TU Delft

Delft University of Technology

Shear failure of prestressed girders in regions without flexural cracks

Roosen, M.A.

DOI
10.4233/uuid:e3615629-cfe2-4fc7-920d-5bc2e776e7c5

Publication date
2021

Document Version
Final published version

Citation (APA)
Roosen, M. A. (2021). *Shear failure of prestressed girders in regions without flexural cracks*. [Dissertation (TU Delft), Delft University of Technology]. https://doi.org/10.4233/uuid:e3615629-cfe2-4fc7-920d-5bc2e776e7c5

Important note
To cite this publication, please use the final published version (if applicable).
Please check the document version above.

Copyright
Other than for strictly personal use, it is not permitted to download, forward or distribute the text or part of it, without the consent of the author(s) and/or copyright holder(s), unless the work is under an open content license such as Creative Commons.

Takedown policy
Please contact us and provide details if you believe this document breaches copyrights.
We will remove access to the work immediately and investigate your claim.

This work is downloaded from Delft University of Technology.
For technical reasons the number of authors shown on this cover page is limited to a maximum of 10.

SHEAR FAILURE OF PRESTRESSED GIRDERS IN REGIONS WITHOUT FLEXURAL CRACKS

M.A. Roosen

SHEAR FAILURE OF PRESTRESSED GIRDERS IN REGIONS WITHOUT FLEXURAL CRACKS

Marco Alexander ROOSEN

SHEAR FAILURE OF PRESTRESSED GIRDERS IN REGIONS WITHOUT FLEXURAL CRACKS

Dissertation

for the purpose of obtaining the degree of doctor
at Delft University of Technology
by the authority of the Rector Magnificus Prof.dr.ir. T.H.J.J. van der Hagen
chair of the Board for Doctorates
to be defended publicly on Monday 29 March 2021 at 17:30 o'clock

by

Marco Alexander ROOSEN

Master of Science in Civil Engineering, Delft University of Technology, the Netherlands
born in Helmond, the Netherlands

This dissertation has been approved by the promotors.

Composition of the doctoral committee:

Reactor Magnificus,	chairperson
Prof.dr.ir. M.A.N. Hendriks	Delft University of Technology and Norwegian University of Science and Technology, Norway, promotor
Dr.ir. Y. Yang	Delft University of Technology, copromotor

Independent members:

Prof.dr.ir. J.G. Rots	Delft University of Technology
Prof. E.C. Bentz	University of Toronto, Canada
Prof.dr.-ing J. Hegger	RWTH Aachen University, Germany
Dr.ir. S.A.A.M. Fennis	Rijkswaterstaat
Prof.dr.ir. H.E.J.G. Schlangen	Technische Universiteit Delft, reserve member

Other member:

Dr.ir. C. van der Veen	Delft University of Technology

Prof.dr.ir. D.A. Hordijk has contributed greatly to the preparation of this dissertation.

This research was sponsored by Rijkswaterstaat, Ministry of Infrastructure and Water Management

Cover photo: ‘Brug over de Rotte’, by M.A. Roosen

©2021 M.A. Roosen, Pijnacker, the Netherlands

Printed by: Ipskamp Printing
ISBN 978-94-6421-285-3
An electronic version of this dissertation is available at http://repository.tudelft.nl/.

Summary

Bridges and viaducts in the Dutch Highway network have been used more intensively by traffic in recent decades. As a result, the current traffic loads are higher than those taken into account during the design. This is an important reason for Rijkswaterstaat (RWS) to assess the structural safety of its older bridges and viaducts. Some of these older structures contain prestressed girders with an I-shape and with a low amount of shear reinforcement. For these bridges it frequently turns out that it is not possible to demonstrate sufficient structural safety. Particularly in the regions close to the supports where the shear forces are high, the shear resistance often appears to be insufficient according to the current guidelines. These are also the regions where no flexural cracks occur because prestressing is present and the moment caused by the load is low. When no flexural cracks are present, these regions can be assessed in two ways: (i) by assuming failure when a diagonal tension crack develops in the web (diagonal tension cracking), or (ii) by determining the resistance after a diagonal tension crack forms, taking into account the contribution of the stirrups, aggregate interlock and the shear transfer by the uncracked flanges. Depending on the amount of shear reinforcement and the level of prestressing, the highest and thus the governing shear resistance will be found from one of these two assessments.

According to the current guidelines for the structural assessment of bridges, the resistance to diagonal tension cracking is determined by equating the maximum principal tensile stress in the web and the axial tensile strength of the concrete. Two comments can be made regarding this approach: (i) the determination of the maximum principal tension stress is less accurate due to the use of a number of simplifications (ii) the actual tensile strength will be affected by the presence of principal compressive stresses (‘biaxial behaviour’) and a ‘statistical size effect’. The latter refers to the phenomenon that if the area with high tensile stresses increases, also the probability of encountering a spot with a lower tensile strength increases. The first part of the research therefore focuses on the question how these aspects affect the accuracy of the predicted resistance.

In order to investigate diagonal tension cracking, a database has been compiled with relevant experiments from literature. For experiments without flexural cracks, the principal tensile stresses were determined by using linear elastic finite element analyses. It is investigated how accurately the numerically found maximum principal tensile stress can be approximated analytically and how this accuracy is affected by using common simplifications. Furthermore, it was investigated whether the experimentally found resistance to diagonal tension cracking could be predicted more accurately when the biaxial behaviour and the statistical size effect are considered. For this part of the research only experiments without flexural cracks are considered, to exclude a potential

influence of the flexural cracks at the edge of the region without flexural cracks on the assumed linear elastic stress distribution in this region. Furthermore, it is investigated whether it is also possible to accurately predict the resistance to diagonal tension cracking for experiments with flexural cracks, when the principal tensile stresses are determined by a linear elastic calculation and it is assumed that these are not affected by flexural cracks in the vicinity. Based on the gathered insights, analytical models have been proposed that make it possible to accurately determine the resistance to diagonal tension cracking: 'model A1' for girders without flexural cracks and 'model A2' for girders with flexural cracks.

From the linear-elastic finite element analyses of experiments without flexural cracks, it was found that diagonal tension cracking occurs at a maximum principal tensile stress lower than the axial tensile strength. Considering the biaxial behaviour or the statistical size effect separately did not result in more consistent predictions. However, when both phenomena are combined, it was found that the resistance to diagonal tension cracking can be predicted very accurately. Another important finding is that the principal tensile stresses in the regions without flexural cracks are lower, and less accurately to predict, when flexural cracks are present at the edge of this region. Nevertheless, it has been demonstrated that for both girders with and without flexural cracks, the resistance to diagonal tension cracking can be accurately determined using the proposed analytical models. For girders with flexural cracks at the edge of the regions without flexural cracks, the overestimation of the maximum principal tensile stress is compensated by assuming a higher tensile strength of the web. Eventually, design values have been derived for both model A1 and model A2, that correspond to an assumed failure probability. By taking the most conservative value of both models, it is possible to use only one model for the design value, referred to as model A. Model A can be used in practice by engineers regardless of the presence of flexural cracks.

When a sufficient amount of shear reinforcement is present, the resistance after diagonal tension cracking will be higher than the resistance to diagonal tension cracking. The theoretical models for girders with stirrups, as used in current design and assessment guidelines, are not intended for regions without flexural cracks. Hence, these models do not take into account (i) the low longitudinal strain, which increases the contribution of the aggregate interlock, and (ii) the shear stress transferred by the uncracked flanges. The second part of the research therefore focuses on the question how the shear force is transferred in these regions and what parameters and conditions affect this shear transfer.

The variable angle truss model, as used in the Eurocode, was found to significantly underestimate the shear resistance of prestressed girders in regions without flexural cracks, especially when a low amount of shear reinforcement is present. That is why, as part of this research, an analytical model has been developed to determine this resistance more

accurately, referred to as ‘model B1’. This model is based on the Modified Compression Field Theory (MCFT). This theory is also suitable to determine the shear resistance for lower amounts of transverse reinforcement. Moreover, the MCFT is able to account for the low longitudinal strain that is typical for regions without flexural cracks. As the first step in the development of the model, the maximum shear stress at mid-depth of the girder height is investigated. This is done specifically for regions without flexural cracks by assuming zero longitudinal strain. For a series of parameters, representative for existing bridges and viaducts, the maximum shear stress has been determined with the MCFT. Subsequently, the shear stress distribution along the diagonal tension crack was investigated by using a non-linear sectional analyses programme based on the MCFT. This programme was subsequently also used to investigate the distribution of the shear stresses in the uncracked flanges. Eventually, model B1 was derived which includes all parameters that significantly affect the shear resistance. In order to evaluate the accuracy of model B1, a database has been compiled with relevant experiments from literature.

The results of the parameter study using the MCFT show that for regions without flexural cracks, the shear resistance in the web is maximum (i) when the aggregate interlock in the crack starts to decrease due to the opening of the crack or (ii) when the concrete is about to crush. The maximum shear resistance found from the more complex MCFT calculations are approximated with simple equations that will be part of the proposed analytical model. These simple equations result in almost the same predicted resistance as found from the MCFT. The maximum shear stress at mid-depth of the girder height, appears to be representative for the resistance along the diagonal tension crack. In addition, when the web fails, a part of the shear force will be transferred by the uncracked flanges. In the proposed model, the total resistance is determined by multiplying the resistance at mid-depth of the girder height by the mean girder width and the effective shear depth. For the effective shear depth a simple equation has been derived. This equation results in almost the same ratios between the maximum shear stress at mid-depth and the total shear resistance as those found with the advanced sectional programme based on the MCFT. Eventually, the experimentally found resistances were compared to the resistance predicted with model B1 for the relevant experiments of the database which demonstrates that the proposed model can determine the shear resistance consistently. A design value has also been derived for model B1, that corresponds to an assumed failure probability.

The resistance in model B1 consists of contributions of aggregate interlock and stirrups. It is also possible to arithmetically ascribe this resistance entirely to the stirrups. Although this way of formulating does not correspond to physical behaviour, the formulation is nevertheless attractive because it is also applied in the currently used variable angle truss model. This model is derived in this dissertation as alternative for

model B1 and is referred to as ‘the variable angle truss model modified for regions without flexural cracks’ or simply ‘model B2’.

The main result of the research is that analytical models have become available that are able to accurately predict the shear resistance in regions without flexural cracks. Using these models, it is possible to make substantiated decisions about whether to maintain, strengthen or replace prestressed bridges and viaducts. Another important result is that the models are less conservative than the models currently in use. For approximately 75 prestressed bridges in the Dutch Highway network, it is not possible to demonstrate sufficient shear resistance in the regions without flexural cracks when the current models are used. However, when the models are used as proposed in this dissertation, it will be possible to demonstrate sufficient shear resistance for approximately 65 of these 75 bridges.

Samenvatting

Bruggen en viaducten in het Nederlandse hoofdwegennet worden de afgelopen decennia steeds intensiever door het verkeer gebruikt. Hierdoor is de huidige verkeersbelasting hoger dan die waarmee tijdens het ontwerp rekening is gehouden. Dit is voor Rijkswaterstaat (RWS) een belangrijke aanleiding om de constructieve veiligheid van zijn oudere bruggen en viaducten te beoordelen. Een deel van deze oudere kunstwerken bestaat uit voorgespannen I-vormige liggers met weinig beugelwapening. Voor deze kunstwerken blijkt het regelmatig niet mogelijk te zijn om aan te tonen dat de constructieve veiligheid voldoende is. Met name in de gebieden nabij de opleggingen, waar de optredende dwarskrachten hoog zijn, blijkt de dwarskrachtcapaciteit volgens de huidige richtlijnen vaak onvoldoende. Dit zijn eveneens de gebieden waar geen buigscheuren ontstaan omdat voorspanning aanwezig is en het optredende moment uit de belasting laag is. Wanneer geen buigscheuren aanwezig zijn, kunnen deze gebieden op twee manieren worden beoordeeld: (i) door uit te gaan van bezwijken wanneer in het lijf een afschuiftrekscheur ontstaat (afschuiftrekbreuk), of (ii) door de weerstand te bepalen na het ontstaan van een afschuiftrekscheur, waarbij rekening wordt gehouden met de bijdrage van de beugels, scheurwrijving en dwarskrachtoverdracht door de niet-gescheurde flenzen. Afhankelijk van de hoeveelheid beugels en de voorspangraad zal uit één van beide beoordelingen de hoogste en dus maatgevende dwarskrachtweerstand volgen.

In de vigerende richtlijnen voor het beoordelen van kunstwerken wordt de weerstand tegen afschuiftrekbreuk bepaald door de maximale hoofdtrekspanning in het lijf gelijk te stellen aan de axiale treksterkte van het beton. Ten aanzien van deze aanpak zijn een tweetal kanttekeningen te maken: (i) de bepaling van de maximale hoofdtrekspanning gebeurt minder nauwkeurig door het gebruik van een aantal vereenvoudigingen en (ii) de aanwezige treksterkte zal worden beïnvloed door hoofddrukspanningen die aanwezig zijn (‘twee-assig gedrag’) en door een ‘statistisch afmetingeneffect’. Met dit laatste wordt het fenomeen bedoeld dat de kans op het aantreffen van een plek met een lagere treksterkte groter is naarmate het gebied met hoge trekspanningen groter is. Het eerste deel van het onderzoek richt zich daarom op de vraag hoe deze aspecten de nauwkeurigheid van de voorspelde weerstand beïnvloeden.

Om het ontstaan van afschuiftrekscheuren te kunnen onderzoeken is een database samengesteld met relevante experimenten uit de literatuur. Voor experimenten zonder buigscheuren zijn de hoofdtrekspanningen bepaald met lineair-elastische eindige-elementenanalyses. Onderzocht is hoe nauwkeurig de numeriek gevonden maximale hoofdtrekspanning analytisch te benaderen is en hoe deze nauwkeurigheid wordt beïnvloed wanneer gangbare vereenvoudigingen worden gebruikt. Verder is onderzocht of

de experimenteel gevonden weerstand tegen afschuiftrekbreuk nauwkeuriger te voorspellen is wanneer het bi-axiale gedrag en het statistische afmetingeneffect worden beschouwd. Voor dit deel van het onderzoek zijn alleen de experimenten zonder buigscheuren beschouwd. Hierdoor wordt een mogelijke invloed van de buigscheuren aan de rand van het gebied zonder buigscheuren op de aangenomen lineair elastische spanningsverdeling in dit gebied uitgesloten. Bovendien is onderzocht of het ook voor de experimenten met buigscheuren mogelijk is om de weerstand tegen afschuiftrekscheuren nauwkeurig te voorspellen wanneer de hoofdtrekspanningen worden bepaald met een lineair elastisch berekening en wordt aangenomen dat deze niet worden beïnvloed door de nabijheid van buigscheuren. Op basis van de opgedane inzichten zijn analytisch modellen voorgesteld die het mogelijk maken om de weerstand tegen het ontstaan van afschuiftrekscheuren nauwkeurig te bepalen: model A1 voor liggers zonder buigscheuren en model A2 voor liggers met buigscheuren.

Uit de lineair-elastische eindige-elementenanalyses van experimenten zonder buigscheuren volgt dat afschuiftrekscheuren ontstaan bij een maximale hoofdtrekspanning die lager is dan de axiale treksterkte. Het beschouwen van de bi-axiale treksterkte of het statistische afmetingeneffect afzonderlijk resulteert niet in consistentere voorspellingen. Wanneer beide fenomenen worden gecombineerd kan de weerstand tegen afschuiftrekbreuk echter zeer nauwkeurig worden voorspeld. Een andere belangrijke bevinding is dat de hoofdtrekspanningen in de gebieden zonder buigscheuren lager zijn, en minder nauwkeurig te voorspellen, wanneer buigscheuren aanwezig zijn aan de rand van dit gebied. Desalniettemin is aangetoond dat zowel voor liggers met, als voor liggers zonder buigscheuren, de weerstand tegen afschuiftrekbreuk nauwkeurig kan worden bepaald met de voorgestelde analytische modellen. Voor liggers met buigscheuren aan de rand van het gebied zonder buigscheuren, kan de overschatting van de maximale hoofdtrekspanning worden gecompenseerd door het aannemen van een hogere treksterkte van het lijf. Uiteindelijk zijn voor zowel model A1 als voor model A2 rekenwaarden afgeleid die horen bij een aangenomen faalkans. Door uit te gaan van de meest conservatieve waarde van beide modellen, is het mogelijk om in de praktijk slechts één model te hanteren voor de rekenwaarde. Dit model, aangeduid als model A, kan dus worden gebruikt ongeacht of buigscheuren aanwezigheid zijn.

Wanneer voldoende beugelwapening aanwezig is, zal de weerstand na het ontstaan van een afschuiftrekscheur hoger zijn dan de weerstand tegen afschuiftrekbreuk. De theoretische modellen voor liggers met beugels, zoals gebruikt in de vigerende ontwerp en beoordelingsrichtlijnen, zijn niet bedoeld voor gebieden zonder buigscheuren. Deze modellen houden namelijk geen rekening met (i) de lage rek in langsrichting, die de bijdrage van de scheurwrijving verhoogt en (ii) de afdracht van schuifspanningen in de niet-gescheurde flenzen. Het tweede deel van het onderzoek richt zich daarom op de

vraag hoe de dwarskracht in deze gebieden wordt overgedragen en wat de parameters en condities zijn die deze overdracht beïnvloeden.

Het vakwerkmodel met variabele hoek, zoals gebruikt in de Eurocode, blijkt de dwarskrachtweerstand van voorgespannen liggers in gebieden zonder buigscheuren sterk te onderschatten, zeker wanneer weinig beugelwapening aanwezig is. Daarom is als onderdeel van dit onderzoek een analytisch model ontwikkeld om deze weerstand nauwkeuriger te kunnen bepalen. Dit model wordt aangeduid als model B1. Voor dit model is de 'Modified Compression Field Theory' (MCFT) als basis genomen, omdat deze ook geschikt is om de dwarskrachtweerstand te bepalen voor lage hoeveelheden dwarswapening. Daarnaast is de MCFT in staat rekening te houden met de lage rek in langsrichting die typerend is voor gebieden zonder buigscheuren. De eerste stap in de ontwikkeling van het model is het onderzoeken van de maximale schuifspanning halverwege de liggerhoogte. Dit is specifiek gedaan voor gebieden zonder buigscheuren door uit te gaan van een rek in langsrichting van nul. Voor een reeks van parameters, die representatief is voor de bestaande bruggen en viaducten, is de maximale schuifspanning bepaald met de MCFT. Daarna is het verloop van de schuifspanningen over de afschuiftrekscheur onderzocht door gebruik te maken van een niet-lineair eindige-elementenprogramma voor doorsneden dat is gebaseerd op de MCFT. Dit programma is vervolgens ook gebruikt om het verloop van de schuifspanningen in de niet-gescheurde flenzen te onderzoeken. Uiteindelijk is een analytisch model afgeleid waarin alle parameters die de dwarskrachtweerstand significant beïnvloeden zijn opgenomen. Om de nauwkeurigheid van het voorgestelde model te kunnen evalueren is een database samengesteld met relevante experimenten uit de literatuur.

De resultaten van de parameterstudie met de MCFT tonen aan dat voor gebieden zonder buigscheuren de dwarskrachtweerstand in het lijf maximaal is (i) wanneer de scheurwrijving begint af te nemen door het openen van de scheur of (ii) wanneer het beton op het punt staat te verbrijzelen. De maximale dwarskrachtweerstand die volgt uit de meer complexe MCFT berekeningen zijn benaderd met eenvoudige formules die worden gebruikt in het voorgestelde analytische model. Deze eenvoudige formules resulteren in vrijwel dezelfde voorspelde weerstand als de weerstand die volgt uit de MCFT. De maximale schuifspanning op een hoogte halverwege de ligger, blijkt representatief te zijn voor de weerstand over de afschuiftrekscheur. Op het moment dat het lijf bezwijkt, zal ook een deel van de dwarskracht worden overgedragen door de niet-gescheurde delen, met name de flenzen. In het voorgestelde model B1, wordt de totale weerstand bepaald door de weerstand halverwege de liggerhoogte te vermenigvuldigen met de gemiddelde liggerbreedte en de effectieve dwarskrachthoogte. Voor de effectieve dwarskrachthoogte is een eenvoudige formule afgeleid. Deze formule leidt tot nagenoeg dezelfde verhoudingen tussen de maximale schuifspanning halverwege de ligger en de totale

dwarskrachtweerstand als de verhoudingen die worden gevonden met het geavanceerde doorsnede-programma gebaseerd op de MCFT. Uiteindelijk is voor de relevante experimenten van de database de experimenteel gevonden weerstand vergeleken met de voorspelde weerstand volgens model B1. Hieruit blijkt dat model B1 de dwarskrachtweerstand consistent kan bepalen. Ook voor model B1 is een ontwerpwaarde afgeleid horende bij een aangenomen faalkans.

In het voorgestelde model B1 wordt de weerstand bepaald op basis van bijdrages van scheurwrijving en beugels. Het is ook mogelijk deze weerstand rekenkundig geheel toe te schrijven aan de beugels. Hoewel deze formulering minder goed aansluit bij het fysische gedrag, is de formulering toch aantrekkelijk omdat deze aansluit bij het momenteel gebruikte vakwerkmodel. Dit model is in dit proefschrift afgeleid als alternatief voor het model B1 en wordt aangeduid als ‘het vakwerkmodel aangepast voor gebieden zonder buigscheuren’ of kortweg ‘model B2’.

Het belangrijkste resultaat van het onderzoek is dat nieuwe analytische modellen beschikbaar zijn gekomen die de dwarskrachtweerstand in gebieden zonder buigscheuren nauwkeurig kunnen voorspellen. Met het gebruik van deze modellen is het mogelijk om gefundeerde beslissingen te nemen over het kunnen handhaven, of moeten versterken of vervangen, van voorgespannen bruggen en viaducten. Een ander belangrijk resultaat is dat de modellen minder conservatief zijn dan de modellen die momenteel worden gebruikt. Bij gebruik van de huidige modellen is het voor ongeveer 75 voorgespannen bruggen in het Nederlandse Hoofdwegennet niet mogelijk om voldoende dwarskrachtweerststand aan te tonen in de gebieden zonder buigscheuren. Wanneer echter de modellen worden gebruikt zoals voorgesteld in dit proefschrift, zal het alsnog mogelijk zijn om voldoende dwarskrachtweerstand aan te tonen voor ongeveer 65 van deze 75 bruggen.

Table of contents

Summary i

Samenvatting v

1 Introduction 1
1.1 Research relevance and objectives 2
1.2 Shear resistance of prestressed girders without stirrups 4
1.3 Shear resistance of prestressed girders with stirrups 6
1.4 Knowledge gaps and research questions 7
1.5 Research methodology 9
1.6 Outline of the dissertation 12

PART 1: RESISTANCE TO DIAGONAL TENSION CRACKING

2 Literature review on diagonal tension cracking 17
2.1 Resistance to diagonal tension cracking 17
2.1.1 Diagonal tension cracking 17
2.1.2 Methods to determine the principal tensile stress 20
2.1.3 Distribution of principal tensile stresses in a prestressed girder 25
2.1.4 Methods to determine the tensile strength of concrete 26
2.1.5 Models from literature 31
2.2 Database on diagonal tension cracking 35
2.2.1 Selection criteria 35
2.2.2 Overview of selected experiments 36
2.3 Findings from literature review 39

3 Resistance to diagonal tension cracking 41
3.1 Experimentally found tensile strength of the web 43
3.2 Bi-axial behaviour and statistical size effect 46
3.3 Principal tensile stresses in disturbed areas 53
3.4 Aspects affecting the accuracy for girders without flexural cracks 57
3.5 Aspects affecting the accuracy for girders with flexural cracks 59

4 Proposed models for diagonal tension cracking 65
4.1 Model A1: girders without flexural cracks 65
4.2 Model A2: girders with flexural cracks 69
4.3 Design values for the proposed models 70

PART 2: SHEAR RESISTANCE AFTER DIAGONAL TENSION CRACKING

5 Literature review on shear resistance of prestressed girders with stirrups 75
5.1 Models from literature 75
5.1.1 Variable angle truss model 75
5.1.2 Empirical model of MacGregor et al. 81
5.1.3 Modified Compression Field Theory 85
5.1.4 Models for girders based on the MCFT 91
5.1.5 Model of Bentz et al. 93
5.1.6 Model of Esfandiari 98
5.1.7 Empirical model of Leonhardt 102
5.1.8 Arch action models 104
5.2 Comparison of models from literature 106
5.3 Database on shear failure of prestressed girders with stirrups 109
5.3.1 Selection criteria 109
5.3.2 Overview of selected experiments 112
5.4 Findings from literature review and further approach 115

6 Shear resistance at mid-depth of the web 119
6.1 Longitudinal strain of the web in regions without flexural cracks 120
6.2 Failure modes of the web in regions without flexural cracks 122
6.2.1 Possible failure modes of the web 122
6.2.2 Method to determine the shear resistance of a failure mode 123
6.3 Shear resistance determined using the MCFT 128
6.4 Proposed approximation equations 131
6.5 Comparison approached resistances with models from literature 134
6.5.1 Model of Bentz et al. 135
6.5.2 Variable angle truss model 138

7 Shear transfer along the crack and in uncracked concrete 143
7.1 Overview of shear transfer mechanism in a girder 144
7.2 Shear transfer along a diagonal tension crack 146
7.3 Shear transfer in uncracked concrete 151

8 Proposed model for shear resistance of girders with stirrups 157
8.1 Method to determine the regions without flexural cracks 157
8.2 Minimum and maximum shear resistance 161
8.3 Model B1: shear resistance of prestressed girders with stirrups 163
8.4 Accuracy of the proposed model 165
8.4.1 Selection of experiments for the evaluation of the accuracy 165
8.4.2 Accuracy of model B1 169
8.4.3 Comparison with models from literature 173
8.5 Design value of model B1 175
8.6 Model B2: modified variable angle truss model 178
8.7 Minimum shear reinforcement ratio 182

9 Conclusions and recommendations 187
9.1 Scientific results 187
9.1.1 Resistance to diagonal tension cracking 187
9.1.2 Shear resistance of prestressed girders with stirrups 189
9.2 Answers to research questions 192
9.3 Summary of proposed models and their application conditions 194
9.3.1 Overview shear resistance models for a prestressed girder 195
9.3.2 Model A: resistance to diagonal tension cracking 197
9.3.3 Model B1: shear resistance of prestressed girders with stirrups 198
9.4 Implications for the structural assessments of bridges 200
9.4.1 Implications for both proposed models 200
9.4.2 Implications for resistance to diagonal tension cracking 201
9.4.3 Implications for girders with stirrups 201
9.5 Future research 202

References 205

Appendices

Appendix A: Database on diagonal tension cracking 213
Appendix B: Categorization of experiments on whether flexural cracks are present 217
Appendix C: Ratio of σ_{1max} and f_{ctm} for experiments without flexural cracks 221
Appendix D: Ratio of σ_{1max} and f_{ctm} considering bi-axial behaviour and statistical size effect 223

Appendix E: Type of diagonal tension cracking and statistical properties for the ratio of σ_{1max} and f_{ctm} 225
Appendix F: Database on shear failure of prestressed girders with stirrups 229
Appendix G: Resistances of membrane elements determined with the MCFT for $\varepsilon_x = 0$, $s_\theta = 300$ mm, $d_{max} = 32$ mm 233
Appendix H: Ratio of the resistance determined with the MCFT and with the proposed approximation equations & other models 235
Appendix I: Ratio of the resistance of girders according to *Response* and predicted using Equations 7.5 and 7.8 to 7.10. 237
Appendix J: Comparison of ε_x at the least compressed chord between *Response* and the proposed method 239
Appendix K: Shear resistance according to the proposed model for prestressed girders with stirrups 241
Appendix L: Selection of experiments for the evaluation of the accuracy of the proposed model based on ε_x 245
Appendix M: Selection of experiments for the evaluation of the accuracy of the proposed model based on $V'_{R,c}$ and V'_{Rmax} 249
Appendix N: Accuracy of models for the determination of the shear resistance of prestressed girders with stirrups 251
Appendix O: Effect on resistance of assuming $s_\theta = 300$ mm and $d_{max} = 31.5$ mm 253
Appendix P: Steps to determine the shear resistance for models from literature 255

Notations 257

Dankwoord 265

Curriculum Vitae 269

1

Introduction

Prestressed girders will fail in shear when the applied shear force exceeds the shear resistance. A distinction can be made between shear failure in regions with and without flexural cracks. This is explained in Figure 1.1 which shows a single span prestressed girder with an I-shaped cross-section loaded by two point loads. The bending moment is maximum between the two point loads and causes a tensile force in the bottom flange. This tensile force causes flexural cracks, starting from the bottom flange. The flexural cracks between the point loads are vertical because of the absence of shear force. Between the point loads and the supports, the girder is exposed to both moment and shear force. In the parts of the girder that are exposed to a substantial moment, flexural cracks develop in the bottom flange and will, due to the presence of a shear force, extend to diagonal cracks in the web. These cracks are defined as flexural shear cracks. The parts of the girder that are less exposed to the moment caused by the point loads, will remain free of flexural cracks, because prestress is present that reduces the tensile force in the bottom flange. The high shear force in these parts causes high principal tensile stresses in the web that can cause diagonal cracks in the web. These cracks are defined as diagonal tension cracks. Eventually, a girder can fail in shear in the region with or without flexural cracks. In this dissertation shear failure of prestressed girders in regions without flexural cracks is investigated.

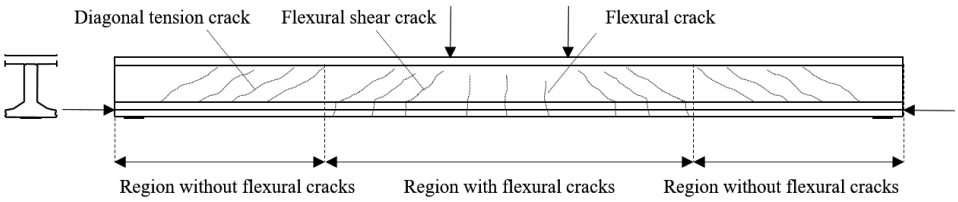

Figure 1.1. Regions of a prestressed girder with and without flexural cracks

The shear resistance in regions without flexural cracks is different than in regions with flexural cracks. There are two reasons for this: the first reason is that the stress conditions that cause diagonal tension cracking are different from the stress conditions that lead to flexural shear cracking; the second reason is that the shear transfer after diagonal cracking differs between both regions. Both reasons will be further explained in this dissertation.

The first topic of this dissertation concerns diagonal tension cracking. For prestressed girders without stirrups, the resistance to diagonal tension cracking is commonly considered as the shear resistance. This topic is relevant for prestressed girders that contain nonconforming stirrups or for girders with a low amount of shear reinforcement. The second topic of this dissertation concerns the shear resistance of prestressed girders with stirrups in regions without flexural cracks. This topic relates to prestressed girders that contain an amount of shear reinforcement which is sufficient to resist additional shear force after diagonal tension cracking.

Section 1.1 describes the relevance and the objectives of this research. Sections 1.2 and 1.3 describe the models that are currently used to assess shear resistance in regions without flexural cracks for existing bridges in the Dutch Highway network. For each model it is evaluated whether the model is indeed suitable to determine the shear resistance in regions without flexural cracks. The models for girders without stirrups are described in Section 1.2 and the models for girders with stirrups in Section 1.3. Section 1.4 describes the knowledge gaps and research questions that are found from the discussion of the currently used models. Section 1.5 explains the methodology used for the research and Section 1.6 provides an outline of the dissertation.

1.1 Research relevance and objectives

In the middle of the last century, the first prestressed structures were built in the Netherlands. The principle of prestressing enabled structural engineers to design longer and more slender bridges. The usage of prestressing has become more common since then. Up-to-date, about 3300 bridges in the Dutch Highway network are prestressed (Klatter 2019).

Bridges and viaducts in Dutch Highway network have been used more intensively by traffic in recent decades. As a result, the current traffic loads are higher than that taken into account during the design. This is an important reason for Rijkswaterstaat, which is part of the Dutch Ministry of Infrastructure and Water Management, to assess the structural safety of its existing bridges and viaducts. A second reason to carry out this assessment is the evolution of the theoretical models used in the design codes to determine the shear resistance.

Preliminary assessments (RWS 2018, De Boer et al. 2016, Kamp 2017a, b, c) showed that it is demanding to demonstrate sufficient shear resistance for a group of existing bridges that contain girders with flanges and a thin web, that were designed before the design code of 1974 (NEN 1974) was enforced. The introduction of NEN 1974 has been a major change for the design practice, as since then a minimum amount of stirrups was

prescribed. According to a recent inventory, 630 prestressed bridges in the Dutch Highway network contain girders with flanges and a thin web and were designed before the design code of 1974 was enforced. These 630 bridges concern 80 post-tensioned bulb-T-girders, 460 pre-tensioned precast girders and 90 post-tensioned box girder bridges (Figure 1.2). For 107 (bulb-T-girders and precast girders) of these 630 older bridges a preliminary assessment has been carried out using the guideline for the assessment of existing structures issued by Rijkswaterstaat (RWS 2013). For 21 of these 107 bridges, it was not possible to demonstrate sufficient shear resistance. The shear resistance was found insufficient in the region with flexural cracks for 6 bridges and in the regions without flexural cracks for 15 bridges. For the entire group of 540 older bulb-T-girders and precast girders, it can be expected, based on extrapolation, that for approximately 75 of these bridges it will not be possible to demonstrate sufficient shear resistance in the regions without flexural cracks.

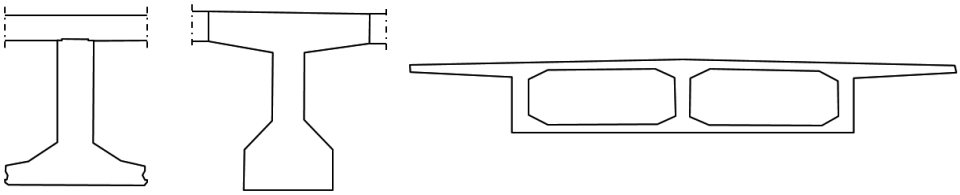

Figure 1.2. Cross-sections of (from left to right) pre-tensioned precast girders with an in situ slab, post-tensioned bulb-T girders and box girder bridges

To be able to make substantiated decisions about the structural safety of bridges there is a need for models that can accurately determine the shear resistance in regions without flexural cracks. This concerns both a model to determine the resistance to diagonal tension cracking and, for prestressed girders with stirrups, a model for the shear resistance specifically intended for regions without flexural cracks.

Many assumptions have been made in developing the currently used model for diagonal tension cracking (Section 1.2). These assumptions eventually have resulted in a simple model that is easy to use in engineering practice. Because the large number of bridges for which it is demanding to demonstrate sufficient shear resistance in the regions without flexural cracks, there is a need to understand how the assumptions affect the accuracy of the predicted resistance and whether refinements are possible to improve the accuracy of the predictions.

The currently used models for the shear resistance of girders with stirrups (Section 1.3) are not intended for regions without flexural cracks. Conditions for these regions, such as a low longitudinal strain and shear transfer by the uncracked flanges, are not considered by the currently used models. There is a need to understand how these conditions affect the shear resistance.

Based on these considerations, the objectives of this dissertation are:

1. To understand how the shear force is transferred in regions without flexural cracks and determine the major parameters and conditions that affects the shear transfer.
2. To derive a model that is capable of accurately determining the resistance to diagonal tension cracking.
3. To derive a model that is capable of accurately determining the shear resistance of girders with stirrups in regions without flexural cracks.

To be able to apply the models in engineering practice, it is not only the objective to derive models for the mean resistance, but also for the design value of the resistance that corresponds to an assumed failure probability. Eventually, it should be possible to make substantiated decisions regarding maintaining, strengthening or renewal of prestressed bridges based on the proposed models.

1.2 Shear resistance of prestressed girders without stirrups

All existing prestressed bridges in the Dutch Highway network contain shear reinforcement. However, not all shear reinforcement is considered as effective. This ineffective shear reinforcement does not fulfil the design requirements and is defined as 'nonconforming shear reinforcement'. Examples of nonconforming shear reinforcement layouts are shown in Figure 1.3.

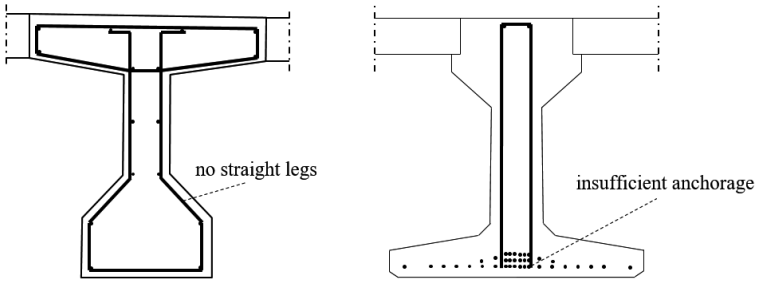

Figure 1.3. Examples of shear reinforcement layouts that are considered ineffective

The bulb-T beam, shown in the left of Figure 1.3, contains shear reinforcement with kinked legs that could possibly burst out. The inverted T-beam, shown in the right of Figure 1.3, contains shear reinforcement insufficiently anchored in the tensile zone. In preliminary assessments, the contribution of this nonconforming shear reinforcement to the shear resistance is neglected, because it is unknown to what extend the stirrups contribute to the shear resistance. Therefore, the girders are considered as members without stirrups. For prestressed girders without stirrups, the resistance to diagonal tension

cracking is considered as the shear resistance, as will be explained in Chapter 2. Therefore, the resistance to diagonal tension cracking can be used to determine the shear resistance of prestressed girders with nonconforming shear reinforcement. The resistance to diagonal tension cracking is also governing for girders with an amount of shear reinforcement that is so low that no additional shear can be resisted after diagonal tension cracking.

According to the Eurocode (NEN 2005) the principal tensile stresses of a single span prestressed member without stirrups, should be limited by the uniaxial tensile strength of concrete for regions which are uncracked in bending. The guideline for the assessment of existing structures (RWS 2013) extends the application of this requirement from 'single span members' to 'structures'. This implies that also bridges that contain continuously supported girders can be assessed using this requirement and even complete bridges, simply or continuously supported. The requirement is based on the principle that concrete cracks at a load that causes a maximum principal tensile stress equal to the uniaxial tensile strength of concrete. It is assumed that the principal tensile stresses can be governing anywhere in the web. Although this principle is simple and might seem indisputable, two remarks can be made to this approach.

The first remark concerns that the maximum principal tension stress is determined less accurately due to the use of a number of simplifications. As a simplification the principal stresses are calculated from the cross sectional forces assuming that the Euler Bernoulli girder theory is valid. Also, the presence of vertical stresses is neglected for simplicity. Both simplifications are questionable for cross-sections that are close to the support or a concentrated load. However, these cross-sections usually turn out to be critical in assessments. Another relevant simplification that could affect the accuracy of the predicted maximum principal tensile stress, is the assumption that the principal tensile stresses in the region free of flexural cracks are not affected by the flexural crack at the edge of this region.

The second remark concerns the suitability of the uniaxial concrete tensile strength as limitation for the maximum principal tensile stress. From tests on bi-axially loaded small membranes, it is know that the tensile strength reduces when the lateral principal compressive stresses increase. This is called bi-axial behaviour and is for instance investigated by Kupfer et al. (1969). Moreover, the tensile strength was found to depend on the size of the region subjected to high tensile stresses (Collins et al. 1997). If the size of this region increases, the member cracks at lower principal tensile stresses. In this dissertation this phenomenon is defined as the statistical size effect. The actual tensile strength will be affected by the presence of principal compressive stresses and the statistical size effect.

1.3 Shear resistance of prestressed girders with stirrups

A part of the existing bridges in the Dutch Highway network contain stirrups that do fulfil the design requirements which are thus considered as effective. According to the currently used guideline for the assessment of existing structures (RWS 2013) three models can be used to determine the shear resistance for girders with stirrups in regions without flexural cracks. The highest of the predicted resistances is considered as governing. The three models are:

1. The model for the resistance to diagonal tension cracking (RWS 2013, NEN 2005).
2. The model for the shear resistance in regions with flexural cracks (RWS 2013).
3. The variable angle truss model according to the Eurocode (NEN 2005).

The first model can only be applied to determine the shear resistance in regions without flexural cracks. The second and third model are applied for regions both with and without flexural cracks. For each model it will be evaluated below whether it is suitable to determine the shear resistance in regions without flexural cracks.

The first model that could be applied to determine the shear resistance in regions without flexural cracks, is the model that determines the resistance to diagonal tension cracking. This approach is based on the principle that the resistance of girders with stirrups is at least the resistance of the girders neglecting the presence of stirrups. As existing bridges in the Dutch Highway network contain a low amount of shear reinforcement, it is indeed possible that diagonal tension cracking is governing for the resistance. This is the case if the amount of shear reinforcement is so low that the highest resistance is found at diagonal tension cracking. However, for higher amounts of shear reinforcement, additional shear force can be resisted after diagonal tension cracking. For these bridges, the resistance will be underestimated if the ultimate resistance is equalised to the resistance to diagonal tension cracking. Therefore, there is also a need to develop a model that is capable to determine the shear resistance in the regions without flexural cracks considering the presence of stirrups. The suitability of the currently used model to determine the resistance to diagonal tension cracking is already discussed in Section 1.2.

The second possible approach is to use the resistance model derived for regions with flexural cracks (RWS 2013). The model consists of a contribution of stirrups and a contribution of concrete. The use of this model for the regions without flexural cracks is based on the assumption that the resistance in regions without flexural cracks is higher than that in regions with flexural cracks. This is attributed to a higher contribution of the concrete to the shear resistance (Leonhardt et al. 1973). This assumption is further discussed in this dissertation (Section 5.1.7). The concrete contribution in the model consists of two parts: (i) a part that causes decompression of the most tensioned flange

and (ii) a part empirically derived for flexural shear cracking of reinforced concrete girders without stirrups. The model is thus derived to determine the resistance along a flexural shear crack. Because no flexural shear cracks are present in regions without flexural cracks the model is fictional for regions without flexural cracks. The model is not further considered in this dissertation as it does not contribute to a better understanding of transfer of the shear force in regions without flexural cracks.

The third model that could be applied to determine the shear resistance in regions without flexural cracks is the variable angle truss model. This model is a lower bound approach based on the theory of plasticity (Walraven 2002). According to the theory of plasticity the largest resistance is found when the stirrups yield and the concrete struts crush at the same time. It is noted that the effective strength of the concrete struts is calibrated using experiments with higher amounts of shear reinforcement. For lower amounts of shear reinforcement failure due to crushing of the struts may not be governing. Instead failure of the struts due to sliding along the (initial) crack may be governing (Nielsen et al. 2011). For the later mechanism, calibration on the strength of struts has not been reported in literature. Moreover, as the strength of struts is also not calibrated for the conditions present in regions without flexural cracks, it is questionable whether the variable angle truss model is suitable to predict the shear resistance in these regions.

1.4 Knowledge gaps and research questions

The objectives of this dissertation are (i) to develop a model that is capable of accurately determining the resistance to diagonal tension cracking and (ii) to develop a model that is capable of accurately determining the shear resistance of girders with stirrups in regions without flexural cracks.

Based on the description and evaluation of the models currently used (Section 1.2), the following knowledge gaps are identified for diagonal tension cracking:

1. From tests on bi-axially loaded small membranes, it is known that the tensile strength is lower if a compressive stress is present perpendicular to the tensile stress. Models that describe this behaviour are available in literature (Kupfer et al. 1969). Moreover, if the size of a region subjected to tensile stresses increases, the member cracks at a lower principal tensile stress (Collins et al. 1997). For both phenomena it is unknown however, whether the relations as described in literature are directly applicable for the tensile strength of the web which should be assumed to predict diagonal tension cracking of girders.
2. The stresses in the girder around the supports and concentrated loads will be disturbed, therefore the Euler Bernoulli girder theory is not valid in these regions. Moreover, the presence of vertical stresses affect the principal tensile stresses around

the supports and concentrated loads. It is unknown how these phenomena affect the maximum principal tensile stress.

3. Flexural cracks on the edge of regions without flexural cracks could affect the stress distribution in the regions without flexural cracks. Currently the maximum principal tensile stress in the regions without flexural cracks is determined by means of a linear elastic calculation and a possible influence of the vicinity of flexural cracks is not considered.

The identified knowledge gaps can respectively be reformulated into the following research questions:

A. Does the accuracy of the predictions increase if bi-axial behaviour and statistical size effect are taken into account?

B. How are the principal stresses distributed around the supports and the concentrated loads and is it possible to determine the maximum principal tensile stress using the Euler-Bernoulli girder theory and by neglecting the vertical stresses?

C. How does the presence of a flexural crack at the edge of the region without flexural cracks affect the distribution of principal tensile stresses in this region?

Based on the description and evaluation of the currently used models for the shear resistance in regions without flexural cracks of girders with stirrups (Section 1.3), the following knowledge gaps are identified:

4. Besides crushing of the concrete struts, crack sliding along the initial crack appears to be a possible failure mode. An example is shown in Figure 1.4, in which failure occurs due to sliding along the major diagonal tension crack, without crushing of the concrete. It is unclear to what extent the failure mode affects the shear resistance in regions without flexural cracks. None of the currently used resistance models (Section 1.3) distinguish these shear failure modes and the associated shear resistances.

5. In regions without flexural cracks, the longitudinal strains in the web will be negative for almost the entire region. If the longitudinal strains decrease, also the crack widths will decrease. Due to these smaller crack widths, higher shear stresses can be transferred in the cracks by aggregate interlock. This makes it plausible that, in regions without flexural cracks, the web is able to resist more shear force than in regions with flexural cracks. It is unclear to what extent the shear resistance is affected by the low longitudinal strain. None of the currently used resistance models (Section 1.3) consider the effect of the longitudinal strain on the shear resistance. It is noted that, when the longitudinal strain in the web is negative, diagonal tension cracks can still occur. This is because it is not the longitudinal stresses associated with the longitudinal

strains that determine the occurrence of a diagonal tension crack, but the principal tensile stresses, which are also largely affected by the shear stresses.

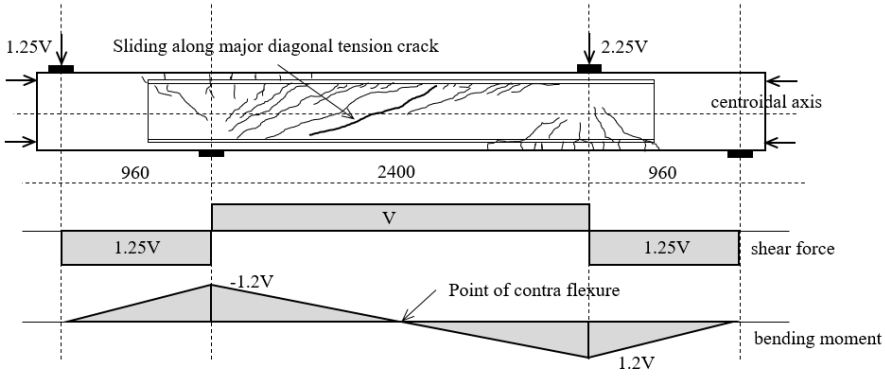

Figure 1.4. Crack patterns for experiment LB10 just before failure (Xie 2009)

6. In regions without flexural cracks, a part of the shear force will be transferred by the uncracked concrete (mainly at the flanges). This is shown in Figure 1.4 in which the flanges above and below the critical diagonal tension crack remain uncracked at a load just before failure. It is unclear to what extent the uncracked concrete above and below the diagonal tension crack contributes to the transfer of shear force in regions without flexural cracks. None of the currently used resistance models (Section 1.3) consider this contribution explicitly.

Again, the identified knowledge gaps can respectively be reformulated into the following research questions:

D. What are the possible shear failure modes for prestressed girders with stirrups in the regions without flexural cracks and is it possible to relate the shear resistance to the potential failure modes?

E. How does the low longitudinal strain, that is associated with regions without flexural cracks, affect the shear force transfer mechanism along the diagonal tension crack?

F. How can the contribution of the shear force transferred by the uncracked flanges be determined and how is this contribution affected by the cross sectional properties?

1.5 Research methodology

Two topics are considered in this dissertation. These concern the resistance to diagonal tension cracking (first topic) and the shear resistance of prestressed girders with stirrups in regions without flexural cracks (second topic). With respect to the first topic, the resistance to diagonal tension cracking is investigated using models that assume a linear elastic stress distribution. With respect to the second topic, the investigation of the shear

resistance of prestressed girders with stirrups is investigated using models that consider the non-linear elastic behaviour of the reinforcement steel, prestressing steel and concrete. An identical methodology regarding literature study is used for both topics:

- An overview of relevant models that predict the shear resistance is compiled and subsequently these models are mutually compared.
- An evaluation is made regarding the following questions: (i) to what extend the models are suitable for determining the shear resistance in the regions without flexural cracks and (ii) to what extend the research questions could be answered based on the literature study.
- The results of the literature review are used to determine the approach to develop a new model.
- A database of relevant experiments described in literature is compiled, which eventually is used to evaluate the accuracy of the proposed model.

The following methodology is used to study the resistance to diagonal tension cracking (first topic):

- The effect of bi-axial behaviour and statistical size effect on the strength of the web are investigated using equations found in literature derived for membrane elements, to predict diagonal tension cracking in girders. These models are used in this study to predict the shear behaviour of girders. To ensure that these phenomena can be investigated without any disturbance caused by the presence of flexural cracks, the evaluation is carried out for experiments on girders free of flexural cracks.
- The disturbed areas around the concentrated loads (supports and externally applied loads) are analysed by carrying out linear elastic finite element analyses. It is assumed that these analyses predict the distribution of principal tensile stresses perfectly. Then, it is investigated how the maximum principal tensile stresses according to the linear elastic finite element analyses can be approached by using the Euler-Bernoulli girder theory. Also, for this purpose only experiments without flexural cracks are used, to ensure that the principal stress distribution can be investigated without any disturbance caused by the presence of flexural cracks.
- The effect of flexural cracks is investigated using experiments on girders with flexural cracks. It is assumed that the other phenomena are sufficiently investigated based on experiments without flexural cracks and that the deviations are only due to the presence of flexural cracks. It is investigated whether it is possible to accurately predict the resistance to diagonal tension cracking using the assumption that the principal stresses are not disturbed in the vicinity of flexural cracks.

The shear resistance of prestressed girders with stirrups in regions without flexural cracks (second topic) is investigated in two steps. Firstly, the resistance at the mid-depth of the web by aggregate interlock and stirrups is determined for regions without flexural cracks. Secondly, the distribution of shear transfer mechanism along the diagonal tension crack and through the flanges is investigated.

The model that is proposed for the shear resistance of the web at mid-depth is derived using the Modified Compression Field Theory (MCFT, Vecchio et al. 1986). The MCFT is used to derive the resistance per failure mode for membranes for a strain condition associated with the regions of a girder without flexural cracks. The resistances per failure mode are derived for certain combinations of parameters. The ranges of these parameters are representative for the intended application of the model (Table 1.1). For the proposed model, the shear resistance at mid-depth of the web is based on the failure modes and associated resistances, derived for the membrane elements.

Table 1.1. Main parameters for bridges with a web and flanges designed before 1974

Parameter	minimum	maximum	
Shear reinforcement ratio (ρ_w)	0.04%	0.70%	
Mean value of concrete cylinder compressive strength (f_{cm})	43	84	N/mm^2
Mean yield strength of shear reinforcing (f_{ywm})	280	560	N/mm^2
Stress in concrete in longitudinal direction at centre of gravity (σ_{cp})	-10.7	-2.4	N/mm^2
Ratio stress in concrete in longitudinal direction at centre of gravity and mean value of concrete cylinder compressive strength (σ_{cp} / f_{cm})	-0.20	-0.04	-
Maximum aggregate size (d_{max})	31.5		mm

The distribution of shear transfer mechanism along the cracks and through the flanges is further analysed using a nonlinear sectional analysis programme for girders based on the MCFT. It is investigated whether the resistance at mid-depth is representative for the resistance along the crack. Moreover, it is investigated what parameters are decisive for the contribution of the uncracked concrete to the total shear resistance. A sensitivity analysis is carried out to determine the effect of the cross sectional properties on the shear resistance contribution of the uncracked concrete. The results are used to derive a model for the shear resistance of a prestressed girder.

Design equations for practice are determined for both models (first and second topic), based on the statistical properties of the test-to-predicted shear resistance ratio. These design values are determined using the approach described in Annex D7.3 of NEN (2011).

The proposed models for both the first and the second topic are intended to determine shear resistance for prestressed bridges, consisting of a web and flanges, for the regions

without flexural cracks. The models are derived considering explicitly the ranges of the main parameters that are representative for the bridges in the Dutch Highway network. In Table 1.1 the ranges of parameters are listed that are assumed to significantly affect the resistance of one or both proposed models. The table is based on data inventories of 9 pre-tensioned precast girders, 22 post-tensioned bulb-T girders and 19 box girder bridges. All these bridges are designed with a design code prior to the design code of 1974 (NEN 1974) and contain girders with a web and flanges. If all bridges would have been inventoried, it is likely a wider range of parameters would have been found. Nevertheless, the table can be used as an indication of the range of parameters for which the models are intended. The derived models are intended for both pre-tensioned and post-tensioned girders, girders with straight or curved tendon profiles and both simply supported and continuously supported girders. The models are derived for normal weight concrete.

1.6 Outline of the dissertation

The research is divided in two parts (Figure 1.5). The first part of the dissertation concerns shear resistance of prestressed girders to diagonal tension cracking regardless of whether stirrups are present (Chapters 2–4). The second part of the dissertation concerns shear resistance of prestressed girders with stirrups after diagonal tension cracking (Chapters 5–8).

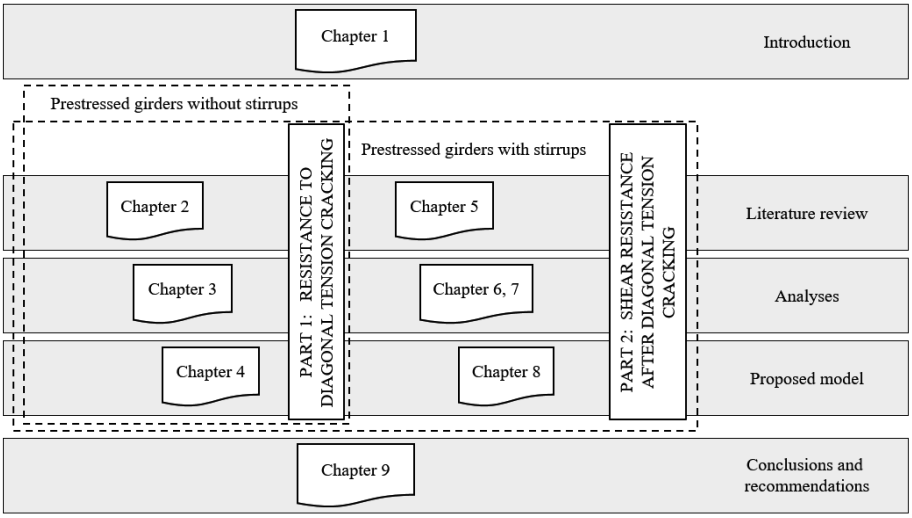

Figure 1.5. Overview of chapters

It is possible that the resistance to diagonal tension cracking is higher than the resistance after diagonal tension cracking. Therefore, the resistance to diagonal tension cracking

can also be governing for the shear resistance of prestressed girders with a low shear reinforcement ratio, the box around the prestressed girders with stirrups is also drawn around chapters 2 to 4. Figure 1.5 further shows which of the chapters concern the literature review, the analyses and the proposed models.

Chapter 2 summarizes relevant literature regarding the determination of the resistance to diagonal tension cracking. Also, an overview of experiments available from literature is provided. These experiments are eventually used for the validation of the proposed model. Chapter 3 investigates how the tensile strength of the web is affected by the principal compressive stresses (bi-axial behaviour) and by the size of the region subjected to high principal tensile stresses (statistical size effect). Moreover, this chapter investigates how the maximum principal tensile stress around the concentrated loads (disturbed areas) can be approximated using the Euler-Bernoulli girder theory and how the distribution of the principal tensile stresses in the region without flexural cracks is affected by the presence of flexural cracks on the edge of this region. Chapter 4 describes the proposed analytical models for diagonal tension cracking (Table 1.2). These concern model A1, for girders that remain free of flexural cracks (Section 4.1) and model A2, for girders in which, beside the regions without flexural cracks, also regions with flexural cracks are present (Section 4.2). For both models also the design value is derived for a target reliability. As these design values are approximately the same for both models, it is proposed to use just one model for engineering practice, referred to as model A, regardless of whether flexural cracks are present (Section 4.3, shown bold in Table 1.2).

Table 1.2 Overview of newly proposed analytical models

			Section	Main equation(s)
Resistance to diagonal tension cracking	Model A1: Proposed model for girders without flexural cracks	Mean value	4.1	4.1 to 4.4
	Model A2: Proposed model for girders with flexural cracks	Mean value	4.2	4.2 to 4.5
	Model A: Proposed model (regardless of whether flexural cracks are present)	**Design value**	**4.3**	**4.9 or 4.10**
Resistance after diagonal tension cracking (for girders with stirrups)	**Model B1: Proposed model**	Mean value	8.3	8.6 to 8.8
		Design value	**8.5**	**8.18 to 8.20**
	Model B2: Alternative model, variable angle truss model modified for regions without flexural cracks	Mean value	8.6	8.21 to 8.24
		Design value	8.6	8.25

Chapter 5 summarizes relevant literature regarding the shear resistance of prestressed girders with stirrups in regions without flexural cracks. Also, an overview of available experiments from literature of girders with stirrups that failed in shear is provided. These experiments are eventually used for the validation of the proposed model. Chapter 6

derives equations for the shear resistance at the mid-depth of the web for regions without flexural cracks. These equations are based on calculations of the resistances of membrane elements for a strain condition associated with regions without flexural cracks. Chapter 7 investigates the distribution of aggregate interlock and stirrup stresses along the diagonal tension crack. It investigates whether the resistance at mid-depth is representative for the resistance along the crack. Also, the contribution of the uncracked concrete to the total shear resistance is investigated. Chapter 8 describes the proposed analytical model for shear resistance of girders with stirrups in regions without flexural cracks, referred to as 'model B1' (Table 1.2). Also, the application conditions are described and the minimum and maximum shear resistances. Moreover, the accuracy of model B1 is evaluated, using test data from the database on shear failure for girders with stirrups. Furthermore, a design equation for practice is determined for model B1 for a target reliability (shown bold in Table 1.2). At the end of this chapter a model is derived that could be used as an alternative for the proposed model. In this model the shear resistance is totally ascribed to the stirrups. Although this way of formulating does not correspond to physical behaviour, the formulation is nevertheless attractive because it is also applied in the variable angle truss model which is currently used in structural assessments. This alternative model is referred to as 'variable angle truss model modified for regions without flexural cracks'' or simply 'model B2' (Table 1.2).

Chapter 9 summarizes the results of this dissertation, gives recommendations regarding the use of the models in practice and for future research.

PART 1: RESISTANCE TO DIAGONAL TENSION CRACKING

2

Literature review on diagonal tension cracking

This chapter describes a literature review on diagonal tension cracking. Section 2.1 summarizes relevant literature regarding the determination of the resistance to diagonal tension cracking. Section 2.2 provides an overview of available experiments in literature with diagonal tension cracks. Section 2.3 summarizes the literature findings and describes the approach that will be used to eventually propose a model.

2.1 Resistance to diagonal tension cracking

Section 2.1.1 gives a definition for diagonal tension cracking and explains why diagonal tension crack is considered as measure for the ultimate capacity of girders without stirrups. Moreover, an overview of the models that will be further considered in this chapter is given. Section 2.1.2 explains how the principal tensile stresses can be determined and describes conditions and phenomena that could affect the accuracy of the calculated principal tensile stresses. Section 2.1.3 explains, with an example, how the principal tensile stress are distributed in a girder and where in the girder the maximum principal tensile stresses can be expected. Section 2.1.4 describes the material tests that can be used to derive the tensile strength of concrete and explains some phenomena which affect the tensile strength. Section 2.1.5 summarizes the models from literature.

In this chapter, the findings from the literature review are frequently complemented with considerations. These consideration are aimed to contribute to the development of an accurate model for the predictions of diagonal tension cracking.

2.1.1 Diagonal tension cracking

Based on observations from experiments, Hanson categorized two different types of diagonal cracks (Hanson 1964, see Figure 2.1): diagonal tension cracks and flexural shear cracks. Diagonal tension cracks were defined as diagonal cracks that start from a point in the web. Flexural cracks that develop into inclined cracks were categorized as flexural shear cracks. Flexural cracks can cause an increase of the principal tensile stresses in the web above the flexural crack and therefore trigger the formation of inclined cracks in the web (Figure 2.1). Hanson (1964) also categorized diagonal cracks triggered by flexural cracks as flexural shear cracks.

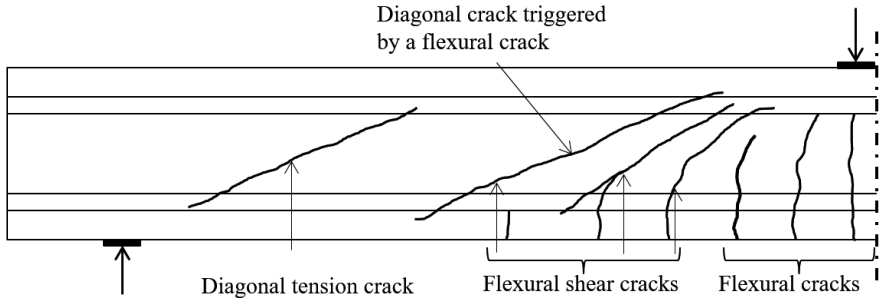

Figure 2.1. Type of cracking according to Hanson (Hanson 1964).

Like Hanson, MacGregor et al. (1960) distinguished two types of cracks: web shear cracks, which is a synonym for diagonal tension cracks, and flexural shear cracks. Web shear cracks were defined as cracks that occur in the web before flexural cracks appear in its vicinity. Flexural shear cracks were defined as inclined cracks that extend from an initiating flexural crack. Also MacGregor et al. (1960) defined inclined cracks, that forms over or beside an initiating flexural crack, as a flexural shear crack.

In this dissertation diagonal tension cracks are defined as diagonal cracks that start in the web in the region without flexural cracks. In contrast to the given definitions in literature, this definition includes the diagonal cracks that are triggered by a flexural crack (figure 2.1). The definition is adapted because the purpose of the eventually proposed model is the determination of the resistance to diagonal tension cracking in the regions without flexural cracks, regardless of what triggered diagonal tension cracking.

Jena et al. (1972) report that especially girders with a large shear span fail instantly after the formation of the first diagonal tension crack. As part of this dissertation, it is investigated whether this dependency indeed exists. Therefore, experimental data of thirty five experiments on prestressed girders without stirrups is used. This concerns experiments carried out by Sozen et al. (1967), Arthur (1965), Elzanaty et al. (1986) and Choulli (2005). In Figure 2.2 the ratio of the experimentally obtained ultimate resistance $V'_{R,exp}$ and the experimentally obtained resistance to diagonal tension cracking $V'_{R,c,exp}$ is shown. The apostrophes indicate that the resistances relate to the region without flexural cracks. About half (seventeen) of the prestressed girders failed instantly at diagonal tension cracking, shown by a $V'_{R,exp} / V'_{R,c,exp}$ of unity. The other half of the girders could resist additional load after diagonal tension cracking. The data points do not show a strong dependency between a/d and whether failure occurred instantly at diagonal tension cracking. The statement of Jena et al. (1972) could therefore not be confirmed. Figure 2.2 also shows the depth of the girders. The figure demonstrates that there is also no clear relation between the depth of the girders and whether failure occurred instantly at diagonal tension cracking. In literature, general agreement exists on considering the

occurrence of the first diagonal tension crack as measure for the ultimate capacity for girders without shear reinforcement. This is because it is difficult to predict the behaviour after diagonal tension cracking (Walraven 1987).

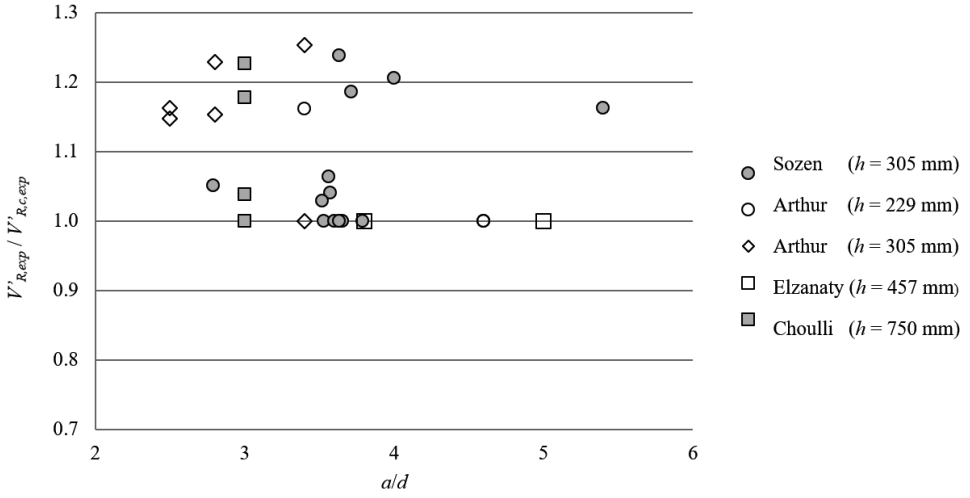

Figure 2.2. Experimentally found ultimate resistance / resistance to diagonal tension cracking

From literature some observations are described regarding diagonal tension cracking. Arthur (1965) reported three types of failure for girders without stirrups initiated by diagonal tension cracking: (i) failure due to a single crack that develops from the support to the load point (ii) failure due to the formation of a series of multiple diagonal tension cracks (web distortion) and (iii) failure due to the formation of a series of multiple diagonal tension cracks (web distortion) followed by crushing of the compression flange under the load point. Another observation is that diagonal tension cracks develop instantly over a large part of the web depth or the complete web depth (Hanson 1964, Choulli et al. 2008, Elzanaty et al. 1986). Furthermore, several investigators (Hanson 1964, Leonhardt et al. 1973, Sozen et al. 1959) observed that diagonal tension cracking can occur after a period of sustained load.

Models that can be used to determine the resistance to diagonal tension cracking can be found in design codes. In this chapter, three models are considered:

1. the Eurocode 2 (NEN 2005), in this chapter referred to as the 'Eurocode model'
2. the Model Code 2010 (*fib* 2012), in this chapter referred to as the 'MC2010 LoA1 model'
3. the ACI (ACI 2008), in this chapter referred to as the 'ACI model'

The Model Code 2010 contains two levels of approximations (LoA). Level 1 indicates that the model is more conservative but easier to use than level 2 (Muttoni et al. 2013).

The model considered in this chapter concerns the level 1 approximation. The model described as level 2 approximation corresponds to the Eurocode model and will not be further explained.

All models are based on the same leading assumption that diagonal tension cracking occurs when the maximum principal tensile stress σ_{1max} in the web equals the concrete tensile strength of the web. The models differ in the simplifications used to determine σ_{1max}. The Eurocode model bases σ_{1max} on σ_1 throughout web whereas the MC2010 LoA1 model and the ACI model only consider σ_1 along the centroidal axis. The models also differ in the tensile strength of the web that is used.

The Eurocode model uses the uniaxial tensile strength f_{ctm} as limit for the tensile strength of the web. Also the MC2010 LoA1 uses f_{ctm} but reduces the shear stress resistance with 20% to compensate that the principal tensile stresses are only considered along the centroidal axis. The ACI model, on the other hand, uses the cracking strength of concrete f_{cr}, which is defined as $0.332\sqrt{f'_c}$, in which f'_c is the specified compressive strength of concrete according to the ACI. It is however already noticed that f_{cr} is significantly lower than f_{ctm}. For values of f_{cm} between 35 and 105 N/mm^2, f_{cr} varies between 57% and 64% of f_{ctm}. It is found in literature (Elzanaty et al. 1986) that f_{cr} is a conservatively chosen value of the splitting strength of concrete $f_{ctm,sp}$. Just like the MC2010 LoA1 model, the value is chosen conservatively to compensate for the fact that σ_{1max} is underestimated because it is based on σ_1 along the centroidal axis. Moreover, a low value is chosen because the tensile strength is expected to decrease due to shrinkage. Based on back calculations of experiments in which diagonal tension cracking occurred (Hanson 1964), it is confirmed that the chosen value is conservative. From these back calculations, it was found that the average principal tensile stress in the centre of gravity at diagonal cracking was $0.457\sqrt{f_{cm}}$, which is higher than the cracking strength of concrete according to the ACI. In this research, the tensile strength that can be used to predict diagonal tension cracking of the web of a prestressed girder is generally defined as $f_{ctm,web}$, which will be discussed further in Section 2.1.5 and Chapter 3.

2.1.2 Methods to determine the principal tensile stress

This section explains how the principal tensile stresses can be determined analytically. The method described in this section is used in the considered models. Cracks occur perpendicular to the principal tensile stress (Figure 2.3) when σ_1 equals the tensile strength of concrete. Therefore, the distribution of the principal tensile stresses is of importance for the prediction of the resistance to diagonal tension cracking in a prestressed girder.

Starting from the geometry and loading conditions (Figure 2.3), the principal tensile stress in a cross-section (location x) and a point over the depth (z), under an applied load F, can be determined in three steps:

1. Determine the cross-sectional forces (M_E, V_E and N_E) for the considered cross-section.
2. Determine the shear stress (τ) and the normal stress in the longitudinal direction (σ_x). These stresses are determined at a certain depth z in the cross-section and are based on the sectional forces.
3. Determine the principal tensile stress σ_1 for the considered point (x, z). This stress is determined from τ and σ_x.

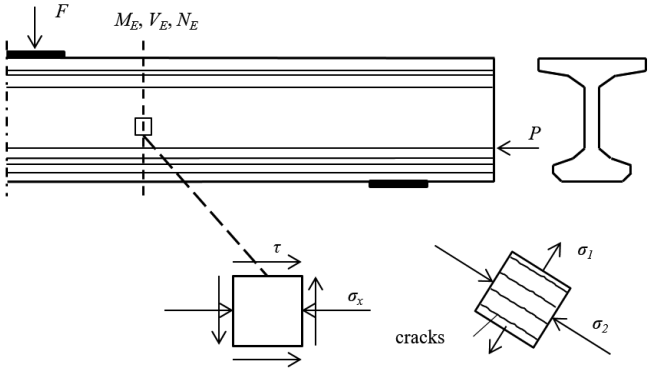

Figure 2.3. General method to determine principal tensile stresses in a prestressed girder.

For monolithic girders, τ and σ_x can be determined using Equations (2.1) and (2.2).

$$\tau\,(z) = \frac{V_E S_c(z)}{b_w(z)\, I_c} \tag{2.1}$$

$$\sigma_x(z) = \frac{N_E}{A_c} + \frac{M_E\, z}{I_c} \tag{2.2}$$

In these equations, I_c is the second moment of area, S_c is the first moment of area, b_w is the width of the web and z is the considered vertical distance to the centroidal axis. The subscript c indicate that the cross-sectional properties are only based on the concrete.

Also the stiffness of the reinforcing and prestressing steel affect the principal stress distribution. The presence of steel could be considered by using the transformed cross-sectional properties instead. However, this effect is neglected for all of the three considered models. The parameter z indicates that the associated parameter varies, or could vary, over the depth of the cross-section.

The Equations 2.1 and 2.2 are based on the assumption that the concrete is uncracked and that linear elastic stress strain relations are applicable. The equations are therefore intended to be used for the areas of a prestressed girder without flexural cracks. The distribution of the principal tensile stresses in the regions without flexural cracks could be affected by flexural cracks at the edge of this region. Because Equations 2.1 and 2.2 are used in the models, this potential disturbance of the principal stress distribution is ignored. According to Leonhardt (1973), the maximum principal tensile stress in the regions without flexural cracks increase due to flexural cracks in the region with flexural cracks. This could be compensated by assuming a lower tensile strength of the web. The tensile strength also reduces due to the presence of lateral principal compressive stresses and due to the presence of residual stresses are accounted. Therefore, it is suggested to use a tensile strength of the web of $0.3f_{c,cu,200}{}^{2/3}$. In this equation $f_{c,cu,200}$ is the concrete compressive strength determined by a cube with a rib length of 200 mm. If values of f_{cm} are considered between 35 and 105 N/mm^2, this equation corresponds to a suggested tensile strength of the web between 58% and 67% of f_{ctm}.

Equation 2.2 is based on the Euler Bernoulli assumption (plain cross-sections remain plain). This is however questionable for a cross-section close to the support or close to the loading plate (non-Bernoulli areas or disturbed areas). This is of importance because the maximum principal tensile stress is typically found around these concentrated loads (see Section 2.1.3 in which an example is given).

The maximum and minimum principal stresses (respectively σ_1 and σ_2) can be found from the stresses in longitudinal and vertical direction (respectively σ_x and σ_z) by Equation 2.3. In this equation, tensile is defined as positive and compression as negative which is a common rule in structural mechanics. This is in contrast to the three codes cited, in which compression is defined as positive. Therefore, the appearance of the equations in this dissertation differs from the code provisions.

$$\sigma_{1,2} = \frac{\sigma_x + \sigma_z}{2} \pm \sqrt{\left(\frac{\sigma_x - \sigma_z}{2}\right)^2 + \tau^2} \tag{2.3}$$

If the vertical stress σ_z is neglected, σ_x is replaced by $\sigma_x(z)$ and τ is replaced by $\tau(z)$, in which z indicates that the stresses are considered for a certain depth in a considered cross-section, Equation 2.4 can be found from Equation 2.3.

$$\sigma_1(z) = \frac{\sigma_x(z)}{2} + \sqrt{\left(\frac{\sigma_x(z)}{2}\right)^2 + \tau(z)^2} \tag{2.4}$$

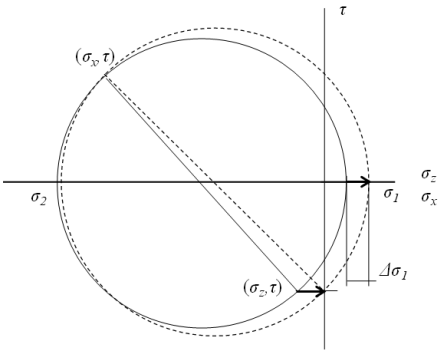

Figure 2.4. Effect of ignoring σ_z on determining σ_1.

Around concentrated forces, like in the support area, σ_z is negative (compression). For a negative value of σ_z, it is a conservative assumption to neglect σ_z. This is illustrated in Figure 2.4 in which σ_x is assumed negative. If σ_z is not neglected, Mohr's circle runs through the points (σ_x, τ) and (σ_z, τ). This circle is shown as a continuous line. Mohr's circle associated with neglecting σ_z runs through the points (σ_x, τ) and $(0, \tau)$. This circle is shown as a dashed line. By neglecting σ_z, the centre of Mohr's circle shifts to the right. Moreover, the diameter of the circle increases. This leads to an increase of σ_1 ($\Delta\sigma_1$ in Figure 2.4). If σ_1 is overestimated, the resistance to diagonal cracking is underestimated, which is conservative. For positive values of σ_x, the increase of σ_1 is less significant. This is because, despite the centre of Mohr's circle still shifts to the right, the radius of the circle decreases.

The extent to which σ_1 is overestimated by neglecting σ_z depends on mutual ratios of the stresses. This is illustrated in Figure 2.5 for different values of the stresses. Equation 2.4, in which σ_z is neglected, is divided by Equation 2.3, in which σ_z is accounted for. The figure shows that the effect of neglecting σ_z becomes more significant for high values of σ_z and low values of τ and σ_x.

If Equation 2.4 is used, the maximum principal tensile stress is located in a cross section at the intersection of the web and a flange exactly next to the concentrated external load or the support reaction. This is because the bending moment has a maximum value at these cross sections. However, the vertical stresses (σ_z) that reduce the maximum principal stresses are neglected in Equation 2.4. Using Equation 2.3 instead would reduce the maximum principal tensile stresses. Therefore, according to the Eurocode model and MC2010 LoA1 model, the principal tensile stresses do not have to be considered for cross-sections that are closer to the support than the point which is the intersection of an axis through the centre of gravity and a 45° inclined line from the inner edge of the support (Figure 2.6). Also according to the ACI model cross-sections directly next to the support do not have to be considered. For prestressed members, a critical section at a

distance $h/2$ from the support is prescribed in ACI (2008) The equations used in the ACI will be explained in Section 2.5.

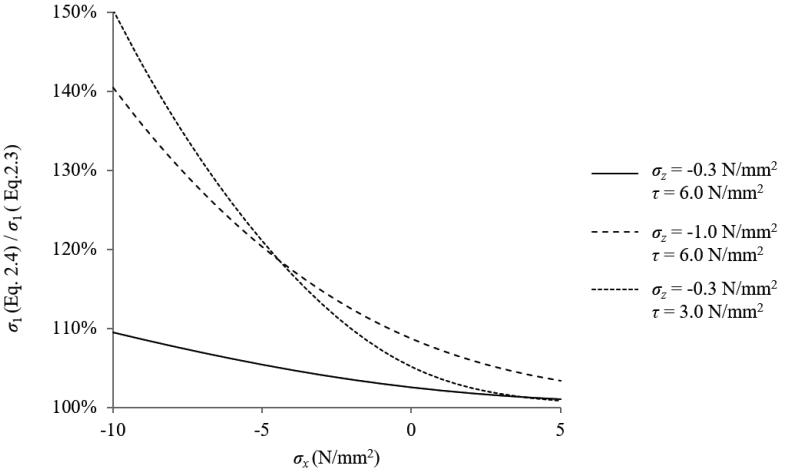

Figure 2.5. Overestimation of σ_1 by ignoring σ_z as function of σ_z, σ_x and τ

In girders with post-tensioned ducts there is a risk that the ducts are not fully grouted. If a duct is not fully grouted, b_w is reduced and consequentially τ and σ_1 increase (Equations 2.1 and 2.4). Therefore, according to the Eurocode, if grouted ducts are applied, the web width should be reduced with 50% of the outer diameter of the duct Φ if $\Phi > b_w/8$ (NEN 2005). For non-grouted ducts, which are outside the scope of the current research, the prescribed reduction is 1.2Φ.

The presence of smooth cable ducts reduces the capability of cross-sections to transfer principal tensile stresses. This was given as explanation for the overestimation of the predicted resistance to diagonal tension cracking by Herbrand et al. (2015). This overestimation was found for experiments carried out on continuous prestressed girders with smooth ducts (Herbrand et al. 2013, Herbrand et al. 2017).

For pre-tensioned prestressing steel, the principal stress distribution is affected by the transfer of the prestress by bond along the transmission length. The longitudinal stress σ_x caused by the prestressing steel should be reduced depending on the distance of the considered cross-section from the starting point of the transmission length (according to the Eurocode model and MC2010 LoA1 model). Also the shear stress τ caused by the prestressing steel should be reduced depending on the this distance, when kinked prestressing strands are applied. Equations for this type of pre-tensioned prestressing steel can be found in *fib* (2012), numbered as 7.3.46 and 7.4.47.

2.1.3 Distribution of principal tensile stresses in a prestressed girder

A main difference between the three considered models (as pointed out in Section 2.1.1) is the area considered to determine the maximum value of σ_1. According to the Eurocode model all possible locations of the web need to be examined to determine the maximum value of σ_1. The MC2010 LoA1 model and the ACI model limit this examination to the centroidal axis. In this section an example of the principal tensile stress distribution in a prestressed girder is given. With this example, insight is given of the impact of limiting the area examined to determine the maximum value of σ_1.

Experiment HAP1W, reported by Choulli (2005), is chosen as an example. This concerns a simply supported I-shaped girder with pre-tensioned horizontal prestressing steel. At a certain load (F) diagonal tension cracks were observed in the experiment. This is called the load that causes diagonal tension cracking. At this load that causes diagonal tension cracking, no flexural cracks were observed in the experiment.

The distribution of the principal tensile stresses at the load that causes diagonal tension cracking is illustrated in Figure 2.6. The principal tensile stress is calculated for points on the intersection of the centroidal axis and 4 axes parallel to the centroidal axis and three cross-sections. The stresses are determined using the three steps described in Section 2.1.2. Cross-section A is located at the point which is the intersection of the centroidal axis and a line inclined from the inner edge of the loading plate at an angle of 45°. Cross-section B is at the location of zero moment. Cross-sections C is located at the point which is the intersection of the centroidal axis and a line inclined from the inner edge of the support at an angle of 45°.

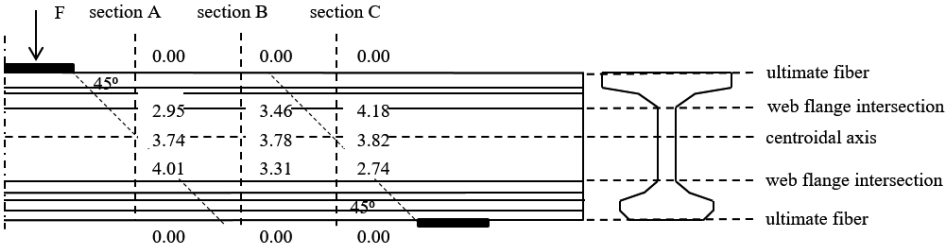

Figure 2.6. Principal tensile stresses (N/mm^2) at diagonal tension cracking load for HAP1W.

The highest principal tensile stresses are found in the web. This is because of the smaller width of the web (b_w) which leads to high shear stresses an therefore high principal tensile stresses (Equations 2.1 and 2.4). In the considered cross-sections, the ultimate fibres in the top and bottom flange remain under compression. As $\tau = 0$ in the ultimate fibres of the considered cross-sections, the resulting principal tensile stress σ_1 is equal to zero (Equation 2.4), as shown in Figure 2.6.

In cross-section A the absolute value of the positive moment due to the load F is larger than the absolute value of the negative moment due to the prestressing. As a result of the positive moment, the lowest σ_x in the web is found on the intersection of the web and the bottom flange (σ_x = -6.37 N/mm^2). This is lower than σ_x in the centre of gravity (σ_x = -9.56 N/mm^2). Although τ is lower at the intersection of the web and the bottom flange (τ = 6.55 N/mm^2) than in the centre of gravity (τ = 7.12 N/mm^2), the effect of the lower σ_x on σ_1 is more significant. This results in a higher σ_1 at the intersection of the web and the bottom flange (σ_1 = 4.10 N/mm^2) than at the centre of gravity (σ_1 = 3.80 N/mm^2).

Cross-section B is at the location of zero moment as result from a combined effect of the external load and the prestressing. As σ_x is constant over the depth, the variation of τ is decisive for the highest principal tensile stress. The maximum value of σ_1 is located in the centre of gravity because the maximum value of τ is located in the centre of gravity.

In cross-section C the absolute value of the negative moment due to the prestressing is larger than the absolute value of the positive moment due to the load F. The resulting negative moment, leads to the observation that the lowest σ_x in the web is found at the intersection of the web and the top flange. This is lower than σ_x in the centre of gravity. Although τ is lower, the effect of the lower σ_x on σ_1 is more significant, resulting in a maximum σ_1 at the intersection of the web and the top flange in cross-section C. In this example, the highest principal stress is found at the intersection of the top flange and the web and is about 9% higher than the highest principal stresses along the centroidal axis.

2.1.4 Methods to determine the tensile strength of concrete

As described at the end of Section 2.1.1, the considered models assume diagonal tension cracking for different tensile strengths of the web: the Eurocode model uses the uniaxial tensile strength f_{ctm} and the ACI model uses the cracking strength of concrete f_{cr}. Equation are available to derive both f_{ctm} and f_{cr} from the concrete cylinder compressive strength (these will be explained later). Reineck et al. (2012) found that the uniaxial tensile strength can be accurately derived from the cylinder compressive strength. This was shown by comparing the uniaxial tensile strength derived from cylinder compressive test and the uniaxial tensile strength derived from splitting test for numerous experiments for which both material test were carried out. The main reasons that f_{ctm} and f_{cr} differ, is that they are based on different types of tests. In this section, three types of tests are explained that reveal various phenomena that will affect the tensile strength of the web that should be assumed in girders (figure 2.7).

Uniaxial tensile tests

Uniaxial tests are performed on prismatic specimen with notches, uniaxial loaded in tension (Hordijk 1991, Figure 2.7). The concept of the test is that the stress distribution at the crack location is undisturbed by the loading conditions. Therefore, these uniaxial tests are considered as 'pure tension test'. It is difficult to perform uniaxial tensile tests. The uniaxial tensile tests appear to be sensitive to the way the tests are carried out. Therefore, uniaxial tensile test are typically performed for research purpose. In engineering practice, the uniaxial tensile strength is determined from concrete cylinder compressive tests. For this purpose, empirical relations have been derived from batches of both uniaxial tension tests and cylinder compressive test. Both the Eurocode (NEN 2005) and the Model Code 2010 (*fib 2012*) use the same empirical relations between the cylinder compressive strength and the uniaxial tensile strength. These expressions are given in Equation 2.5, for strength classes of concrete equal to or smaller than C50/60, and Equation 2.6, for strength classes of concrete larger than C50/60. These equations are applicable for normal weight concrete.

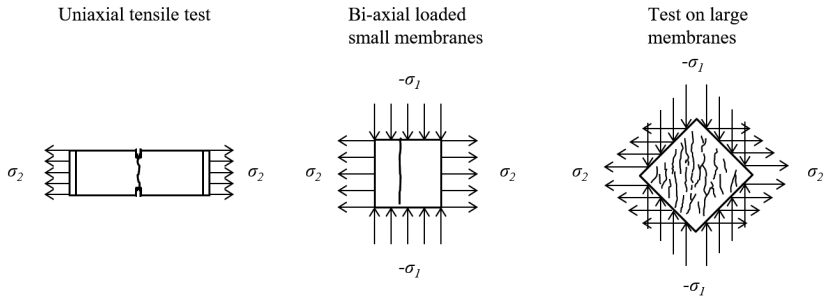

Figure 2.7. Uniaxial tensile test (Hordijk 1991), bi-axial test on small membranes (Kupfer 1969) and test on large reinforced membrane elements (Vecchio et al. 1994)

$$f_{ctm} = 0.30 {f_{ck}}^{2/3} \tag{2.5}$$

$$f_{ctm} = 2.12 \ln(1 + f_{cm}/10) \tag{2.6}$$

Also splitting tensile tests (on cylinders) and flexural tension tests (or modulus of rupture tests) can be used to indirectly determine the uniaxial tensile strength of concrete. The tensile strength from these material tests deviates from the uniaxial tensile strength because the stress distribution is affected by the loading conditions. Also for splitting tensile tests and flexural tension tests, the uniaxial tensile strength can be determined by empirical relations between both tensile strengths. The Eurocode (NEN 2005) prescribed for instance the equation $f_{ctm} = 0.9 f_{ctm,sp}$ to derive the uniaxial tensile strength from the splitting strength. According to Reineck et al. (2012) splitting tests are preferred

for the determination of the uniaxial tensile strength, above flexural tensile tests. However, no general agreement exists in literature about the empirical relations between the splitting tensile strength and the uniaxial tensile strength (*fib* 2012).

Tests on bi-axially loaded small membrane elements

From tests on these elements it is found that lateral principal compressive stresses reduce the tensile strength of concrete. This phenomenon is called bi-axial behaviour. Bi-axial behaviour is investigated by Kupfer who developed a test setup to investigate small membrane elements loaded by tension stresses and perpendicular to it compression stresses (200 by 200 by 50 mm^3, Figure 2.7). The compressive load was applied with brush bearing plates that were flexible enough to follow the concrete deformations without generating appreciable force into the membrane element (Kupfer et al. 1969, Kupfer 1973). Huber (2016) collected the experiments of bi-axial loaded small membrane elements of various researchers (Kupfer et al. 1969, Hussein 1998, Hampel 2006). The results are shown in Figure 2.8. This figure shows the combination of σ_2/f_{cm} and σ_1/f_{ctm} at which the membranes cracked. The tensile strength, as ratio of the uniaxial tensile strength, was found to decrease with decreasing principal compressive stresses (as ratio of the compressive strength). From the figure it also appears that this reduction is larger for higher strength classes of concrete.

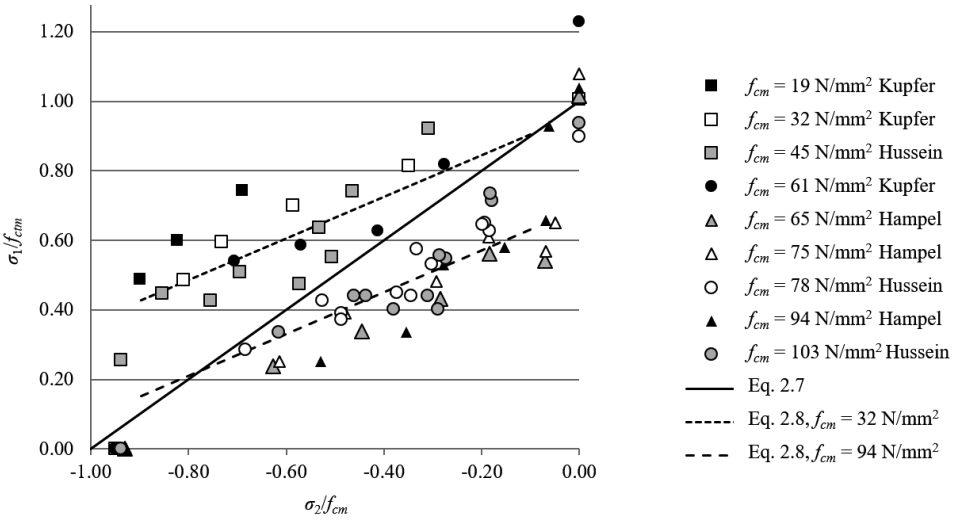

Figure 2.8. Experimentally found and predicted combination of σ_2 / f_{cm} and σ_1 / f_{ctm} that causes cracking

The Mohr-Coulomb linear approximation, which is given by Equation 2.7, is included in Figure 2.8. The subscript '*eff*' is used to indicate that the tensile strength of concrete is depending on the lateral principal compressive stress, as introduced by Huber (2016). According to this equation, the tensile strength is zero when $\sigma_2 = -f_{cm}$. The tensile

strength linear increases to the uniaxial concrete tensile strength when $\sigma_2 = 0$. Note that, according to figure 2.8, the Mohr-Coulomb equation leads to an overestimation of the tensile strength for concrete with higher compressive strengths. This is especially the case for high values of σ_2 / f_{cm} (i.e. less negative). It is further noted that these high values of the compressive stress are typical for diagonal tension cracking of the web of pre-stressed girders (Jena et al. 1972).

$$f_{ctm,eff} = \left[1.0 + \frac{\sigma_2}{f_{cm}}\right] f_{ctm} \tag{2.7}$$

Based on the data collected (Figure 2.8), Huber (2016) derived an empirical equation to determine the effective tensile strength of concrete. Both the effect of the compressive stresses and the effect of the concrete compressive strength on the tensile strength are taken into account, (Equation 2.8). Huber suggest to limit the application of the equation to $-0.9 \leq \sigma_2 / f_{cm} \leq -0.1$ as the equation only reflects the experimental data in this range. In Figure 2.8 the predictions according to this equation are included, both for a low concrete compressive strength (f_{cm} = 32 N/mm^2) and for a high concrete compressive strength (f_{cm} = 94 N/mm^2). Note that, according to Figure 2.8, values of $f_{ctm,eff}$ close to f_{ctm} are found only when $\sigma_2 = 0$ and the reduction of f_{ctm} appears to become significant, even when σ_2 / f_{cm} is just below zero.

$$f_{ctm,eff} = \left[1.6 - 0.2\, f_{cm}{}^{1/3} - 0.6\, \frac{\sigma_2}{f_{cm}}\right] f_{ctm} \tag{2.8}$$

The Eurocode model assumes diagonal tension cracking when the maximum principal tensile stress is equal to the uniaxial tension strength of concrete. Based on the result of the membrane elements, it is expected that the resistance to diagonal tension cracking is overestimated using this code, because the effect of the bi-axial behaviour is not considered.

Tests on large membrane elements

The tensile strength can also be derived from tests on large reinforced membrane elements (Figure 2.7). An example of a series of test on membranes is the research programme carried out by Vecchio et al. (1994). The membrane elements are loaded with loading keys, which are cast into the experiment. Membrane elements were tested with dimensions of 890 mm by 890 mm by 70 mm. The membranes were tested with various combinations of in-plane shear and bi-axial stresses (both tensile and compressive stresses). Figure 2.9 shows the principal tensile stresses at cracking (f_{cr}, cracking strength) versus the cylinder compressive strength of concrete. This principal tensile stress can simply be determined from the reported shear stress and the horizontal and the vertical stresses at which cracking occurred, using Equation 2.3.

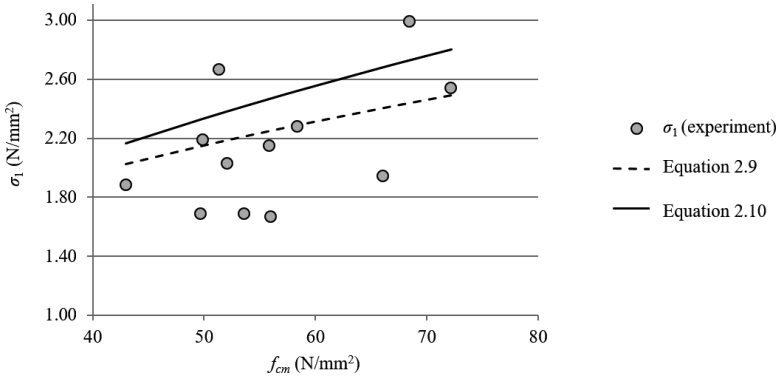

Figure 2.9. Principal tensile stress at cracking for membranes tested by Vecchio et al. (1994)

Bentz (2000) derived an empirical relation between the cracking strength and the cylinder compressive strength (Equation 2.9) using test results of 83 large membrane elements, which were tested in Toronto and Houston. These include tests of Vecchio et al. (1994) which are shown in Figure 2.9. Figure 2.9 also shows the predicted cracking strength predicted by Equation 2.9.

$$f_{cr} = 0.45\, {f_{cm}}^{0.4}\ (N/mm^2) \tag{2.9}$$

$$f_{cr} = 0.332\, \sqrt{f_{cm}}\ (N/mm^2) \tag{2.10}$$

In Equation 2.10 corresponds to the relation between as used in the ACI code (ACI 2008) only f_{cm} is used instead of f'_c. Figure 2.9 also shows the cracking strength predicted by Equation 2.10. The tensile strength based on this equation was found to overestimate the experimentally found tensile strength (Bentz 2000). This is confirmed by Figure 2.9. Equation 2.9 corresponds better with the experimentally found strength than Equation 2.10, especially for higher strength concrete.

The tensile strength according to Equation 2.9 is significantly lower than the uniaxial tensile strength (Equations 2.5 and 2.6). This can be explained by the size of the membrane elements. For large membranes the chance of encountering the weakest and controlling piece of concrete is larger than for small membranes (Bentz 2000). According to Collins et al. (1997) the tensile strength is about inversely proportional to the fourth root of the size. In this dissertation this is defined as the statistical size effect. Another consideration could be that the tensile strength is reduced due to bi-axial behaviour. As the membrane elements are bi-axial loaded it is plausible that the tensile strength is reduced by the lateral principal compressive stresses. However, the principal compressive stresses at the membrane tests are typically low which limits this effect of bi-axial behaviour.

It is noted that underestimation of the cracking strength for membrane elements, using Equation 2.10, is not per definition also present when determining the resistance to diagonal tension cracking of girders. This is because, as already described in Section 2.1.1, Equation 2.10 was found to result in conservative predictions of the resistance to diagonal tension cracking (Hanson 1964).

2.1.5 Models from literature

This section describes and compares the considered models. All models assume that the resistance to diagonal tension cracking can be found by determining the shear force at which the predicted maximum value of σ_1 equals $f_{ctm,web}$.

When the Eurocode model is used, the resistance to diagonal tension cracking, $V'_{R,c}$, can be calculated by carrying out the following steps:

1. Consider the first cross-section (at distance x) that should be considered (for instance cross-section A or C in Figure 2.6).
2. Consider a point on the cross-section (z). For instance the intersection of the web and the bottom flange (see for example Figure 2.6).
3. Assume a load (F) and calculate the sectional forces M_E, N_E and V_E in the cross-section.
4. Determine $\sigma_x(z)$ in the considered point (z) from the sectional forces (Equation 2.2).
5. Determine the shear stress that can be resisted ($\tau'_{R,c}(z)$) in the considered point (z) based on $\sigma_x(z)$ and f_{ctm} by using Equation 2.12 (which will be explained later). The apostrophe in $\tau'_{R,c}(z)$ indicated that the shear resistance concern the regions without flexural cracks and the subscript c indicates that the resistance is based on the concrete.
6. Determine the associated shear force $V'_{R,c}$ from $\tau'_{R,c}$ using the cross-sectional properties (Equation 2.1).
7. Adapt the load (F) until the shear force V_E equals the shear resistance $V'_{R,c}$. When both are equal σ_1 equals f_{ctm} and the shear resistance ($V'_{R,c}$) for the considered point is known.
8. Repeat the steps 1 to 7 for all points (z) in the cross-section.
9. Equal the resistance of the cross-section $V'_{R,c}$ with the lowest $V'_{R,c}(z)$ for all points (z) in the cross-section. The lowest resistance is normally found at the web-flange interfaces or at the centre of gravity (Section 2.1.3).

10. Repeat steps 1 to 9 for all cross-sections. The lowest resistance is normally found in cross-sections A (negative moment governing), B (shear force governing) or C (positive moment governing) as explained in Section 2.1.3.

11. The resistance to diagonal tension cracking ($V'_{R,c}$) of the girder is determined by the lowest of $V'_{R,c}$ off all the cross-sections.

As for using the Eurocode model a lot of iterative steps are necessary, the use of for instance a spread sheet is convenient.

Step 5 determines the shear stress that can be resisted in the considered point (z), $\tau'_{R,c}(z)$, based on $\sigma_x(z)$ and $f_{ctm,web}$. To determine $\tau'_{R,c}(z)$ Equation 2.4 is first rearranged in Equation 2.11. Equation 2.12 is found when $\tau(z)$ is equalized to $\tau'_{R,c}(z)$ and σ_1 is equalized to $f_{ctm,web}$.

$$\tau(z)^2 = {\sigma_1}^2 - \sigma_1 \sigma_x(z) \tag{2.11}$$

$$\tau'_{R,c}(z) = \sqrt{{f_{ctm,web}}^2 - f_{ctm,web}\, \sigma_x(z)} \tag{2.12}$$

An iterative calculation is not necessary when the ACI model or the MC2010 LoA1 model are used, because $\sigma_{1\max}$ is based on σ_1 along the centroidal axis. This is because σ_x is no longer dependant on the applied external load. When an external concentrated load is applied, the first cross-section from the support is governing (Section 2.1.2). This is because the self-weight causes a maximum shear force in this cross-section.

The equations that describe the three models are listed in Table 2.1. To make the models comparable, the vertical component of prestress force ($V_{R,p}$) is omitted in the equations according to the ACI (2008). This is because according to the Eurocode and Model Code 2010, $V_{R,p}$ is considered as reduction of the load instead of a component of the shear resistance (equivalent load method).

Basically, three differences between the models exists:

1. Whether σ_{1max} is only based on σ_1 along the centroidal axis or over the area considered throughout the web area (column σ_x in Table 2.1).
2. The tensile strength of the web used to determine $\tau'_{R,c}$ ($\tau'_{R,c}$ in Table 2.1).
3. The equation used to determine $V'_{R,c}$ from $\tau'_{R,c}$ and the cross-sectional properties (column $V'_{R,c}$ in Table 2.1).

The first difference between the models is the area in which σ_1 is considered to determine the maximum value of σ_1. According to the MC2010 LoA1 model and the ACI model, σ_1 is only considered along the centroidal axis. The stress in longitudinal direction at the centre of gravity σ_{cp} can be determined using Equation 2.16. According to the Eurocode

model, the depth of the cross is considered to determine σ_{1max}. Consequently σ_x should be determined at different depths (z) using Equation 2.13.

Table 2.1. Models to determine the resistance to diagonal tension cracking

Model	σ_x	$\tau'_{R,c}$	$V'_{R,c}$
Eurocode	$\sigma_x(z) = \frac{N_E}{A_c} + \frac{M_E z}{I_c}$ (2.13)	$\sqrt{{f_{ctm}}^2 - \sigma_x(z) f_{ctm}}$ (2.14)	$\frac{I_c\, b(z)}{S_c(z)}\, \tau'_{R,c}$ (2.15)
MC2010 LoA1	$\sigma_{cp} = \frac{N_E}{A_c}$ (2.16)	$0.8\sqrt{{f_{ctm}}^2 - \sigma_{cp} f_{ctm}}$ (2.17)	$\frac{I_c\, b_w}{S_{c,cg}}\, \tau'_{R,c}$ (2.18)
ACI		$0.291\sqrt{f'_c} + 0.3\,\sigma_{cp}$ (2.19)	$b_w\, d_p\, \tau'_{R,c}$ (2.20)

The second difference between the models is the assumed concrete tensile strength of the web at which diagonal cracking occurs. According to the Eurocode model, diagonal tension cracking is predicted assuming $f_{ctm,web} = f_{ctm.}$ With this assumption, Equation (2.14) is directly derived from Equation 2.12. The MC2010 LoA1 model is based on the same assumption. However, because σ_{1max} is not considered at the most unfavourable location, and is consequently underestimated, the resistance of the shear stress is reduced to 80% (Eq. 2.17). According to the ACI model, diagonal tension cracking is predicted assuming $f_{ctm,web} = 0.332\ \sqrt{f'_c}\ (= f_{cr})$ in which f'_c is the specified compressive strength of concrete according to the ACI (according to the ACI, $f'_c = 1.1 f_{cm} + 4.8$, in N/mm^2, for $f'_c \geq 34$ N/mm2). With this assumption, a similar equation could be expected as for the other models. However, it was found that this equation could be closely approached using Equation 2.19 (Xie 2009).

The third difference between the models is the equation used to relate the shear stress resistance $\tau'_{R,c}$ at the considered depth to the shear force resistance $V'_{R,c}$ of the cross-section. As according to the Eurocode model several points over the depth (z) are considered, the cross-sectional properties at the considered depth are used to determine the associates shear force (Equation 2.15). As according to the MC2010 LoA1 model only the centroidal axis is considered to determine σ_{1max}, the cross-sectional properties at the centre of gravity are used to determine the associated shear force (Equation 2.18). Equation 2.20, which is used in the ACI model, is a simplification of Equation 2.18. In this equation $b_w\, d_p$ has replaced $I_c\, b_w / S_{c,cg}$. The effect of this simplification is illustrated in Figure 2.10. In this figure, a cross-section with flanges with a depth of $h/5$ and a variable flange width (b+2Δb) is considered. It is assumed that $d_p = 0.9h$. On the vertical axis the

factor is shown necessary to determine the shear force, divided by bh, from the shear stress τ. The dashed line $V = \tau\ b\ 0.9h$ represents the simplified ACI equation. The solid line represents the exact factor as used in Equation 2.18. As shown in the Figure 2.10, the ACI equation overestimates the shear force resistance for a given shear stress resistance. Therefore, the simplification used in the ACI (2008) is unconservative. The overestimation has a maximum value for a rectangular cross-section ($\Delta b = 0$) and decreases for larger flange widths. As the ACI equation uses d_p instead of h, the overestimation also depends on d_p.

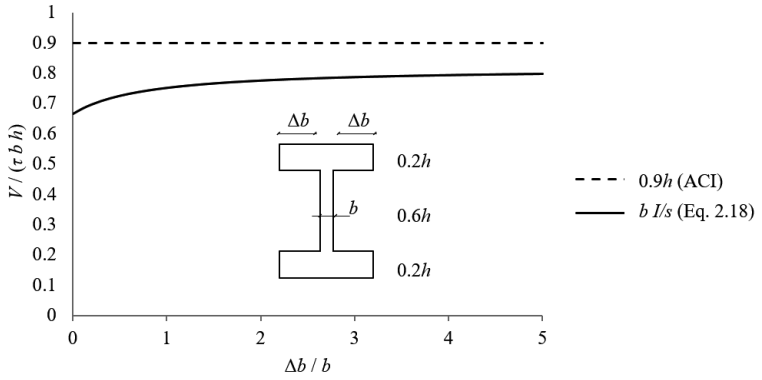

Figure 2.10. Factor to relate V and τbh, exactly and simplified as used in the ACI

The Eurocode model is only intended for prestressed single span members without shear reinforcement. Also the MC2010 LoA1 model is only applicable for hollow core slabs and similar structural members. The ACI (2008) is on the other hand intended for prestressed members both simply and continuously supported.

Beside the three considered models, also empirical models were derived by various researchers. Hicks (1958), Sethunarayanan (1960), Olesen et al. (1967) and Arthur (1965) suggested empirical relations to determine the resistance to diagonal tension cracking as a function of the ratio of the shear span a over effective depth d or girder depth h. Also Jena et al. (1972) developed an empirical model. In contrast to the other empirical models, this empirical model used experiments on both simply and continuously supported girders. Therefore the empirical model of Jena et al. (1972) is shown as an example of an empirical model (Equation 2.21).

$$f_{ctm,web} = f_{cm,cube}\left(0.0164 + \frac{h\ 0.0857}{a}\right) \tag{2.21}$$

The tensile strength of the web depends on the ratio of the shear span to girder depth (a/h). According to this model, $\sigma_{1\max}$ is only based on σ_1 along the centroidal axis. Data

from experiments with prestressing with and without bond were used as the behaviour for diagonal tension cracking was considered to be identical for both conditions.

2.2 Database on diagonal tension cracking

To be able to study diagonal tension cracking, experiments have been inventoried from literature. These experiments are used to compile a database which will be used to evaluate the accuracy of the predictions of the eventually proposed model. This section describes the database that is composed of experiments on prestressed girders with and without stirrups, in which diagonal tension cracking was observed. Section 2.2.1 explains the criteria that are used to determine whether experiments can be included in the diagonal tension cracking database. Section 2.2.2 provides an overview of the selected experiments.

2.2.1 Selection criteria

This section is based on literature survey on shear tests in which diagonal tension cracking is reported. The survey results in a diagonal tension cracking database (Appendix A).

The literature survey covered by the presented database includes the following overviews and databases:

- an overview in a state-of-the art report on shear in prestressed concrete members (Walraven 1987).
- an overview of experiments used for verification of a shear design method (Collins et al. 1996).
- a shear database on prestressed members (Nakamura 2011).
- an overview of prestressed girders of a database with shear test on structural concrete beams (Reineck et al. 2012).

All these overviews and databases consist of collection on members with and without stirrups. From experiments it was found that the presence of stirrups does not affect the resistance to diagonal tension cracking (Elzanaty et al. 1986). Therefore, both types are considered in this part of the research.

For the considered experiments with prestressed girders, the main selection criterion is whether diagonal tension cracks occurs. Diagonal tension cracks are defined as diagonal cracks in the web of a girder in the region without flexural cracks (Section 2.1.1). The selection is further based on the following criteria and considerations:

- Only experiments that contain sufficient information to predict the resistance to diagonal tension cracking are included. If, for example, the associate load that causes diagonal tension cracking is unknown, the experiment is not included in the database.
- Both simply and continuously supported girders are collected as this is the intended use of the models proposed in this research.
- Only girders that are prestressed are selected. Sometimes one, or several experiments from a series of tests on prestressed girders, did not contain prestress to investigate the effect of the absence of prestressing. These experiments are not included in the database.
- Only experiments with normal weight concrete are selected.
- It is unlikely that the absence or presence of bonding of the prestressing steel would affect the cracking of the concrete. Therefore experiments are selected independently of the type of prestressing.
- Experiments are selected independent of whether the formation of a diagonal tensions cracks was triggered by the formation of a flexural crack. This is because the purpose of the eventually proposed model is to determine the resistance to diagonal tension cracking in the regions without flexural cracks regardless of what triggered diagonal tension cracking.
- It should be avoided to develop a model that is intended for large girders in practice based on test results of small girders, without considering the influence of the size on the structural behaviour. For instance, in small girders the effect of tension softening behaviour on the development of flexural cracks is more emphatically present than in larger girders. To limit the chance that deviant behaviour of small girders affects the evaluation of models, only experiments with a member depth larger than 450 mm are selected. The selection criterion can be considered as relatively strict compared to criteria used by other researchers. For instance Avendano et al. (2008), Hawkins et al. (2007), Birrcher et al. (2009) and Reineck et al. (2012) used a minimum girder depth of 305, 508, 305 and 70 mm respectively as selection criteria for their databases. An important goal of the current research is to investigate if the predictions according to the eventually proposed model is consistent for different girder depths larger than 450 mm.

2.2.2 Overview of selected experiments

The diagonal tension database is included in Appendix A. An overview of the selected experiments and associated ranges of parameters is given in table 2.2. These parameters concern the girder depth h, the web width b_w, the mean concrete cylinder compressive

strength f_{cm}, the stress in longitudinal direction caused by the prestressing in the centroidal axis σ_{cp} and the ratio of σ_{cp} and f_{cm}. In total seventy experiments that meet the selection criteria as described in section 2.2.1 are selected. Both simply and continuously supported girders are included in the database.

Table 2.2. Overview database on diagonal tension cracking

Researcher (year)	Identification (numbers of experiments)	Support conditions	h	b_w	f_{cm}	σ_{cp}	σ_{cp} / f_{cm}
			mm	mm	N/mm^2	N/mm^2	-
Elzanaty et al. (1986)	CW1, CW2, CW3, CW4, CW5, CW6, CW7, CW8, CW9, CW10,CW11, CW12, CW13, CW14, CW15, CW16, CW17 (17)	Simply supported	457	51	40/ 79	-11.3/ -7.9	-0.20/ -0.11
Choulli (2005)	HAP1E, HAP1TE, HAP1TW, HAP1TW, HCP1TW, HCP1TE, HCP2TE, HAP1W, HAP2TW, HAP2E, HAP2W, HCP2TW (12)	Simply supported	750	100	81/ 99	-9.6/ -6.3	-0.12/ -0.07
Hanson (1964)	F-X1A, F-X1B, F-1A, F-1B, F-2A, F-2B, F-3A, F-3B, F-4A, F-4B, F-5A, F-5B, F-7A, F-7B, F-8A, F-8B, F-10A, F-10B, F-11A, F-11B, F-12A, F-12B, F-13A, F-19A, F-19B (25)	Simply supported	457	76	44/ 51	-6.4/ -5.8	-0.15/ -0.12
Leonhardt et al. (1973)	ŢP2, ŢP4 (2)	Simply Supported	900, 970	80, 150	24/ 47	-5.6/ -6.5	-0.24/ -0.14
Xie (2009)	LB2, LB3, LB7, LB8, LB10, LB11 (6)	Continuously Supported	504, 506	72, 74	62/ 64	-11.2/ -3.5	-0.20/ -0.11
Rupf et al. (2013)	SR21, SR22, SR23, SR24, SR25, SR26, SR29, SR30 (8)	Continuously supported	780	150	30/ 37	-2.3/ -4.8	-0.14/ -0.07

The main selection criterion is whether diagonal tension cracking occurred. This is argued in the remaining part of this section for each of the series of experiments. It is noted that the values of $V'_{R,c,exp}$ listed in Appendix A, are without self-weight. This experimentally found shear force is compared with the predicted shear resistance for the external load wherein the self-weight is subtracted.

A part of the experiments described in the research report of Elzanaty et al. (1986) was designed to fail as a result of 'web shear failure' (CW-series). The experimentally found resistance to diagonal cracking is reported. In the report, it is described that these diagonal cracks are web shear cracks which is an equivalent of diagonal tension cracking. Therefore, all experiments of the CW-series are selected. The descriptions and photos of the crack pattern confirmed this selection as shown by the photo of experiment CW8 (Figure 2.12).

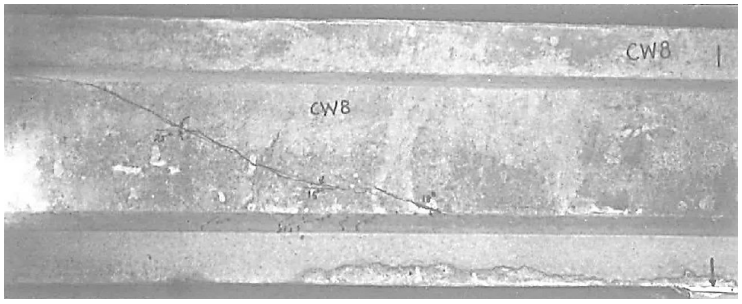

Figure 2.12. Photo at diagonal tension cracking of experiment CW8 (Elzanaty et al. 1986).

The load at first cracking is reported in the dissertation of Choulli (2005). It is described that the first cracks that appeared were diagonal cracks in the web. Therefore, all experiments are selected. It is difficult to confirm this selection based on the photos, as both flexural shear cracks and diagonal tension cracks are visible on the photos. Therefore, the selection is mainly based on the description.

The dissertation of Hanson (1964) reports the experimentally found resistances to significant shear cracking. This concerns both diagonal tension cracking and flexural shear cracking. From the crack diagrams at significant shear cracking it could be determined for which experiments diagonal tension cracking occurred, which were all selected. For a part of the experiments diagonal tension cracking was triggered by a flexural crack and for a part it was not.

The research report of Leonhardt et al. (1973) reports the experimentally found resistance to diagonal cracking. For two experiments it could be determined from photos that the diagonal cracks concerns diagonal tension cracks. Both these experiments are selected.

In the dissertation of Xie (2009) the experimentally found resistance to inclined web shear cracking was reported for all considered experiments. Some experiments were not selected as they were loaded in tension or without prestress. All other experiments were selected. The descriptions and figures of the crack pattern at diagonal cracking stage confirm the selection.

In the reports of Rupf (2014) and Rupf et al. (2012, 2013), the experimentally found resistance to inclined cracking was not reported. However, from figures concerning the crack openings vectors at each load step, it was possible to determine whether diagonal tension cracks occurred and between which load steps. Subsequently, by interpreting the stirrups strain measurements at different locations, it was possible to determine the exact load at diagonal tension cracking. All experiments in which diagonal cracking was observed were selected.

2.3 Findings from literature review

This literature study reveals that the models described in literature use different approaches to determine the maximum principal tensile stress (Sections 2.1.1, 2.1.2, 2.1.3 and 2.1.5). It is unclear if the resistance to diagonal tension cracking can be accurately determined if the maximum principal tensile stress is only based on the principal tensile stresses along the centroidal axis. It is also unknown whether the accuracy increases when the maximum principal tensile stress throughout the web is used. According to all cited codes, it is not necessary to consider the principal tensile stresses around the support (as explained in Section 2.1.2). However, a substantiation is lacking of the size of this area. And finally, it is uncertain whether the models from literature rightly assume that the flexural crack on the edge of the region without flexural cracks does not affect the stress distribution in this region (Section 2.1.2).

The literature study also reveals that the assumed tensile strength of the web differs for each of the considered models (Sections 2.1.1, 2.1.4, 2.1.5). The statistical size effect seems to be the main cause that the ACI model assumes a lower tensile strength than the Eurocode model (Section 2.1.4). It is unclear whether this lower strength is indeed necessary to prevent an overestimation of the resistance to diagonal tension cracking. Also, no answer has been found on whether the effect of bi-axial behaviour can be omitted despite that this effect is clearly shown by tests on small membrane elements (Section 2.1.4).

3

Resistance to diagonal tension cracking

This chapter describes analyses regarding several phenomena that can affect the resistance to diagonal tension cracking. The models that will be proposed in Chapter 4 are based on these analyses.

This chapter investigates four phenomena based on the following questions:

1. How is the tensile strength of the web affected by the lateral principal compressive stresses (bi-axial behaviour, Section 2.1.4)?
2. How is the tensile strength of the web affected by the size of the area subjected to high principal tensile stresses (statistical size effect, Section 2.1.4)?
3. How can the maximum principal tensile stress around the concentrated loads (disturbed areas) be approximated using equations based on the Euler Bernoulli girder theory?
4. How is the distribution of the principal tensile stresses affected by the presence of flexural cracks on the edge of the region of the girder free of flexural cracks?

Whether or not flexural cracks are present before the formation of diagonal tension cracks (phenomenon 4), appears to have a significant effect on the diagonal cracking process. Therefore, the tensile strength of the web (phenomena 1 and 2) and the disturbed areas (phenomenon 3) are investigated considering experiments that are free of flexural cracks at the instant a diagonal tension crack forms (Sections 3.1 – 3.4). This ensures that the mentioned phenomena can by investigated without any disturbance caused by the presence of flexural cracks. Section 3.5, on the other hand, considers experiments in which flexural cracks are present at the instant a diagonal tension crack forms. The differences are then ascribed to the effect of the flexural cracks on principal tensile stresses in the region without flexural cracks. Hence, the other phenomena are considered sufficiently investigated in the preceding sections.

Section 3.1 (roughly) derives the tensile strength of the web using the principal tensile stresses found from linear elastic finite element analyses at the load that caused diagonal tension cracking. In this section, the tensile strength of the web is derived assuming no effect of the principal compressive stresses on the tensile strength and no statistical size effect. Subsequently, Section 3.2 investigates whether considering a statistical size effect

and bi-axial behaviour improves the consistency of the predictions. Section 3.3 investigates the effect of concentrated loads on the principal tensile stress distribution. Moreover, this section investigates whether the maximum principal tensile stresses can be accurately approximated using equations based on the Euler Bernoulli girder theory. Section 3.4 investigates, for girders without flexural cracks, what the effect is on the accuracy, when the maximum principal tensile stresses σ_{1max} is based on σ_1 along the centroidal axis instead of σ_1 over the entire web area. Section 3.5 investigates how the presence of flexural cracks, on the edge of the regions without flexural cracks, affects diagonal tension cracking in the regions without flexural cracks.

Figure 3.1 provides an overview of the methodology used to analyse the described phenomena. The methodology will be explained more extensively in the following sections.

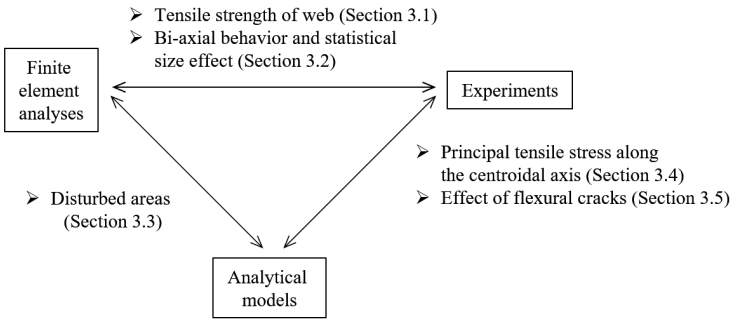

Figure 3.1. Overview of the used methodology

Equations 2.1 to 2.4 of Chapter 2 are repeated an renumbered to Equations 3.1 to 3.4, to make this chapter more self-contained. These equations are based on the Euler Bernoulli girder theory. For monolithic structures, the shear stress ($\tau(z)$) and the stress in the concrete in the longitudinal direction ($\sigma_x(z)$) can be determined from the sectional forces (M, V and N) using Equation 3.1 and 3.2. The principal stresses σ_1 and σ_2 can be determined from τ, σ_x and σ_z using equation 3.3.

$$\tau\,(z) = \frac{V S_c(z)}{b_w(z)\, I_c} \tag{3.1}$$

$$\sigma_x(z) = \frac{N}{A_c} + \frac{M\, z}{I_c} \tag{3.2}$$

$$\sigma_{1,2}(z) = \frac{\sigma_x(z) + \sigma_z(z)}{2} \pm \sqrt{\left(\frac{\sigma_x(z) - \sigma_z(z)}{2}\right)^2 + \tau(z)^2} \tag{3.3}$$

$$\sigma_{1,2}(z) = \frac{\sigma_x(z)}{2} \pm \sqrt{\left(\frac{\sigma_x(z)}{2}\right)^2 + \tau(z)^2} \tag{3.4}$$

In Equation 3.3 σ_z is the stress in the concrete in vertical direction. To determine the principal tensile stress σ_1 the '±' should be read as plus. To determine the principal compressive stress σ_2 the '±' should be read as minus. Alternatively, the principal tensile stresses can be determined using Equation 3.4 in which the vertical stresses σ_z are neglected. In the equations I_c is the second moment of area, S_c is the first moment of area, A_c is the area of concrete cross-section, b_w is the width of the web and z is the vertical distance from the centroidal axis. The subscript c indicates that the cross-sectional properties concern the concrete. The parameter z indicates that the associated parameter varies, or could vary, over the height z of the cross-section.

3.1 Experimentally found tensile strength of the web

As described in Section 2.1.4, there is no general agreement in literature on the tensile strength of the web that should be used to determine diagonal tension cracking. If the results of material tests are present, such as a concrete cylinder compressive test, the tensile strength of the web can be determined using different equations (Equations 2.5 to 2.10). For a given strength class of concrete, these equations result in mutually different values of the tensile strength of the web.

Although the Equations 2.5 to 2.10 are used for diagonal tension cracking of girders, none of these equations are based on test results on girders. To evaluate which equation is most suitable for girders, this section will investigate the tensile strength of the web using experiments from the diagonal tension cracking database (Section 2.2). The tensile strength of the web is assumed to be equal to the maximum principal tensile stress in the web at the load that caused diagonal tension cracking. The maximum principal tensile stress of the web can be determined from linear elastic finite element analyses. The highest principal stresses are typically found around the disturbed areas (Section 2.1.3). By using a finite element analyses, the principal stresses in the disturbed areas can be determined accurately. Equations 3.1, 3.2 and 3.4 are not suitable to predict the stresses in these disturbed areas (Section 3.3).

To investigate the tensile strength of the web, only experiments are used in which no flexural cracks are present at diagonal tension cracking. In Section 3.5 it will be demonstrated that flexural cracks can affect the diagonal cracking process significantly. By considering experiments without flexural cracks, this influence is avoided. For experiments without cracks, linear elastic analyses are appropriate to investigate the distribution of the principal tensile stresses. In the current section, it is assumed that there is no effect of bi-axial behaviour and no statistical size effect. These two phenomena will be further investigated in Section 3.2.

Experiments without flexural cracks are selected from the database on diagonal tension cracking (Appendix A). The substantiation whether experiments are considered as experiment with or without flexural cracks is given in Appendix B. Whether flexural cracks are present is based on both the descriptions in the associated research reports and hand calculations. The longitudinal stress in the ultimate fibre (σ_x) at the cross-section of the point load is determined using a hand calculation for the load that caused diagonal tension cracking. If σ_x is (significantly) smaller than the flexural tensile strength of concrete, $f_{ctm,fl}$, it is assumed that no flexural cracks are present. For this selection criterion, the flexural tensile strength is determined using Equation 3.5 (NEN 2005). In this equation, h is the girder height and f_{ctm} is the uniaxial tensile strength of concrete.

$$f_{ctm,fl} = \max\left(\left(1.6 - \frac{h}{1000}\right) f_{ctm}, f_{ctm}\right) \tag{3.5}$$

Sixteen experiments could be categorized as 'experiments without flexural cracks'. This concerns experiments of Elzanaty et al. (1986), Choulli (2005) and Hanson (1964) and Leonhardt et al. (1973). Eleven of these experiments remained free of flexural cracks according to both the descriptions in the associated reports and according to the hand calculations. Five experiments are selected for which it was not reported whether flexural cracks were observed before diagonal tension cracking. These experiments were selected based on only the results of the hand calculations. Because for these experiments a description was missing to confirm that no flexural cracks were present, only experiments are selected for which σ_x is significantly smaller than the flexural tensile strength of concrete ($\sigma_x \leq 0.75\ f_{ctm,fl}$). To ensure that only experiments free of flexural cracks are considered, experiments were not selected if hand calculations resulted in the prediction that flexural cracks should be present but the reports described that the experiments remained free of flexural cracks. Appendix B lists the results of the hand calculation, whether flexural cracks are reported and the final categorization.

Linear elastic finite element analyses are carried out for twelve experiments of Elzanaty et al. (1986) and Choulli (2005) and two experiments of Hanson (1964). For the two selected experiments of Leonhardt et al. (1973) no finite element analyses are carried out (Table 3.1). The finite element analyses of the experiments of Choulli and Elzanaty et al. are described in Kroeze (2018) and the finite element analyses of the experiments of Hanson are described in Sugianto (2019). These reports describe how the girders are modelled, which analyses are carried out, how the models are verified and what the results of the analyses are. The analyses are carried out using the finite element programme DIANA. The girders are discretised with a 2D quadrilateral plane stress elements with a linear interpolation of the displacements. The thickness of the experiment is modelled using a thickness function. To gain accurate results a mesh was used

of 25 x 25 mm^2. The reinforcing and prestressing steel are modelled as embedded reinforcement.

Table 3.1 Number of experiments without flexural cracks used in analyses

	Elzanaty et al. (1986) and Choulli (2005)	Hanson (1964)	Leonhardt et al. (1973)
Experiments	CW1, CW2, CW4, CW5, CW8, CW13, CW14, CW16, CW17, HAP1E, HAPTE, HAP1W	F-1A and F-1B	ŢP2 and ŢP4
Linear elastic finite element analyses	12	2	-
Section 3.1 Experimentally found tensile strength of web	12	2	-
Section 3.2 bi-axial behaviour	12	-	-
Section 3.2 bi-axial behaviour and statistical size effect	12	2	-
Section 3.3 disturbed areas	12	2	-
Section 3.4 aspects affecting the accuracy for girders without flexural cracks	12	2	2

Figure 3.2 shows an example of a finite element model of experiment HAP1E. (Choulli 2005) The principal (tensile) stresses are determined for the load that caused diagonal cracking.

Figure 3.2. Finite element model of experiment HAP1E (Kroeze 2018)

For the selected experiments, the maximum principal tensile stress in the web at diagonal tension cracking (σ_{1max}) is determined. The found distribution of the principal tensile stresses is further analysed in Section 3.3. The tensile strength of the web is expressed as a fraction of the uniaxial tensile strength of concrete. The uniaxial tensile strength is derived from the cylinder compressive test even if splitting tests are available. This approach is chosen because it corresponds to the approach used in practice to determinate the tensile strength. Moreover, Reineck et al. (2012) describe that the uniaxial tensile strength can be accurately derived from the concrete cylinder compressive strength. This is found by comparing the uniaxial tensile strength derived from cylinder compressive test and the uniaxial tensile strength derived from splitting test for experiments where both material test are carried out. Equation 3.6 is used to determine f_{ctm} for experiments in which $f_{cm} \leq 54$ N/mm^2 and Equation 3.7 for experiments in which $f_{cm} > 54$ N/mm^2.

This corresponds with the equations applicable for experiments as described by Reineck et al. (2012).

Although the limit of f_{cm} = 54 N/mm^2 corresponds to NEN (2005), it could be considered to use 58 N/mm^2 instead to prevent a discontinuity at the transition of Equation 3.6 to 3.7. This discontinuity is not present in NEN (2005) in which the relation $f_{ctm} = 0.30\ (f_{cm} - 8)^{2/3}$ is used instead of Equation 3.6 and which is applicable for structures in practice (which show a larger variation of the concrete compression strength than for experiments carried out under laboratory conditions). However, the limit of f_{cm} = 54 N/mm^2 is maintained, as this corresponds to the equations proposed by Reineck et al. (2012).

$$f_{ctm} = 0.30\ (f_{cm} - 4\ )^{2/3} \tag{3.6}$$

$$f_{ctm} = 2.12\ \ln(1 + \ f_{cm}/10) \tag{3.7}$$

For fourteen experiments without flexural cracks, linear elastic finite element analyses are carried out (Table 3.1). The maximum principal tensile stress σ_{1max} is set equal to the maximum value for σ_1 for all points of the mesh and is listed in Appendix C. Appendix C also lists σ_{1max}/f_{ctm} for each experiment. A mean value of σ_{1max}/f_{ctm} is found of 0.84. If it is assumed that the stress distribution simulated by the finite element analyses is accurate and that diagonal cracks form when the maximum principal tensile stress equals the tensile strength of concrete, the average tensile strength of the web should correspond to Equation 3.8.

$$f_{ctm,web} = \ 0.84 f_{ctm} \tag{3.8}$$

The found tensile strength of the web is lower than f_{ctm} which is used in NEN (2005). In all these equations the effect of bi-axial behaviour and a statistical size effect are not explicitly considered. These phenomena will be further investigated in Section 3.2.

The coefficient of variation of $\sigma_{1max}/\ f_{ctm}$ is found to be 6.7% (Appendix C). Despite that bi-axial behaviour and a statistical size effect are not explicitly considered, diagonal tension cracking of girders without flexural cracks can be predicted rather consistent using linear elastic finite element analyses.

3.2 Bi-axial behaviour and statistical size effect

The average principal tensile stresses in the web at which diagonal tension cracks form is lower than the uniaxial tensile strength of concrete as found in Section 3.1. In literature two possible phenomena are described that support this finding (Section 2.1.4). The first phenomenon is bi-axial behaviour. From tests on bi-axially loaded small membranes, it

is found that the tensile strength reduces with increasing lateral compressive stresses. The second phenomenon is a statistical size effect. The statistical size effect concerns the phenomenon that if a larger region of a member is subjected to high tensile stresses, the chance of encountering a weak spot increases and the member cracks at lower principal tensile stresses. This section investigates both phenomena.

Firstly, it is investigated whether the strength of the web can be predicted accurately using two models from literature that describe bi-axial behaviour (which will be explained hereafter), ignoring the presence of a statistical size effect. For this investigation the results of the finite element analyses are used. In contradiction to Section 3.1, the analyses are not only based on the found principal tensile stress σ_1, but also on the lateral principal compressive stress σ_2. The bi-axial strength (defined as $f_{ctm,eff}$) is found by multiplying the uniaxial tensile strength f_{ctm} (according to Equations 3.6 and 3.7) with a factor. The first investigated model from literature is the Mohr-Coulomb approximation as described in Section 2.1.4 (Equation 2.7). The factor used in this model is listed in Table 3.2. According to this factor, the tensile strength reduces linearly from f_{ctm} at $\sigma_2 = 0$ to zero at $\sigma_2 = -f_{cm}$. The second investigated model from literature is the empirically relation derived by Huber (2016). This relation is also described in Section 2.1.4 (Equation 2.8, which is applicable for $-0.9 \leq \sigma_2 / f_{cm} \leq -0.1$). Also the factor used in this model is listed in Table 3.2. According to this equation, the reduction of f_{ctm} does not only depend on σ_2, but also on the concrete cylinder compressive strength f_{cm}.

Table 3.2. Factors by which f_{ctm} has to be multiplied o account for bi-axial behaviour

No bi-axial behaviour	Mohr-Coulomb Approximation (Section 2.1.4)	Huber (2016) (Section 2.1.4)
1	$1.0 + \frac{\sigma_2}{f_{cm}}$ (Equation 2.7)	$1.6 - 0.2\, f_{cm}{}^{\frac{1}{3}} - 0.6\, \frac{\sigma_2}{f_{cm}}$ (Equation 2.8)

To determine whether the accuracy increases using the factors from literature (Table 3.2), the results of the twelve finite element analyses carried out by Kroeze (2018) are considered (Table 3.1). In this study, σ_1 and σ_2 are determined for the load that causes diagonal tension cracking for each point of the mesh. By combining these values with f_{cm}, the values of $\sigma_1/f_{ctm,eff}$ could be determined. For each experiment, the maximum of $\sigma_1/f_{ctm,eff}$ is listed in Appendix D, for both the Mohr-Coulomb approximation (Equation 2.7) and the equation found by Huber (Equation 2.8).

The results for the twelve experiments are shown in Table 3.3, Figure 3.3, Figure 3.4 and Figure 3.5. The mean value and coefficient of variation for the situation that no bi-axial behaviour in considered deviates somewhat from Section 3.1. This deviation is

caused by the two additional experiments that are considered in Section 3.1 (Table 3.1, Appendix D).

Table 3.3. Statistical properties of $\sigma_{1max}/f_{ctm,eff}$ for depending on model for bi-axial behaviour

		No bi-axial behaviour	Mohr-Coulomb approximation (Equation 2.7)	Huber (2016) (Equation 2.8)
$\sigma_{1max}/f_{ctm,eff}$	Mean	0.83	1.01	1.29
	Coefficient of variation	5.2%	6.7%	8.2%

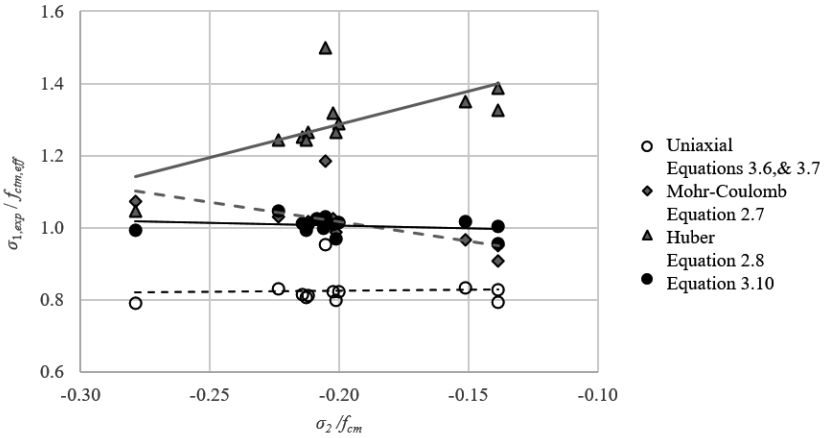

Figure 3.3. $\sigma_{1max}/f_{ctm,eff}$ versus σ_2/f_{cm} using f_{ctm} and three models for bi-axial strength

For the considered experiments, f_{cm} varies between $41 \leq f_{cm} \leq 99$ N/mm^2, as shown in Figure 3.4. This complies with the range found for existing bridges in the Dutch Highways, for which f_{cm} varies between $43 \leq f_{cm} \leq 84$ N/mm^2 (Table 1.1).

Figure 3.5 shows that considered experiments σ_{cp}/f_{cm} varies between $-0.20 \leq \sigma_{cp}/f_{cm} \leq -0.10$. This party complies with the range for existing bridges in the Dutch Highways, for which σ_{cp}/f_{cm} varies between $-0.20 \leq \sigma_{cp}/f_{cm} \leq -0.04$ (Table 1.1). Only for $-0.10 \leq \sigma_{cp}/f_{cm} \leq -0.04$, for which it could be expected that the effect of bi-axial behaviour is less significant, no experimentally data is available.

It is found that using the Mohr-Coulomb approximation (grey diamonds, dashed grey trend line) results in $\sigma_{1max} / f_{ctm,eff}$ of almost unity (Table 3.3). However, for high values of σ_2/f_{cm} and for high values of f_{cm}, the predicted strength of the web is overestimated (Figure 3.3 and 3.4). If the equation derived by Huber (grey triangles, continuous grey trend line) is used it is found that the tensile strength of the web was significantly underestimated (Table 3.3), especially for high values of σ_2 / f_{cm} (Figure 3.3) and high

values of f_{cm} (Figure 3.4). Moreover, it was found that the consistency of the predictions for both models slightly decreases compared to simply using the uniaxial strength and neglecting the bi-axial behaviour (white circles, dashed black trend line in Figures 3.3 and 3.4). Based on these results, it is plausible that bi-axial behaviour is the cause that the web cracks at principal tensile stresses below the uniaxial tensile strength, as was found in Section 3.1. However, regarding the increase of the coefficient of variation of the predictions, the difference cannot be satisfactorily explained by only considering the existing models for bi-axial strength.

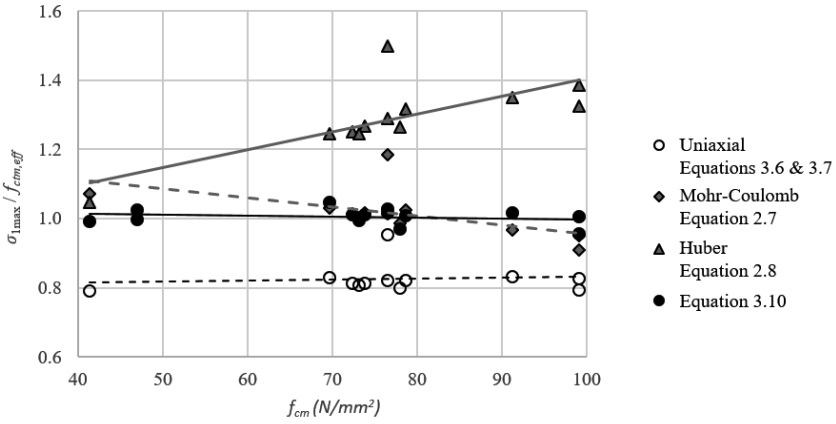

Figure 3.4. $\sigma_{1max}/f_{ctm,eff}$ versus f_{cm} using f_{ctm} and three models for bi-axial strength

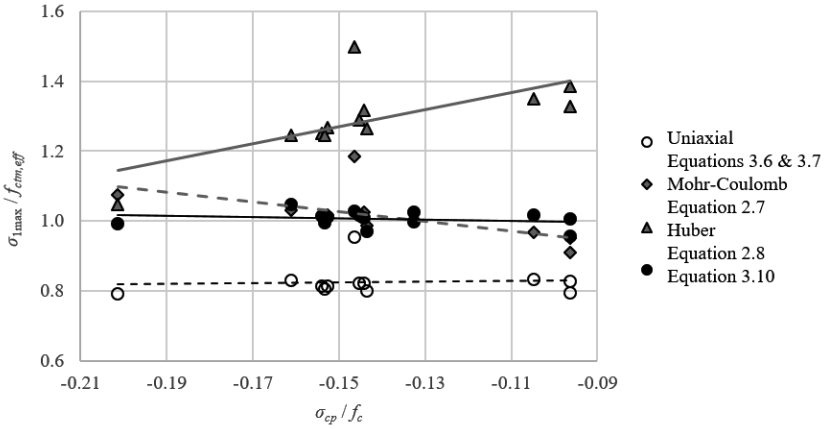

Figure 3.5. $\sigma_{1max}/f_{ctm,eff}$ versus σ_{cp}/f_{cm} using f_{ctm} and three models for bi-axial strength

In the second part of this section, a statistical size effect is considered in addition to the bi-axial behaviour as discussed in the first part of this section. An equation is derived for the tensile strength of the web that considers both phenomena.

The suggested equation is based on four assumptions:

1. The bi-axial behaviour is well described using the Mohr-Coulomb approximation.
2. The tensile strength is inversely proportional to the fourth root of the size (Collins, 1997).
3. This size corresponds to the length along the longitudinal axis over which the principal tensile stresses are between 90% and 100% of the maximum principal tensile stresses (this length is defined as $l_{\sigma 1}$).
4. The principal tensile stress (σ_{1m}) and principal compressive stress (σ_{2m}) at the point at the mid-length of $l_{\sigma 1}$ and at mid-height of the points defining $l_{\sigma 1}$ are representative for the stresses at which diagonal tension cracking occurs (Figure 3.6).

The factor by which the bi-axial tensile strength has to be multiplied to consider a statistical size effect will be derived using four of the experiments that are categorized as 'No flexural cracks present' (Figure 3.6). For these experiments the area of the web in which σ_1 is between the 90% and 100% of $\sigma_{1\max}$ are shown in dark grey in Figure 3.6. The principal tensile stresses are based on the results of the finite element analyses carried out by Kroeze (2018) and Sugianto (2019). The concrete tensile strength is not a fixed value but will have a spatial variation. It is likely that diagonal tensile cracks will initiate from the location with the lowest tensile strength. Cracks are expected in the area associated with $l_{\sigma 1}$, shown as light grey parallelograms in Figure 3.6 (which is confirmed by observations).

The results of finite element analyses are used to determine $l_{\sigma 1}$ for each of the four girders. It is assumed that the tensile strength is inversely proportional to the fourth root of a critical size, defined as $l_{\sigma 1}$. The factor for the statistical size effect is defined as $(l_0/l_{\sigma 1})^{1/4}$ (Equation 3.9). The parameter l_0 is introduced to determine the value of $l_{\sigma 1}$ for which no size effect is present. Equation 3.9 is the equation for the tensile strength $f_{ctm,2s}$ in which both the factor for bi-axial behaviour according to the Mohr-Coulomb approximation and the factor for a statistical size effect are combined. The parameter l_0 is determined based on the four experiments by equating $f_{ctm,2s}$ and σ_{1m} at a point at the mid-length of $l_{\sigma 1}$ and at mid-height of the points defining $l_{\sigma 1}$ (halfway the length of the white arrows as shown in Figure 3.6). The results are shown in Table 3.4. A mean l_0 was found of 710 mm from the four experiments (Table 3.4). In the derived for the tensile strength of the web (Equation 3.10) a slightly higher value is used for l_0 of 750 mm (as rounded gross value).

$$f_{ctm,2s} = \left(1.0 + {}^{\sigma_{2m}}/_{f_{cm}}\right)\left({}^{l_0}/_{l_{\sigma 1}}\right)^{1/4} f_{ctm} \tag{3.9}$$

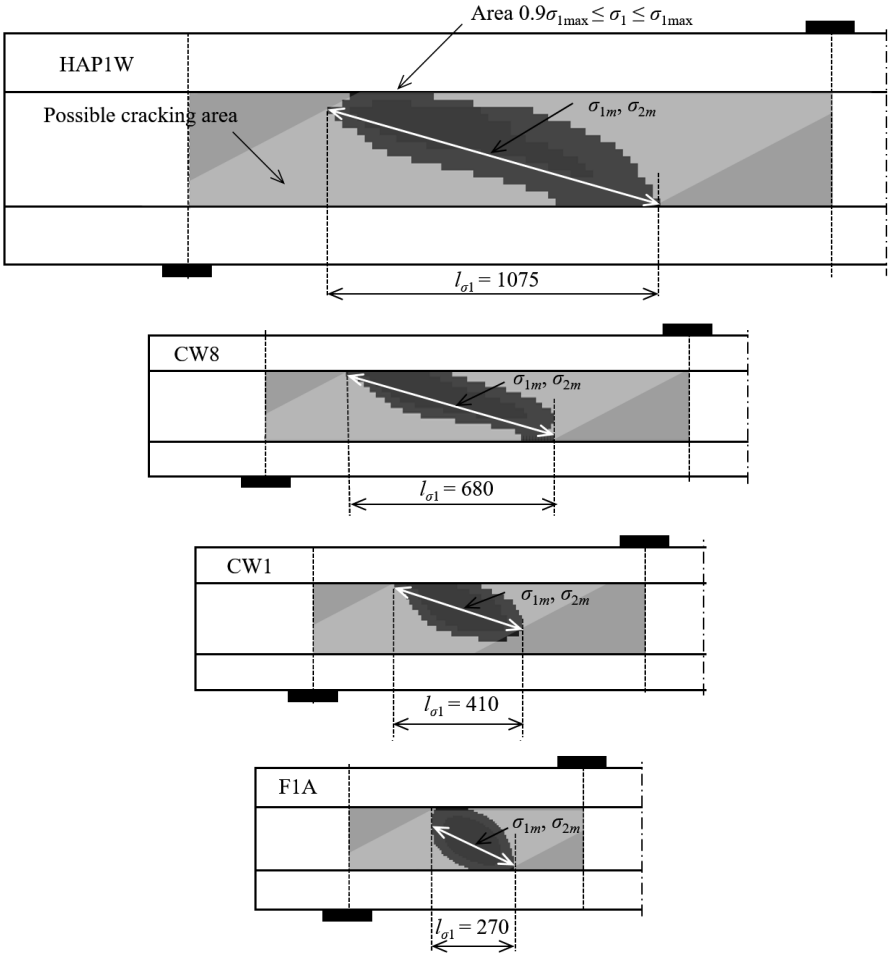

Figure 3.6. areas in which $0.9\sigma_{1max} \le \sigma_1 \le \sigma_{1max}$ and $l_{\sigma 1}$ used to derive a statistical size effect

Table 3.4. Data used for derivation of a statistical size effect factor l_0

Experiment	f_{cm}	f_{ctm}	σ_{2m}	$1.0 + \frac{\sigma_2}{f_{cm}}$	$f_{ctm,eff}$	σ_{1m}	$\frac{\sigma_{1m}}{f_{ctm,eff}}$	$l_{\sigma 1}$	l_0
	N/mm^2	N/mm^2	N/mm^2	-	N/mm^2	N/mm^2	-	mm	mm
HAP1W	99.2	5.07	-13.7	0.86	4.36	3.81	0.87	1075	620
CW8	41.4	3.35	-11.5	0.72	2.42	2.59	1.07	680	890
CW1	76.6	4.58	-15.7	0.79	3.64	4.35	1.20	410	840
F1A	47.0	3.68	-9.7	0.79	2.93	3.37	1.15	270	480
Mean									710

$$f_{ctm,2s} = \left(1.0 + {}^{\sigma_{2m}}/_{f_{cm}}\right)\left({}^{750}/_{l_{\sigma 1}}\right)^{1/4} f_{ctm} \tag{3.10}$$

To investigate whether the strength of the web can be predicted more accurately if both bi-axial behaviour and a statistical size effect are considered, $\sigma_{1max}/f_{ctm,2s}$ is determined for all of the 14 experiments without flexural cracks for which linear elastic finite element analyses are carried out (Table 3.1). The area in which the principal tensile stress are higher than 90% of the maximum principal tensile stress, $l_{\sigma 1}$, σ_{1m} and σ_{2m} are determined in the same way as for the four experiments of Figure 3.6 that were used to derive l_0. The tensile strength of the web is determined from Equation 3.10. The results for the fourteen experiments are shown in Appendix D, Figure 3.3, Figure 3.4 and Figure 3.5 (black circles and a continuous black trend line).

Table 3.5 compares the results of the derived equation for the tensile strength of the web (Equations 3.10) and the results of using the uniaxial tensile strength of concrete. It is found that both the mean value and the coefficient of variation significantly improves if a statistical size effect and bi-axial behaviour is considered. Moreover, the predictions were found to be consistent for the considered ranges of σ_2 / f_{cm} (as found from Figure 3.3) and f_{cm} (as found from Figure 3.4).

Table 3.5. Statistical properties of σ_{1max} / f_{ctm} for bi-axial behaviour and a statistical size effect

$f_{ctm,web}$		f_{ctm} (Equations 3.6, 3.7)	$f_{ctm,2s}$ (Equations 3.6, 3.7, 3.10)
Statistical size effect		no	yes
Bi-axial behaviour		no	yes
σ_{1max}/f_{ctm}	Mean	0.84	1.01
	Coefficient of variation	6.7%	2.3%

As the derived tensile strength is found to result in particular accurate predictions, it is not necessary to further reconsidered the four assumptions that are used to derive Equation 3.10. In Section 3.1 it was found that the tensile strength of the web is about 84% of the uniaxial tensile strength. The difference can satisfactorily be explained by considering both the bi-axial strength and a statistical size effect.

In the current section the principal stresses are determined numerical and only for girders without flexural cracks. Sections 3.4 and 3.5 investigate the accuracy of the predicted resistance, without considering bi-axial behaviour and a statistical size effect, when the principal stresses are analytical determination, for girders both with and without flexural cracks. Based on the results of Section 3.4 and 3.5, and some additional considerations, bi-axial behaviour and a statistical size effect will not be part of the models proposed models in Chapter 4. This is further argued in Chapter 4.

It is noted that it could also be considered to relate the tensile strength to the size 'surface' or 'volume'. This is not further investigated considering the consistent predictions of Equation 3.10[1].

3.3 Principal tensile stresses in disturbed areas

In this section the disturbed areas are analysed. The distribution of the principal stresses, as found from the finite element analyses for experiments without flexural cracks (Section 3.2) will be further evaluated. Subsequently the results of the finite element analyses are compared to the results of the analytical equation which derives the maximum principal tensile stress from the cross sectional forces using Equations 3.1, 3.2 and 3.4. Finally, it is evaluated if it is possible to approximate the results of the finite element

[1] In a recent research the 'cracking size effect' has been investigated (Bentz 2019, Bentz 2020). The 'cracking size effect' is a synonym for the 'statistical size effect' as used in this dissertation. The recent research reveals that it is possible to relate the cracking strength of concrete to the volume within which the tensile stress is at least equal to 85% of the maximum value (the Highly Stressed Volume, abbreviated as HSV). This relation is referred to as the 'unified tension model'. The model is justified with 511 tension tests, consisting of flexural tests, direct tension tests, split cylinder tests and shells. The 'unified tension model' relates the tensile strength to the highly stressed volume, which seems in contrast to the derived model in this dissertation (Equation 3.10). In Equation 3.10, the tensile stress is related to a length along the longitudinal axis, related to an highly stressed surface. It is however noted that no diagonal tension tests with girders were used to justify the unified tension model. A possible reason for the difference between both models, is whether a significant gradient of the (principal) tensile stresses is present in the associated tests. For direct tensile tests, split cylinder tests and the shell tests, the stresses are uniformly distributed over the whole highly stressed volume and no redistribution is possible when at the weakest spot the tensile stress is equal to the tensile strength. For diagonal the tension test on girders, on the other hand, the principle tensile stress is only locally equal to the tensile strength, and the area around the weakest spot can resist additional stresses. This could potentially postpone diagonal tension cracking. The possibility to redistribute stresses could be a possible explanation for the difference between both models. It is noted that the model derived in this dissertation (Equation 3.10) also takes into account the conditions that the principal compressive stress differs in every spot of the highly stressed surface. In the tests for the unified tensile model, on the other hand, a constant value could be assumed for σ_2/f_{cm} for each type of tests (0-10%, which was significantly lower than 14-28% found for the diagonal tension tests on girders). It is not yet clear how the different values of the principal compressive stress should be taken into account when the unified tensile model is applied. These conditions currently complicate a direct application of the 'unified tension model' for the prediction of diagonal tension cracking.

analyses by limiting the considered area around the concentrated loads for which the maximum principal stress are determined using Equations 3.1, 3.2 and 3.4 (Figure 3.7).

Figure 3.7 shows girder HAP1E of the Choulli test series (Choulli 2005). The relation between the cross sectional forces and the distribution of the principal tensile stresses, based on Equations 3.1, 3.2 and 3.4, is already described in Section 2.1.3. The principal stress distribution can be exemplified by only considering the principal stress distribution along the axis that coincides with the intersection of the top flange and the web, the centroidal axis and the axis that coincide with the intersection of the web and the bottom flange. These considered axes are shown in Figure 3.7.

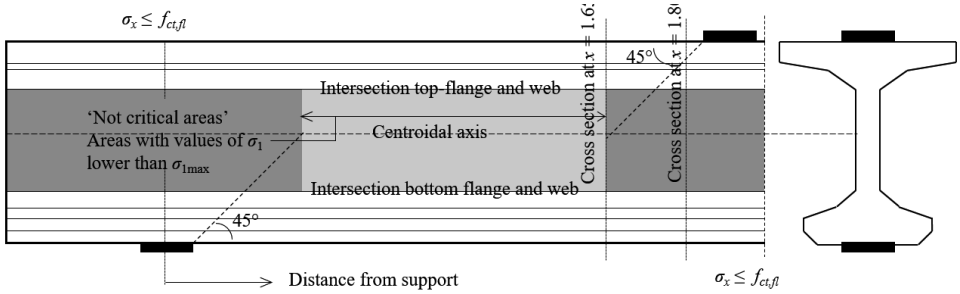

Figure 3.7. Location of considered axis, cross-sections and areas of experiment HAP1E

Figure 3.8 shows the distribution of the principal tensile stresses along each defined axis. The continuous black lines show the principal tensile stresses as found from the finite element analyses. The dashed lines show the principal tensile stresses as found from the cross sectional forces using Equation 3.1, 3.2 and 3.4.

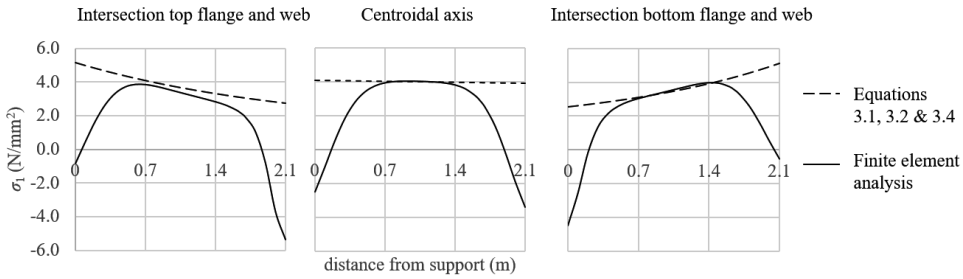

Figure 3.8. Distribution of σ_1 along defined axes determined both numerical and analytical

It appears that at the location of the concentrated forces (support plate at x = 0 m and loading plate at x = 2.1 m) the principal tensile stresses are significantly overestimated using Equation 3.1, 3.2 and 3.4. It also appears that in the middle region (the areas which are not 'disturbed') the principal tensile stresses are more accurately approached using Equation 3.1, 3.2 and 3.4.

To further investigate the cause of the deviation, a cross-section in the disturbed area is considered at a location 300 mm from the point load, at x = 1.8 m (Figure 3.7). The distribution of the longitudinal stresses σ_x, the vertical stresses σ_z, the shear stresses τ and the resulting σ_1 along the cross-section (z direction) are shown in Figure 3.9. The stresses are shown both as result of the finite element analyses (dots) and derived from the cross sectional forces using Equations 3.1, 3.2 and 3.4 (continuous line).

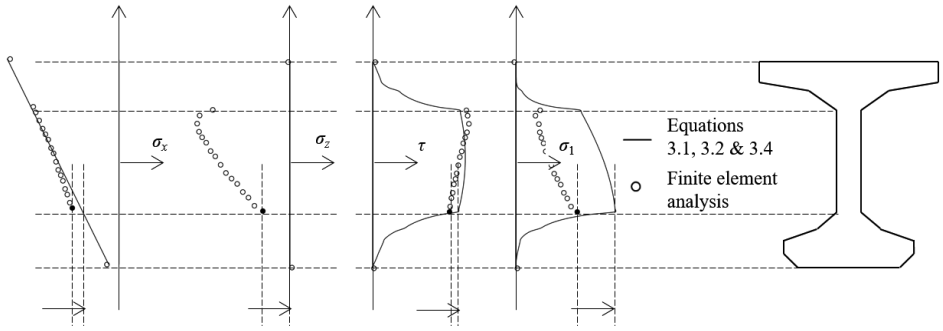

Figure 3.9. σ_x, σ_z , τ and σ_1 along cross-section at x = 1.8 m

In Table 3.6, the principal tensile stresses are more extensively compared at x = 1.8 m, at the location of z in which the maximum value of σ_1 is found (black dots in Figure 3.9). As shown in Table 3.6, the principal tensile stress is significantly overestimated using Equations 3.1, 3.2 and 3.4 compared to the principal tensile stresses found from the finite element analyses (which are considered as accurate). Using Equation 3.2 results in an overestimation of the longitudinal stresses (Figure 3.9). A higher longitudinal stress (less compression) results in a higher principal tensile stress (Equation 3.3). This is the first cause of the overestimation of σ_1 by the analytical equations. Equations 3.4 conservatively neglects any contribution of the vertical stresses (Section 2.1.2). Figure 3.9 shows that, at the considered location, a negative (compression) vertical stress is present that will result in a lower principal tensile stress (Equation 3.3). This is the second cause of the overestimation of σ_1 by using the analytical equations. Using Equation 3.1 also results in an overestimation of the shear stresses. A higher shear stress results in a higher principal tensile stress (Equation 3.3). This is the third cause of the overestimation of σ_1 by using the analytical equations. All three causes were found to have a comparable contribution to the overestimation of σ_1 for the considered girder.

Table 3.6. σ_x, σ_z , τ and σ_1 at x = 1.8 m and 1.6 m at the intersection of web and bottom flange

	x	σ_x	σ_z	τ	σ_1
	m	N/mm^2	N/mm^2	N/mm^2	N/mm^2
Finite element analyses	1.80	-7.05	-0.90	5.81	2.60
Analytical Equations 3.1, 3.2 and 3.4	1.80	-5.30	0.00	6.69	4.55
Finite element analyses	1.65	-7.76	-0.38	6.51	3.41
Analytical Equations 3.1, 3.2 and 3.4	1.65	-6.17	0.00	6.70	4.29

Apparently, the principal tensile stresses are overestimated around the disturbed area if Equations 3.1, 3.2 and 3.4 are used. The finite element analyses demonstrate that the maximum principal tensile stress is not located in an area close to the support (Figure 3.8). If the stresses are considered further away from the support the stresses determined with analytical equations correspond better with the stresses determined with the finite element analyses (Figure 3.8). Therefore, the analytical equation could still be suitable to predicted the maximum principal tensile stresses under the condition that an area around the support is not considered. This is a logical approach because the maximum principal tensile stress is not located close to the support (Figure 3.7). This approach corresponds to the Eurocode (NEN 2005) and the Model Code 2010 (*fib* 2012), that prescribe that the principal tensile stresses do not have to be considered for cross-sections closer to the support than the point that is the intersection of the elastic centroidal axis and a 45° inclined line from the inner edge of the support (Figure 3.7). Whether this definition of the 'not critical area' results in accurate predictions of the maximum principal tensile stress is evaluated. For the evaluation, the prescribed area is assumed to be applicable for both the support and the concentrated load. These areas are shown in Figure 3.7 in dark grey. As a consequence, the maximum principal tensile stress will only be based on the principal tensile stresses in the light grey area.

Firstly, the suggested dimensions of the 'not critical area' is evaluated by reconsidering the stress distribution of girder HAP1E. Table 3.6 shows the stresses at the intersection of the bottom flange and the web for the location x = 1.65 m which corresponds to the edge of the area that has to be considered as described by NEN (2005) and *fib* (2012). As appears from Table 3.6, the predictions of the longitudinal stress and the shear stress according to the Equations 3.1 and 3.2 are more similar to the stresses found from the finite element analyses, although the equations still slightly overestimate the stresses. Also the absolute value of the vertical stress is less at x = 1.65 than at x = 1.8 m, although still significant. As a consequence, the principal tensile stress is still overestimated at this location (σ_1 = 4.29 N/mm^2 instead of 3.41 N/mm^2). However, according to the finite element analyses the maximum value of σ_1 was located at a cross-section further away

from the concentrated load. According to the finite element analyses the maximum principal tensile stress $\sigma_{1max} = 4.19$ N/mm^2, which is just slightly less than the value found using Equations 3.1, 3.2 ad 3.4 at $x = 1.65$ m ($\sigma_1 = 4.29$ N/mm^2).

Secondly, the suggested dimensions of the 'not critical area' is evaluated by considering the fourteen experiments for which linear elastic finite element analyses are carried out (Table 3.1). For these experiments σ_1 is determined using Equations 3.1, 3.2 and 3.4, and σ_{1max} equals the maximum of σ_1 in the web (light grey area in Figure 3.7). These values for σ_{1max} are compared to σ_{1max} according to the finite element analyses (Appendix C). The last column of Appendix C shows that the mean value of the ratio σ_{1max} according to Equations 3.1, 3.2 and 3.4 and σ_{1max} according to the linear elastic finite element analyses equals 1.06, with an associated coefficient of variation of 2.9%. It was found that the assumed dimensions of the 'not critical area' results in a rather accurate prediction of $\sigma_{1max.}$ Despite the significant deviations of σ_1 in the areas close to the point loads, Equations 3.1, 3.2 and 3.4 are still found to be rather suitable to predict the maximum σ_1, if the considered area is limited to the light grey area shown in Figure 3.7. This is relevant as it avoids extensive finite element analyses in practice. However, it is emphasized that this is only demonstrated for girders that remain free of flexural cracks (in which $\sigma_x \leq f_{ctm,fl}$ both at the support and at point load). Section 3.5 will demonstrate that this approach is not suitable in areas where the point loads causes flexural cracks in the flanges of the girder ($\sigma_x > f_{ctm,fl}$).

If a distributed load, or a combination of a distributed load and a point load are applied, the shear stresses will increase toward the support. This phenomenon is not included in the considerations of this section. On the other hand, neglecting the vertical stresses will still result in an overestimation of the principal tensile stress at the critical spot using the analytical equations, also for distributed load. Moreover, determining the longitudinal stress using the analytical equations will, also for distributed loads, result in an overestimation of the principal tensile stress. Nevertheless, the difference in loading conditions will be a reason to include some conservatism when the design value for the eventually proposed model is derived for girders without flexural cracks (Section 4.3). This is because distribution of the shear stresses in bridges is, due to the presence of distributed loads, less favourable, compared to the experiments used to derive the design value, which were loaded with concentrated loads.

3.4 Aspects affecting the accuracy for girders without flexural cracks

This section only concerns girders without flexural cracks for which a model will be proposed in Section 4.1. This section investigates the effect on the accuracy when the maximum principal tensile stresses σ_{1max} is based on σ_1 along the centroidal axis instead

of σ_1 over the web area. The effect is investigated by comparing accuracy of the predictions according to both models, using the experimentally found load that caused diagonal tension cracking (Figure 3.1). The maximum principal tensile stress σ_{1max} is determined using Equations 3.1, 3.2 and 3.4. for the 16 experiments without flexural cracks (Table 3.1), both for the model considering σ_1 over the (light grey) web area and for the model that considers σ_1 only along the centroidal axis (Figure 3.7). The maximum principal tensile stresses are compared to the uniaxial tensile strength. The results are listed in Appendix C ('Maximum σ_1 in the web' and 'Maximum σ_1 along the centroidal axis'). When the experimental results are used to determine the mean value of a proposed models, only the coefficient of variation will be relevant for the judgement of which model is the most accurate. The results are shown in Table 3.7.

Table 3.7. Effect of considered area for σ_{1max} on the statistical properties of σ_{1max}/f_{ctm}

		Maximum σ_1 in the web	Maximum σ_1 in the along the centroidal axis
Number of experiments		16	16
σ_{1max}/f_{ctm}	Mean	0.89	0.79
	Coefficient of variation	5.2%	11.8%

As appears from Table 3.7, the most accurate predictions are found if σ_{1max} is based on σ_1 over the web area. This approach will therefore be used in the proposed model for girders without flexural cracks in Section 4.1. In this section a assuming tensile strength of the web $f_{ctm,web}$ will be assumed of $0.89f_{ctm}$. By assuming a tensile strength of the web of $0.89f_{ctm}$, the mean value of $\sigma_1/f_{ctm,web}$ for the 16 considered experiments becomes unity. The proposed tensile strength of the web is somewhat higher than the value $0.84f_{ctm}$ found in Section 3.1. This corresponds to the finding of Section 3.3, that σ_{1max} is average 6% higher according to Equations 3.1, 3.2 and 3.4 than according to the finite element analyses (Appendix C).

If σ_{1max} would be based on σ_1 along the centroidal axis, a strength of the web $f_{ctm,web}$ should be assumed of $0.79f_{ctm}$. This value is somewhat lower than the value $0.84f_{ctm}$ derived in Section 3.1. If the σ_{1max} is located at another location than the centroidal axis, which will be generally the case (Section 2.1.3), then this model will lead to an underestimation of σ_{1max}. This explains the lower value of $f_{ctm,web}$ which should be assumed when this model is used. The coefficient of variation significantly increases compared to the model that considers σ_1 over the entire height of the web (light grey area in Figure 3.6). This difference will be explained using the results of the experiment ŢP2 of Leonhardt for which σ_1/f_{ctm} is shown in Figure 3.10. The principal tensile stress σ_1 is determined from the cross sectional forces using Equations 3.1, 3.2 and 3.4. As shown in Figure 3.10, a maximum value for σ_1 is found at intersection of the top-flange and the

web. This value ($0.81f_{ctm}$) is significantly higher than the maximum of σ_1 along the centroidal axis ($0.55f_{ctm}$). Therefore, it is plausible that the formation of diagonal tension cracks is initiated around the location at which $\sigma_1 = 0.81f_{ctm}$. If σ_{1max} would have been only based on σ_1 along the centroidal axis, the resistance to diagonal tension cracking would have been underestimated significantly. Therefore, the model that is proposed in Section 4.1 considers σ_1 over the complete height of the web (light grey area of Figure 3.6) instead of only at the centroidal axis.

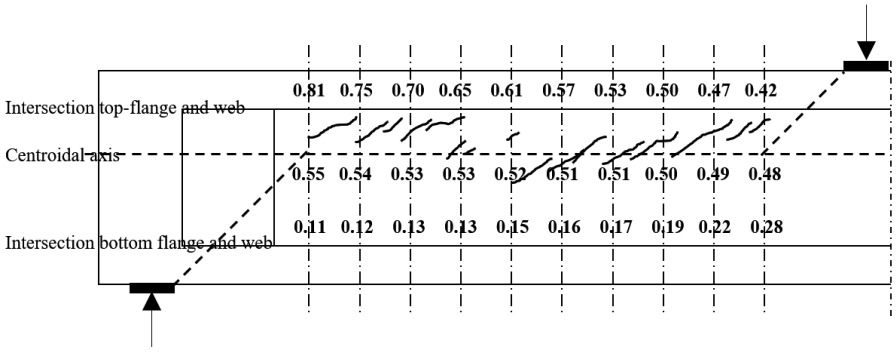

Figure 3.10. σ_{1max} / f_{ctm} at the load causing diagonal tension cracking for experiment TP2

3.5 Aspects affecting the accuracy for girders with flexural cracks

In the previous sections, the resistance to diagonal tension cracking of girders without flexural cracks is investigated. Determining the maximum principal tensile stress for these girders from linear elastic analyses is rather indisputable. As the effect of flexural cracks on cracking process was not present, experiments on girders without flexural cracks were suitable to investigate the effect of bi-axial behaviour, a statistical size effect and the distribution of principal tensile stresses around concentrated loads. Also for girders with flexural cracks it is common to determine the maximum principal tensile stress in the region without flexural cracks using Equations 3.1, 3.2 and 3.4. These equations assume a linear elastic stress distribution in the regions without flexural cracks, not disturbed by flexural cracks. For girders with flexural cracks this assumption is disputable. Flexural cracks at the edge of the region without flexural cracks can affect the stress distribution in regions without flexural cracks (Leonhardt et al. 1973). Moreover, as will be explained later in this section, flexural cracking itself could initiate diagonal tension cracking in the regions without flexural cracks.

The effect of flexural cracks on diagonal tension cracking is investigated using experiments from the diagonal tension cracking database (Section 2.2) with flexural cracks. The method to determine whether flexural cracks are present is already described in

Section 3.1 (and listed in Appendix B). As explained in Section 3.1, 16 of the 70 experiments in the diagonal cracking database were categorized as 'girders without flexural cracks' (these are used for the analyses in Sections 3.1 to 3.4). In this section, experiments will be used in which flexural cracks were present at diagonal tension cracking (Appendix B). Of the 70 experiments in the diagonal cracking database 43 were categorized as 'girders with flexural cracks'. To ensure the right categorization, only experiments were categorized for which hand calculations and the observations correspond. For 11 experiments, the calculations and observations did not match and these experiments were categorized as 'Unknown'(Appendix B) and were not further used for the analyses in the current section.

This section will illustrate that for a part of the experiments with flexural cracks, diagonal tension cracking were initiated by flexural cracks. To relate the experiments to whether a flexural crack caused diagonal tension cracking, the experiments are categorized in three types of diagonal tension cracking, based on a method that will be explained further in this section (Appendix E):

- type a: no flexural cracks are present (these correspond to the ones in Appendix B, these are not further used in this section, but included for completeness)
- type b: flexural cracks are present but these flexural cracks did not cause diagonal tension cracking
- type c: flexural cracks are present and these flexural cracks caused diagonal tension cracking.

Cracking type b will now be discussed. Even if flexural cracks are present, diagonal cracks can form independently of the formation of these flexural cracks. In other words, flexural cracks are present but do not cause diagonal tension cracking. An example for this type of diagonal tension cracking is shown in Figure 3.11, for the end part of the simply supported girder of experiment F2-B of Hanson (1964).

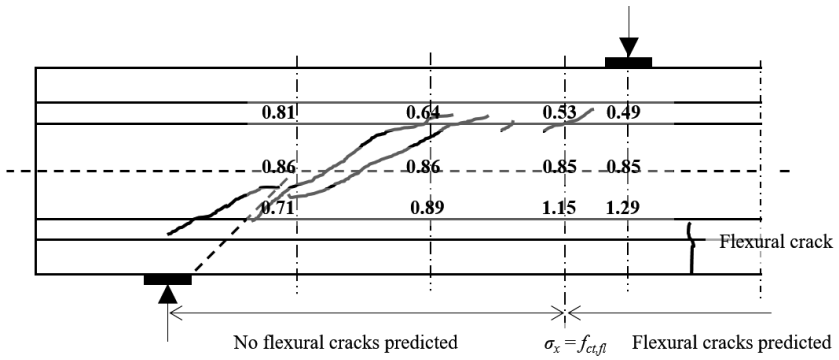

Figure 3.11. σ_{1max} / f_{ctm} at the load causing diagonal tension cracking for experiment F2-B

The regions with and without flexural cracks are predicted for the load that causes diagonal tension cracking and these are shown in this figure by the condition $\sigma_x = f_{ctm,fl}$. Figure 3.11 shows that the observed flexural crack is indeed located in the region in which flexural cracks are predicted. From Figure 3.11 it also appears that the diagonal tension cracks did not form in the vicinity of the flexural crack. This is an indication that the diagonal cracking was not caused by the formation of the flexural crack. This figure also shows σ_1 / f_{ctm} along three axis: the intersection of the top flange and the web, the centroidal axis and the intersection of the web and the bottom flange. The principal tensile stresses σ_1 are determined at load that causes diagonal tension cracking using Equations 3.1, 3.2 and 3.4. Although it is unclear what point is responsible for the initiation of the diagonal tension crack, it is clear that the principal tensile stress are significant over a large part of the web. The significant principal tensile stresses and the distance of the observed flexural crack to the diagonal tension crack makes it plausible that the stress condition in the web it selves caused diagonal tension cracking.

The 43 experiments with flexural cracks (Appendix B) are categorized as 'type b' if two conditions are met: (i) From the observations (a cracking pattern or a photo) it is clear that diagonal tension cracks did not form in the vicinity of a flexural crack and (ii) from calculations (Equations 3.1, 3.2 and 3.4) it is found that the principal tensile stresses are significant in the web (close to the strength of the web). It was found that 12 of the 43 experiments meet both these conditions (Appendix E).

Cracking type c will now be discussed. The formation of a flexural crack can be the cause for diagonal tension cracking. An example for this type of diagonal tension cracking is shown in Figure 3.12, for the continuously supported girder of experiment SR25 reported in Rupf et al. (2012). This figure presents the region between the point of contraflexure and the middle support. The regions with flexural cracks is predicted using the condition $\sigma_x = f_{ctm,fl}$ and the regions are shown in Figure 3.12. This figure shows that the observed flexural cracks are indeed closely related to this predicted region.

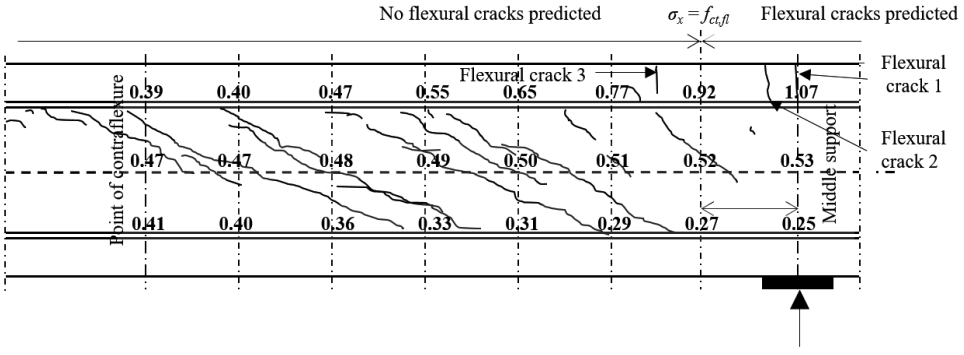

Figure 3.12. σ_{1max} / f_{ctm} at the load causing diagonal tension cracking for experiment SR25

Before diagonal tension cracks formed, only the shallow flexural crack straight above the middle support was present (described as 'Flexural crack 1' in Figure 3.12). At the load that causes diagonal tension cracking, the other flexural cracks (described as Flexural cracks 2 and 3 in Figure 3.12) and the diagonal cracks formed at once at the same load step (this finding is based on drawings of the cracks at each load stage combined with strain measurements of the stirrups). Figure 3.12 shows that diagonal tension cracks form directly below Flexural crack 3. This is an indication that the diagonal cracking was caused by the formation Flexural crack 3. Figure 3.12 shows σ_1 / f_{ctm}, in which σ_1 is determined from Equations 3.1, 3.2 and 3.4. The distribution of this ratio shows that the principal tensile stresses are significantly lower than the tensile strength of the web, over almost the entire web. Despite the low principal stresses in the web, diagonal tensile cracks formed in the entire considered part of the girder. It is plausible that flexural crack 3 caused an increase in the principal tensile stresses in the web below, which triggered the diagonal tension crack. This makes it plausible that the flexural crack caused diagonal tension cracking of the web.

The 43 experiments with flexural cracks are categorized as type c if two conditions are met: (i) From the observations (a cracking pattern or a photo) it is clear that diagonal tension cracks form in the vicinity of a flexural crack and (ii) from calculations it is found that the principal tensile stresses are rather low in the web. It was found that 25 of the 43 experiments meet both conditions (Appendix E).

Apparently, the principal tensile stress distribution, predicted using Equations 3.1, 3.2 and 3.4, is affected by the formation of flexural cracks. It is investigated whether the model as proposed in Section 3.4 is still suitable to predict diagonal tension cracking for the experiments categorized as crack types b and c (Appendix E). To investigate this, the web area without flexural cracks are considered (light grey areas in Figure 3.13). This includes the cross-section at which $\sigma_x = f_{ctm,fl}$. In this cross-section the principal tensile stress in the web will be maximum at the intersection of the tensile flange and the web. At this point, the longitudinal stresses will be lower than in the ultimate fibre. The value of principal tensile stress at this point also depends on the magnitude of the shear stresses. The higher the principal tensile stress is at this point, the more likely it is that the flexural cracks will trigger diagonal tension cracking in this point. When this point is also considered (light grey areas of Figure 3.13), the model could potentially be suitable to predict diagonal tension cracking, also if diagonal tension cracking is caused by flexural cracks (crack type c). This will now be evaluated.

In the regions of Figure 13 with flexural cracks, flexural shear is assumed to be governing and in the regions without flexural cracks, diagonal tension cracking. Figure 3.13 show the areas in which σ_1 were considered to determined $\sigma_{1\max}$ (light grey areas). In the

dark grey area at the support, the principal tensile stresses are not considered, as described in Section 3.3. For all of the 70 experiments, the light grey regions are determined and subsequently the maximum principal tensile stresses in these regions are determined at the load causing diagonal tension cracking (using Equations 3.1, 3.2 and 3.4). The found values for σ_{1max}, and σ_{1max} / f_{ctm}, are listed in Appendix E. Only the results for the experiments that could clearly be categorized as cracking types a, b and c are further considered.

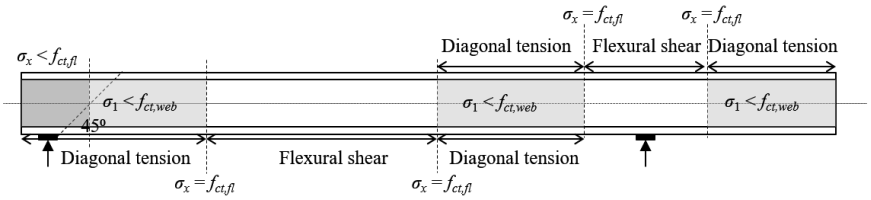

Figure 3.13. Proposed model for the resistance to diagonal tension cracking

Table 3.8 summarizes the statistical properties per cracking type as found from Appendix E. The statistical properties for the 16 experiments without flexural cracks correspond to Table 3.7 and are included for completeness and as reference. The mean values found for σ_{1max} / f_{ctm} for cracking type b and c are higher than that of cracking type a. As the tensile strength of the concrete is not affected by type of cracking, the higher ratios will be caused by an overestimation of σ_{1max}. For cracking type b and c, the coefficient of variation is found to be higher than for cracking type a. This indicates that diagonal tension cracking is less accurate to determine if flexural cracks are present.

Table 3.8. Statistical properties of σ_{1max}/f_{ctm} depending on type of diagonal tension cracking

	No flexural cracks (Section 3.4)	Flexural cracks present (Section 3.5)		
Type of diagonal tension cracking	(type a)	Diagonal tension cracks not caused by flexural cracks (type b)	Diagonal tension cracks caused by flexural cracks (type c)	Total (type b & type c)
Number of experiments	16	12	25	37
Mean σ_{1max}/f_{ctm}	0.89	1.12	0.96	1.01
Coefficient of variation σ_{1max}/f_{ctm}	5.2%	7.6%	10.9%	12.3%

The proposed model for girders with flexural cracks in Section 4.2 will therefore assume a tensile strength of the web $f_{ctm,web}$ of $1.01f_{ctm}$. By assuming a tensile strength of the web of $1.01f_{ctm}$, the mean value of $\sigma_1/f_{ctm,web}$ for the 37 considered experiments becomes unity.

This assumed value for the tensile strength of the web is higher than the one proposed for girders without flexural cracks (which was $0.89f_{ctm}$, Section 3.4). Apparently, the principal tensile stresses are somewhat overestimated for girders with flexural cracks. This overestimation can be compensated by assuming a higher tensile strength of the web. It is not necessary to make a distinction between whether diagonal tension cracks are caused by flexural cracks or not (between crack types *b* and *c*). Hence, with a coefficient of variation of 12.3% it is possible to rather accurately predict the resistance to diagonal tension cracking for girders with flexural cracks.

4

Proposed models for diagonal tension cracking

The current chapter describes the analytical models that are proposed to determine the resistance to diagonal tension cracking. The proposed models are based on the results of the analyses of Chapter 3. Also an overview is given of simplifications that are regarded as acceptable considering the accuracy found. Moreover some points of attention are enumerated that should be considered when determining the maximum principal tensile stress. Section 9.3 provides further guidance on the application of the models for engineering practice.

This chapter proposes two different models for diagonal tension cracking. Section 4.1 proposes a model for girders without flexural cracks, referred to as 'model A1'. Section 4.2 proposes a model for girders with flexural cracks, referred to as 'model A2'. Section 4.3 derives the design value for the proposed models, for a target reliability, that can be used in engineering practice. Because the design values of both models do not differ much, the most conservative value is chosen to be applicable for both models. As a result, it is possible to use one model to predict the resistance to diagonal tension cracking in engineering practice, Model A, regardless of whether flexural cracks are present.

The models that are proposed assume that diagonal cracks form in the web of a prestressed girder if the maximum principal tensile stress equals the derived tensile strength of the web. The models are applicable for both simply and continuously supported prestressed girders.

Equations from previous chapters are repeated (and renumbered) to make this chapter more self-contained.

4.1 Model A1: girders without flexural cracks

The analytical model proposed to determine the resistance to diagonal tension cracking for girders without flexural cracks is referred to as 'model A1' and is shown in Figure 4.1. Figure 4.1 also shows how the analyses of Chapter 3 are used in the proposed model by referring to the relevant sections.

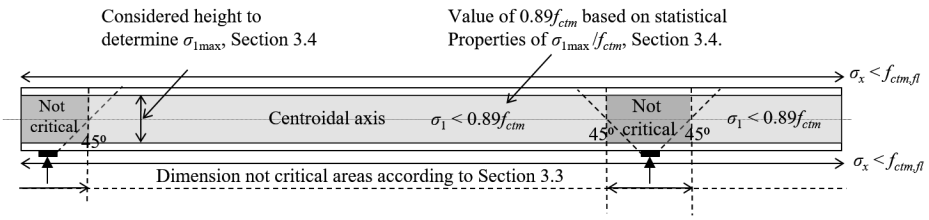

Figure 4.1. Model A1 –diagonal tension cracking for girders without flexural cracks

For girders without flexural cracks, in which no flexural cracks or flexural shear cracks are present, sufficient resistance to diagonal tension cracking is present if the maximum principle tensile stress in the web σ_{1max} is smaller than $0.89f_{ctm}$ (Equation 4.1). If a diagonal tension crack forms, a girder without (sufficient) stirrups is considered as failed (Section 2.1.1).

$$\sigma_{1\max} \leq 0.89 f_{ctm} \tag{4.1}$$

The fraction of 0.89 corresponds to the average σ_{1max} / f_{ctm} found from back calculations of experiments at the load that causes diagonal tension cracking (Section 3.4, Table 3.7). The maximum principal tensile stress σ_{1max} should be based on the maximum of σ_1 in the light grey regions of Figure 4.1.

Principal tensile stresses can be determined using Equation 4.2.

$$\sigma_1(z) = \frac{\sigma_x(z)}{2} + \sqrt{\left(\frac{\sigma_x(z)}{2}\right)^2 + \tau(z)^2} \tag{4.2}$$

In Equation 4.2, $\sigma_x(z)$ is the normal stress in the longitudinal direction and $\tau(z)$ is the shear stress, both determined assuming a linear elastic stress distribution. For monolithic structures, $\sigma_x(z)$ can be determined by Equation 4.3, and $\tau(z)$ by Equation 4.4. In these equations z is the considered distance from the centroidal axis, I_c is the second moment of area, $S_c(z)$ is the first moment of area, A_c is the area of the concrete cross-section and $b_w(z)$ is the width of the web.

$$\sigma_x(z) = \frac{N_E}{A_c} + \frac{M_E\, z}{I_c} \tag{4.3}$$

$$\tau(z) = \frac{V_E S_c(z)}{b_w(z)\, I_c} \tag{4.4}$$

The maximum principal tensile stresses σ_{1max} should be based on σ_1 over the height of the girder (light grey area of Figure 4.1). When, as a simplification, σ_{1max} would have been based on σ_1 along the centroidal axis, the consistency of the predicted resistance to

diagonal tension cracking decreases significantly (Section 3.4). This simplification is therefore not used in model A1.

Around the support of a simply supported girder, σ_{1max} is located outside the dark grey region as shown in Figure 4.1. This region is defined by a vertical line through the point that is the intersection of the elastic centroidal axis and the 45° inclined line from the inner edge of the support. This dark grey region is not critical because of the presence of σ_z, which is neglected in Equation 4.5, and the favourable distributions of σ_x and τ (Section 3.4). It is noted that simply supported girders are designed in a way that the moment due to prestressing will not cause flexural cracks in the ultimate fibre at the top flange at the girder ends. If this is the case, the condition $\sigma_x < f_{ctm,fl}$ will automatically be met at the girder ends. Also the cross-section above the intermediate support could remain free of flexural cracks. If this is the case, the same considerations are applicable as for the end support. Therefore, if the condition $\sigma_x < f_{ctm,fl}$ is met, it is also for the intermediate supports not necessary to consider the principal tensile stresses in the dark grey region as shown in Figure 4.1.

Equation 4.3 shows that $\sigma_x(z)$ depends on M_E (Equation 4.6). Therefore, also σ_1 depends on M_E (Equation 4.5). In engineering practice, it is often unclear if a load combination that results in a maximum V_E will also cause the highest σ_{1max}. Therefore, different load combinations should be considered to determine σ_{1max} (Hegger et al. 2015).

Model A1 uses the following assumptions which makes it possible to assess bridges in a rather simple way:

- Diagonal cracks form at the instant the maximum principal stress equals the tensile strength of concrete.
- Bi-axial behaviour of concrete is not considered.
- A statistical size effect is not considered.
- The presence of stirrups does not affect the resistance to diagonal tension cracking.
- The longitudinal and shear stresses are determined from the cross-sectional properties of concrete A_c, $S_c(z)$ and I_c, and the effect of the stiffness of the reinforcing and prestressing steel on these stresses is not considered.

Considering the high accuracy of the predicted resistances, the effect of these assumptions on the predicted resistance is limited.

The model assumes that diagonal cracks form at the instant the maximum principal stress equals the tensile strength of concrete. In a nonlinear finite element analyses (Slobbe et al. 2017), it was found that diagonal tension cracks did not directly form at the instant that the tensile strength of the concrete is reached at one location. This is

because, at the load step before diagonal tension cracking, the principal tensile strains already exceeded the tensile strain associated with the tensile strength. Apparently some redistribution occurred. Due to tension softening, the tensile strength does not immediately drop to zero. However, as the proposed model is found to be accurate there is little reason to further investigate this possible effect of redistribution.

As described in Section 3.2, the tensile strength depends on the lateral principal compressive stresses (bi-axial behaviour). If the level of prestressing increases, σ_{cp}/f_{cm} decreases, consequentially σ_2/f_{cm} decreases and also the tensile strength decreases due to bi-axial behaviour (Equation 2.7). As a consequence, diagonal tension cracking will occur at a lower principal tensile stress. However, bi-axial behaviour is already implicitly considered by assuming a tensile strength of the web of 89% in the proposed model. Moreover, it is likely that $0.89f_{ctm}$ is an upper bound for bridges in practice. For existing bridges in the Dutch Highways (designed with a design code before 1974, Table 1.1) σ_{cp}/f_{cm} varies between $-0.20 \leq \sigma_{cp}/f_{cm} \leq -0.04$. For the experiments considered to derive $f_{ctm,web,}$ σ_{cp}/f_{cm} varies between $-0.28 \leq \sigma_{cp}/f_{cm} \leq -0.13$. For bridges in practice it is also likely that areas with high principal tensile stresses will be rather small and will not significantly affect the resistance to diagonal tension cracking[2]. Therefore, and given the accuracy found (Table 3.8), bi-axial behaviour and statistical size effect are no part of the proposed model. Besides, bi-axial behaviour and size effect can be considered by applying Equation 3.10 (Section 3.3) if for a specific structure there is still reason to consider these phenomena.

For girders without shear reinforcement, diagonal tension cracking is a brittle failure mode in which the girders are not able to redistribute the stresses after cracking. Therefore, all phenomena that could affect the principal tensile stress should be considered. Depending on the type of structures and whether the structure is post-tensioned or pretensioned, the following points of attention should be considered when determining maximum principal tensile stress:

– If the considered structures consist of both a precast part and a cast in-situ part, the construction phases should be taken into account. Moreover, the different moduli of elasticity of both parts should be considered.

[2] A recent research, in which the 'cracking size effect' has been investigated (Bentz 2019, Bentz 2020), shows that a lower bound of the cracking size effect is found for 30 litres of the Highly Stressed Volume (HSV). This HSV is defined as the volume within which the tensile stress is at least equal to 85% of the maximum value. For higher volumes of the HSV, the cracking strength does not further reduce. This lower bound is found by considering the results of numerous tension tests. This is an additional argument for not considering the statistical size effect for the structural assessment of existing bridges.

– If the equations are applied for cross-sections within the transmission length of the structure, both $\sigma_x(z)$ and $\tau(z)$ should be determined considering the prestress is not fully introduced. Equations for this application can be found in *fib* (2012), numbered as 7.3.46 and 7.4-47.
– A reduction of $b_w(z)$ should be considered to account for the risk that the ducts are not fully grouted for post-tensioned structures. An equation for this application can be found in NEN (2005), numbered as 6.16.
– The effects of imposed deformations should be considered (temperature, support settlement, shrinkage and creep).
– The effects of transverse bending should be considered.

Especially the regions on both sides of the mid support, imposed deformations could affect the maximum principal tensile stress. Section 9.3.1 describes further considerations for the application of the proposed models for these support conditions.

4.2 Model A2: girders with flexural cracks

The analytical model proposed to determine the resistance to diagonal tension cracking for girders with flexural cracks is referred to as 'model A2' and is shown in Figure 4.2. Figure 4.2 also shows how the analyses of Chapter 3 are used in the proposed model by referring to the relevant sections.

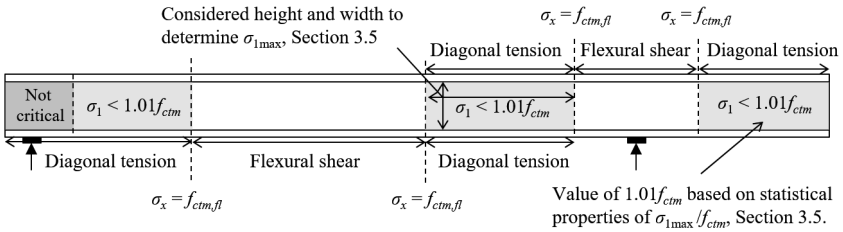

Figure 4.2. Model A2 –diagonal tension cracking for girders with flexural cracks

Model A2 is only applicable for the regions of the girders with flexural cracks (Figure 4.2), that remain free of flexural cracks (light grey areas in Figure 4.2). The regions without flexural cracks are limited by the condition $\sigma_x < f_{ctm,fl}$. For regions in which flexural cracks are present, diagonal cracks will develop from these flexural cracks. These regions are shown white in Figure 4.2. The resistance to flexural shear cracking should be based on appropriate resistance models. This is further explained in Section 9.3.1, in which the equations given by the Eurocode (NEN 2005) are used as an example of how to determine the shear resistance in the regions with flexural cracks.

For girders with flexural cracks, sufficient resistance to diagonal tension cracking is present if the maximum principle tensile stress $\sigma_{1\max}$ is smaller than $1.01 f_{ctm}$ (Equation 4.5).

$$\sigma_{1\max} \leq 1.01 f_{ctm} \tag{4.5}$$

The fraction of 1.01 corresponds to the average $\sigma_{1\max} / f_{ctm}$ found from back calculations of experiments at the load that causes diagonal tension cracking (Section 3.5, Table 3.8).

Just like for model A1, the maximum principal tensile stresses $\sigma_{1\max}$ should be based on σ_1 over the height of the girder (light grey area of Figure 4.2). When, as a simplification, $\sigma_{1\max}$ would have been based on σ_1 along the centroidal axis, the consistency of the predicted resistance to diagonal tension cracking decreases significantly (Section 3.5). This simplification is therefore not used in model A2.

Figure 4.2 shows the regions with flexural cracks ($\sigma_x > f_{ctm,fl}$, as white areas) and the regions without flexural cracks ($\sigma_x < f_{ctm,fl}$, as grey areas). The flexural cracks at the edge of the light grey regions can initiate diagonal tension cracking. Whether this cracking mode will occur can be determined by examining the principal tensile stresses along the edge of the light grey region (Section 3.5). Eventually, diagonal tension cracking is predicted if the principal tensile stresses are equal to the tensile strength of the web (Equation 4.5) anywhere in the light grey area in Figure 4 2, regardless of whether these are caused by flexural cracks.

Model A2 uses the same simplifications as model A1. Just like model A1, it is considered as unnecessary to further investigate these simplifications considering the accuracy of the predicted resistances. Due to the presence of flexural cracks, the variation increases significantly when flexural cracks are present (Table 3.8). This is an additional argument for girders with flexural cracks that it is not worth the effort to consider bi-axial behaviour and size effect. For model A2, the same points of attention should be considered when determining the maximum principal tensile stress as for model A1, given the brittle failure mode.

4.3 Design values for the proposed models

This section determines the design value for the tensile strength of the web that can be used to determine the resistance to diagonal tension cracking. The design value is derived to reach a failure probability of 10^{-4} for a 50 year reference period, which corresponds to a target reliability index $\beta_t = 3.8$. If another failure probability is envisaged, the same approach can be used to determine the associated design value for the tensile strength of the web. The design value for the tensile strength is based on the

statistical properties of σ_{1max}/f_{ctm} as found in Section 3.5, listed in Table 3.8 and in Appendix E. These statistical properties concern the uncertainty of the resistance model. The uncertainties regarding the model, the geometry and the material are implicitly included. The design value for the tensile strength is derived using the approach described in Annex D7.3 of the NEN (2011). It is noted that the design value for the tensile strength is related to the resistance of the model and is no material property.

The design value X_d for the basic variable X, which equals σ_{1max}/f_{ctm}, can be determined using Equation 4.6 as described in NEN (2011). X is assumed to follow a lognormal distribution, which is a common distribution function for the resistance and is also used in the design value format of the Eurocode.

$$X_d = \eta_d e^{(m_y - k_{d,n} s_y)} \tag{4.6}$$

$$m_y = {}^1/_n \sum \ln(X) \tag{4.7}$$

$$s_y = \sqrt{\ln({V_x}^2 + 1)} \tag{4.8}$$

In Equation 4.6, η_d is de design value of the conversion factor and should cover all uncertainties in a real structure that are not covered by the considered experiments. For the derivation of the design value for the tensile strength, a factor of 1/1.15 is used, to be consistent with the design value format of the Eurocode. The design value for the fractile factor ($k_{d,\eta}$) can be found from Table D2 in NEN (2011). Table D2 assumes that the design value corresponds to $\alpha_R\beta_t$, in which α_R is the first-order reliability method sensitivity factor for the resistance, which equals 0.8, and β_t is the target reliability index which is equated to 3.8. Equation 4.7 concerns the equation for m_y, which is the mean of the basic variable in a lognormal distribution and Equation 4.8 concerns the equation for s_y, which is the coefficient of variation in a lognormal distribution. In Equation 4.8, V_x is the coefficient of variation.

For model A1, the design value X_d is determined for the statistical properties of the 16 experiments without flexural cracks (Table 3.8, Appendix E). The design value X_d is derived by applying these statistical data in Equations 4.6 to 4.8. A design value X_d is found of 0.652 (Table 4.1), which means that $\sigma_{1Ed,max} \leq 0.652 f_{ctm}$. If the relation $f_{ctk} = 0.7 f_{ctm}$ is used, this equation can also be written as $\sigma_{1Ed,max} \leq 0.931 f_{ctk}$. If subsequently a partial factor γ_c is used of 1.5, which means that $f_{ctd} = f_{ctk} / 1.5$, the equations can be rewritten as $\sigma_{1Ed,max} \leq 1.40 f_{ctd}$.

Also for model A2, the design value X_d is determined, but now for the statistical properties of the 37 experiments with flexural cracks (Table 3.8, Appendix E). A design value

X_d is found of 0.599 (Table 4.1), meaning that $\sigma_{1Ed,\max} \leq 0.599 f_{ctm}$, which can be rewritten, using the same assumptions as for model A1, as $\sigma_{1Ed,\max} \leq 1.28 f_{ctd}$.

Table 4.1. Derivation of design value X_d for diagonal tension cracking

	n	m_y	s_y	$k_{d,\eta}$	X_d
Model A1	16	-0.121	5.2%	3.19	0.652
Model A2	37	0.007	12.2%	3.11	0.599

Although it is somewhat conservative for model A1, it is for simplicity proposed to use a design value of $1.28 f_{ctd}$ for both models (Equation 4.9). The design value of the resistance to diagonal tension cracking is referred to as model A and can be applied in practice irrespectively of whether flexural cracks are present. It is noted that some conservatism is desirable for model A1, to compensate for the less favourable distribution of the shear stresses in bridges, which are loaded with distributed loads, compared to the experiments used to derive the design value, which are loaded with a concentrated load (Section 3.3). As a consequence of using one design value, it is possible to use just one model for diagonal tension cracking for application in engineering practice.

$$\sigma_{1\max,Ed} \leq 1.28 f_{ctd} \tag{4.9}$$

It is noted that instead of limiting the design value of the maximum principal tensile stress σ_{1Ed} to $1.28 f_{ctd}$ and using a $\gamma_c = 1.5$ is also possible, if preferred, to limit σ_{1Ed} to $1.00 f_{ctd}$ and use a partial factor γ_c of 1.17.

The design value of the resistance to diagonal tension cracking that corresponds to this condition is defined as $V'_{Rd,c}$. For monolithic structures, Equation 4.10 can be derived if Equation 4.9 is combined with Equations 2.14 and 2.15. The apostrophe in $V'_{Rd,c}$ indicates that the equation is only applicable in regions without flexural cracks.

$$V'_{Rd,c} = \frac{I_c b_w(z)}{s_c(z)} \sqrt{(1.28 f_{ctd})^2 + \sigma_x(z)(1.28 f_{ctd})} \tag{4.10}$$

PART 2: SHEAR RESISTANCE AFTER DIAGONAL TENSION CRACKING

5

Literature review on prestressed girders with stirrups

This chapter describes a literature review on shear resistance of girder with stirrups. Section 5.1 provides an overview of models from literature intended to determine the shear resistance of prestressed girders with stirrups. Section 5.2 mutually compares the models of Section 5.1. Section 5.3 describes a database that is compiled out of experiments from literature on prestressed girders with stirrups for which failure could be related to diagonal tension cracks. Section 5.4 evaluates to what extend the research questions are answered based on the literature study. Based on these answers, an approach is chosen to derive the model for the determination of the shear resistance in regions without flexural cracks.

5.1 Models from literature

This section provides an overview of models from literature that are intended to determine shear resistance of prestressed girders with stirrups. The models are intended to determine shear resistance in general or shear resistance in regions without flexural cracks specifically. The models that are described are the variable angle truss model (Section 5.1.1), an empirical model derived by MacGregor et al. (Section 5.1.2), models based on the Modified Compression Field Theory (Sections 5.1.3-5.1.6), an empirical model suggested by Leonhardt (Section 5.1.7) and a model based on arch action as suggested by Huber (Section 5.1.8).

In this chapter, the findings from the literature review are frequently complemented with considerations. These consideration are aimed to contribute to the development of an accurate model for the resistance of prestressed girders with stirrups in regions without flexural cracks.

5.1.1 Variable angle truss model

The variable angle truss model, as used in the Eurocode (NEN 2005), is intended to determine both the shear and moment resistance of reinforced and prestressed members with stirrups. In this section the determination of shear resistance is explained. No distinction is made between the resistance in regions with and without flexural cracks. Walraven described the model in several publications (Walraven et al. 1995, 1999, Walraven 2002). In these publications the method is referred as ‘variable inclination strut method’. The explanation of the variable angle truss model given in this section is

based on the model described in these publications. The alternative name 'variable angle truss model' is used by Collins et al. (1997) and this name is adopted in this dissertation.

The variable angle truss model is based on equilibrium, assuming the presence of a smeared truss in the girder. The shear transfer mechanisms of the variable angle truss model are illustrated in Figure 5.1, for a free body diagram that is cut along a compressive strut. Figure 5.1 could be interpreted as if the vertical components are only resisted by the stirrups and there is no contribution of aggregate interlock. However, θ is the angle of the compressive strut which does not corresponds to angle of the cracks. Because aggregate interlock is present, the angle of the compressive struts is smaller the angle of the cracks. The variable angle truss model therefore implicitly takes into account the contribution of aggregate interlock.

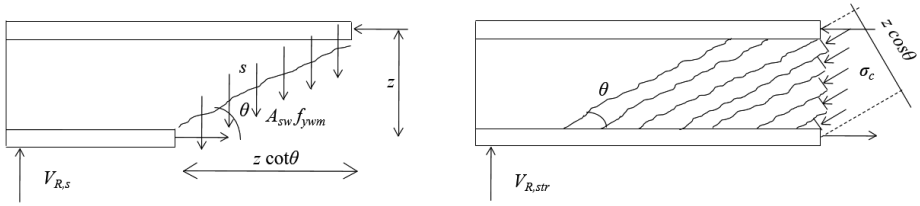

Figure 5.1. Variable angle truss model (Walraven 2002)

Vertical components of the truss are represented by the stirrups. For stirrups that are applied perpendicular to the longitudinal axis, the maximum shear that can be resisted by stirrups ($V_{R,s}$) is represented by Equation 5.1.

$$V_{R,s} = {}^{A_{sw}}/_{S}\; z\, f_{ywm}\, \cot\theta \tag{5.1}$$

In this equation, A_{sw} is the area of the stirrups, s is the spacing of stirrups, f_{ywm} is the yield strength of the stirrups in tension and θ is the inclination of the compressive struts. The distance between the chords parallel to the longitudinal axis is assumed to be equal to the internal lever arm z.

The internal lever arm is the distance between the centre of the tensile forces in longitudinal direction in the steel and the centre of the longitudinal compressive stresses in the concrete. It is unclear how this internal level arm should be determined according to the variable angle truss model. From the background document of the Eurocode, in which the variable angle truss model in included, it appears that the lever arm is set to a defined ratio of the effective depth d. The internal lever arm for reinforced structures is assumed to be equal to $0.9d$, independently whether flanges are present. The equation for the internal lever arm for prestressed concrete is not explicitly described. However, in the

background document predictions of the resistance were carried out for the variable angle truss model (Walraven 2002). As part of the current dissertation these predictions were analysed. This was done for the predictions of the experiments carried out by Lyngberg (1976), Hanson et al. (1964), Leonhardt et al. (1973) and Levi et al. (1993). It was found that an internal lever arm of $0.95d$ was assumed for prestressing steel.

The equation for the effective depth of the combined prestressing and reinforcing steel is not explicitly described in the Eurocode (NEN 2005). By analysing the predictions in the background document, as part of the current dissertation, it was found that for these girders a weighted mean value was used to determine the internal lever arm z (Equation 5.2). In Equation 5.2, z_p is the internal lever arm of prestressing steel, z_s is the internal lever arm of reinforcing steel, A_p is the area of prestressing steel and A_s is the area of reinforcing steel.

$$z = \left(z_s A_s + z_p A_p\right)/\left(A_s + A_p\right) \tag{5.2}$$

Diagonal struts of the truss are represented by concrete(Figure 5.1, right part). The area perpendicular to the compressive struts equals to $b_w\, z\, \cos\theta$. In this equation b_w is the width of the web. The force in the compressive struts is equal to $V_{R,str}/\sin\theta$. The strength of the struts is assumed to be equal to $\alpha_{cw}\, \nu\, f_{cm}$, in which f_{cm} is the concrete compressive strength of a cylinder, ν is the concrete effectiveness factor and α_{cw} is a factor addressing the effect of prestressing. The ultimate shear associated with the crushing of the compressive strut is given by Equation 5.3.

$$V_{R,str} = b_w\, z\, \alpha_{cw} \nu\, f_{cm}\, \sin\theta\, \cos\theta \tag{5.3}$$

The background of the effectiveness factor for concrete ν is given by Nielsen et al. (2011). The effectiveness factor is introduced because the concrete compressive strength of the web is smaller than the concrete compressive strength of a cylinder (f_{cm}). The main reason is that the concrete is cracked and cracking reduces the strength. The transfer of stresses from the reinforcement to the concrete between macro cracks, causes micro cracks. These micro cracks are assumed to be the main reason for the strength reduction in compressive struts. The strength reduction is affected by the compressive strength of concrete, the diameter of the reinforcement, the reinforcement ratio, texture of the surface of the bars and reinforcement stresses. However, based on an extensive experimental test programme it was found that it was sufficient to base the effectiveness factor only on the concrete compressive strength. Based on the experimental test programme, two equation were derived: $\nu = 0.8 - f_{cm} / 200$, applicable for values of f_{cm} up to 75 N/mm^2, and $\nu = 1.9 / f_{cm}^{0.34}$ for values of f_{cm} between 75 and 100 N/mm^2. As a conservative simplification Equation 5.4 was suggested applicable for all values of f_{cm}

(Nielsen et al. 2011). This equation is adopted in the Eurocode (NEN 2005). The equations above are derived for experiments with a significant amount of shear reinforcement, of which the consequence will be discussed hereafter.

$$\nu = 0.6\,(1 - {}^{f_{cm}}\!/_{250}) \tag{5.4}$$

The factor α_{cw} addresses the effect of prestressing on the strength of the compressive struts. The factor depends on the ratio of the stress in the concrete in longitudinal direction in the centre of gravity (σ_{cp}) and the mean concrete cylinder strength (f_{cm}). For $0 \leq \sigma_{cp}/f_{cm} \leq 0.25 f_{cm}$, $\alpha_{cw} = 1 + \sigma_{cp}/f_{cm}$, for $0.25 f_{cm} \leq \sigma_{cp}/f_{cm} \leq 0.50 f_{cm}$, $\alpha_{cw} = 1.25$ and for $0.50 f_{cm} \leq \sigma_{cp}/f_{cm} \leq f_{cm}$, $\alpha_{cw} = 2.5(1 - \sigma_{cp}/f_{cm})$. The equations assume that for concrete compressive stresses up to a value of $0.6 f_{cm}$, the strength of the concrete struts increases by the presence of prestressing. The equations were validated by carrying out predictions for the resistances with and without α_{cw} and comparing these with the experimentally found resistances (Walraven 2002). Both the level of overestimation of the resistance and the scatter were found to reduce, if α_{cw} according to the given equations is applied.

The variable angle truss model is a lower bound approach based on the theory of plasticity. According to the theory of plasticity the largest resistance is found if the stirrups yield and the concrete struts crush at the same time. To meet this condition, the maximum resistance of the stirrups according to Equation 5.1 must be equal to the maximum resistance associated with crushing of the compressive struts according to Equation 5.3. By assuming both equations are equal, the strut inclination according to Equation 5.5 is found. Equation 5.6 shows the equation for ψ_{vat} which is used in Equation 5.5. The subscript 'vat' is used to distinguish between the factor ψ_{vat} which is frequently used in literature and which equals to $\rho_{sw} f_{ywm} / f_{cm}$.

$$\tan\theta = \sqrt{{}^{\psi_{vat}}\!/_{(1-\psi_{vat})}} \tag{5.5}$$

$$\psi_{vat} = \rho_z f_{ywm} / \nu\, \alpha_{cw} f_{cm} \tag{5.6}$$

If the value of ψ_{vat} decreases, the model will predict a decrease of the angle of the compressive struts, activating more stirrups (Equation 5.5). As a result of the smaller inclination of the struts, the stress in the struts increases (Equation 5.3). This decrease of the angle of the compressive struts is possible until the stress in the concrete reaches its compressive strength. This predicted behaviour is confirmed with experiments (Walraven et al. 1995, Walraven et al. 1999). These experiments concern normal, lightweight and high strength reinforced concrete girders with shear reinforcement ratios between 0.36% and 3.86%. In these experiments, the principal strains in the web of the experiments were measured using LVDT's. These are compared to the strut inclination

θ as predicted using the variable angle truss model. The predictions show good similarity with the measurements.

In the variable angle truss model, the maximum angle of the compressive strut is assumed to be 45°, which is associated with crushing of concrete without the yielding of the stirrups ($V_{R,\max}$). Also this behaviour is confirmed with the experiments (Walraven et al. 1995, Walraven et al. 1999). Yielding of stirrups and crushing of concrete was observed for experiments with low values of ψ_{vat}. For experiments with high values of ψ_{vat}, crushing of concrete before yielding of stirrups was observed.

The inclination of the compressive struts is limited to 21.8°. As explained, the concrete effectiveness factor v according to Equation 5.4 is derived by Nielsen et al. (2011) using experiments with values of $\psi_{vat} > 0.05v$ (which correspondents with a values of ψ_{vat} of about 0.023). Nielsen did not investigate the application for lower values of ψ_{vat}. According to Nielsen et al. (2011) the effectiveness factor v is the product of v_c, that represents the strength reduction by micro cracks, and v_s, which is the sliding reduction factor. However, Nielsen assumed that if sufficient stirrups are present, crack sliding does not have to be taken into account and v_s equals 1. For low values of ψ_{vat} the variable angle truss method was found to overestimate the shear resistance. This was found using experiments on non-prestressed girders (Walraven 2002). Apparently the strength of the compressive struts is overestimated using Equation 5.4 for low values of ψ_{vat}. The overestimation could be compensated by setting a limit of θ of 21.8° ($\cot\theta = 2.5$). This leads to conservative predictions for low values of ψ_{vat}.

As part of this dissertation it is argued to what extend the variable angle truss model is suitable for the determination of the shear resistance in regions without flexural cracks. Two considerations are described.

The first consideration, regarding regions without flexural cracks, concerns the effect of the longitudinal strain on the shear resistance. For reinforced concrete girders, without prestressing, the longitudinal strain in the critical cross-section is significantly larger than zero. Large longitudinal strains result in lower shear resistance. For prestressed girders on the other hand, the longitudinal strains are lower. Due to the smaller crack width, a higher shear force can be transferred in the cracks by aggregate interlock. To take into account this additional contribution, the variable angle truss should allow a smaller strut angle. However, the model is independent of the longitudinal strain and valid for both girders with and without flexural cracks. Therefore, the model has no mechanism which could take into account this additional contribution for prestressed girders while remain conservative for reinforced concrete girders.

The second consideration, regarding prestressed girders in general, concerns the conservatism of the prediction for prestressed girders. This is investigated, as part of this

dissertation, using experiments on 76 prestressed I and T shaped girders that failed in shear that are reported in the background document of the Eurocode (Walraven 2002). The resistances for these experiments are predicted using the variable angle truss model. The predicted resistances are compared to the experimentally found resistances. The determined mean value and the coefficient of variation of the experimentally found to predicted resistance ratio are shown in Table 5.1. A distinction is made between whether the lower limit for θ was found to be governing. The predictions for the 40 experiments for which the lower limit was found governing were found to be extremely conservative and inconsistent (Table 5.1). The predictions for the 36 experiments for which the lower limit was not governing the predictions, were found to be much less conservative and much more consistent.

Table 5.1. Test-to-predicted shear resistance ratio for variable angle truss model

	Lower limit for θ (21.8°) found as governing	
	no	yes
Number of experiments	36	40
Mean $V_{R,exp}/V_{R,vat}$	1.22	2.03
Coefficient of variation $V_{R,exp}/V_{R,vat}$	13%	39%

For reinforced concrete the variable angle truss model overestimates the resistance for low values of ψ_{vat} (Walraven 2002). This is the reason to limit θ to 21.8°. It is additionally investigated, as part of this dissertation, if for prestressed girders the resistance is also overestimated if θ is not limited. Figure 5.2 shows the predictions (lines) and the experimentally found resistances (dots) for the 76 experiments of the back-ground document (Walraven 2002). The continuous line shows the predicted resistance without limitation of θ and the dashed line with limitation of θ ('cut-off').

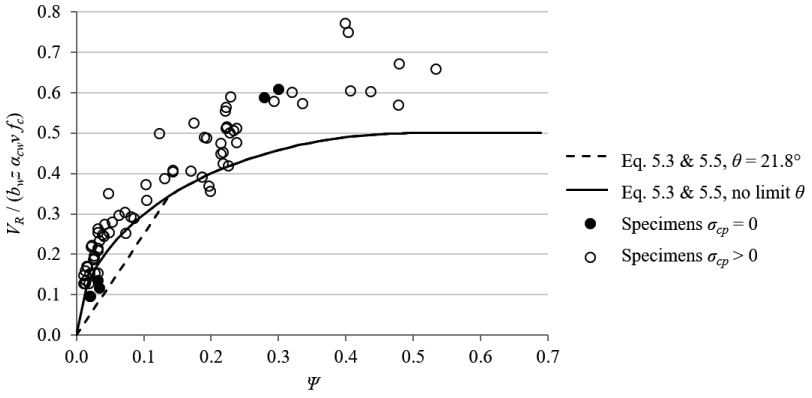

Figure 5.2. Experimentally found and predicted resistances for 76 experiments with & without limit θ

As appears from the figure, the number of experiments for which the resistance is overestimated without limitation of θ, is limited. Moreover, some of these experiments, appeared to be reinforced experiments without prestressing (black dots in Figure 5.2). These were probably selected because the experiments were part of a series of experiments that mainly contained experiments with prestressing. Based on the data, it is questionable if the reported limitation of the inclination of the comprise struts is also necessary for prestressed girders.

As described by Nielsen et al. (2011), not only crushing of the concrete struts, but also crack sliding along the initial crack appears to be a possible failure mode, especially for girder with a low amount of shear reinforcement. However, an appropriate concrete effectiveness factor for this failure mode is yet unknown.

5.1.2 Empirical model of MacGregor et al.

MacGregor et al. (1960) derived a model which is intended to determine shear and moment resistance for prestressed girders with stirrups. The shear resistance models for prestressed girders in the ACI (2008) are based on this model. In this section the determination of shear resistance is explained. In the model, a distinction is made between the resistance to flexural shear failure ($V_{R,FSF}$) and web shear failure ($V_{R,WSF}$). The minimum of both determines the governing failure mode (Table 5.2, Equation 5.10).

Table 5.2. Overview model MacGregor et al. (1960)

Resistance to flexural shear failure	$V_{R,FSF}$	=	$V_{R,FSC}$	+	$V_{R,s}$	(5.7)
Resistance to web shear failure	$V_{R,WSF}$	=	$V_{R,DTC}$	+	$V_{R,s}$	(5.8)
Resistance to diagonal cracking $V_{R,DC}$		=	Minimum ($V_{R,FSC}$, $V_{R,DTC}$)			(5.9)
Resistance to shear failure V_R =	Minimum ($V_{R,FSF}$, $V_{R,WSF}$)					(5.10)

MacGregor et al. (1960) derived a model based on the assumption that the shear resistance is equal to the resistance to diagonal cracking ($V_{R,DC}$) plus a contribution of stirrups ($V_{R,s}$). These shear transfer mechanisms are shown in Figure 5.3. This figure is drawn in a similar way as Figure 5.1 (variable angle truss model) so these models can easily be compared. It is noted that diagonal cracking is not a shear transfer mechanism after diagonal cracking. The physical relevance of this figure is thus limited. Diagonal cracking can be diagonal tension cracking or flexural shear cracking (Figure 1.1). The minimum of both determines which cracking mode is governing (Table 5.2, Equation 5.9).

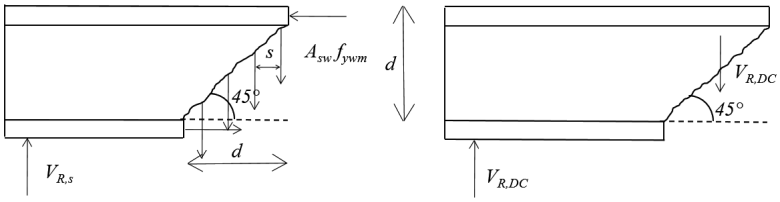

Figure 5.3. Empirical model MacGregor et al. (1960)

The resistance to both diagonal tension cracking ($V_{R,DTC}$) as flexural cracking ($V_{R,FC}$) are based on the concrete tensile strength (which will be explained hereafter). Additionally, three relations are determined empirically:

- The increase in resistance between flexural shear cracking and flexural shear failure.
- The increase in resistance between diagonal tension cracking and web shear failure.
- The increase in the resistance between flexural cracking ($V_{R,FC}$) and flexural shear cracking ($V_{R,FSC}$).

The empirical relations are based on experiments carried out by MacGregor et al. (1960) and experiments carried out by Sozen et al. (1959).

In the model that MacGregor used for the prediction of diagonal tensile cracking, the tensile strength of the web is based on the shear stress resistance along the centroidal axis (as described in Section 2.1.5). Unlike Equation 2.17, the tensile strength of the web is assumed to be 80% of the flexural tensile strength ($0.8f_{ctm,fl}$). The flexural tensile strength was subsequently derived from f_{cm} which was determined by carrying out compressive test on cylinders. The equation $f_{ctm,fl} = 21 / (4 + 83/ f_{cm})$ was used, expressed in N/mm^2. This equation was derived for small-coarse aggregate by Sozen et al. (1959). The predicted diagonal cracking resistance was found to be accurate. This was found by MacGregor et al. (1960) by comparing the predicted and experimentally found resistances for 32 experiments (experiments of both MacGregor et al. and Sozen et al.). Unlike Equations 2.16, 2.17 and 2.18, the stresses were based on the presence of both concrete and reinforcement. Thus in Equation 5.11, I and S_{cg} are used that are based on the presence of both materials ('transformed cross-sections').

$$V_{R,DTC} = \frac{I\, b_w}{S_{cg}} \sqrt{0.8f_{ctm,fl}{}^2 - \sigma_{cg} 0.8f_{ctm,fl}} \tag{5.11}$$

MacGregor's model assumes that the resistance to flexural shear cracking consists of two components (Equation 5.12). The first component is the resistance to flexural cracking ($V_{R,FC}$). $V_{R,FC}$ is determined by calculating the shear force at which the tensile stress in the ultimate fiber equals $f_{ctm,fl}$. Thus $V_{R,FC}$ depends on the forces in each cross-section

and will differ along the girder axis. The second component is the shear force needed to transform the flexural crack into a flexural shear crack. This term is determined empirically from experiments in which a flexural crack were observed that turned into a flexural shear crack. To derive this empirical relation, an initiating shear crack was assumed at a location that is the sum of 1/4 of the girder height and 1/6 of the shear span from the concentrated load. The increase of shear force to transform the flexural crack into a flexural shear was related to the resistance to diagonal tension cracking. A value of 1/15 $V_{R,DTC}$ was found appropriate (Equation 5.12, Figure 5.4).

$$V_{R,FSC} = V_{R,FC} + \frac{1}{15} V_{R,DTC} \tag{5.12}$$

Figure 5.4 was reproduced as part of this dissertation using the data of MacGregor (1960). In this figure both the experimentally found and the predicted resistance to diagonal cracking are shown as ratio of the predicted resistance to diagonal tension cracking. Both the predicted resistances to diagonal tension cracking (Equation 5.11, horizontal dashed line) and to flexural shear cracking (continuous line, Equation 5.12) are shown. Also a distinction is made between observed flexural shear cracking (black coloured circles) and observed diagonal tension cracking (not-coloured circles). Figure 5.4 demonstrated that Equations 5.11 and 5.12 are rather accurate. Moreover, the suitability of Equation 5.9 is demonstrated, which predicts the governing diagonal cracking mode (lowest resistance approach, Section 2.1.7).

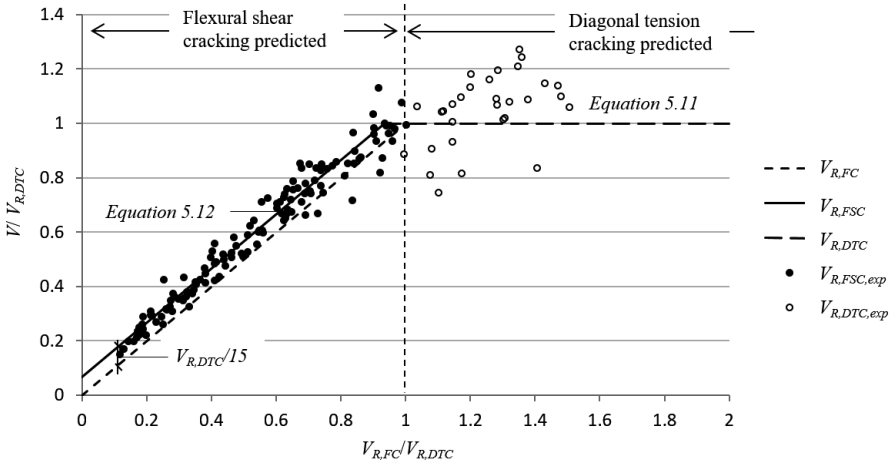

Figure 5.4. Predicted and experimentally found diagonal cracking resistance (MacGregor et al. 1960)

MacGregor determined the added resistance of the stirrups empirically. For this purpose the 16 prestressed experiments were selected, that contained stirrups and failed in shear. No distinction was made between the initial diagonal cracking modes. Associated ranges

of parameters are shown in Table 5.3. Experiments of which the identification start with B, have a web width of 76 mm. Experiments of which the identification start with C have a web width of 38 mm. The girder of which the identification starts with F is combined with a composite slab. The contribution of stirrups (Equation 5.13) was determined by subtracting the predicted resistance to diagonal cracking (Equations 5.9, 5.11 and 5.12) from the experimentally found ultimate resistance.

Table 5.3. Experiments selected for empirical relation Equation 5.11 and associated parameters ranges

Researcher (year)	Identification (number of experiments)	Prestressing	Support conditions	h	a/d	σ_{cp}	ρ_w	f_{cm}	d_{max}
				mm	-	N/mm^2	%	N/mm^2	mm
MacGregor et al. (1960)	BW.14.34, BW.14.38, BW.14.58, BW14.60, BW.18.15S, CW.13.28, CW.14.17, CW.14.22, CW.14.23, CW.14.37, CW.14.39, CW.14.47, CW.14.50, CW.14.51, CW.14.54, FW.14.06	Straight pre-tensioned tendons	Simply supported	305	2.8-7.0	2.2-6.0	0.14-1.04	17-53	9

The empirically found coefficient of 1.1 (Equation 5.13) equals a cracking angle of 42°. This is rather steep compared to observed cracking angles in prestressed girders. MacGregor et al. gave as possible explanation for the low coefficient of 1.1, that the stirrups near the end of the inclined crack may not have been stressed to the yield point.

$$V_{R,s} = 1.1\, A_{sw}\, f_{yw}\, {}^{d}/_{s} \tag{5.13}$$

As part of this dissertation the data in the report were further analysed. It is investigated whether also experiments that failed in web shear were part of the experiments. Although this could not be confirmed, it was found that the initial cracking mode concerned flexural shear cracking for 7 experiments and diagonal tension cracking for 9 experiments. The empirical model of MacGregor et al. was used to determine the ACI shear provisions (ACI 2008). Some modifications were made:

- For the equation to determine the flexural cracking strength $f_{ctm,fl} = 0.498\ \sqrt{f_{cm}}$ is used instead of $f_{ctm,fl} = 21 / (4 + 83/ f_{cm})$, both expressed in N/mm^2. This affects $V_{R,FC.}$
- $V_{R,DTC}$ is based on the cracking strength f_{cr} (Equation 2.10) instead of $0.8 f_{ctm,fl}$

– To relate the shear stress resistance $\tau'_{R,c}$ at the centre of gravity to the shear force resistance of the cross-section, the simplified Equation 2.19 is used instead of Equation 5.11.
– The shear force necessary to transform a flexural crack into a flexural shear crack is set to $0.0498\sqrt{f_{cm}}\,b_w z$ (=$0.171 V_{R,DTC}$) instead of $1/15 V_{R,DTC}$ (=$0.067 V_{R,DTC}$)
– The empirical found factor 1.1 (Equation 5.13) for the contribution of stirrups ($V_{R,s}$) is conservatively set to 1.

If web shear resistance is governing, the resistance for prestressed girders with stirrups according to the ACI (2008), is represented by Equation 5.14. In this equation the resistance to diagonal tension cracking is based on d_p. The contribution of the stirrups is based on d, which is the distance from extreme compression fiber to centroid of longitudinal tension reinforcement. In the ACI a minimum value of $0.8h$ is prescribed for d and d_p.

$$V_{R,STF} = b_w\, d_p \left(0.291\sqrt{f'_c} + 0.3\,\sigma_{cp}\right) + A_{sw}\, f_{wym}\, {}^{d}/_{s} \tag{5.14}$$

In literature many researchers investigated the accuracy of the ACI code provisions. In this literature review the accuracy investigated by Esfandiari et al. (2009) is reported as this specifically concerns prestressed girders with stirrups. For 88 simply supported girders, a mean value of the test-to-predicted shear resistance ratio was found of 1.08 and an associated coefficient of variation of 25%. In this research no distinction was made between the accuracy for regions with or without flexural cracks. For an empirically derived model a low level of conservatism can be expected. This is because all shear transfer mechanism are implicitly included in an empirical model. The predictions were however found not so consistent.

5.1.3 Modified Compression Field Theory

The Modified Compression Field Theory (MCFT) is a theory capable to predict the load-deformation response of membrane elements (Vecchio et al. 1986, Bentz et al. 2006a). The MCFT is also used to derive a model to determine shear resistance for girders (Bentz et al. 2006a, Esfandiari 2009). The main principles of the MCFT are explained in this section. In Section 5.1.4 it is explained how the MCFT is made applicable to predict shear resistance for girders. For this dissertation, two models are considered that predict shear resistance for girders that are based on the MCFT. This concerns the model of Bentz et al. (2006a), which is explained in Section 5.1.5 and the model of Esfandiari (2009), which is explained in Section 5.1.6.

The MCFT consists of 15 equations which are listed in Tables 5.4 and 5.5. Since the original version of the MCFT several adaptions have been made. In this section, the version of the MCFT that is also used in *Response* is explained (Bentz 2000, Bentz et al. 2001). This is a non-linear sectional analyses programme for girders, also referred as R2K. The original notation of the parameters used in the equations are replaced by notations in accordance to the Model Code 2010 (*fib* 2012). Also the original notions are shown in the explanation of the parameters.

The MCFT treats cracked concrete as a new material with its own empirically found stress-strain relations. Equilibrium, compatibility and stress-strain relations are expressed as average stresses and strains (Table 5.4).

Table 5.4. Average stresses and strains equations of the MCFT (Bentz et al. 2006a).

Average stresses	Average strains	Stress–strain relationships
		Reinforcement
$\sigma_x = \rho_x \sigma_{sx} + \sigma_1 - \tau \cot\theta$ (5.15)	$\tan^2\theta = \frac{\varepsilon_x + \varepsilon_2}{\varepsilon_z + \varepsilon_2}$ (5.18)	$\sigma_{sx} = E_s\,\varepsilon_x \le f_{yx}$ (5.21)
$\sigma_z = \rho_z \sigma_{sz} + \sigma_1 - \tau \tan\theta$ (5.16)	$\varepsilon_1 = \varepsilon_x + \varepsilon_z + \varepsilon_2$ (5.19)	$\sigma_{sz} = E_s\,\varepsilon_z \le f_{yz}$ (5.22)
		Concrete
$\tau = {(\sigma_1 + \sigma_2)}/{(\tan\theta + \cot\theta)}$ (5.17)	$\gamma_{xz} = 2(\varepsilon_x + \varepsilon_2)\cot\theta$ (5.20)	$\sigma_2 = \frac{f_{cm}}{0.8 + 170\,\varepsilon_1}\left(2\,\frac{\varepsilon_2}{\varepsilon_c} - \left(\frac{\varepsilon_2}{\varepsilon_c}\right)^2\right)$ (5.23)
		$\sigma_1 = {0.33\sqrt{f_{cm}}}/{(1 + \sqrt{500\varepsilon_1})}$ (5.24)

For concrete stresses the two principal stress directions are considered (Figure 5.5). This results in principal tensile stresses (σ_1, original notation f_1) and principal compressive stresses (σ_2, original notation f_2). Steel stresses are considered in the axial directions. The average reinforcement stress per unit length is the product of the average reinforcement stresses (σ_{sx} in x-direction, original notation f_{sx} and σ_{sz} in z-direction, original notation f_{sz}) and the reinforcement ratio (respectively ρ_x and ρ_z). The applied stresses on the membrane element (σ_x, σ_z, τ, original notations f_x, f_z, v) should be in equilibrium with average stresses in the concrete and steel.

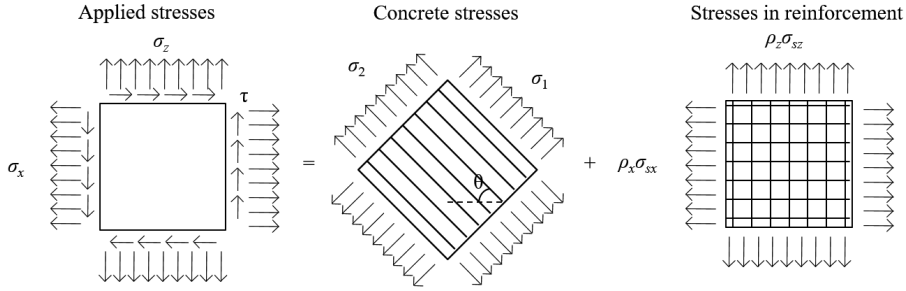

Figure 5.5. Average stresses according to MCFT (first two figures, Vecchio et al. 1986).

From this principle Equations 5.15 – 5.17 are derived. The angle of inclination of the principal compressive stresses θ (original notation θ_c) and the angle of inclination of the principal strains θ_ε (original notation θ) are assumed to be equal. This assumption is made despite measurements show that θ and θ_ε deviate somewhat. For simplification the notation θ is used in Table 5.4. According to the Compression Field Theory, the predecessor of the MCFT, a value of $\sigma_1 = 0$ is assumed as stress-strain relation instead of 5.24.

The average strain equations (Equations 5.18 – 5.20) relate the averages strains (ε_x, ε_z, γ_{xz}) and the principal strains (ε_1, ε_2, θ). The strains in the concrete are assumed to be equal to the strains in principal direction. In Figure 5.6, ε_1 is the principal tensile strain in concrete and ε_2 the principal compression strain in concrete. The strains in the steel are assumed to be equal to the longitudinal average strains ε_x, ε_z. The equations are transformation equations used to transform the strains to a different coordinate system. For instance as described by Verruijt (1987).

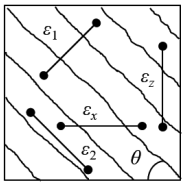

Figure 5.6. Average strain parameters according to MCFT (Vecchio et al. 1986)

In the MCFT bilinear stress-strain relations are used for reinforcement (Equations 5.21 and 5.22). However, in *Response* also tension hardening behaviour is considered. The constitutive equations of the "new material" cracked concrete are determined empirically, initially based on 30 tests on reinforced membrane elements (890 mm x 890 mm x 90 mm). The relations have later been confirmed with 250 experiments performed at the University of Toronto (Bentz 2000). Empirical relations could be derived from the applied stresses and the measured strains. Consequently, the average stresses include stresses between cracks, stresses at cracks, interface shear in cracks and dowel action.

And the average concrete strain (ε_1) contains local strains at cracks, strains between the cracks, bond slip and crack slip (Bentz 2000). Hence, the average stress – strain relations differ significantly from the relations measured in for example splitting tests or cylinder compression tests.

Equation 5.23 describes the empirically found relation for cracked concrete in compression. The equation is visualised in Figure 5.7. The concrete strength ($f_{cm,red}$) is represented as ratio of the maximum compressive strength of a cylinder test (f_{cm}). The strains are represented as ratio of ε_c, the strain associated with f_{cm}. The principal compressive stress σ_2, was found to depend on not only the principal compressive strain ε_2 but also the principal tensile strain ε_1. For uncracked concrete no reduction of f_{cm} is necessary ($f_{cm,red} = f_{cm}$) and the stress strain relation does not differ from a concrete cylinder test (Figure 5.7, figure on the left, minimum value of $\sigma_2 = f_{cm}$). For cracked concrete a reduced value of f_{cm} was found, $f_{cm,red}$ (Figure 5.7, figure on the right). It was found that the strength of concrete under compression reduces with increasing values of principal tensile strains ε_1 according to Equation 5.23.

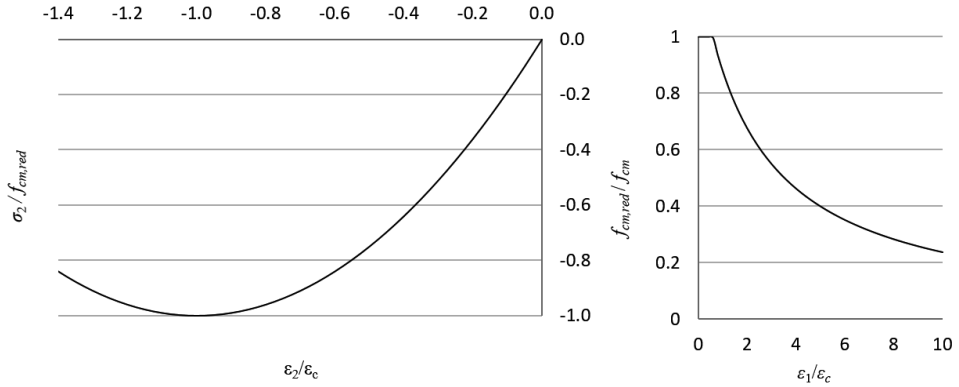

Figure 5.7. Average stress- average strain relations for concrete in compression (Eq. 5.23)

For uncracked concrete the principal tensile stress increases linear with the principal strain ($\sigma_1 = \varepsilon_1 E_s$). The version of the MCFT used by *Response*, uses Equation 2.9 for the cracking strength of concrete f_{cr}. Equation 5.24 describes the empirically found (high scatter) stress strain relation for cracked concrete in tension. After cracking the average tensile strength reduces with increasing values of ε_1. The relation is visualised in Figure 5.8. The principal tensile stress should be limited if the average stress cannot be resisted locally at the crack (see hereafter), it is unsafe to apply the MCFT without this crack-check. The crack check ensures that the principal tensile stress can be resisted locally by the steel (yielding strength minus average stress) and the aggregate interlock at the crack.

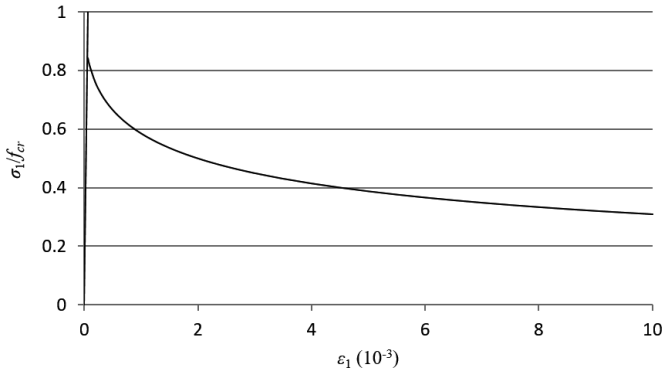

Figure 5.8. Average stress- average strain relation for concrete in tension (Equation 5.24)

At a crack the stresses in the reinforcement ($\sigma_{sx,cr}$ and $\sigma_{sz,cr}$ for respectively the stress in the reinforcement in x and z direction, original notations f_{sxcr} and f_{szcr}) are higher than the average stresses σ_{sx} and σ_{sz}. The concrete tensile stress is zero at the crack which is lower than the stresses of the uncracked concrete between two existing cracks. According to the MCFT the use of average stresses is allowed under the conditions that the average stresses can be resisted locally at a crack. If the computed stresses exceed the resistance at the crack, the average stresses σ_1 is reduced until equilibrium at the crack surface is possible. Equations concerning the crack conditions are listed in Table 5.5.

Table 5.5. Crack conditions equations of the MCFT (Bentz et al. 2006a).

Stresses at cracks	Crack widths	Max. shear stress on crack
$\sigma_{sx,cr} = (\sigma_x + \tau \cot\theta + \tau_{ci} \cot\theta)/\rho_x$	$w = s_\theta \cdot \varepsilon_1$	$\tau_{ci,max} = \dfrac{0.18\sqrt{f_{cm}}}{0.31 + \dfrac{24\,w}{(d_{max}+16)}}$
(5.25)	(5.27)	(5.29)
$\sigma_{sz,cr} = (\sigma_z + \tau \tan\theta - \tau_{ci} \tan\theta)/\rho_z$	$s_\theta = 1/\left(\dfrac{\sin\theta}{s_x} + \dfrac{\cos\theta}{s_z}\right)$	
(5.26)	(5.28)	

In Figure 5.9 the external applied stresses and the internal stresses at the crack are shown. In this figure τ_{ci} is the shear stress on the crack surface due to aggregate interlock. Equation 5.25 and 5.26 are found if the applied loads are equal to the stresses at the surface for both directions. Equilibrium can be achieved with different combinations of the stress in the reinforcement at the crack and τ_{ci}. The solution used in the MCFT is to only assume shear stresses at the crack when the resistance of the reinforcement is insufficient to resist the applied stresses. If the average stresses cannot be resisted locally at a crack, σ_1 should be reduced until equilibrium is possible.

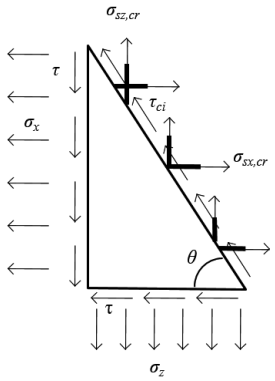

Figure 5.9. Transmission of stresses across a crack (MCFT, based upon Bentz et al. 2006b)

The MCFT assumes that the maximum value of τ_{ci}, which is $\tau_{ci,\max}$, only depends on the crack width w. Based on results of experiments carried out by Walraven, (Walraven 1980, 1981) an empirical equation was derived between the crack width and $\tau_{ci,\max}$ (Equation 5.29). Equation 5.29 results in reasonably accurate approximations despite that the tangential displacement is eliminated, which is argued by Yang (2014). The maximum shear on the crack increases for higher strength concrete classes or larger maximum aggregate sizes ($d_{\max}$, original notation a). The crack width is assumed to be the product of the principal tension strain ε_1 and the crack spacing s_θ (Equation 5.27). The diagonal crack spacing at an angle θ is calculated from the cracks spacing in both orthogonal directions (s_x and s_z, Equation 5.28).

According to the MCFT three conditions can be governing at failure for cracked concrete:

1. Crushing of the concrete (minimum value of σ_2).
2. Slipping of the crack (maximum value of σ_1).
3. Yielding of the longitudinal reinforcement (maximum value of σ_1).

Several assumptions are made in the development of the MCFT. It is assumed that, stress and strains can be considered as average values, perfect bond exist between steel and concrete, the stress-strain relations of concrete and steel are independent and the inclination of principal compressive stress and strain coincide. The effect of these assumptions on the accuracy appears to be limited. Bentz et al. compared the resistances according to the MCFT with the experimentally found resistance of 102 experiments with membrane elements (Bentz et al. 2006b) loaded in pure shear or shear combined with uniaxial stress ($\sigma_z = 0$). This resulted in a mean ratio of test-to-predicted resistance of 1.01 and a CoV of 12.2%. The accuracy regarding models for shear resistance for girders based on the MCFT is discussed in Section 5.1.5 and 5.1.6.

5.1.4 Models for girders based on the MCFT

In this section it is explained how the MCFT, intended for membrane elements, is made applicable to predict shear resistance for girders. Two girder models will be considered which determine the shear resistance (Sections 5.1.5 and 5.1.6). The part of the method that is equal for both models is described in this section. This section is based on the Simplified Modified Compression Field Theory (Bentz et al. 2006b) and the background article of the CSA (Bentz et al. 2006a). The models are intended to determine shear and moment resistance for reinforced and prestressed members with and without stirrups. In this section the determination of shear resistance of girders with stirrups is explained. No distinction is made for models that determine the shear resistance for regions with and without flexural cracks. The models are based on equilibrium and compatibility. The shear transfer mechanisms of the models are illustrated in Figure 5.10 for a free body diagram that is cut though along a diagonal crack. This figure is drawn in a similar way as Figure 5.1 (variable angle truss model) and Figure 5.3 (empirical model used in ACI), so these models can easily be compared.

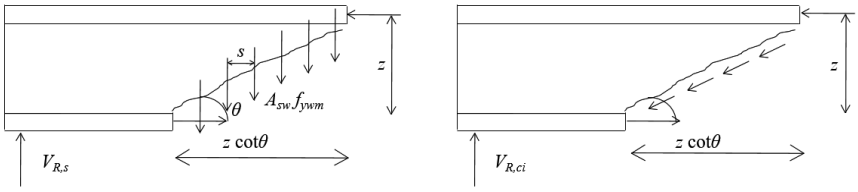

Figure 5.10. Girder model based on MCFT, based on Bentz (2006b)

As shown in Figure 5.10, the shear resistance of a girder consist of contributions of the stirrups ($V_{R,s}$) and of aggregate interlock ($V_{R,ci}$). It is assumed that the stirrups yield along the horizontal projection of the diagonal crack (z cotθ). The aggregate interlock consists of the shear stress (which corresponds to τ_{ci} according to Figure 5.9) over the length of the crack.

The shear resistance of the flexural compression zone is assumed to be larger than that of the cracked zone. With this assumption, the resistance of the cracked zone will control the shear strength of the girder (Bentz et al. 2006a). To explain this, Figure 5.11 is drawn as part of this dissertation. In this example only the most tensioned flange is cracked by bending. It is assumed that failure occurs in the cracked zone. In that case, the shear resistance in the cracked zone is governing for the ultimate failure.

The contribution of the uncracked concrete is considered implicitly by assuming a larger contribution of the stirrups and aggregate interlock. Both contributions are considered along the internal lever arm multiplied with cotθ. As shown in Figure 5.11, the internal

lever arm is partly located in the flexural compression zone. So neglecting the contribution of the uncracked concrete is compensated by assuming contributions of aggregate interlock and stirrups along a larger length of the crack. As the shear resistance approaches zero at the top of the cross-section, z is chosen and not the full effective depth d (Figure 5.11).

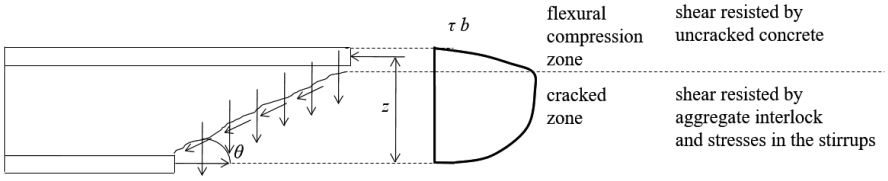

Figure 5.11. Zones of shear stress multiplied with width over the height of the girder

The models assume no contribution of dowel action by the longitudinal reinforcement to shear resistance.

The shear resistance for girders with concrete using normal weight aggregate is represented in Equation 5.30. In this equation β is the concrete contribution factor (aggregate interlock) and θ is the angle of inclination of the principal compressive stress. This angle is assumed to correspond with the angle of diagonal cracks. The vertical component of prestress force ($V_{R,p}$), which is present in the original model (Bentz et al. 2006a), is not taken over in Equation 5.30. In this research $V_{R,p}$ is considered as a reduction of the load instead of as a component of the shear resistance. This way the described models of this chapter are mutually comparable. The shear strength is limited by the crushing resistance of concrete in diagonal compression, without yielding of the stirrups, which is shown by Equation 5.31, and will be explained hereafter.

$$V_R = \beta \sqrt{f_{cm}}\, b_w\, z + A_{sw}\, f_{ywm}\, z \cot\theta / s \tag{5.30}$$

$$V_{R,max} = 0.25\, f_{cm}\, b_w\, z \tag{5.31}$$

The shear stress resistance of a cross-section is only determined at the mid-depth of the cross-section. It is assumed that the aggregate interlock resistance of the complex crack geometry may be estimated at the mid-depth and that this can represent the entire crack surface. Also the number of stirrups that are crossed by the crack is simply based on the angle of the diagonal crack at the mid-depth. By multiplying the shear stress with the shear area $b_w z$, the shear resistance of the cross-section is found. In this way, a theory intended for membrane elements is made applicable for girders.

Parameters θ and β in Equation 5.30 can be related to the equations of the MCFT. As the two considered models are used for sectional analyses of girders, it is assumed that σ_z is

zero. Moreover, it is assumed that the stirrups yield at failure. Hence, crushing of concrete before the stirrups yield is considered as a separate limitation of the shear resistance (Equation 5.31). As $\sigma_z = 0$ and $\sigma_{sz} = \sigma_{sz,cr} = f_{ywm}$, Equation 5.16 can be rewritten as Equation 5.32 and Equation 5.26 can be rewritten as Equation 5.33. In these equations, both σ_1 as τ_{ci} can be expressed in terms of $\sqrt{f_{cm}}$ as can be seen from Equations 5.24 and 5.29. Therefore, Equations 5.32 and 5.33 can formulated as Equation 5.34 (Bentz et al. 2006b). Equation 5.30 is found if both sides of Equation 5.34 are multiplied with the shear area $b_w z$.

The predictions of β and θ are described as part of the models of Bentz et al. (Section 5.1.5) and Esfandiari (Section 5.1.6.). The parameters β and θ depend on the normalized applied shear (τ/f_{cm}) the longitudinal strain ε_x and the effective crack spacing size (Bentz et al. 2006a). If these are determined, β and θ can be found using tables (AASHTO 2004). To simplify the application of the model, the two considered models determine β and θ independently of the normalized applied shear. As a consequence, no tables have to be used, which make the models more appealing for applications in practice. The models are deemed to be applicable for both regions with and without flexural cracks.

$$\tau = \rho_z f_{yw} \cot\theta + \sigma_1 \cot\theta \tag{5.32}$$

$$\tau = \rho_z f_{yw} \cot\theta + \tau_{ci} \tag{5.33}$$

$$\tau = \rho_z f_{yw} \cot\theta + \beta\sqrt{f_{cm}} \tag{5.34}$$

Also the upper limit of the shear $V_{R,\max}$ (Equation 5.31) is derived from the MCFT. This concerns the crushing resistance of the cracked concrete without yielding of the transverse reinforcement. As the condition concerns crushing of the concrete, ε_2 is assumed to be –2 mm/m. Because the transverse reinforcement is not yielding, the strain ε_z is lower than 2 mm/m. As a lower strain on longitudinal direction increases the maximum resistance, conservatively ε_z = 2 mm/m is assumed. The longitudinal strain ε_x will be lower than 2 mm/m (because the longitudinal reinforcement is not yielding). As a lower strain increases the resistance, conservatively $\varepsilon_x = 2$ mm/m is assumed. Using these values in respectively Equations 5.18, 5.19, 5.23, 5.24 and 5.17, a value for the shear stress $\tau_{R,\max}$ is found of $0.28 f_{cm}$. Conservatively, a value of $\tau_{R,\max} = 0.25 f_{cm}$ was chosen. Equation 5.31 is found if $\tau_{R,\max}$ is multiplied with the shear area $b_w z$ (Bentz et al. 2006b).

5.1.5 Model of Bentz et al.

The model of Bentz et al. is intended to determine shear and moment resistance for reinforced and prestressed members with and without stirrups. In this section the determination of shear resistance for girders with stirrups is explained. No explicit distinction is made between regions with and without flexural cracks, although a relation between

the failure mode and the magnitude of the longitudinal strain is obvious. The model of Bentz et al. is used in the Canadian Highway Bridge Design Code (CSA 2006). The model is partly explained in Section 5.1.4. In this section the derivation of equations for β and θ is explained. The equation for β is derived for elements without transverse reinforcement and the equation for θ is derived for elements with transverse reinforcement. These derivations are explained based on the background article of the design code (Bentz et al. 2006a). The Simplified Modified Compression Field Theory (Bentz et al. 2006b) is used to demonstrate that the derived equations can be combined to determine the shear resistance for elements with transverse reinforcement.

The equation for β is based on MCFT calculations for membrane element without transverse reinforcement. The value of β can be determined using the equations of the MCFT (Table 5.4 and Table 5.5) for a range of values of the longitudinal strain ε_x, the crack spacing s_θ, the maximum aggregate size d_{max} and the concrete cylinder compressive strength f_{cm}. To demonstrate this, as part of this dissertation, the crack width is determined for a crack spacing s_θ of 300 mm, a concrete strength of 60 N/mm^2 and different values of ε_x. These are calculated using an example described by Bentz et al. (2006b). The results are shown in Figure 5.12 (dots).

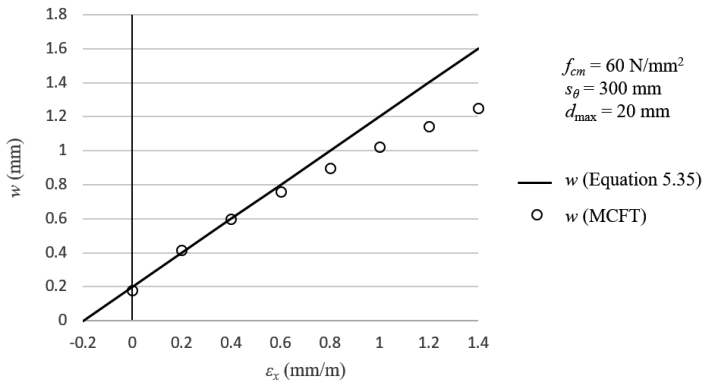

Figure 5.12. Crack width versus the longitudinal strain conform the MCFT and Equation 5.35

A simply linear equation (Equation 5.35) was found to be a rather good approach of the relation between ε_x and w according to the MCFT (Figure 5.12). Especially for values of steel up to 400 N/mm^2 for which for shear failure the strain at mid-depth is expected to be lower than 1 mm/m. Also for other values of f_{cm} Equation 5.35 approached the calculated values of the crack width reasonably (Bentz et al. 2006a). The value of β can easily be found by substituting Equation 5.35 in Equation 5.29. If a value of the maximum aggregate size d_{max} is assumed of 20 mm, Equation 5.36 is found for β. The

equation shows that contribution of the aggregate interlock decreases if the crack opening increases. To prevent negative crack widths the minimum allowable value of ε_x is set to –0.2 mm/m (which is found by setting w to 0 mm in Equation 5.35).

$$w = 0.0002 + \varepsilon_x \tag{5.35}$$

$$\beta = {}^{0.4}/_{(1 + 1500\varepsilon_x)} \tag{5.36}$$

The crack width (and the aggregate interlock resistance) does not only depend on the longitudinal strain ε_x but also on the diagonal crack spacing s_θ (Equation 5.27). Equation 5.36 is derived for a crack spacing of 300 mm. For different values of the crack spacing, Equation 5.36 has to be multiplied with 1300/(1000+s_θ). For girders without stirrups the crack spacing depends on the girder height. The crack spacing increases proportional with the girder height and so does the crack width. Therefore, an increase of girder height leads to a decrease of aggregate interlock and deeper girders fail at lower stresses ('size effect'). However, for girders with stirrups the crack spacing is controlled and no significant size effect is expected. For girders with stirrups it is assumed that the crack spacing s does not exceed 300 mm.

The equation of the angle of the compressive stresses θ, is based on MCFT calculations for membrane elements with transverse reinforcement. Based on the theory of plasticity, shear can be resisted at a range of possible values of θ. However, θ should be low enough to ensure yielding of the stirrups and high enough to prevent crushing of the concrete. The range in which both conditions are met, decreases if the shear load increases. Therefore, the MCFT calculations are conservatively made for the maximum value of the shear load $\tau/f_{cm} = 0.25$ (Section 5.1.4). The calculations are carried out for a range of values of the longitudinal strain ε_x and several values of the concrete cylinder compressive strengths f_{cm}. Moreover, it is assumed that $\sigma_z = 0$. In Figure 5.13 the resulting upper and lower limit of the angle are shown as function ε_x. The figure shows the most narrow results for all ranges of f_{cm}, noticing that the effect of f_{cm} on the figure is not significant. The area in which both conditions are met (areas that are not grey) was found to be rather small. Equation 5.37 fits in between the found relations for the upper and lower limit.

$$\theta = 29 + 7000\varepsilon_x \tag{5.37}$$

Although the equation for β is derived for elements without transverse reinforcement and the equation for θ is derived based on elements with transverse reinforcement, Bentz et al. propose to use Equations 5.36 and 5.37 for elements with and without transverse reinforcement (Bentz et al. 2006a). After yielding of the transverse reinforcement, θ and

β reduce as a consequence of an increase of ε_1. Consequently, the contribution of aggregate interlock decreases and the contribution of the transverse reinforcement increases. Therefore, Bentz et al. consider it as a conservative approach to predict θ at a maximum value of the aggregate interlock. Therefore, MCFT calculations for a maximum value of τ_{ci} are used to verify the suitability of the application of Equations 5.36 and 5.37 for elements that contain transverse reinforcement.

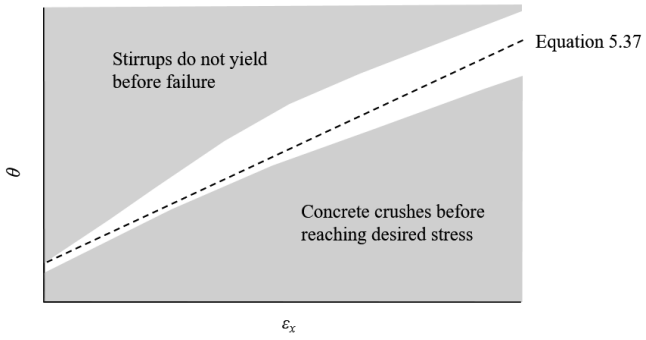

Figure 5.13. Limits of the angle of the compressive stresses for $\tau/f_{cm} = 0.25$ (Bentz et al. 2006a)

In Figure 5.14, the predictions of β and θ are show in relation to the longitudinal strain for membrane element with transverse reinforcement. The dashed lines show the predicted values of β according to Equation 5.36 and the prediction of θ according to 5.37. The grey areas show the values of θ and β predicted according to the MCFT for a maximum value of τ_{ci} and a value for s_θ *of* 300 mm and with a range of values for $\rho_z f_{ywm}/f_{cm}$. The kink in the graphs shows that for high values of $\rho_z f_{ywm}/f_{cm}$, the crushing of concrete before yielding of the transverse reinforcement becomes governing ($\tau/f_{cm} = 0.25$).

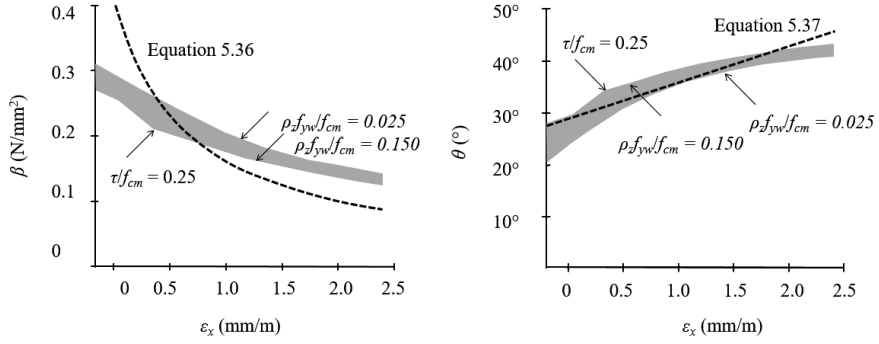

Figure 5.14. Comparison β and θ between MCFT & Equations 5.36 and 5.37 at maximum τ_{ci} (Bentz et al. 2006b)

If the Equations 5.36 and 5.37 are used, the predicted values for β and θ appear to be conservative in comparison with the predictions of the MCFT for most values of ε_x.

However, for small values of ε_x, the values of β are too high, which results in unconservative predictions of the aggregate interlock component. On the other hand, θ is predicted too high for low value of ε_x, which is a conservative result. It is obvious that for regions without flexural cracks, low values of the longitudinal strain are of specific interest.

Several assumptions are summarized regarding the development of the Simplified Modified Compression Field Theory (which corresponds with Equations 5.36 and 5.37 for membrane elements with transverse reinforcement). It is assumed that w can be approached directly from ε_x with a linear relation, that θ can be approached directly from ε_x with a linear relation and the same equations for θ and β can be used for elements with and without transverse reinforcement. The effect of the assumptions on the accuracy appears to be limited. Bentz et al. compared the resistances according to the Simplified Modified Compression Field Theory with the experimentally found resistance of 102 experiments on membrane elements (Bentz et al. 2006b) loaded in pure shear or shear combined with uniaxial stress ($\sigma_z = 0$). This resulted in a mean ratio of test-to-predicted resistance of 1.11 and a CoV of 13.0%.

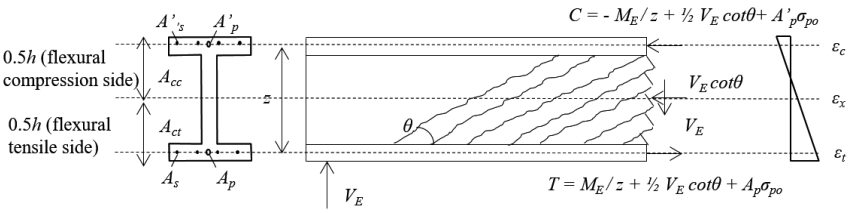

Figure 5.15. Model to determine longitudinal strain (Bentz et al. 2006a)

Also the method to determine ε_x is part of the model of Bentz et al.. This method is illustrated in Figure 5.15. As the shear resistance is only determined at the mid-depth of a cross-section, also ε_x is determined at the mid-depth. The modelled girder consist of a compressive chord and a tensile chord. The compressive force $C = -M_E/z + 0.5V_E cot\theta + A'_p \sigma_{p'o}$, in which M_E is the moment due to the external load, z is the internal lever arm, V_E is the shear due to the external load, A'_p is the area of the prestressing steel at the compressive side of the girder and $\sigma_{p'0}$ is the initial stress in the prestressing steel at the compressive side of the girder. The internal lever arm is assumed to be equal to 0.9 times the effective depth. The tensile force $T = M_E/z + 0.5V_E cot\theta + A_p \sigma_{po}$, in which A_p is the area of the prestressing steel at the tensile side of the girder and σ_{p0} is the initial stress in the prestressing steel at the tensile side of the girder. It is suggested (Bentz et al. 2006a) to use conservatively V_E instead of $0.5V_E cot\theta$ for simplicity. The strain in the tensioned chord $\varepsilon_t = T /(E_s A_s + E_p A_p)$. If the tension chord is not cracked the stiffness should be increased by the stiffness of the uncracked concrete ($E_s A_s + E_p A_p + E_c A_{ct}$), in

which A_{ct} is based on the area of concrete within $0.5h$ of the ultimate fiber (Figure 5.15). The strain in the compressive chord $\varepsilon_c = D / (E_s A_s + E_p A_p + E_c A_{cc})$. Finally, ε_x is assumed to be equal to $(\varepsilon_t + \varepsilon_c)/2$. It is suggested to conservatively assume $\varepsilon_c = 0$ so $\varepsilon_x = \varepsilon_t/2$. However, as this research concerns shear resistance in regions without flexural cracks, which is characterised by small longitudinal strains, this suggested simplification is not further used in this dissertation.

The accuracy of the model of Bentz et al., was investigated by Esfandiari et al.(2009) for 88 simply supported girders. This reference is used as this specifically concerns prestressed girders with stirrups. This investigation was already reported in Section 5.1.2 for the accuracy of the model of MacGregor et al.. For the model of Bentz et al., a mean value of the test-to-predicted shear resistance ratio was found of 1.31 and an associated coefficient of variation of 16%. In his research no distinction was made between the accuracy for regions with or without flexural cracks.

5.1.6 Model of Esfandiari

Like the model of Bentz et al., the model of Esfandiari is intended to determine shear and moment resistance for reinforced and prestressed members with and without stirrups. In this section the determination of shear resistance for girders with stirrups is explained. Also in the model of Esfandiari, no explicit distinction is made between the flexural shear resistance in regions with and without flexural cracks, although a relation between the failure modes and the magnitude of the longitudinal strain is obvious. The model is partly explained in Section 5.1.4. In this section the derivation of the equations for β and θ is explained. This section is based on Esfandiari (2009) and Esfandiari et al. (2009).

Esfandiari carried out MCFT analyses on membrane elements with different amounts of longitudinal and transverse reinforcement (Esfandiari 2009). The results for two elements with the same amount of longitudinal reinforcement but a different amount of transverse reinforcement, are shown in Figure 5.16. In this figure the ratio of the shear stress and concrete strength is presented versus the shear strain. After yielding of the transverse reinforcement, ε_x increases and θ and β decrease. This implies that the resistance by aggregate interlock decreases and the resistance by the transverse reinforcement increases. Depending on the magnitude of both shear transfer mechanism, the total resistance could decrease (Figure 5.16, membrane element with low ρ_z) or increase (Figure 5.16, membrane element with high ρ_z) after first yielding. A further increase of γ_{xz} eventually causes concrete crushing for both elements. Significant differences are found in values of θ and β for both physical conditions. Hence, first yielding of stirrups or crushing of concrete could be associated with the highest resistance and be the governing failure mechanism.

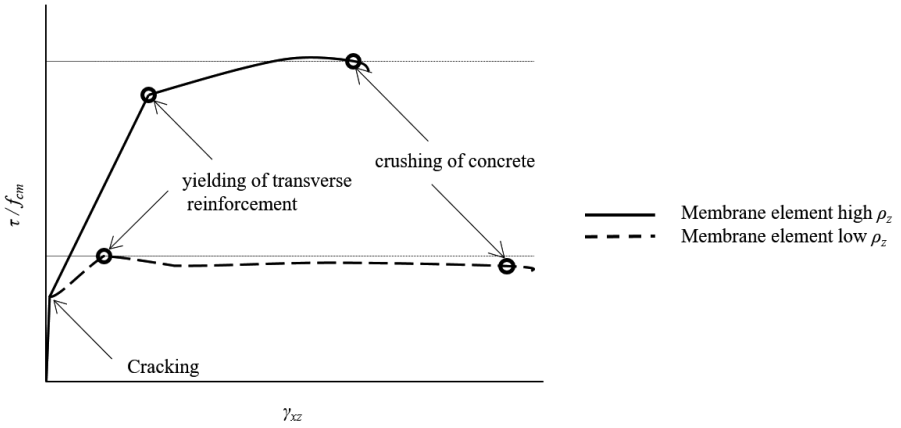

Figure 5.16. Shear response for two membrane elements, based on Esfandiari (2009)

At first yielding of the transverse reinforcement, values of θ and β were determined as function of ε_x from MCFT analyses on membrane elements (Esfandiari 2009). The parameter $\rho_z f_{ywm}/f_{cm}$ was used to fit the trend predicted by the MCFT. Equations 5.38 - 5.41 were found as rather good approximations of θ and β at yielding of the transverse reinforcement. In these equations, ε_y is the yielding strain of the transverse reinforcement.

$$\theta = \theta_0 + \Delta\theta\ \varepsilon_x \tag{5.38}$$

$$\theta_0 = \left(85\frac{\rho_z f_{yw}}{f_{cm}} + 19.3\right)\left(1.1 - 50\ \epsilon_y\right) \tag{5.39}$$

$$\Delta\theta = 1000\left(37.5\left(1.4 - 200\varepsilon_y\right) - \theta_0\right) \tag{5.40}$$

$$\beta = 0.18\left(1.6 - 300\varepsilon_y\right) \tag{5.41}$$

The results are presented as example in Figure 5.17 for values of f_{cm} of 40 N/mm^2 and f_{ywm} of 400 N/mm^2 and values of ρ_z of both 0.002 and 0.010. The solid lines are the predictions according to the MCFT membrane element predictions. According to Equation 5.39, the angle of principal compression depends on the parameter $\rho_z f_{ywm}/f_{cm}$. The concrete contribution factor β according to Equation 5.41 is a fixed value and is presented with a dashed line. Figure 5.17 shows that the results of the model of Esfandiari matches the results of the MCFT well, although for low shear reinforcement ratios, which are typical for the Dutch Highway bridges designed with a design code prior to the design code of 1974, the predictions of β are conservative.

Figure 5.17 furthermore shows that β is significantly overestimated for low longitudinal strains for the condition of first yielding, when the model according to Bentz et al. is used. For these conditions, the aggregate interlock is overestimated. On the other hand,

also θ is overestimated for these conditions and the contributions of the stirrups is therefore underestimated. Eventually, the overestimation of the contribution of aggregate interlock is compensated by the underestimation of the contribution of stirrups. This is found from the comparison of the predicted and experimentally found resistance for 102 membranes (Bentz et al. 2006b) and 88 simply supported prestressed girders (Esfandiari et al. 2009), as described in Section 5.1.5.

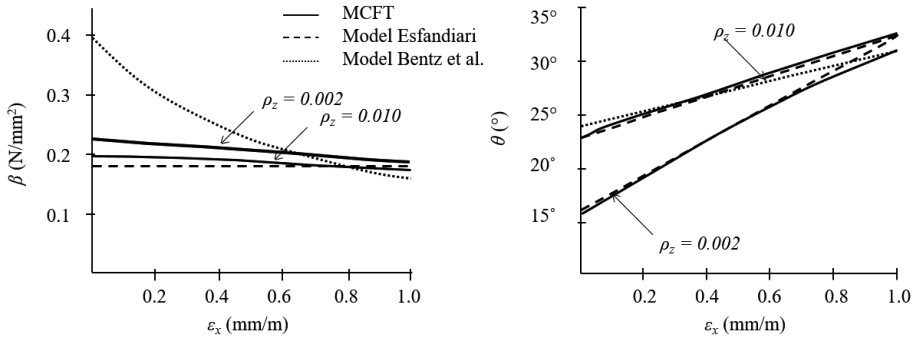

Figure 5.17 Comparison β and θ between MCFT & Eqns. 5.38-5.41 at first yielding (Esfandiari 2009)

Also at concrete crushing, values of θ and β were determined as function of ε_x from MCFT analyses on membrane element and the parameter $\rho_z f_{ywm}/f_{cm}$ was used to fit the trend predicted by the MCFT. Equations 5.38, 5.42 - 5.44 were found as approximation of θ and β at crushing of the concrete.

$$\theta_0 = 119\frac{\rho_z f_{yw}}{f_{cm}} + 15.6 \tag{5.42}$$

$$\Delta\theta = 15{,}000\frac{\rho_z f_{yw}}{f_{cm}} + 2000 \tag{5.43}$$

$$\beta = 0.65\ \frac{\rho_z f_{yw}}{f_{cm}} + 0.030 \tag{5.44}$$

The results are presented as example in Figure 5.18, again for values of f_{cm} of 40 N/mm^2 and of f_{ywm} of 400 N/mm^2 and values of ρ_z of both 0.002 and 0.010. According to Equation 5.44, the concrete contribution factor β depends on the parameter $\rho_z f_{ywm}/f_{cm}$. According to Equations 5.42 and 5.43, also the angle of principal compression depends on the parameter $\rho_z f_{ywm}/f_{cm}$. From Figure 5.18 is found that the results of the model of Esfandiari and the results of the MCFT match well, although some conservatism exist regarding β for low longitudinal strains.

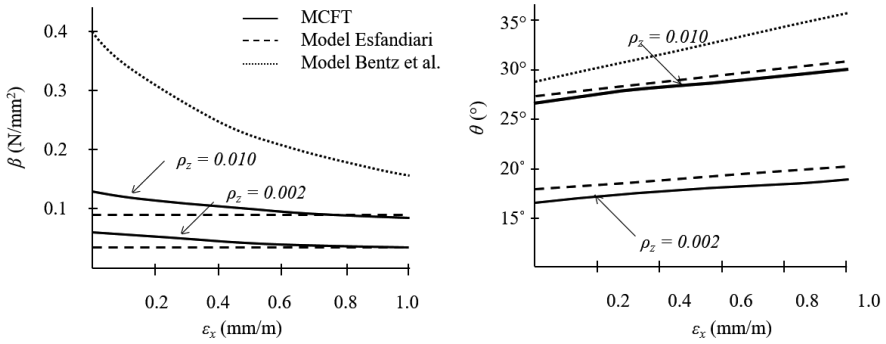

Figure 5.18 Comparison β and θ between MCFT and Equations 5.42-5.44 at concrete crushing (Esfandiari 2009)

Figure 5.18 furthermore shows that β is also significantly overestimated for low longitudinal strains for the condition of concrete crushing when the model according to Bentz et al. is used. But just like for the condition of first yielding, the overestimation of the contribution of aggregate interlock (overestimation of β) is compensated by an underestimation of the contribution of stirrups (overestimation of θ).

The shear stress that can be resisted can be determined from Equation 5.34 based on the determined values of θ and β. The governing resistance equals the highest resistance that is found for both physical conditions (first yielding and crushing). The failure mode associated with the highest resistance is the predicted failure mode.

The equations were fitted for values of ε_x between 0 and 1.0 mm/m. Within these limits the equations generally match well with the predictions of full MCFT analyses. However, the predicted values for both θ and β are more conservative for low values of ε_x, which can be associated with regions without flexural cracks. The predictions are especially conservative in combination with low values of ρ_z.

Also the method to determine ε_x is part of the model of Esfandiari. For the longitudinal component of the shear force carried by the web, the angle θ is calculated. This is in contrast to the approach used by Bentz et al. for which the angle is assumed (Section 5.1.5 and Figure 5.15). Moreover, this longitudinal component is only accounted for in the cracked web. Also tension stiffing of the tensioned flange and the presence of longitudinal reinforcement in the web are accounted for in the approach used by Esfandiari. Furthermore, the location at which the prestressing steel in the web are present is accounted for explicitly. These refinements result in an extensive set of equations (Esfandiari 2009) and more accurate predictions of ε_x compared to the model of Bentz et al.. However, the model still suggests to use the equation $\varepsilon_x = \varepsilon_t/2$ instead of $\varepsilon_x = (\varepsilon_t +$

ε_c)/2. As shear failure in regions without flexural cracks is characterised by small longitudinal strains, the effect of this simplification can be significant.

Esfandiari et al.(2009) investigated the accuracy of his model for 88 simply supported prestressed girders with stirrups. This investigation was already reported in Section 5.1.2 and 5.1.6 for the accuracy of the model of respectively MacGregor et al. and Bentz et al.. For the model of Esfandiari a mean value of the test-to-predicted shear resistance ratio was found of 1.27 and an associated coefficient of variation of 17%. In this research no distinction was made between the accuracy for regions with or without flexural cracks. Esfandiari concluded that the model becomes more conservative for $\varepsilon_x < 0.1$ mm/m.

5.1.7 Empirical model of Leonhardt

Leonhardt et al. (1973) suggested an empirical model based on experiments with post-tensioned girders with an I and T shaped cross-section. The experiments contained straight and inclined prestressing cables and the level of prestressing varied between the experiments. The described empirical model according to Leonhardt is intended to determine the shear resistance for prestressed members with stirrups in regions free of flexural cracks.

Based on the cracking pattern at failure, different zones were distinguished (Figure 5.19). This concerns zone A, which is free of cracks, zone B, which contains diagonal tension cracks and no flexural cracks, and zone C, which contains both flexural cracks and flexural shear cracks. For each zone Leonhardt et al. derived different models to determine the shear resistance.

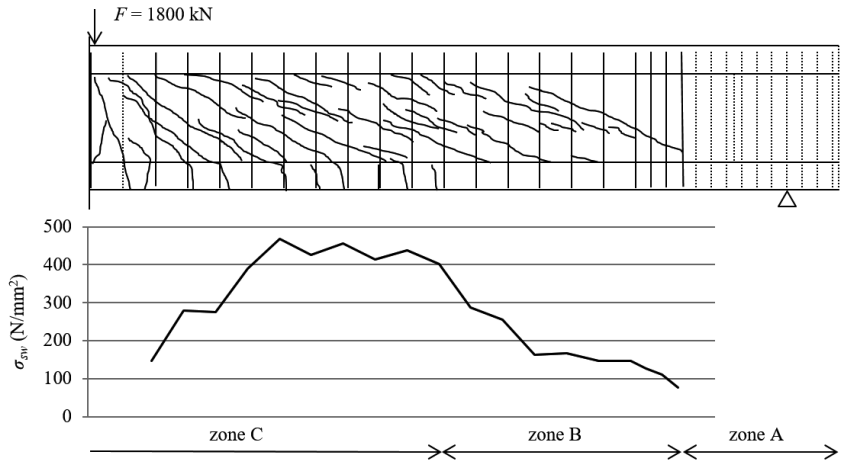

Figure 5.19. Crack pattern, cracking zones and max. stirrups stresses for IP1 (Leonhardt et al. 1973)

As part of the experiment, the strains in the stirrups were measured at four locations over the length of the stirrups. In Figure 5.19 the stress associated with the maximum of the measured strains is shown for experiments IP1 at the last load step before failure (a load of 1800 kN). Although the shear force was equal in both zones, the maximum stresses in zone B were found to be significant lower than in zone C. Leonhardt assumed that this was due to the contribution of the compressive and tensile chords to the shear resistance, as both chords remain uncracked and have a high stiffness. For zone B, Leonhardt suggested to use the linear elastics principal tensile stress distribution as basis for the determination of the shear resistance. This was assumed justified as the diagonal tensile cracks were fine hair cracks at the instant the experiments failed.

The stresses in the stirrups have a component in the direction of the maximum principal tensile stress. From equilibrium it is found that this component equals $\rho_w \sigma_{sw}$, in which ρ_w is the transverse reinforcement ratio (original notation μ_s) and σ_{sw} (original notation $\sigma_{eBü}$) is the stress in the stirrups. The measured stresses in the stirrups are lower than calculated from the principal tensile stresses. Therefore, a 'reduction parameter' σ_{cR} was introduced (original notation σ_{1D}) which is determined empirically using the data of five tested experiments at various load stages and Equation 5.45. In this equation σ_1 (original notation σ_{1M}) is the principal tensile stress at the centroidal axis determined from a linear elastic calculation. For σ_{sw}, the stress in the stirrups associated with the maximum of the four measured strains is used.

$$\sigma_{cR} = \sigma_1 - \rho_w \sigma_{sw} \tag{5.45}$$

The contribution of the concrete is determined for the 5 experiments at different load stages (in total 30 calculations). A value for σ_{cR} of $0.25 f_{cm}^{2/3}$ was found to be a lower limit for all obtained results. The maximum principal tensile stress that can be resisted according to the model of Leonhardt (σ_{1R}) is given in Equation 5.46. In this equation f_{cm} is used instead of the cube compressive strength (which was based on cubes sized 200 mm) which was used by Leonhardt et al.. To converse the cube compressive strength into a cylinder compressive strength the conversion equations of Reineck et al. (2012) are used. The last part of Equation 5.46 is based on the assumption that at failure the stirrups will yield.

$$\sigma_{1R} = 0.25 f_{cm}^{2/3} + \rho_w f_{yw} \tag{5.46}$$

Some critical remarks are make regarding Leonhardt's model as part of this dissertation. The contribution of the concrete is empirically derived and mainly based on load stages before failure. The contribution of concrete could possibly reduce at higher load stages,

when the crack further opens. Moreover, only for two of the five considered experiments, the failure could be related to diagonal tension cracks (Section 5.2.2). The gathered empirical data for various load steps is thus limited to ensure the behaviour at shear failure in regions without flexural cracks is covered for all possible situations. In addition, some experiments did show the development of significant stirrups stresses in zone B (ŢP2 and ŢP4). Also the measurements of experiment IP1, which is shown in Figure 5.19, shows significant stresses developed in the stirrups in the zone B at an earlier load step. At this earlier load step, the zone with flexural cracks was smaller and zone B larger. The significant stresses developed in the area what subsequently 'became' a C zone. It is also mentioned that equilibrium for stresses along the girder axis is not considered in the model suggested by Leonhardt.

5.1.8 Arch action models

In this section, arch action models are explained for prestressed girders with stirrups. Both shear and moment resistance can be determined using arch action models. In this section the determination of shear resistance is explained. In arch action models a compressive strut is modelled that makes equilibrium with a part of the external loads (F) and the prestressing forces (P), see Figure 5.20. As shown in this figure, the arch profile should suit the loading. The longitudinal component of the arch is in equilibrium with the longitudinal component of the prestressing. The vertical component of the arch can resist a part of the vertical external load. Arch action models are used together with truss analogy models that resist the remaining part of the external load. Examples of arch action models are described in the Model Code 1990 (*fib* 1993), Huber (2016), Huber et al. (2016a, b, c), Gleich et al. (2015, 2016, 2018). Arch action models differ in the approach of composing the shape of the compressive arch and the way the truss analogy model was applied. The model of Huber (2016) is intended for the region without flexural cracks (zone B as described in Section 5.1.7). Therefore, the model of Huber will be further described in this section.

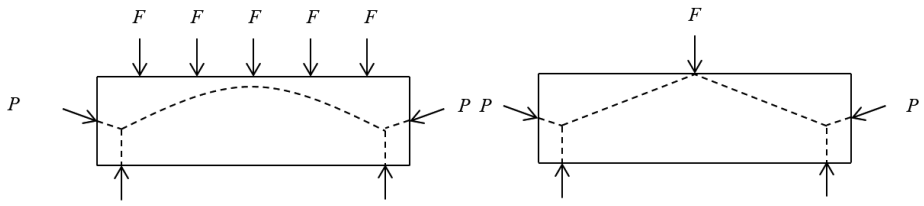

Figure 5.20. Arch profiles adapted to different load patterns according to Model Code 1990 (*fib* 1993)

According to the model of Huber, the shear resistance in a region without flexural cracks, consists of a contribution of the vertical component of the inclined compressive

strut V_{cc} and a contribution of stirrups $V_{R,s}$ (Equation 5.47). The model for shear resistance assumes no contribution of aggregate interlock ($V_{R,ci}$) to the shear resistance.

$$V_R = V_{R,s} + V_{cc} \tag{5.47}$$

The critical cross-section for the resistance is assumed to be at a distance x_{crit} from the support, that is equal to the depth of the beam (h) minus the distance between the ultimate top fiber and the centre of gravity of the cross-section ($z_{c,0}$), see Figure 5.21.

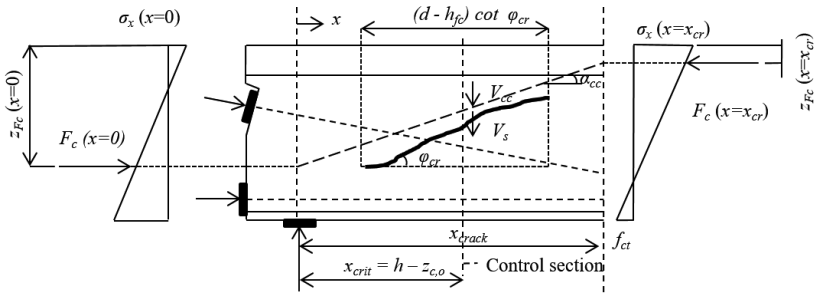

Figure 5.21. Compression arch model Huber (Huber 2016)

V_{cc} is defined as the vertical component of the inclination of the compression strut. To determine the inclination of the compression strut, two cross-sections are considered. The first cross-section is located at the support ($x = 0$). The second cross-section is located at the location of the first flexural crack ($x = x_{cr}$) . In this cross-section the longitudinal stress σ_x in the ultimate fiber equals the uniaxial tensile strength f_{ctm}. For both cross-sections, the distance z_{Fc} between the ultimate fiber and the resulting concrete compressive force (F_c) is found from the stress distribution over the cross-section. This is determined from the cross-section forces using Hooke's law. The angle of the compressive strut α_{cc} can be determined from Equation 5.48. As a simplification, the force in the compression strut is assumed to be equal to the component of the prestressing force parallel to the girder axis (P_x). With this assumption Equation 5.49 is found.

$$\alpha_{cc} = \arctan\left(\frac{z_{Fc(x=0)} - z_{Fc(x=x_{cr})}}{x_{cr}}\right) \tag{5.48}$$

$$V_{cc} = P_x \sin\alpha_{cc} \tag{5.49}$$

The contribution of the reinforcement is given by Equation 5.50. The angle of the crack is assumed to be equal to φ_{cr}, which is the angle of the principal stresses at a load that causes a diagonal tension crack. This is the case if the principal tensile stress in the web equals the biaxial concrete tensile strength $f_{ctm,eff}$ (Equation 2.8 in Section 2.1.4). The angle φ_{cr} varies over the height of girder. As a simplification, φ_{cr} is based on the principal

stresses at the centre of gravity. Rotation of the crack after formation of the crack is assumed to be obstructed by the uncracked compression zones between the crack and the ultimate fiber on both sides of the crack. It is further assumed that the stirrups are yielding along a length cot φ_{cr} multiplied with the effective depth d minus the height of the compression flange h_{fc}.

$$V_{R,s} = \frac{A_{sw}}{s_w}\left(d - h_{fc}\right) \cdot f_{ywm} \cdot \cot \varphi_{cr} \tag{5.50}$$

There are some critical remarks to make regarding the model of Huber. As no comparison with experiments is done, because these were assumed to be not available, the model is not validated. It is unknown if the model can predict the shear resistance accurately. Moreover, the model assumes no contribution of aggregate interlock as the rotation of the compressive strut is obstructed by the uncracked flanges. This assumption is in contrast to observations of experiments for which the flange remained free of flexural cracks in the shear critical region, carried out by Rupf et al. (2013). For these experiments, the inclination of the principal compressive strains was measured at the last load step just before failure. These measured angles were found to be significantly lower than the observed angle of the cracks. This clearly indicates that the compressive struts have rotated between the formation of the diagonal cracks and the ultimate failure of the girder.

5.2 Comparison of models from literature

In this section, models as described in Section 5.1 are mutually compared. These comparisons concern the following aspects:

1. the applicability for regions without flexural cracks
2. the assumed failure mode
3. the contribution of the stirrups to the shear resistance
4. the contribution of the concrete to the shear resistance
5. the contribution of the uncracked concrete to the shear resistance

The first aspects concerns the applicability for regions without flexural cracks. All models are intended to determine the shear resistance of prestressed girders with stirrups in regions without flexural cracks either specifically or in combination with regions with flexural cracks. Two models are specifically intended for regions without flexural cracks and cannot be used for regions with flexural cracks. These concern the models of Leonhardt and Huber. The model of MacGregor et al. describes the resistance to web-shear failure and flexural shear failure. In the region without flexural cracks the resistance to web-shear failure will always be governing. This is because the resistance to flexural

shear failure equals the resistance to flexural shear cracking and an additional term. The models of Bentz et al. and Esfandiari do not explicitly distinguishes regions with and without flexural cracks. However, the longitudinal strain at the mid-depth of the girder (ε_x) significantly affects the predicted resistance. As the values for the longitudinal strain at the mid-depth associated with regions without flexural cracks will be lower than for regions with flexural cracks, the associated shear resistance will be higher. The variable angle truss model, does not distinguishes the resistance in regions with and without flexural cracks.

The second aspect concerns the assumed failure mode. All models determine the shear resistance under the condition that failure due to concrete crushing before yielding of the stirrups, is not governing. To capture this condition, each model describes an associated equation for this maximum shear resistance. Only the model of Esfandiari predicts the governing shear failure mode. This concerns either failure at first yielding of stirrups or failure due to stirrups yielding and concrete crushing simultaneously. According to the variable angle truss model, failure occurs due to the simultaneously crushing of concrete and yielding of stirrups. Also the model of Huber assumes that at failure the stirrups yield, but the resistance of the compressive struts is verified independently. The model of Bentz does not explicitly predict the failure mode. The models of MacGregor et al. and Leonhardt are empirical and do not further distinct specific failure mechanisms.

The third aspect concerns the contribution of the stirrups to the shear resistance. The models determine the contribution of the stirrups to the shear resistance ($V_{R,s}$) differently. The equations used in the models are shown in Table 5.6. All models assume yielding of the stirrups at failure. All models also assume yielding along the horizontal projection of a diagonal crack. Only the horizontal projection of the diagonal crack differs per model. According to the variable angle truss model the angle θ is found for the condition that the shear force associated with crushing of the compressive struts is equal to the shear force at yielding of the stirrups. In the variable angle truss model θ concerns the angle of the compressive strut and can be lower than the angle of the cracks. The contribution of aggregate interlock is implicitly included in θ. If the ranges of parameters according to Table 1.1 are applied, the values for θ are found as listed in Table 5.6. The variable angle truss model bases the horizontal projection of a diagonal crack on the internal lever arm. The cracking angle according to the model of MacGregor et al. is determined as final part of the empirical model (a value of 42˚ was found that was conservatively set to 45˚). MacGregor already recognised that the angle was too steep compared to observations (Section 5.1.2). The model according to MacGregor et al. bases the horizontal projection of a diagonal crack on the effective depth d. The cracking angle according to the model of Bentz et al. depends on ε_x. According to the model of Esfandiari the cracking angle depends not only on ε_x but also on f_{ywm}, f_{cm}, and ρ_z and on

the failure mode. If the range of parameters according to Table 1.1 is applied and it is further assumed that $-0.2 \leq \varepsilon_x \leq 0$ mm/m (which is typical for regions without flexural cracks), values for θ are found as listed in Table 5.6 ('indication θ)'. Both models base the horizontal projection of a diagonal crack on the internal lever arm. According to the model of Huber it is assumed that the diagonal crack does not extend into the most compressed flange but remains in the web. Therefore, the horizontal projection of a diagonal crack is based on the height of the effective depth minus the height of the compression flange. Huber assumes that the angle of the crack equals φ_{cr}, which is the angle of the principal stresses at a load that causes a diagonal tension crack.

Table 5.6. Comparison between models regarding contributions of aggregate interlock & stirrups for $-0.2 \leq \varepsilon_x \leq 0$

Model	Variable angle truss model (Section 5.1.1)	MacGregor et al. (Section 5.1.2)	Bentz et al. (section 5.1.5)	Esfandiari (Section 5.1.6)	Huber (Section 5.1.8)
$V_{R,s}$	$A_{sw}/s\, f_{ywm}\, z \cot\theta$	$A_{sw}/s\, f_{ywm}\, d$	$A_{sw}/s\, f_{ywm}\, z \cot\theta$	$A_{sw}/s\, f_{ywm}\, z \cot\theta$	$A_{sw}/s\, f_{ywm}\, (d - h_{fc})\cot\varphi_{cr}$
Indication θ	$22° \leq \theta \leq 25°$	(θ =45°)	$28° \leq \theta \leq 29°$	$15° \leq \theta \leq 26°$	
$V_{R,ci}$	Implicitly via θ	$0.291\sqrt{f_{cm}}\, b_w\, d_p + 0.3\sigma_{cp}\, b_w\, d_p$	$\beta\sqrt{f_{cm}}\, b_w\, z$	$\beta\sqrt{f_{cm}}\, b_w\, z$	None
Indication β			$0.40 \leq \beta \leq 0.57$	$0.03 \leq \beta \leq 0.21$	

The fourth aspect concerns the contribution of the concrete to the shear resistance. The models determine the contribution of the aggregate interlock ($V_{R,ci}$) differently. The variable strut model has no separate term to predict the contribution of aggregate interlock. Hence, aggregate interlock is implicitly considered by allowing an angle of the compressive struts less than the cracking angle. According to the model of MacGregor et al., the contribution of the concrete equals the resistance to diagonal tension cracking. This explains the presence of σ_{cp} which is not present in the other models. The models according to Bentz et al. and Esfandiari explicitly predict the contribution of aggregate interlock. The contribution of the aggregate interlock, expressed in β, according to the models of Bentz et al., depends on ε_x. According to the model of Esfandiari the concrete contribution depends not only on ε_x but also on f_{ywm}, f_{cm}, and ρ_z and on the failure mode. If the range of parameters according to Table 1.1 is applied and it is also assumed that $-0.2 \leq \varepsilon_x \leq 0$ mm/m, values for β are found as listed in Table 5.6 ('indication β)'. The model of Huber does not take into account the contribution of aggregate interlock.

The fifth aspect concerns the contribution of the uncracked concrete to the shear resistance. None of the described models explicitly considers the contribution of the uncracked flanges to the shear resistance.

5.3 Database on shear failure of prestressed girder with stirrups

To be able to study the resistance of prestressed girders with stirrups in regions without flexural cracks, experiments have been inventoried from literature. These experiments are used to compile a database. These inventoried experiments will be used for specific analyses (Chapter 7). These experiments will also be used to evaluate the accuracy of the proposed model (Chapter 8).

This section describes the database that is compiled of experiments on prestressed girders with stirrups for which failure could be related to diagonal tension cracks. Section 5.3.1 explains the choice of the criterion 'failure related to diagonal tension cracks' as main criterion for the selection. This is used instead of 'failure in a region without flexural cracks', which is the scope of the current research. Section 5.3.1 further explains the other selection criteria that are used. Section 5.3.2 provides an overview of the selected experiments.

5.3.1 Selection criteria

In literature no reports are found that explicitly mention whether failure occurred in a region with or without flexural cracks. Many reports were found from literature on the other hand of experiments for which failure could be related to diagonal tension cracks. Therefore, it was possible to compile a database of experiments for which failure could be related to diagonal tension cracks. This is the main reason why 'failure related to diagonal tension cracks' is chosen as main selection criterion instead of 'failure in a region without flexural cracks'.

For these experiments it is however uncertain if failure also occurred in an region that remained free of flexural cracks until failure. This is illustrated in Figure 5.22. The left part of the figure shows the crack pattern at diagonal tension cracking. Shallow flexural cracks are present at this load stage, but just outside the region which could be critical for shear failure. The right part of the figure shows the crack pattern at failure. At this load stage, flexural cracks have penetrated into the region critical for shear failure. These cracks are shallow and did not merge with the diagonal tension cracks. Nevertheless, flexural cracks were present in the region in which the girder failed. Hence, although it was explicitly reported that the failure could be related to diagonal tension cracks, failure took place in a region with flexural cracks.

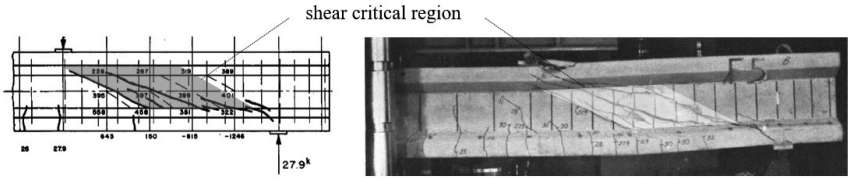

Figure 5.22. Crack pattern at diagonal tension cracking & at failure (experiment F5B, Hanson 1964a).

In contrast to Figure 5.22, it is frequently not clear from reports from literature whether failure occurred in a region with or without flexural cracks. Therefore, the presence of flexural cracks is not based on observations of experiments. The presence of flexural cracks will be calculated instead. These calculations are carried out based on a method, described in Section 8.1. This method will be used to further select experiments that failed in regions without flexural cracks. Eventually, the accuracies of the models are based on the experiments for which no flexural cracks are predicted in the shear critical region.

The literature survey which is covered by the presented database, includes the following overviews and databases:

- an overview listed in a state-of-the art report on shear in prestressed concrete members (Walraven 1987).
- an overview of experiments used for verification of a shear design method (Collins et al. 1996).
- a shear database on prestressed members (Nakamura 2011).
- an overview of prestressed girders of a database with shear test on structural concrete girders (Reineck et al. 2012).

All these overviews and databases consist of a part with and a part without stirrups. Considering the purpose of the database, only the parts with stirrups are considered.

The main selection criterion is whether shear failure can be related to diagonal tension cracks. Experiments for which failure was related to flexure cracks or flexural shear cracks are not included in the database. Also experiments that failed within the transmission length of pre-tensioned tendons are excluded.

The section is based on the following criteria and considerations:

- Only reports and dissertations that contain sufficient information to predict the shear resistance are included.
- Both simply and continuously supported girders are collected, because both supporting conditions are part of the intended application of the developed model (Section 1.5).

- Only normal weight concrete is considered as this is the intended application (Section 1.5).
- Only experiments with vertical stirrups are considered.
- The behaviour of shear failure between girders with bonded and unbonded prestressing steel can differ fundamentally. This is because for girders with only unbonded prestressing steel the only equilibrium model is a tied arch (Walraven 1987). This is the case unless girders contain also reinforcement or if flexural cracks are only present over a limited length. As unbonded prestressing steel are not applied in prestressed bridge girders in the Dutch Highways, experiments with unbonded prestressing steel are not selected in the database. An exception is the experiment carried out by Xie (2009), which could be selected, because in addition to unbonded prestress also bonded reinforcement was applied.
- The developed model is not intended for girders that have insufficient stirrups to prevent failure after diagonal tension cracking. The resistance of these girders does not differ from the resistance of girders without stirrups. Therefore, girders that instantly fail after diagonal tension cracking are not included in the database. For a part of experiments with a low shear reinforcement ratio, the resistance is higher than the resistance to diagonal tension cracking. In advance it can be difficult to determine if this additional resistance is due to the presence of stirrups. Hence a part of the girders without stirrups has some residual resistance after diagonal tension cracking (Chapter 2.1.1. and Figure 2.2). In Section 8.4.1 both the resistance to diagonal tension cracking and the resistance considering the presence of stirrups are predicted. Experiments are selected for which the predicted resistance, if the presence of stirrups in considered, is higher than the predicted resistance to diagonal tension cracking.
- The ratio of the shear span to the effective depth (a/d) could be chosen as selection criterion. In literature, a/d is a common selection criterion if only the behaviour of slender girders is investigated. By selecting only experiments with a large a/d, the increase to the resistance due to direct transfer mechanism is limited (Section 5.1.8). For instance a minimum a/d of 2.4 is used in the Reineck database for slender girders (Reineck et al. 2012). The same limit is applied by Bentz to select experiments to verify the accuracy of the sectional analyses programme *Response* (Bentz 2000). Most models are intended to describe sectional behaviour and conservatively neglect any contribution of direct load transfer mechanism. Also the model that is developed as part of this research is intended to describe sectional behaviour. It is however uncertain if a minimum a/d of 2.4 is a valid limit for prestressed girders that fail in the region without flexural cracks. Therefore, a/d is not used as selection criterion. Part of the research is to investigate if the predictions according to the proposed model for

shear resistance in regions without flexural cracks are affected by a/d. This is an additionally objective of the current research.

– It should be avoided to base models that are intended for large girders in practice on test results of small experiments, considering the influence of the sizes of girders to their structural behaviour. Crack spacing in small girders is small compared to higher girders if girders do not contain stirrups. As a result the aggregate interlock component is much higher in small girders compared to deeper girders. This is called a 'size effect'. However, for girders with stirrups, crack spacing is controlled and no significant size effect is expected (Bentz et al. 2006a). Nevertheless, to limit the chance that deviant behaviour of small girders affects the development or evaluation of models, only experiments with a member height larger than 450 mm are selected. The selection criterion can be considered as relatively strict compared to criteria used by other researchers to compile their databases. For instance Avendano et al. (2008), Hawkins et al. (2007), Birrcher et al. (2009) and Reineck et al. (2012) used respectively a minimum girder height of 305, 508, 305 and 70 mm as selection criteria for their databases. An additional goal of the current research is to investigate whether the predictions are consistent for different girder heights according to proposed model for the shear resistance in regions without flexural cracks.

5.3.2 Overview of selected experiments

The database of shear failure related to diagonal tension cracks of girders with stirrups is included in Appendix F. An overview of the selected experiments and associated ranges of parameters is given in table 5.7. Figure 5.23 illustrates the described parameters. Fifty seven experiments are selected that meet the selection criteria as described in section 5.3.2. Both simply as continuously supported girders are included. Selected experiments contain both post-tensioned and pre-tensioned tendons. The applied geometries of the tendons of the experiments are straight, draped and curved.

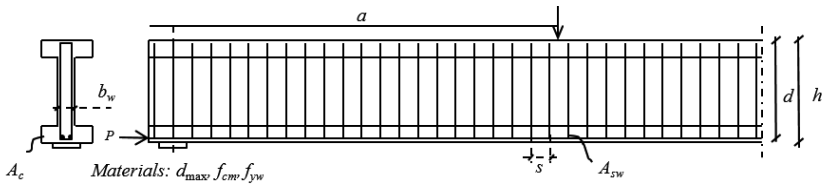

Figure 5.23. Data used to determine the main parameters and characteristics of the experiments

The main selection criterion is if failure could be related to diagonal tension cracks. The selected experiments meet this condition. This is argued in the remaining part of this section.

Table 5.7. Overview database on shear failure related to diagonal tension cracks, girders with stirrups

Researcher (year)	Identification (number of experiments)	Prestressing	Support conditions	h	σ_{cp}	ρ_w	f_{cm}	a/d	d_{max}
				mm	N/mm^2	%	N/mm^2	-	mm
Elzanaty et al. (1986)	CW10,CW11, CW12, CW13, CW14, CW15, CW16, CW17 (8)	Straight pre-tensioned tendons	Simply supported	457	7.9-11.3	0.25-0.79	40-74	3.4-3.7	13
Choulli (2005)	HCP2TE, HCP2TW, HAP2TW, HCP1TE, HCP1TW, HAP1TE, HAP1TW (7)	Straight pre-tensioned tendons	Simply supported	750	6.3-9.6	0.50	81-96	3.0-3.1	12
Hanson (1964)	FX1A, FX1B,F1A, F1B, F2A, F2B, F3A, F3B, F4B, F5A, F5B, F19A (12)	Straight pre-tensioned tendons	Simple supported	457	5.8-6.4	0.20-0.74	44-51	1.9-3.2	19
Leonhardt et al. (1973)	ŢP2, ŢP4 (2)	Draped post-tensioned cable with bond	Simply supported	970, 900	5.5, 6.3	0.70-2.31	24, 47	3.9	15
Rupf et al. (2013)	SR21, SR22, SR23, SR24, SR25, SR26, SR27, SR29, SR30 (9)	Curved post-tensioned cable with bond	Continuously supported	780	2.3-4.9	0.06-0.25	28-37	6.6-6.9	16
Mattock et al. (1961)	S1, S2, S3, S5, S6, S7, S8, S9, S10, S11, S12, S13, S21 (13)	Straight pre-tensioned tendons	Continuously supported	648	8.0	0.37-1.12	42-47	1.0-4.5	19
Xie (2009)	LB2, LB3, LB6, LB7, LB8, LB10 (6)	Straight post-tensioned	Continuously supported	500	4.3-11.2	0.19-0.37	62-64	5.1	10

A part of the experiments of the experiment of Elzanaty et al. (1986) that were designed to fail as result of 'web shear failure' (CW-series) contain stirrups. For these experiments the experimentally found shear resistance is reported. As the failure was related to diagonal tension cracks, all experiments of the CW-series with stirrups are selected. It was reported that flexural cracks were present but that these were all shallow and did not propagate in the web. It is difficult to confirm the selection based on the photos of the failed experiments. Hence, it is unclear from the photos to what extend the flexural cracks were expanded. Therefore, the selection is based on the description. The failure modes reported concern extensive crack opening, sometimes combined with crushing of concrete. For two experiments the diagonal tension cracks propagated through the top flange.

A part of the experiments tested by Choulli (2005) contain stirrups. It was reported that six of the experiments failed as a result of diagonal tension, yielding of the stirrups and crushing of the concrete in the web. Because the failure was associated with diagonal tension, these six experiments were selected for the database. It was difficult to confirm the selection based on the photos. That is because it was unclear from the photos to what extend the flexural shear cracks were expanded. Therefore, the selection is based on the description. Experiment HCP2TW was reported to fail as result of stirrups rupture and concrete crushing. Because it was reported that the rupture occurred in a diagonal tension crack, also this experiment is selected.

In the dissertation of Hanson (1964) a distinction was made between if flexural shear cracks or diagonal tension cracks could be associated with the shear failure mechanism. This was done by studying photographs of the tested girders taken before and after failure. All experiments for which failure was related to diagonal tension cracking are selected. The failure modes reported concern web crushing, stirrups fracture and shear compression.

For two of the experiments in the research report of Leonhardt et al. (1973) that failed in shear, the failure could be associated with diagonal tension cracks. This was determined from the figures in the report that describe the development of the cracks. These two experiments are selected. The associated photos were studied and it was confirmed that failure was related to diagonal tension cracks.

Most of the experiments that were part of the experiment carried out by Rupf et al. (2013) concerned prestressed girders with a flange. It was reported that all these girders failed in the region of the point of contraflexure. Therefore, the experimentally found resistance was related to diagonal tension cracking. All experiments that contained prestress were selected. For two of these experiments photos of the final crack pattern were present that confirmed that failure was related to diagonal tension cracks. Two failure

modes were described. The first concerned failure of the web by large openings of the cracks of the web and rupture of the stirrups. This was observed for experiments with low amounts of shear reinforcement. The second failure mode concerned crushing of concrete simultaneous with yielding of the stirrups. This was observed for higher amounts of shear reinforcement. Although different anchorage conditions were applied in the experiments of Rupf et al., no influence was observed on the shear resistance or the failure mode. However, a potential effect of the anchorage conditions on the predicted resistance cannot be ruled out.

Almost all experiments in the research report of Mattock et al. (1961) failed in shear. For these experiments it was reported that diagonal tension cracks led to failure. The flexural cracks caused by the negative moment were too close to the support and to steeply inclined to lead to shear failure. Besides, it was reported that flexural cracks merged with diagonal tension cracks that developed independently in the web. Nevertheless, all the experiments for which the girder failed in shear are selected, as the diagonal cracks are diagonal tension cracks. For some tests, photos of the failed experiments were present and for several other experiments figures of the cracking pattern. These were studied and it was confirmed that failure was related to diagonal tension cracks. All girders failed due to crushing of the web and simultaneously yielding of the stirrups.

Seven experiments that were part of the experiment carried out by Xie (2009), concerned prestressed girders with stirrups. One experiment suffered some problems with the formwork and was not selected. It was reported that failure occurred due to rupture of the stirrups and sliding along a major inclined web-shear crack for all experiments, so all six remaining experiments are selected. For all experiments, crack diagrams were included in the dissertation for each load stage. The dissertation also includes photos of the girders after failure. These crack pattern and photos confirm that failure was related to diagonal tension cracks.

5.4 Findings from literature review and further approach

This section describes to what extend the research questions could be answered based on the literature study. Based on these answers an approach is chosen to derive the model which is proposed in this dissertation.

Research question D concerns the question ‘What are the possible shear failure modes for prestressed girders with stirrups in the regions without flexural cracks? Is it possible to relate the shear resistance to the possible failure modes?’. From the literature review it is found that the model of Esfandiari distinguishes possible failure modes. The model also relates the shear resistance to these possible failure modes. This makes the approach

that is used to derive the model of Esfandiari also suitable to further investigate the possible shear failure modes in the regions without flexural cracks. Subsequently it is possible to relate the shear resistance to the failure modes.

Research question E concerns the question ‘How does the low longitudinal strain, that is associated with regions without flexural cracks, affect the shear force transfer mechanism along the diagonal tension crack?. From the literature review two approaches are found. The first approach is to relate the shear resistance to the longitudinal strain. This approach is used in the models based on the MCFT (Bentz et al. and Esfandiari). These models relate the contribution of aggregate interlock and stirrups to the strain at mid-depth. As a consequence, low longitudinal strain, which is associated with regions without flexural cracks, will result in high contributions of aggregate interlock and stirrups. A second approach is to develop models that are only applicable in regions without flexural cracks. In this approach the low longitudinal strain, associated with regions without flexural cracks, is considered implicitly. Such an approach is used in the empirical models of Leonhardt and MacGregor et al..

Research question F concerns the question ‘How can the contribution of the shear force transferred by the uncracked flanges be determined? And how is this contribution affected by the cross sectional properties?’ From the literature review it was found that none of the described models consider the contribution of the shear force transferred by the uncracked concrete (flanges) by a separate term. However, the model of Bentz et al., does consider the contribution of the uncracked most compressed zone implicitly. The contribution by aggregate interlock and stirrups was found to be related to the crack length over the cracked height. The model of Bentz et al., determines the total shear resistance based on a cracked length related to the internal lever arm instead of the cracked height. The difference between the internal lever arm and the cracked height results in the contribution of the uncracked compression flange. A possible contribution of the uncracked least compressed zone, is no part of the model of Bentz et al.. The effect of the cross sectional properties on the contribution by the uncracked concrete, is also not considered in the model of Bentz et al..

The approach used to derive the model of Esfandiari will be used to further investigate the possible shear failure modes in the regions without flexural cracks and to relate the shear resistance to the failure modes (Chapter 6). The newly proposed model will thus be based on the Modified Compression Field Theory (Vecchio et al. 1986). This theory is based on extensively studied membrane behaviour and provides insight into the fundamental behaviour of concrete in shear. The resistance of this well-known membrane behaviour was related (Bentz et al., Esfandiari) to the resistance of a girder by making some clear assumptions.

These assumptions are:

- plane sections remain plane,
- transverse stresses are neglected and
- the resistance is assumed to remain constant over the web (Bentz et al. 2006a).

Because the model is based on this rational theory it is plausible that all parameters that affect the resistance are considered. This is in contrast to the other models for shear resistance that are calibrated using results of experiments on girders. This is obvious for the empirical models (MacGregor et al., Leonhardt). But also in the variable angle truss model the strength of the compressive struts is based on experiments on girders. For the newly derived model, experiments on girders will eventually only be used to investigate the accuracy of the developed model.

It could be argued to just use the model of Esfandiari to predict the shear resistance in regions without flexural cracks, instead of developing a new model. From the literature review, the following remarks can be made regarding to what extend the model of Esfandiari is suitable for the prediction of the shear resistance in regions without flexural cracks (Section 5.1.6):

- The model is derived for values of the longitudinal strain between 0 and 1.0 mm/m. For low values of the longitudinal strain, which can be associated with regions without flexural cracks, the predicted values for both θ and β appear to be conservative compared to the predictions using the MCFT (Section 5.1.6).
- From a comparison with experimentally found resistance, the predicted resistance was found to be conservative for $\varepsilon_x < 0.1$ mm/m (Section 5.1.6). This will eventually be evaluated in Section 8.4.3 for experiments that failed in regions without flexural cracks.
- The model of Esfandiari is derived for values of $0.2\% \leq \rho_z \leq 1.0\%$, $30 \leq f_{cm} \leq 60$ N/mm^2 and $d_{max} = 19$ mm (Esfandiari 2009). For the application of the model for the assessment of existing Dutch Highway bridges also values $\rho_z < 0.2\%$ are of interest just like values of $f_{cm} > 60$ N/mm^2 (Table 1.1). Moreover, a value of $d_{max} = 31.5$ mm is applicable for the assessment of existing Dutch Highway bridges build before the year 2000 (based on experience expert).
- No validation is found in literature for the assumption that the resistance remains constant over the web. Also this substantiation is missing for the now investigated condition that both flanges remain uncracked.
- The contribution of the uncracked concrete is not considered in the model of Esfandiari.

In the newly proposed model the longitudinal strain will not be considered explicitly. The low longitudinal strain will implicitly be considered by developing a model that is only applicable for regions without flexural cracks. It is appealing for practice to avoid the complex calculation of longitudinal strain. This simplifies the models and enables engineers to easily apply the model to assess large numbers of bridges. As the model will be based on the MCFT, a fixed value for the longitudinal strain is assumed (Section 6.1). It is however investigated whether the accuracy increases if the longitudinal strain is considered explicitly (Section 8.4.2).

In the newly developed model, the contribution of the uncracked concrete will be considered by assuming a contribution of aggregate interlock and stirrups over a cracked length associated with a height larger than the cracked height just like the model of Bentz et al. does. This height will be derived for the condition that both flanges remain uncracked.

6

Shear resistance at the mid-depth of the web

In this dissertation a model is derived for the shear resistance of prestressed girders with stirrups in regions without flexural cracks. The model describes the transfer of shear force by aggregate interlock, stirrups and uncracked concrete. The current chapter derives equations for the maximum shear stress that can be resisted at the mid-depth of the web by aggregate interlock and stirrups. Chapter 7 demonstrates that the shear stress that can be resisted at mid-depth of the web is representative for shear stress that can be resisted along the diagonal tension crack. Also the additional shear that can be transferred in uncracked concrete is described in Chapter 7. Chapter 8 describes the proposed model and is based on the results of Chapter 6 and 7 (see Figure 6.1).

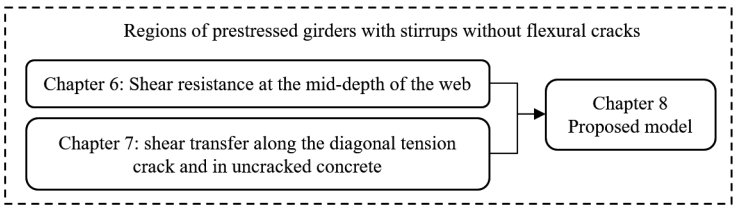

Figure 6.1. Overview of the analysed topics and the allocation of the proposed model per chapter

An overview of the sections is shown in Figure 6.2. The longitudinal strain (ε_x) will not be considered explicitly for the proposed model of Chapter 8. Instead a fixed value is chosen for the regions of a girder without flexural cracks (as announced in Section 5.4). Zero is chosen for this fixed value for ε_x, which is explained in Section 6.1. The shear stress that can be resisted depends on the governing failure mode. Therefore, it is necessary to first determine the possible failure modes for regions without flexural cracks. Section 6.2 determines the possible failure modes for regions without flexural cracks using the approach that was as suggested in Esfandiari (2009) as announced in Section 5.4.

Section 6.3 then describes the shear resistance according to the MCFT for each possible failure mode at $\varepsilon_x = 0$. The resistance is determined using ranges of parameters representative for bridges with a thin web that are designed with a design code prior to the design code of 1974 (NEN 1974), see Table 1.1). Section 6.4 describes the derivation of

the approximation equations for the shear resistance of the mid-depth of the web for $\varepsilon_x = 0$. Consequentially, the resistance can be determined with simplified equations instead of the MCFT. To evaluate the accuracy of the proposed approximation equations, Section 6.5 compares the resistances determined with the MCFT with the resistances obtained with the model of Bentz et al.. Moreover, Section 6.5 compares the resistances determined using the MCFT with the resistances found using the variable angle truss model. By comparing both resistances, the currently used limitation of the inclination of the compressive struts could be evaluated for regions without flexural cracks.

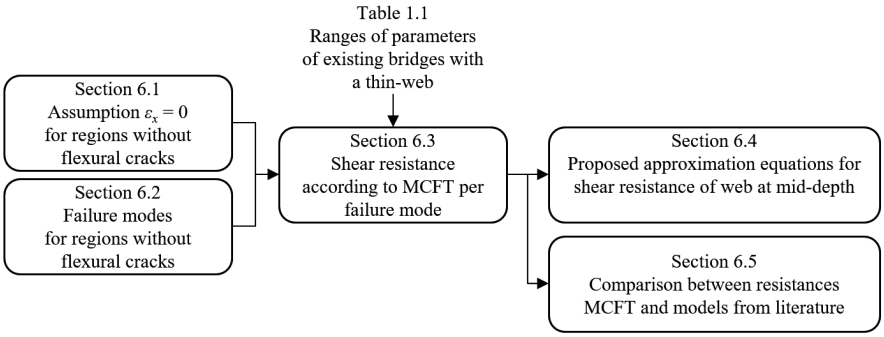

Figure 6.2. Overview and coherence of sections

As the resistance is determined using the MCFT, which is intended for membranes, the term transverse reinforcement is used in this chapter, instead of stirrups. The resistances according to the MCFT are determined using *Membrane* 2000 (Bentz 2000, Bentz et al. 2001) which is a programme that solves the equations of the MCFT as described in Section 5.1.3.

6.1 Longitudinal strains of the web in regions without flexural cracks

In the model proposed in Chapter 8, the shear resistance of the web is based on the resistance calculated with the MCFT. The shear resistance according to the MCFT is related to the longitudinal strain. The shear resistance at mid-depth, investigated in this chapter, thus depends on the longitudinal strain at mid-depth. This longitudinal strain will not be considered explicitly for the proposed model (Chapter 8). This is because, for the regions without flexural cracks, considering the longitudinal strain explicitly will not lead to a more accurate determination of the resistance. This will be demonstrated in Section 8.4.2. Because ε_x does not have to be considered explicitly, complex calculations of the longitudinal strain are not needed, which simplifies the application of the model. Instead of explicitly considering the longitudinal strain, the longitudinal strain is assumed to be zero. In this sections it is explained that ε_x equals zero is a suitable and conservative assumption for regions of a girder without flexural cracks.

In this dissertation, the shear resistance is investigated in regions without flexural cracks (Figure 6.3). A region remains free of flexural cracks, if the stress in the ultimate fibre of the most tensioned flange is smaller than the flexural tensile strength of concrete ($f_{ctm,fl}$). Or, expressed in terms of strains, if the ultimate strain in longitudinal direction in the most tensioned flange ε_t is smaller than the cracking strain ε_{cr} ($= f_{ctm,fl} / E_c$). The cracking strain is about 0.1 mm/m (for $40 \leq f_{cm} \leq 100$ N/mm^2). The longitudinal strain at mid-depth (ε_x) equals ($\varepsilon_c + \varepsilon_t$) / 2, in which ε_c is the strain in the most compressed fibre (Figure 6.3). As $\varepsilon_t \leq 0.10$ and $\varepsilon_c \leq 0$, ε_x will be small or negative (theoretical a maximum value of 0.05 could be found for the maxima $\varepsilon_c = 0$ and $\varepsilon_t = 0.1$ mm/m). Therefore, the assumption of $\varepsilon_x = 0$ at mid-depth could be considered as an upper limit. For lower values of ε_x, the resistance will be higher. A smaller value of ε_x results in a smaller crack width and more aggregate interlock (Figures 5.14, 5.17 and 5.18). A smaller value of ε_x also leads to a higher stirrup contribution, as the cracking angle decreases (Figures 5.14, 5.17 and 5.18). Therefore, it is a conservative assumption to use $\varepsilon_x = 0$ to determine the shear resistances using the MCFT for regions without flexural cracks.

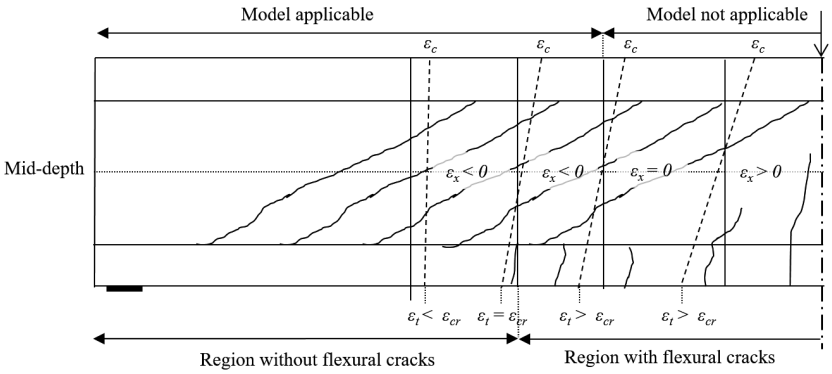

Figure 6.3. Relation between presence of flexural cracks and longitudinal strain at mid-depth

It is noted that, when the longitudinal strain in the web is negative, diagonal tension cracks can still occur (Figure 6.3).. This is because not the longitudinal stresses, that are associated with the longitudinal strains, are decisive for whether a diagonal tension crack occurs, but the principal tensile stresses, that are also largely affected by the shear stresses. This was already demonstrated in Figure 1.5 in which diagonal tension cracks form in the web of a girder in the vicinity of the point of contra flexure.

6.2 Failure modes of the web in regions without flexural cracks

This section determines the shear resistance for a membrane element for a considered failure mode and a considered strain. This approach is suggested in Esfandiari (2009) and described in Section 5.1.6. Esfandiari distinguished failure modes and was able to related the resistance for each failure mode to the strain. Subsections 6.2.1 describes the failure modes that can occur specifically in regions without flexural cracks. Subsection 6.2.2. explains the method to determine the resistance for a failure mode and a strain state in more detail. Moreover, Subsection 6.2.2 explains that the maximum of the determined resistances is governing.

6.2.1 Possible failure modes of the web

The proposed model (Chapter 8) will determine the resistance for two failure modes for $\varepsilon_x = 0$ (Section 6.1):

1. Crushing of the concrete and simultaneous yielding of the transverse reinforcement.
2. Slipping of the crack and simultaneous yielding of the transverse reinforcement.

These two failures modes are also described by Vecchio et al. (1986) as possible failure modes that can be determined using MCFT analyses. A third possible failure mode described in this article, concerns failure due to yielding of the longitudinal reinforcement. This failure mode is not possible in regions without flexural cracks. Therefore, this failure mode is not further considered in this dissertation.

A fourth possible failure mode concerns instant failure due to diagonal tension cracking. This failure could occur if the amount of transverse reinforcement is so low that the membrane element fails directly after diagonal tension cracking. If this is the case, the resistance is comparable to that of a membrane element without transverse reinforcement (Section 2.1.1). As explained in Chapter 2, the resistance to diagonal cracking depends on the stresses in the longitudinal (and potentially transverse) direction and the tensile strength of the concrete. In this dissertation the resistance associated with diagonal tension cracking is called ‘minimum shear resistance’. The determination of this shear resistance is described in Chapters 2 to 4 and Section 8.2. The resistance to diagonal tension cracking is derived analytically and it is not necessary to use the MCFT for this purpose.

A fifth possible failure mode is crushing of the concrete without yielding of the transverse reinforcement. If the amount of transverse reinforcement is high, the concrete can crush before the transverse reinforcement yields. Bentz (2009a) already derived an equation for this upper limit of shear resistance based on the MCFT (Section 5.1.4). In Section 8.2 this derivation is adapted to be suitable to determine the upper limit of the

shear resistance for regions without flexural cracks. It is common to describe the resistance associated with this failure mode as 'maximum shear resistance' (Chapter 5). This definition will also be used in this dissertation.

The described possible failure modes deviate in two aspects from the approach used by Esfandiari. The first aspects concerns yielding of the longitudinal reinforcement (indicated above as 'third failure mode'). As the model of Esfandiari is also applicable for regions with flexural cracks, also failure due to yielding of the longitudinal reinforcement was considered and is a part the model. However, this is not relevant in the current dissertation. The second aspects concerns the failure due to slipping of the crack (indicated above as 'second failure mode'). Esfandiari did not recognize slipping of the crack as failure mode. Instead he defined yielding of the transverse reinforcement as failure mode. As will be shown in Subsection 6.2.2., it is possible to determine the shear stress for several conditions, such as yielding of the traverse reinforcement. Therefore, the analyses (Section 6.3) are also carried out for yielding of the transverse reinforcement ($\varepsilon_x = 0$). It was found that slipping of the crack and yielding of the transverse reinforcement frequently (but not always) resulted in the same shear resistance (Appendix G). However, if this was not the case, the shear stresses associated with the condition sliding of the cracks was found to be higher than the shear stress associated with yielding of the transverse reinforcement for almost all combinations of the considered parameters (Appendix G). The condition associated with the highest shear stress corresponds to the shear resistance. Therefore, failure due to yielding of the transverse reinforcement is not considered as failure mode in this dissertation.

It can be concluded that the proposed model should be suitable to determine the resistance for the first two failure modes. The resistance of the proposed model should eventually be limited to prevent crushing of the compression field without yielding of the stirrups (upper bound). And the proposed model should be combined with the models for diagonal tension cracking which is a lower bound for the shear resistance.

6.2.2 Method to determine the shear resistance of a failure mode

This subsection explains how the resistance of a membrane element can be determined for the two considered failure modes, using the MCFT. This is explained by considering two analyses for a membrane element. The first analysis is intended to demonstrate that sliding of the crack or crushing of the concrete can be governing. The second analysis is intended, in combination with the first analysis, to demonstrate how the shear resistance associated with an investigated strain state (for this investigation $\varepsilon_x = 0$) and an investigated failure mode (for this research crushing of concrete or slipping of the crack) can be determined. It will be described that the resistances can be found by adapting the load increment for a condition associated with a failure, until the longitudinal strain is

zero. This approach is also suggested by Esfandiari (2009), as described in Section 5.1.6. This subsection is intended to explain in more detail how the MCFT is used to determine the resistance of the web of a girder for $\varepsilon_x = 0$.

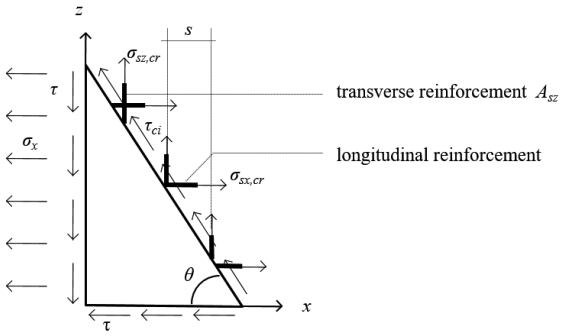

Figure 6.4. Shear transfer across a crack (MCFT, based upon Bentz et al. 2006b)

To explain the two considered failure modes, the explanation of some parameters that follow from the MCFT (Section 5.1.3), are shortly repeated (Figure 6.4). The shear resistance of a cracked membrane element consists of contributions of the transverse reinforcement (τ_s) and of the aggregate interlock (τ_{ci}), according to Equation 6.1. The shear stress transferred by the transverse reinforcement depends on the transverse reinforcement ratio ρ_z (= A_{sz} /(b s), in which b is the depth of the membrane element), the stress in the transverse reinforcement at the crack $\sigma_{sz,cr}$ and the angle of the crack θ (Section 5.1.4.2, Equation 6.2).

$$\tau = \tau_s + \tau_{ci} \tag{6.1}$$

$$\tau_s = \rho_z \sigma_{sz,cr} \cot\theta \tag{6.2}$$

$$\tau_{ci,\max} = \frac{0.18\sqrt{f_{cm}}}{0.31 + \frac{24\,w}{(d_{\max} + 16)}} \tag{6.3a}$$

$$\tau_{ci,max} = \beta\sqrt{f_{cm}} \tag{6.3b}$$

The stress in the transverse reinforcement, the cracking angle and shear stress transferred by aggregate interlock can be found from membrane analyses using the MCFT. If the shear stress transferred by the crack is small, the aggregate interlock stresses follow from equilibrium (Equation 5.26). At this situation, the maximum aggregate interlock stress is not governing ($\tau_{ci} < \tau_{ci,\max}$). If the shear stress transferred by the crack is high, the maximum aggregate interlock stress can be governing ($\tau_{ci} = \tau_{ci,\max}$). This maximum aggregate interlock stress $\tau_{ci,\max}$ depends on the crack width w, the cylinder compressive strength of concrete f_{cm} and the maximum aggregate size $d_{\max}$ (Equation 6.3a, see also

remarks in Section 6.3 regarding higher strength concrete). Equation 6.3a can be simplified by using the parameter β instead of w and d_{max} (Equation 6.3b).

Based on this short repetition of the explanation of some parameters of the MCFT, the first analysis will be described. This analyses is intended to demonstrate that sliding of the crack or crushing of the concrete can be governing. The governing failure mode depends on the amount of transverse reinforcement, the yield strength of the transverse reinforcement and the strength of the concrete. The first analysis is carried out with *Membrane* 2000 (Bentz 2000). The properties of the membrane element are: f_{cm} = 60 N/mm^2, f_{yz} = 250 N/mm^2 (no strain hardening), ρ_z = 0.5%, d_{max} = 31.5 mm and crack spacing parameters $s_x = s_z$ = 400 mm. The element is loaded with load increments of $\delta\sigma_x$ / $\delta\tau$ = -1.82 / 1. The used ratio of load increments and crack spacing parameters lead to ε_x = 0 mm/m at crack slipping and a diagonal crack spacing s_θ of 300 mm. The used load increment will be further explained in combination with the second analyses and in Section 6.3. The shear stress versus shear strain diagram that is found from the membrane analysis is shown in Figure 6.5.

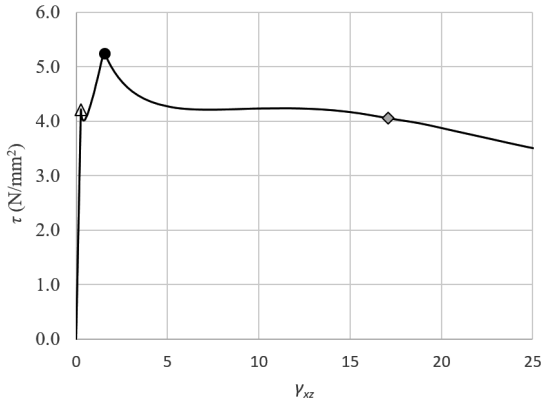

Figure 6.5. Shear stress versus shear strain
(triangle = cracking, circle = crack slipping, diamond = crushing)

Until diagonal cracking, the shear is resisted by the concrete. A diagonal crack forms at the instant the cracking strength is reached (Equation 5.24). The parameters at the load step directly after cracking are shown in Table 6.1. This point is shown in Figure 6.5 with a triangle. At this load step, aggregate interlock stresses are present. Because the crack width is limited, a high value of the maximum aggregate interlock is found (Equation 6.3). At this load, the calculated aggregate interlock stress is less than its maximum (Table 6.1, $\tau_{ci} < \tau_{ci,max}$). As subsequently the load increases, the aggregate interlock stress increases. Simultaneous, the crack width increases and the maximum value of the aggregate interlock decreases. This increase is possible until the crack width has a value

resulting in an aggregate interlock stress that equals the maximum ($\tau_{ci} = \tau_{ci,\max}$). At this load crack slipping occurs. This point is shown in Figure 6.5 with a circle. After diagonal cracking, the stress in the transverse reinforcement at the crack $\sigma_{sz,cr}$ immediately equals the yielding strength ($f_{yz} = 250$ N/mm^2). As also the cracking angle remains about equal, the increase of shear stress between cracking and slipping, can be attributed to the increase of the aggregate interlock stresses (τ, τ_s, τ_{ci}, in Table 6.1).

Table 6.1. Strains, stresses and maximum stresses at different load stages

	strains		at crack							at compression field	
	γ_{xz}	ε_x	θ	τ_s	w	β	$\tau_{ci,max}$	τ_{ci}	τ	σ_2	$\sigma_{2,\max}$
	mm/m	mm/m	°	N/mm^2	mm	-	N/mm^2	N/mm^2	N/mm^2	N/mm^2	N/mm^2
Cracking	0.28	-0.19	26.2	2.54	0.03	0.55	4.29	1.50	4.04	-8.4	-60.0
Slipping	1.58	**0.00**	25.7	2.60	0.49	0.32	**2.51**	**2.51**	5.11	-12.0	-58.1
Crushing	17.1	0.75	18.6	3.71	8.25	0.04	0.31	0.31	4.02	**-13.2**	**-13.2**

After slipping (and yielding of the reinforcement), the cracking angle starts to decrease. The rotation leads to an increase of the contribution of the transverse reinforcement to the shear resistance (Equation 6.2). Simultaneous, as the cracks width increases, the contribution of the aggregate interlock decreases. At increasing loads, also the principal strain ε_1 increases. This results in a reduction of the maximum compressive stresses at the compression field $\sigma_{2,\max}$ (Equation 5.23). Due to the rotation of the compression field, the stress in the compression field σ_2 increases simultaneously. For a certain rotation of the compression field, the compressive stresses at the compression field equals the maximum compressive stress ($\sigma_2 = \sigma_{2,\max}$). At this point the concrete crushes. This point is shown in Figure 6.5 with a square diamond (Table 6.1).

In general two scenarios are possible. The first scenario is that when the load increases, the resistance by the transverse reinforcement due to the rotation of the compression field increases faster than the shear stresses in the aggregate interlock decreases by the crack opening. For this scenario the maximum resistance is found at concrete crushing. The second scenario is that when the load increases, the shear stresses in the aggregate interlock decreases faster than the resistance by the transverse reinforcement increases. For this scenario the maximum resistance is found at crack sliding. This is the case for the considered element (Figure 6.5). The associated failure mode and the maximum shear resistance, depends on the amount of transverse reinforcement, the yield strength and the strength of the concrete (in symbols ψ which equals $\rho_z f_{yz} / f_{cm}$). So depending on ψ, sliding of the crack or crushing of the concrete can be governing.

To derive a model for a girder, the longitudinal strain is the prescribed parameter (Section 6.1). The second analysis demonstrates how to find the shear resistance associated with an fixed strain state (for this investigation $\varepsilon_x = 0$) and an investigated failure mode (for this research crushing of concrete or slipping of the crack). The assumption of a

fixed strain state requires an approach that differs from the first analysis. This is illustrated for the same membrane element as used in the first analysis. In this first analysis the (ratio of the) load was prescribed. The analysis resulted in different values of the longitudinal strain depending on the load step (Table 6.1) and governing failure mode. In the membrane analyses, the fixed strain state $\varepsilon_x = 0$ can be found by adapting the ratio of the load increments $\delta\sigma_x / \delta\tau$ until, for an investigated failure mode, the condition $\varepsilon_x = 0$ is met (iterative process). For both failure modes ($\sigma_2 = \sigma_{2,max}$ or $\tau_{ci} = \tau_{ci,max}$) a resistance can be determined that matches the condition $\varepsilon_x = 0$. Therefore, analyses resulting in $\varepsilon_x = 0$ are carried out for each of the two possible failure modes. Sufficient longitudinal reinforcement is applied to ensure that yielding of the longitudinal reinforcement is not governing. Only the results at $\varepsilon_x = 0$ are of interest for the model that will be developed. The investigated failure modes lead to two shear strain versus shear stress diagrams (Figure 6.6). Associated values of the parameters are shown in Table 6.2. The black dot in Figure 6.6 indicated the point of slipping of the crack for $\varepsilon_x = 0$. The grey diamond indicates the point of crushing of the concrete for $\varepsilon_x = 0$. As the resistance for crack sliding for $\varepsilon_x = 0$ ($\tau = 5.11$ N/mm^2, Table 6.2) is higher than the resistance to concrete crushing for $\varepsilon_x = 0$ ($\tau = 4.35$ N/mm^2, Table 6.2), crack sliding was found to be the governing failure mode for this membrane element.

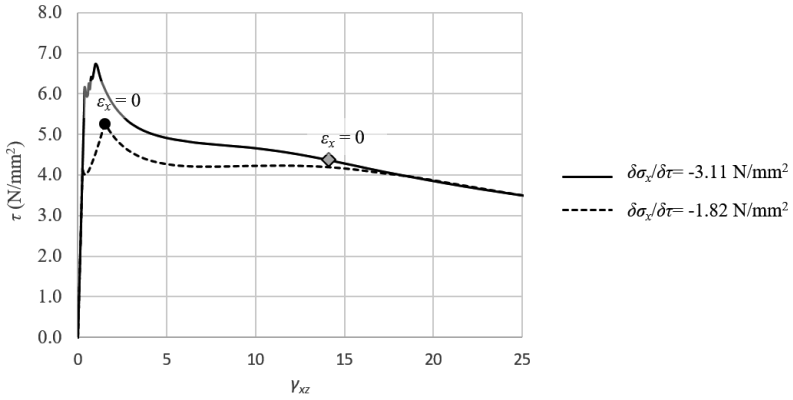

Figure 6.6. Maximum shear at slipping (circle) and crushing (diamond) for $\varepsilon_x = 0$

Table 6.2. Strains, stresses and maximum stresses for $\varepsilon_x = 0$ and $s_\theta = 300$ mm

	load	$s_x =$	at crack							at compression field	
	$\delta\sigma_x/\delta\tau$	s_z	θ	τ_s	w	β	$\tau_{ci,max}$	τ_{ci}	τ	σ_2	$\sigma_{2,max}$
	-	mm	°	N/mm^2	mm	-	N/mm^2	N/mm^2	N/mm^2	N/mm^2	N/mm^2
Slipping	-1.82/1	400	25.7	2.60	0.49	0.32	**2.51**	**2.51**	**5.11**	-12.0	-58.1
Crushing	-3.11/1	376	17.5	3.96	6.70	0.05	0.38	0.38	**4.35**	**-15.1**	**-15.1**

6.3 Shear resistance determined using the MCFT

This section describes the shear resistance according to the MCFT for each possible failure mode at $\varepsilon_x = 0$. Subsection 6.2.2. explained that the resistance for a failure mode should be derived for the condition that corresponds to the failure mode ($\tau_{ci} = \tau_{ci,\max}$ for crack sliding and $\sigma_2 = \sigma_{2,\max}$ for crushing of the compression fields) and $\varepsilon_x = 0$. Also Section 6.2.2 explained that the maximum resistance is governing. This section determines the resistance using ranges of parameters that cover the parameters associated with the bridges with a thin web that are designed with a design code prior to the design code of 1974 (NEN 1974), see Table 1.1. Based on the results of the analyses, approximation equations are derived to determine the shear that can be resisted by the web of a girder in regions without flexural cracks (Section 6.4).

The MCFT (Section 5.1.4) is developed to determine the load-shear response of membrane elements. As mentioned in Section 5.1.4.1, the MCFT is validated using 102 experiments with membrane elements. A mean test-to-predicted resistance ratio was found of 1.01 and an associated coefficient of variation of 12% (Bentz et al. 2006b). For the majority of these membranes only shear loads were applied ($\sigma_x = 0$) or shear loads in combination with longitudinal tension loads ($\sigma_x > 0$). However, for some of these experiments shear loads were applied in combination with longitudinal compressive loads ($\sigma_x < 0$). The accuracy of the predictions for these experiments with compressive loads was similar to the accuracy of the other experiments. Since the loading conditions of some of the reported tests are similar to the stress conditions in the web investigated in the current research, it is assumed that the prediction of MCFT results in an accurate determination of the real behaviour of the structure. Eventually, the proposed model (Chapter 8) is also validated with experiments on girders (Section 8.4).

The resistances are determined using the MCFT for a wide range of parameters. The parameters are determined in such a way that they are representative for the intended application of the model (Table 1.1). In Table 6.3, the parameters are listed and arguments are summarized for the investigated values of the parameters. Forty analyses per failure mode are carried out. The effect of the longitudinal strain parameter ε_x and the diagonal crack spacing parameters s_θ on the accuracy of the predictions is investigated as part of the evaluation of the model (Section 8.4.2). In *Membrane* 2000, the value of $d_{\max}$ is linearly reduced from its actual value at $f_{cm} = 60$ N/mm^2 to zero at $f_{cm} = 80$ N/mm^2. For higher strength concrete the aggregate size is assumed to have no significant effect on the shear strength. This is because in higher strength concrete the cracks run through the aggregates due to the strong paste (Bentz et al. 2006a). Because of the drop in aggregate interlock resistance at these values, not only the minimum and maximum values are examined ($f_{cm} = 40$ N/mm^2 and $f_{cm} = 100$ N/mm^2), but also the two mentioned intermediate values.

Table 6.3. Considered parameters for the membrane analyses

Investigated parameter(s)		Comments
ε_x	0 mm/m	This value relates to the investigated regions without flexural cracks as explained in Section 6.1. The effect on the accuracy of ε_x is investigated in Section 8.4.2.
d_{max}	31.5 mm	Common value for d_{max} applied in Dutch bridges (up to 2000). It is noted that d_{max} reduces from the actual d_{max} at f_{cm} = 60 to zero at f_{cm} = 80 N/mm^2. The model is also validated in Section 8.4.2, using d_{max} as applied in the experiments, which leads to a lower resistance.
s_θ	300 mm	Conservative assumption for elements that contain both transverse and longitudinal reinforcement (Bentz et al. 2006a). In Section 8.4.2, both s_θ = 300 mm and the measured value for s_θ are used to validate the model.
f_{cm}	40, 60 ,80, 100 N/mm^2	Concrete strengths of f_{cm} = 40 and 100 N/mm^2 are considered as minimum and maximum values for the concrete strength for Dutch bridges (Table 1.1). As d_{max} reduces from the actual d_{max} at f_{cm} = 60 to zero at f_{cm} = 80 N/mm^2, these strengths are additional investigated.
f_{yz}	250, 600 N/mm^2 (no strain hardening)	Yielding strength of stirrups of 250 and 600 N/mm^2 are considered as minimum and maximum values of the mean yield strength for stirrups applied in Dutch bridges (Table 1.1).
ρ_z	0.10%, 0.25%, 0.50%, 0.75%, 1.00%	A shear reinforcement ratio of 1.00 % is considered as maximum values applied in Dutch bridges (Table 1.1). It is assumed that diagonal tension cracking is governing for values of ρ_z lower than 0.10%. Older bridges typically contain a low amount of shear reinforcement (an indication for the maximum value for bridges that consist of girders is about 0.30%, for box girder bridges the maximum is about 0.70%).

The method used to derive the resistances will be explained. The analyses are carried out using the Programme *Membrane* 2000 which is a programme that solves the equations of the MCFT (Section 5.1.3, Bentz 2000, Bentz et al. 2001). For each combination of parameters the material properties are entered: f_{cm}, d_{max}, f_{yz}, f_{yx}, ρ_z, ρ_x and the geometry of the concrete and reinforcement. Sufficient longitudinal reinforcement is applied to ensure no yielding of the longitudinal reinforcement. Values for the crack spacing in longitudinal and transverse direction (s_x, s_z) are estimated that would lead to s_θ = 300 mm and are entered in the programme. Firstly, failure due to slipping of the crack is investigated. A value for σ_x is estimated and entered that would lead to ε_x = 0 at crack slipping. A full response analyses is carried out and the strain is determined at the

load step that results in $\tau_{ci} = \tau_{ci,\max}$. At this load step ε_x will initially not be equal to zero. Therefore, σ_x is adapted until the condition $\varepsilon_x = 0$ at crack slipping ($\tau_{ci} = \tau_{ci,\max}$) is met (Figure 6.6). Next, the crack spacing parameters s_x and s_z are adapted until s_θ equals 300 mm. Additionally it is checked if this effects $\varepsilon_x = 0$ at crack slipping and possibly again σ_x is adapted until the condition $\varepsilon_x = 0$ is met. Thereafter, the values of the τ_{ci}, θ are noted (Appendix G) and it is checked if the values match the calculated value of τ using equation 6.1 and 6.2. This check is carried out using $\sigma_{sz,cr} = f_{yz}$, so this also confirms that the transverse steel at the crack is yielding at the instant the cracks slips. Also the input values for the crack spacing parameters are noted (Appendix G). Secondly, failure due to crushing of the compression field is investigated. A similar process is carried out. For this failure, σ_x is determined that leads to $\varepsilon_x = 0$ at crushing of the compression field (Figure 6.6). In other words, the load step at which $\sigma_2 = \sigma_{2,\max}$. The resistances ($\tau_R$) determined with the MCFT for each combinations of f_{cm}, f_{yz}, ρ_z, and for each failure mode are listed in Appendix G. The governing resistance is the maximum of the resistances associated with both failure modes (Appendix H). Also the iterative determined values for s_x (and s_z which value is set equal to s_x) and σ_x are listed.

Beside the results of crack sliding ($\tau_{ci} = \tau_{ci,\max}$) and crushing of the compression fields ($\sigma_2 = \sigma_{2,\max}$) also the resistances associated with yielding of the transverse reinforcement are listed in Appendix G. As noted in Section 6.2.1, in Esfandiari (2009) it was not recognized that slipping of the crack was a failure mode. Instead, yielding of the transverse reinforcement was defined as failure mode. As shown in Appendix G, the shear resistance associated with yielding of the transverse reinforcement was never significant higher than the shear resistance associated with sliding of the cracks. But the shear resistance associated with sliding of the cracks was frequently significant higher than the shear resistance associated with yielding of the transverse reinforcement.

In Figure 6.7, the resistances that are found from the MCFT analyses are plotted versus ψ. The maximum values of ψ differs per graph as a consequence of the different considered values for f_{cm} (the ranges of ρ_z and f_{yz} do not differ). The resistance associated with crack sliding is plotted with black trend lines (and black circles) and the resistance associated with crushing of the compression field is plotted with grey trend lines (and grey diamonds). Both trend lines are second order polynomials and are plotted with the intention to show the trend and the governing failure mode (highest of both trend lines). For the lower strength concrete ($f_{cm} = 40$ N/mm^2 and $f_{cm} = 60$ N/mm^2) crack sliding is found to be the governing failure mode. Also for the higher strength concrete ($f_{cm} = 80$ N/mm^2 and $f_{cm} = 100$ N/mm^2) in combination with lower values of ψ, crack sliding is found to be the governing failure mode. For the higher strength concrete in combination with higher values of ψ, crushing of the compression field is found to be governing. This is because for the higher strength concrete $d_{\max} = 0$ so the maximum resistance due to

aggregate interlock decreases. Therefore, the resistance to crack sliding decreases and failure due to concrete crushing was found to become governing. For the higher strength concrete and low values of ψ, on the other hand, the potential increase of the resistance by crack rotation is relatively low. So despite the low contribution of aggregate interlock, crack sliding is still found to be governing for low values of ψ for these higher strengths of concrete.

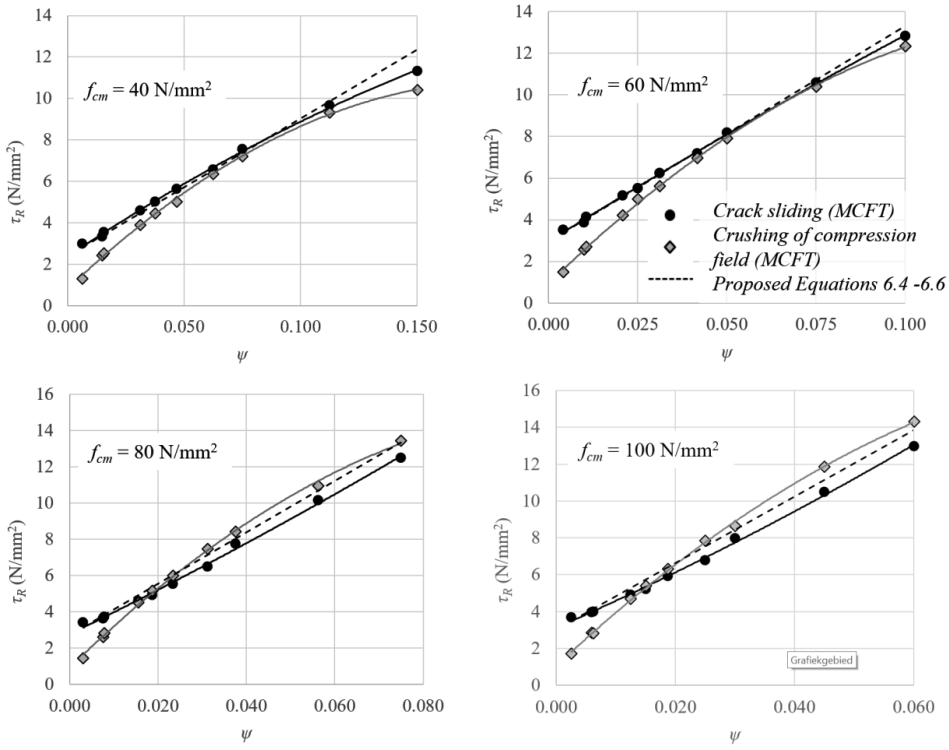

Figure 6.7. Resistance to crack sliding (circles) and concrete crushing (diamonds) at $\varepsilon_x = 0$ versus ψ

6.4 Proposed approximation equations

In Section 6.3, the shear resistance according to the MCFT is determined, for a range of parameters, for both the failure modes crushing of the compression field and slipping of the crack. As explained in section 6.2, the highest of both resistances is governing. In the current section, equations are derived to approximate the resistance found using the MCFT with simple equations. These approximation equations are used for the proposed model (Chapter 8). This prevents that MCFT analyses are necessary for each assessed bridge. In the proposed approximation equations, a distinction is made between the contribution of aggregate interlock to the shear resistance (which corresponds to $\beta\sqrt{f_{cm}}$, as

explained in Section 5.1.4) and the contribution of the stirrups (which corresponds to $\rho_z f_{yz} \cot\theta$, which is also explained in Section 5.1.4).

To derive an approximation equation for the contribution of aggregate interlock, a linear equation $\beta = ea + b\psi$ is assumed. The parameters a and b define the linear model for β, for $f_{cm} \leq 60$ N/mm^2. The parameter e accounts for the drop in the contribution of aggregate interlock for $f_{cm} \geq 80$ N/mm^2 (for which the crack runs through the aggregates). For the contribution of stirrups, a linear equation $\theta = c + d\psi$ is assumed. The values c and d define the linear model for θ. For a combination of a, b, c, d and e, the approached resistance and the resistance according to the MCFT are determined (Section 6.3, Appendix G). Subsequently the mean values of the ratio of both resistances and the associated coefficient of variation are determined using the results of 40 membranes. The values of a, b, c, d and e are adapted until the mean value of the ratio of the resistances equals 1.00 and a minimum coefficient of variation is found (which eventually was 4%). This results in values for a, b, c, d and e of respectively 0.38, -2.5, 26, 0, 0.8 (Equations 6.4 to 6.6).

$$\tau_R = \tau_s + \tau_{ci} = \rho_z f_{yz} \cot\theta + \beta\sqrt{f_{cm}} \tag{6.4}$$

$$\beta = 0.38 - 2.5\psi \qquad \text{for } f_{cm} \leq 60 \text{ N/mm}^2 \tag{6.5}$$

$$\beta = 0.30 - 2.5\psi \qquad \text{for } f_{cm} \geq 80 \text{ N/mm}^2 \tag{6.6}$$

With $\psi = \rho_z f_{yz} / f_{cm}$ and $\theta = 26°$

The following considerations are made regarding the approximation equations:

- As shown in Figure 6.7, for the range of values of ψ, different resistances are found for the two possible failure modes. However, is was found possible to accurately cover the governing (highest) resistance, using just one set of equations (Equations 6.4 to 6.6). This significantly reduces the effort to determine the shear resistance in practice. Moreover, considering both failure modes separately does not lead to a significant increase of accuracy, as the found coefficient for the ratio of the approached resistance and the resistance found from the MCFT was low.
- The resistances according to Equations 6.4 to 6.6 are included in Figure 6.7. In this figure, the results of the approximation equations are compared to the resistance calculated with the MCFT. It is noted that the resistances from the approximation equations should be compared to the highest of the resistance to crack sliding and crushing of the compression field (Section 6.2.1). Equations 6.4 to 6.6 result in a mean value of the ratio of the calculated to approximated resistance of 1.00 and a

coefficient of variation of 4%. Since the coefficient of variation found is so low, apparently all parameters that significantly affect the accuracy are considered. The low coefficient of variation also confirms the suitability of the assumption that the contributions of aggregate interlock and transverse reinforcement depend linear on ψ.

- The largest overestimation for the resistance is found to be 8%. This is found for a membrane with a low strength concrete (f_{cm} = 40 N/mm^2) and with a high values of ψ (ψ =0.150). This overestimation is considered to be acceptable as shear reinforcement ratios of 1% are not expected to be present for existing Dutch bridges (Table 1.1). Only for box-girder bridges, shear reinforcement ratios up to 0.70% are present. Moreover, for these box-girder bridges the concrete cylinder compressive strength will typically be higher than 40 N/mm^2.
- The shear contribution of aggregate interlock is lower for $f_{cm} \geq$ 80 N/mm^2 than for $f_{cm} \leq$ 60 N/mm^2, as explained in Section 6.3. Therefore, the MCFT uses a value for $d_{\max}$ of zero for $f_{cm} \geq$ 80 N/mm^2. This results in a drop in the maximum aggregate interlock resistance according to the MCFT. This can be accounted for by limiting f_{cm} in Equation 6.3 for $\tau_{ci,\max}$ (as done in the model of Bentz et al.), or by adapting the factor β for $f_{cm} \geq$ 80 N/mm^2. It was found that the latter leads to the most accurate approximation.
- It is conservative, considering Equation 6.3a, to interpolate β linearly for 60 < f_{cm} < 80 N/mm^2. This results in a larger reduction of $\tau_{ci,\max}$ than if Equation 6.3a would have been used.
- Note that in Chapters 7 and 8, the parameter f_{yz} which is applicable for membranes, will be replaced by f_{ywm} which is applicable for girders.

Figure 6.8 compares the values of β calculated with the MCFT with the values of β predicted using Equation 6.5 and 6.6. Especially for low values of ψ, the contribution of the aggregate interlock to the shear resistance can be substantial. For the low values of ψ, for which crack sliding is the governing failure mode, the values of β are reasonably approached (Figure 6.8). For higher values of ψ, for which both failure modes can be governing, the β approximation of the MCFT results is poor. However, for higher values of ψ, the contribution of the aggregate interlock to the shear resistance is less significant. This explains why the approximation of the total shear resistance is found accurate despite the poor predictions of β. Therefore, Equation 6.5 to 6.6 are considered as suitable approximation equations for β. Notice that the found drop in the value for β for $f_{cm} \geq$ 80 N/mm^2 according to the MCFT is well captured for low values of ψ, for all concrete strengths by using Equations 6.5 and 6.6. Also the observed trend that relative contribution of the aggregate interlock decreases when ψ increases is well captured with the approximation equations.

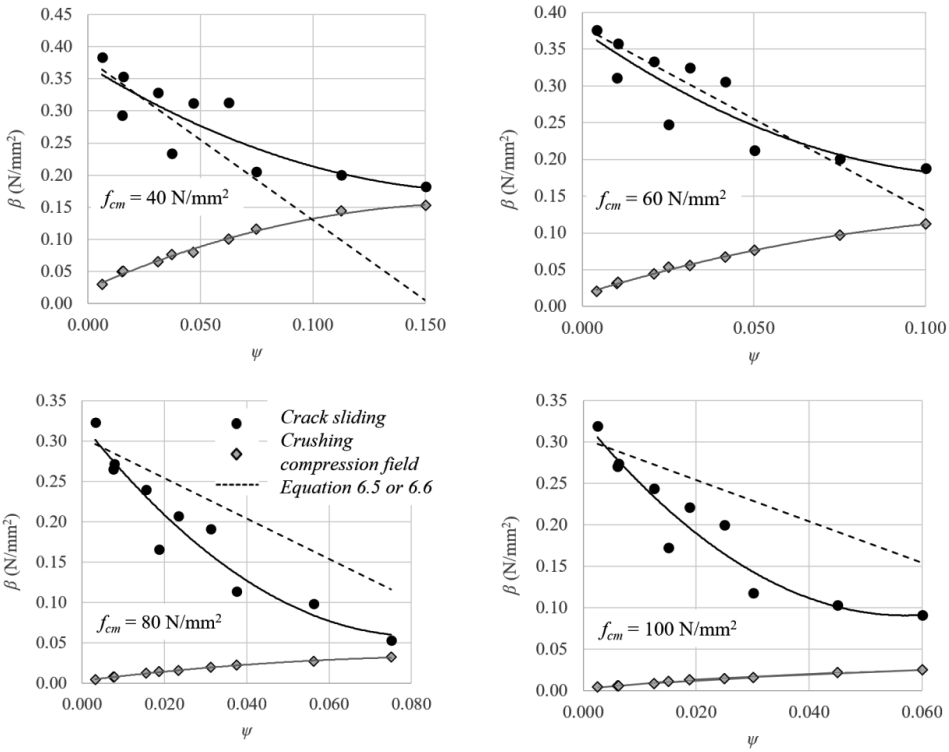

Figure 6.8. β for crack sliding (circles) and concrete crushing (diamonds) at $\varepsilon_x = 0$ versus ψ

Figure 6.9 compares the values for θ calculated with the MCFT to the proposed value for θ of 26°. Crack sliding is found to be governing for all values of ψ for low concrete strengths and for low values of ψ for high concrete strengths. For this failure mode, the approximation of $\theta = 26°$ is reasonable. For high values of ψ, for high concrete strengths, crushing of the compression field is governing. For this failure mode, the approximation of θ is poor. However, the underestimation of θ associated with this failure mode (which causes an overestimation of the contribution of transverse reinforcement), is compensated by an underestimation of β (Figure 6.8). This explains that the approximation of the total shear resistance is accurate. Therefore, the value for θ of 26° is considered as suitable.

6.5 Comparison approached resistances with models from literature

This section compares the resistances for membranes determined with the MCFT for $\varepsilon_x = 0$ (Section 6.3) to the resistances found by using two models from literature as described in Chapter 5. This concerns the model of Bentz et al. (Section 5.1.5) and the variable angle truss model (Section 5.1.1). The model of Bentz is considered to evaluate the proposed approximation equations (Equation 6.4 – 6.6). The variable angle truss

model is considered to evaluate the currently used limitation of the inclination of the compressive struts of 21.8° for regions without flexural cracks, as announced in 5.1.1. (Figure 5.2).

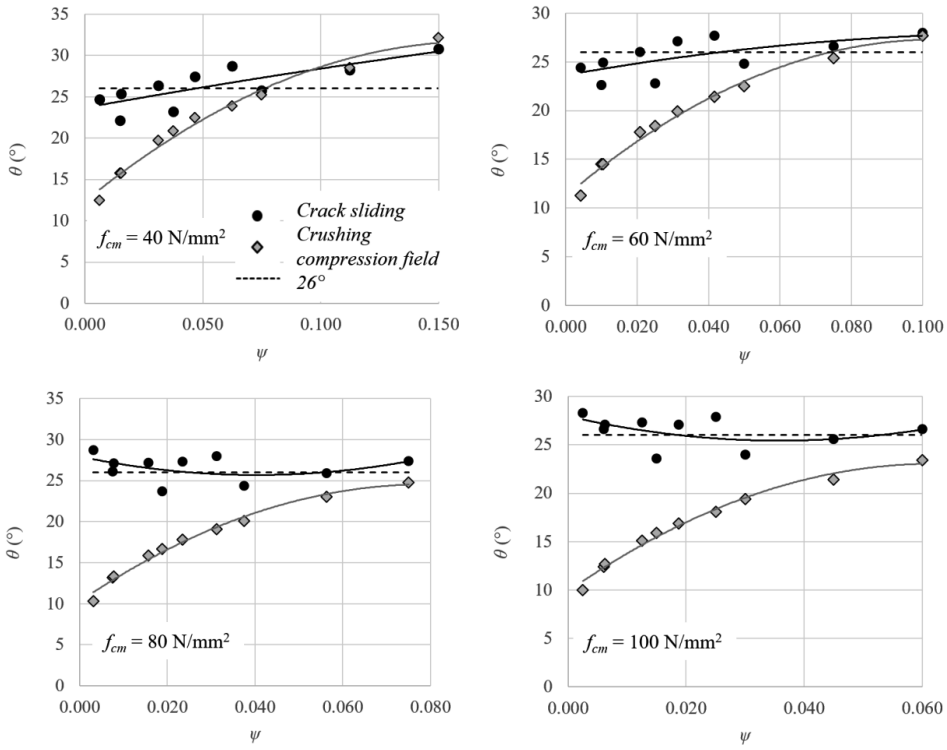

Figure 6.9. θ at to crack sliding (circles) and concrete crushing (diamond) at $\varepsilon_x = 0$ versus ψ

The ratios of the resistances according to the MCFT and the resistances according to the considered models are determined. The mean values and coefficients of variation of the proposed approximation equations (Equations 6.4 to 6.6) and both models are shown in Table 6.4, for zero longitudinal strain. Appendix H lists the ratio of resistance according to MCFT and the models from literature, including some intermediate results, at a longitudinal strain of zero. The derivation of these ratios will be further explained in this section.

6.5.1 Model of Bentz et al.

The approximation equations (Equations 6.4 to 6.6) are intended to accurate approximate the resistance found from the MCFT, for the condition $\varepsilon_x = 0$. Also the model of Bentz et al. is derived from the MCFT for $\varepsilon_x \geq -0.2$. Therefore, the model of Bentz et al. (Section 5.1.5) is considered to evaluate whether the approximation equations indeed

result in more accurate approximation of the resistance found from the MCFT for the condition $\varepsilon_x = 0$.

Table 6.4. Mean value and COV of the ratio of resistance according to the MCFT and according to the models

	Proposed approximation equations Section 6.4	Model of Bentz et al. (Section 5.1.5) Section 6.5.1	Variable angle truss model (Section 5.1.1) Section 6.5.2
Mean	1.00	0.94	1.89
Coefficient of variation	4%	5%	69%

This subsection compares the resistances calculated with the model of Bentz et al. (Section 5.1.5, Bentz et al. 2006a,b, CSA 2006) and the resistances predicted with the MCFT (Section 6.3). The model of Bentz et al. is based on the MCFT and intended for both membrane analyses (Simplified Modified Compression Field Theory, Bentz et al. 2006b) and girder analyses. The model of Bentz et al., and the approximation equations (Section 6.4) both determine the shear resistance with Equation 6.4 (Equation 6.4 is equal to Equation 5.34 in Section 5.1.4). The approximation equations are derived for the condition $\varepsilon_x = 0$. To evaluate the model of Bentz et al. for zero longitudinal strain, ε_x is set to zero. This results in a fixed value for β of 0.4 and a fixed value for θ of 29°. Both the model of Bentz et al. as the proposed approximation equations assume a fixed value for the diagonal crack spacing parameter s_θ of 300 mm. There are some differences between the model of Bentz et al. and approximation equations (Equations 6.4 to 6.6) for the condition $\varepsilon_x = 0$:

1. According to the model of Bentz et al., β and θ are independently of ψ.
2. For girders with stirrups, the resistance according to the model of Bentz et al. is assumed to be independent of d_{max}. The model of Bentz et al. is derived for d_{max} equals 19 mm. It is noted that for values of $f_{cm} \leq 60$ N/mm^2, the MCFT will predict a higher resistance if d_{max} equals 31.5 mm than if d_{max} equals 19 mm.
3. The shear contribution of aggregate interlock is lower for $f_{cm} \geq 80$ N/mm^2 than for $f_{cm} \leq 60$ N/mm^2, as explained in Section 6.3. To account for this effect, the model of Bentz et al. limits f_{cm} to a maximum of 65 N/mm^2 in Equation 6.4. In the approximation equations, on the other hand, β is limited in accordance to Equation 6.6 for $f_{cm} \geq 80$ N/mm^2.

To illustrate the differences, the resistances using the model of Bentz et al. is compared to the resistance according to the MCFT for a membrane element with $f_{cm} = 60$ N/mm^2 and $d_{max} = 31.5$ mm. The results are shown in Figure 6.10. The resistance τ_R calculated

with the MCFT is shown with a solid black trend line (and transparent dots). The contribution of the aggregate interlock τ_{ci} according to the MCFT is shown with a black dotted trend line (and transparent diamonds). The resistance according to the model of Bentz at al. is shown with a solid grey trend line (and grey dots). The model of Bentz assumes a constant value for the contribution of the aggregate interlock τ_{ci}, which is shown with a grey dotted trend line (and grey diamonds). As appear from Figure 6.10, the model of Bentz et al. overestimates the resistance compared to the MCFT. This overestimation can be ascribed to an overestimation of the aggregate interlock for higher values of ψ.

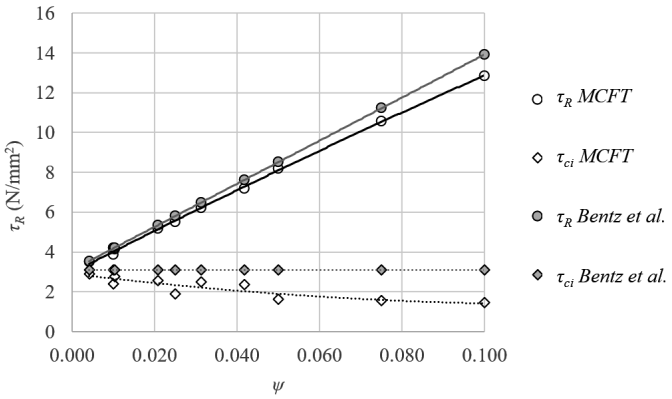

Figure 6.10. Comparison predicted resistances of MCFT with model of Bentz et al. for $\varepsilon_x = 0$

In addition to the analysis for a membrane element with $f_{cm} = 60$ N/mm^2, the comparison is extended to all considered concrete strengths (f_{cm} = 40, 60, 80 and 100 N/mm^2, 40 membranes).

This comparison results in three findings.

1. The model of Bentz et al. results in a mean value of the ratio of the calculated to approximated resistance of 0.94 and a coefficient of variation of 5% (Table 6.4, Appendix H). The coefficients of variation of the model of Bentz et al. and the approximation equations are comparable. However, the model of Bentz et al. overestimates the resistance for the considered ε_x = 0 mm/m. This is the case despite the lower values for $d_{\max}$ (19 mm) for which the model of Bentz et al. is derived.
2. In contrast to the approximation equations in Section 6.4, the trend of a decreasing contribution of aggregate interlock at increasing values of ψ is not present. Hence, in the approximation equations of Bentz et al., a constant value is used.
3. Using the model of Bentz et al., a mean value of the ratio of the calculated to approximated resistance for f_{cm} = 80 N/mm^2 (in which $d_{\max}$ is just zero) is 0.91, with a lowest

value of 0.84. Using the approximation equations of Section 6.4, a mean value of the ratio of the calculated to approximated resistance is found of 1.00 with a lowest value of 0.93. The underestimation can be attributed to using a value of f_{cm} = 65 N/mm^2 in Equation 6.4 to account for the drop in the contribution of aggregate interlock for higher strength concrete ($f_{cm} \geq$ 80 N/mm^2), instead of limiting β in accordance with 6.5 and 6.6.

If only the regions without flexural cracks are considered, the approximation equations are capable to approach the shear resistance according to the MCFT more accurate than the model of Bentz et al.. It is noted that the approximation equations are only suitable to predict the resistance in regions without flexural cracks. The model of Bentz et al., on the other hand, is also suitable to predict the resistance for regions with flexural cracks.

6.5.2 Variable angle truss model

In Section 5.1.1 the hypothesis is made, that if the variable angle truss model is used, no limit is necessary for prestressed girders (Section 5.1.1 and Figure 5.2). In this section it is evaluated whether this can be confirmed, specifically for regions without flexural cracks, by using the resistances found from the MCFT. Therefore, the resistances calculated with the MCFT are compared to the resistances predicted with the variable angle truss model for the condition $\varepsilon_x = 0$ (in the equations and figures the variable angle truss model is abbreviated as VAT). Although the variable angle truss model (Section 5.1.1) is intended for girders, it is also possible to apply the theory to predict the resistance of membranes, by Equations 6.7 to 6.10.

$$\tau_u = \tau_s = \rho_z f_{yz} \cot\theta \tag{6.7}$$

$$\tan\theta = \sqrt{\psi_{vat} / (1 - \psi_{vat})} \tag{6.8}$$

$$\psi_{vat} = \rho_z f_{yz} / \nu\, \alpha_{cw} f_{cm} \tag{6.9}$$

$$\nu = 0.6\,(1 - f_{cm}/250) \tag{6.10}$$

As explained in Section 5.1.1, the factor α_{cw} addresses the effect of prestressing on the strength of the compressive struts. The factor depends on the ratio of the stress in the concrete in longitudinal direction in the centre of gravity (σ_{cp}) and the cylinder compressive strength of concrete (f_{cm}). To be able to compare both models, it is necessary to assume a value for σ_{cp}. For the comparison it is assumed that $\sigma_{cp} = 0.1 f_{cm}$. According to the variable angle truss model, α_{cw} equals to $1 + \sigma_{cp}/f_{cm}$ (for $0 \leq \sigma_{cp}/f_{cm} \leq 0.25 f_{cm}$). The assumption $\sigma_{cp} = 0.1 f_{cm}$ results in a factor α_{cw} of 1.1. With this assumption the resistances can be predicted using the variable angle truss model. The resistances are determined

for the membranes for which the resistance were already calculated using the MCFT (Section 6.3). Note that the variable angle truss model assumes that the resistance is independent of s_θ and $d_{\max}$. Also the longitudinal strain (ε_x) is assumed to have no effect on the resistance, although one could argue that this is implemented to some extend by the factor α_{cw}. It is noted that the version of the Eurocode that is currently under development (CEN 2020), relates the limitation of the angle of the compressive struts to the average axial compressive stresses.

To illustrate the differences, the resistances for the variable angle truss model is compared to the resistance according to the MCFT for a membrane elements with f_{cm} = 60 N/mm^2. In Figure 6.11 the resistance calculated with the MCFT (τ_R) is shown with a solid trend line (and black dots). The contribution of the aggregate interlock τ_{ci} according to the MCFT is shown with a dotted trend line (and transparent diamonds). The contribution of the transverse reinforcement according to the MCFT is the difference between τ_R and τ_{ci} as illustrated with an arrow. The resistance according to the variable angle truss model is shown with a black dashed trend line (and black squares). It is shown that the variable angle truss model underestimates the resistance compared to the MCFT. This underestimation increases for decreasing values of ψ.

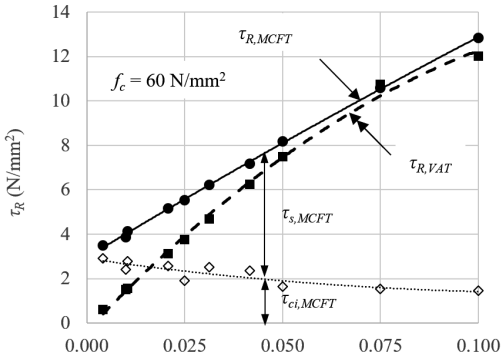

Figure 6.11. Predicted resistances according to the MCFT and the variable angle truss model for ε_x = 0

The underestimation was found to be related to the limitation of the angle of the compressive struts. For the membranes in Figure 6.11, the variable angle truss model predicts only an angle of the compressive strut > 21.8° for values of ψ of 0.075 and 0.100. For these two membranes, the predictions using the variable angle truss model reasonable agree with the results of the MCFT. For lower values of ψ, the minimal angle of the compressive struts is governing and the predictions according to the variable angle truss model deviate from the resistances according to the MCFT. As explained in Section 5.1.1, the effectiveness factor was derived for experiments with higher values for ψ.

Section 5.1.1 also explains that for lower values of ψ , the limit of $\theta = 21.8°$ is governing, which leads to (over)conservative predictions.

Additionally to the results for the membrane elements with $f_{cm} = 60$ N/mm^2, for which the shear strength is shown in Figure 6.11, the comparison is extended to all the considered concrete strengths ($f_{cm} = 40$, 60, 80 and 100 N/mm^2, 40 membranes). A mean value of the ratio of the resistance according to the MCFT and according to the variable angel truss model is found of 1.89 and a coefficient of variation of 69% (Table 6.4). The results are shown in Appendix H. It appears that for 34 of the 40 membranes the lower limit of θ of 21.8° is governing.

It is noted that for reinforced concrete the longitudinal strain in the critical cross-section will be significantly larger than zero. Large longitudinal strains result in low shear resistance. For prestressed girders on the other hand, the longitudinal strains will be lower. In Section 5.1.1 it is shown that the resistance for the considered 76 prestressed girders could be estimated quite accurate without any limitation of θ (Figure 5.2). It is plausible that this can be attributed to the higher resistance due to smaller longitudinal strains. Therefore, it is investigated if the limitation is necessary for predicting the shear resistance at zero longitudinal strain. This is done by comparing $v\alpha_{cw}$, that represents the effective strength of the concrete struts, for the MCFT and the variable angle truss model for the 40 considered membranes. Firstly, $v\alpha_{cw}$ is determined that would result in the same resistances as calculated with the MCFT. For each membrane the resistance is known from the membrane analyses from Section 6.3 (Appendix G). Assuming this shear resistance, θ can be calculated using Equation 6.7, ψ_{VAT} using Equation 6.8 and $v\alpha_{cw}$ using Equation 6.9. The results are the black dots in Figure 6.12. Secondly $v\alpha_{cw}$ is determined according to the variable angle truss model, using Equation 6.10 and the assumption $\alpha_{cw} = 1.1$. This is shown as solid black lines in Figure 6.12. For the lower limit of θ of 21.8°, a value for ψ_{VAT} is found of 0.138 using Equation 6.8. From this value, $v\alpha_{cw}$ associated with the minimal θ can be determined using Equation 6.9. This is shown as continuous grey lines in Figure 6.12. The lowest of both lines is the governing value according to the current variable angle truss model.

As can be seen from Figure 6.12, the lower limit (if governing) results in lower $v\alpha_{cw}$ than calculate with the MCFT (the black dots are all above the grey line representing the lower limit). As expected, the lower limit is found to be too strict. The variable angle truss model without limitation results for most membranes in higher values for $v\alpha_{cw}$ than calculate with the MCFT (the black dots are frequently lower than the black continuous line representing the variable angle truss model without limitation of θ). The hypothesis that no limit is necessary (Section 5.1.1 and Figure 5.2) could not be confirmed based the comparison carried out in this section. On the other hand, it was confirmed that the currently used limitation of θ of 21.8°, is found to be too strict. Section 8.5, suggests an

alternative model in which a more suitable equation for the effective strength of the concrete struts is derived, based on ψ, for zero longitudinal strain.

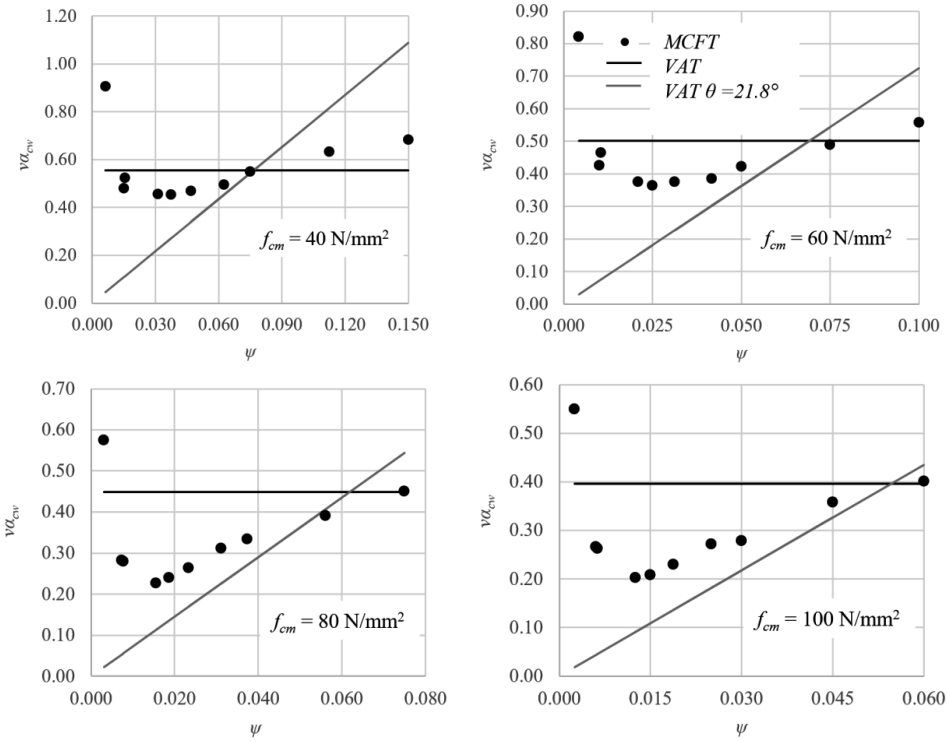

Figure 6.12.Comparison between $\nu\alpha_{cm}$ according to MCFT & predicted with variable angle truss model

7

Shear transfer along the crack and by uncracked concrete

In this dissertation a model is derived for the shear resistance of prestressed girders with stirrups in regions without flexural cracks. The model describes the transfer of shear force by aggregate interlock, stirrups and uncracked concrete. Chapter 6 derives equations for the maximum shear stress that can be resisted at the mid-depth of the web by aggregate interlock and stirrups. The current chapter demonstrates that the shear stress that can be resisted at mid-depth of the web is representative for shear stress that can be resisted along the diagonal tension crack. Also the additional shear that can be transferred by uncracked concrete is described in the current chapter. Chapter 8 describes the proposed model and is based on the results of Chapter 6 and 7 (Figure 6.1).

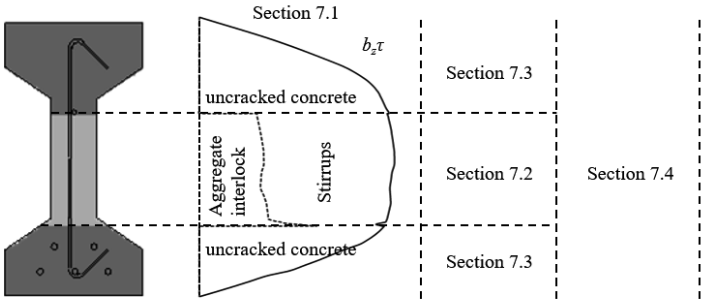

Figure 7.1. Overview and coherence of sections

In Figure 7.1 an overview of the sections of this chapter and their relations is presented. Section 7.1 describes the mechanisms that can contribute to the transfer of the shear force in girders with stirrups in regions without flexural cracks. This section further describes equations to determine the contribution of each shear transfer mechanism to the total shear resistance. Section 7.2 investigates the distribution of aggregate interlock and stirrup stresses along the diagonal tension crack, using *Response* (Bentz 2000). *Response* is a non-linear sectional analyses programme based on the MCFT. Two girders from experiments, which are reported in literature, are analysed that are predicted to fail at a condition that no flexural cracks are present. The decisive failure mechanism of the first girder was crack slipping, while the decisive failure mechanism of the second girder was crushing of the compression field. For both girders, it will be investigated whether the resistance at mid-depth is representative for the resistance along the crack. Section 7.3

describes the contribution of the uncracked concrete to the total shear resistance. Also this contribution is analysed using *Response*. In the proposed model (Chapter 8), the contribution of uncracked concrete is not taken into account explicitly. Instead, it is taken into account by introducing the 'effective shear depth' in the calculation of the shear resistance. An equation is derived to determine the effective shear depth. Section 7.4 summarizes the main results and evaluates to what extend the research questions are answered based on the analyses carried out in Chapter 6 and 7.

7.1 Overview of shear transfer mechanism in a girder

This section describes how shear is transferred in girders with stirrups in regions without flexural cracks. These shear transfer mechanism are illustrated with a free body diagram that is cut through at a diagonal tension crack (Figure 7.2). Shear can be transferred by three mechanism:

1. Shear transfer along the diagonal tension crack by stirrups crossing the diagonal tension crack ($A_{sw}/(b_w\, s)\ \ \sigma_{szcr,z}\ \cot\theta_z$ or $\rho_z\ \sigma_{szcr,z}\ \cot\theta_z$, left part of Figure 7.2)
2. Shear transfer by aggregate interlock stresses ($\tau_{ci,z}$) along the diagonal tension crack (right part of Figure 7.2).
3. Shear transfer by shear stresses in the uncracked concrete ($\tau_{uncr,z}$) above and below the diagonal tension crack (right part of Figure 7.2).

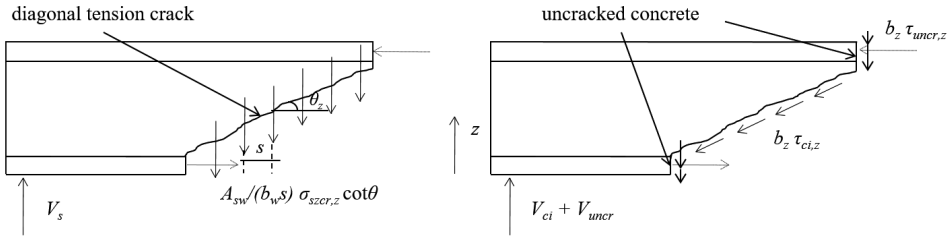

Figure 7.2. Possible shear transfer mechanism in regions without flexural cracks (girder with stirrups)

In the description of the shear transfer by stirrups, A_{sw} is the area of shear reinforcement, b_w is the width of the web, s is the distance between the stirrups, $\sigma_{szcr,z}$ is the stress in the stirrups in the crack and θ_z is the angle of the crack. To make the contributions comparable, the shear transfer by stirrups is considered as distributed stress along the crack. Therefore, the width of the web section is part of the equation. Alternatively the shear transfer by stirrups could be expressed as $\rho_z\ \sigma_{szcr,z}\ \cot\theta_z$ in which ρ_z is the shear reinforcement ratio ($A_s/(b_w\, s)$). The subscription z is used for the parameters that vary along the crack.

For regions without flexural cracks, dowel action of the longitudinal reinforcement is not relevant. At least, as long as the longitudinal reinforcement is located in the flanges

that remain uncracked, which is a reasonable assumption for regions without flexural cracks.

The vertical component of prestressing could be considered as a shear transfer mechanism (cross sectional method). However, in this dissertation the equivalent prestressing method is used instead of the cross sectional method. Therefore, the vertical component of the prestress is considered as a reduction of the load instead of a shear transfer mechanism.

To determine the contribution of each shear transfer mechanism, the stresses need to be integrated along the edge surface of the free body diagram (width and height). The contribution of the three shear transfer mechanisms can be determined from the stresses using Equations 7.1 to 7.3.

$$V_s = {}^{A_{sw}}/_{s} \int \sigma_{szcr,z} \cot\theta_z \, dz \tag{7.1}$$

$$V_{ci} = \int b_z \tau_{ci,z} \, dz \tag{7.2}$$

$$V_{uncr} = \int b_z \tau_{uncr,z} \, dz \tag{7.3}$$

Equation 7.1 describes the contribution of the stirrups to the shear force (V_s). The stresses in the stirrups that cross the crack ($\sigma_{szcr,z}$) and the angle of the crack (θ_z) along the crack, need to be integrated over the height. Equation 7.1 is valid for a constant area of shear reinforcement (A_{sw}) and a constant distance between the stirrups (s). Note that the stirrups contribution does not depend on b_w. Equation 7.2 describes the contribution of the aggregate interlock to the shear force (V_{ci}). This part is found by integrating the aggregate interlock stresses $\tau_{ci,z}$ along the crack multiplied with the associated width of the cross-section b_z, over the height. The stirrups and aggregate interlock resist a part of the shear force only along the diagonal tension crack. For the part of the free body diagram that is not cracked, shear force is resisted by uncracked concrete. The concrete remains uncracked as long as the principal tensile stress does not exceed the concrete tensile strength. Equation 7.3 describes the contribution of the uncracked concrete to the shear force (V_{uncr}). The shear is found by integrating the shear stresses transferred by uncracked concrete ($\tau_{uncr,z}$) multiplied with the associated width of the cross-section, over the height.

The equations are applicable to determine the contributions by the different load transfer mechanisms for an arbitrary load. For the shear force associated with the maximum load, the shear resistance, the subscript R is added to the shear forces (V_{Rs}, V_{Rci}, $V_{R,uncr}$).

The three components will be presented in the next section as distributed shear force (V per h or τ_z times b_z). By expressing all three contributions as shear force per unit height, they can be mutually compared. It is noted that, because the resistance is presented as distributed shear force ($\tau_z b_z$), the typical drop in shear stresses (τ_z) at the transition of the small web and the broad flange, observed if only the shear stresses are shown, is not present. The distributed shear force will show uninterrupted graphs instead (see as example Figure 7.1).

In this chapter *Response* will be used for the analyses (Bentz 2000). *Response* is a non-linear sectional analyses programme based on the MCFT. In addition, *Response* assumes that the girder theory is valid (plane sections remain plane) and that there are no stresses present in traverse direction. *Response* uses a series of bi-axial nodes along the cross-section. *Response* integrates the stresses along the height instead of along the cracks. As the diagonal cracks will form parallel of each other and the angle will not change significantly it is assumed that the *Response* is suitable to analyse the stresses along the crack.

7.2 Shear transfer along a diagonal tension crack

This section investigates if the resistance at mid-depth is representative for the resistance along the entire crack surface. Chapter 6, derives equations for membrane elements that meet the condition $\varepsilon_x = 0$ at mid-depth. For the regions of a girder without flexural cracks, this assumption is conservative, as explained in Section 6.1. If the resistance at mid-depth can represent the resistance along the entire crack surface for regions of a girder without flexural cracks, Equations 6.4 to 6.6 can also be used to determine the maximum shear force that can be transferred by aggregate interlock and stirrups. This can be achieved by multiplying the shear resistance at mid-depth by the surface of the crack.

A part of the height of the girder remains uncracked. Therefore, in addition to the part of the shear force that is transferred in the part of the section with diagonal cracks, also a part of the shear force is transferred by the uncracked parts (mainly the flanges). The contribution of the uncracked concrete to the shear resistance is further investigated in Section 7.3.

The distribution along the diagonal tension crack of the aggregate interlock and stirrups is investigated. Two girders from the database (Section 5.3) are analysed, with two typical failures modes: a girder that was predicted to fail due to slipping of the crack (FX1-A, Hanson 1964) and a girder that was predicted to fail due to crushing of the concrete (HCP1TE, Choulli 2005). The distributions of the shear stresses are analysed using the

programme *Response* (Bentz 2000). The results can be used to investigate the distribution of the aggregate interlock stresses, the stresses in the stirrups at the crack and the cracking angles, along the crack. Also the shear transferred by the uncracked concrete is analysed using *Response*. The distribution over the various transfer mechanism is investigated at maximum shear force predicted by *Response* (the shear resistance).

The *Response* analyses are carried out based on the geometric an material properties which are described in the dissertations in which the experiments are described (Hanson 1964, Choulli 2005, Appendix F). The stress strain diagrams (including the tensile strength of concrete) are derived from the measured cylinder compressive strength of concrete, using the default relations as described in the User Manuel of *Response* (Bentz et al. 2001). The analyses are based on the maximum aggregate size used in the girders. For the girder of Choulli, a maximum aggregate size of zero is used, as $f_{cm} \geq 80\text{N/mm}^2$ (Section 6.3). For the material properties of the reinforcing steel, the stress strain relations are based on data from the material tests. The reinforcing steel is characterised by the yield strength, the ultimate strength, the modulus of elasticity, the strain at strain hardening and the rupture strain. The material properties for the prestressing reinforcement are based on data from material tests, as reported in the dissertations. The material of the prestressing reinforcement is characterised by the ultimate strength, the modulus of elasticity and the rupture strain in combination with the derived Ramsberg-Osgood parameters. The normal force caused by prestressing, as reported in the dissertations, is entered by defining pre-strains. Crack spacing (s) is automatically calculated using the CEB crack spacing equation (Equation 7.4). *Response* uses this equation to determine the crack spacing in the two orthogonal directions separately (s_x an s_z, Equation 5.28). In Equation 7.4, c is the diagonal distance from the considered depth to the nearest reinforcement in the section, d_b is the diameter of the nearest bar and ρ is the percentage of steel within a concrete area of $7.5d_b$ above and below a bar.

$$s = 2c + 0.1\ {}^{d_b}/_{\rho} \tag{7.4}$$

Analyses for the two simply supported girders are performed at cross-sections at a distance of ½ (h - $h_{bf,str}$ - $h_{bf,skw}$) / tan30 to the point load. This is considered as the cross-section that can be associated with the first possible diagonal tension crack. The terms $h_{bf,str}$ and $h_{bf,skw}$ are used for the height of respectively the straight and the skew part of the bottom flange. These terms are subtracted from the girder height as the crack through the bottom flange is about perpendicular to the longitudinal axis. For the two considered simply supported girders, the moment to shear ratio decreases in cross-sections closer to the support. Therefore, the cross-section at a distance of ½ (h - $h_{bf,str}$ - $h_{bf,skw}$) / tan30 to the point load is assumed to be the most critical one. The location of the considered cross-section determines the used load increments.

In Figure 7.3 the results of the *Response* analyses are shown for girder HX1-A (Hanson 1964). The light grey area shows the part of the cross-section that is cracked and the dark grey area shows the uncracked part. Whether a cross-section is cracked depends on whether the principal tensile stresses exceed the concrete tensile strength. As *Response* assumes that no transverse stresses are present, the principal tensile stress depends on the stress in longitudinal direction and the shear stress. The web is cracked because the shear stresses in the web are significantly higher than in the flange (due to the difference in the width) which increases the principal tensile stresses. The longitudinal stresses are affected by the bending moment. In the considered cross-section, the longitudinal stress is higher in the bottom part than in the top part, which increases the principal tensile stress. Therefore, a small part in the top of the web remains uncracked whereas a small part of the skew bottom flange is cracked (Figure 7.3). In the cracked part, shear force is transferred by aggregate interlock and stirrups, whereas in the uncracked part, shear force is transferred by uncracked concrete.

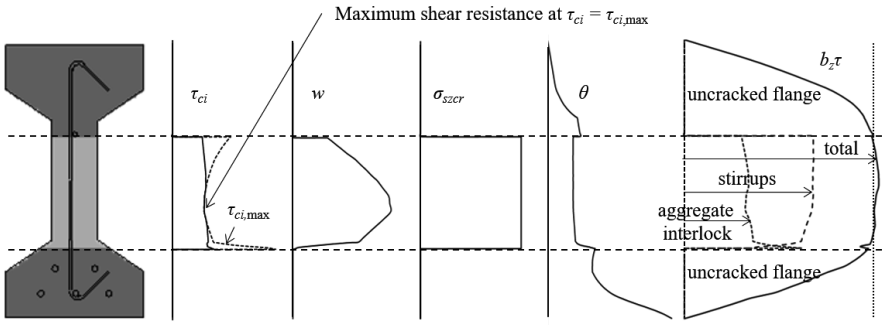

Figure 7.3. Distributed shear force & parameters per shear transfer mechanism (HX1-A, Hanson 1964)

The failure of girder HX1-A is caused by slipping of the crack. This is shown in Figure 7.3, where τ_{ci} equals $\tau_{ci,max}$ at a height just below mid-depth, at the maximum shear force (shear resistance). At this location the crack width (w) is at its maximum. As shown in Figure 7.3, the maximum aggregate interlock stresses decrease with increasing crack widths (Equation 5.29). The distribution of the aggregate interlock stresses is not affected by the distribution of the crack width, as the cracks widths only determines $\tau_{ci,max}$. Along the crack, τ_{ci} follows from equilibrium (Equation 5.25 and 5.26) as explained in Section 5.1.3. As shown in Figure 7.3, it is a plausible assumption for this girder to consider the aggregate interlock stress at mid-depth as representative for the entire crack surface (see $b_z\tau$ for aggregate interlock).

As shown in Figure 7.3, the stresses of the stirrups at the crack (σ_{szcr}) were found to be equal to the yielding strength over the entire cracked height. Moreover, Figure 7.3 shows that the crack angle θ is rather constant over the cracked height. Only in the bottom

flange the crack angle is higher than average, what causes a decrease in the contribution of the stirrups. This decrease in contribution of the stirrups is compensated by an increase of the contribution of aggregate interlock as result of the increasing width of the cross-section. As shown in Figure 7.3, is a plausible assumption for this girder to consider the contribution of the stirrups at mid-depth as representative for the entire crack surface (see $b_z \tau$ for stirrup contribution).

At the maximum shear force (shear resistance) the associated stresses in the compression field (σ_2) are not governing, as these are smaller than the maximum ($\sigma_{2,max}$, Figure 7.4). It is found that HX1-A is predicted to fail as result of slipping of the crack (Figure 7.3) instead of crushing of the compression fields (Figure 7.4).

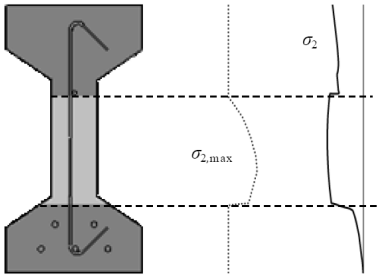

Figure 7.4. Stresses and strength of compression field at maximum shear (HX1-A, Hanson 1964)

The second girder, that is analysed with *Response*, concerns HCPT1E (Choulli 2005). In Figure 7.5, the stresses in the compression field (σ_2) at maximum shear (shear resistance) and the maximum compressive stresses of the compression field ($\sigma_{2,max}$) are shown. The stresses in the compression field ($\sigma_2 = \sigma_{2,max}$) are found to be governing for the shear resistance and therefore, HCPT1E is predicted to fail as result of crushing of the compression fields.

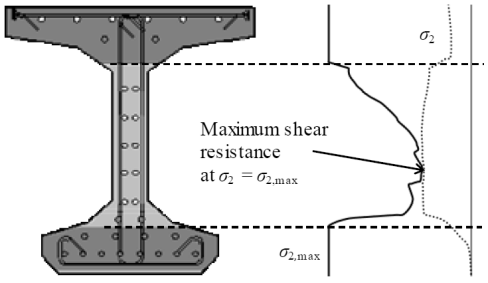

Figure 7.5. Stresses and strength of compression field at maximum shear (HCP1TE, Choulli 2005)

Figure 7.6 shows the distributed shear force and associated parameters per shear transfer mechanism for HCP1TE. Just like girder HX1-A, the cracked area extends more into

the bottom of the cross-section than the top of the cross-section, because the moment affects the longitudinal stresses.

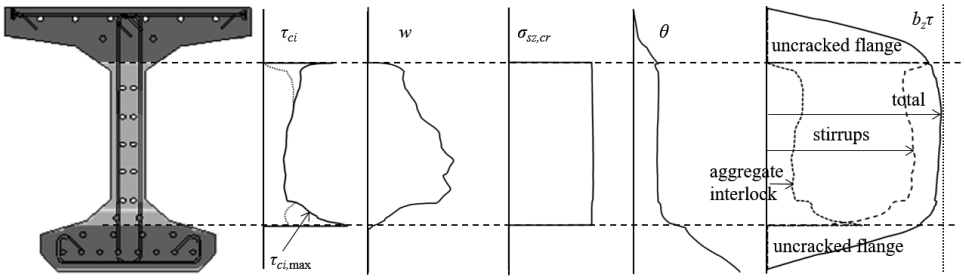

Figure 7.6. Distributed shear force & parameters per shear transfer mechanism (HCP1TE, Choulli 2005)

As described, crushing of the concrete was found governing for girder HCP1TE. In contrast to the girder HX1-A, the girder HCP1TE could resisted additional shear force after $\tau_{ci} = \tau_{ci,max}$. As a consequence, $\tau_{ci,max}$ is decisive for the distribution of τ_{ci} for a considerable part of the cross-section, as shown in Figure 7.6 (area where $\tau_{ci} = \tau_{ci,max}$). The maximum aggregate interlock stresses decreases if the crack width increases (Equation 5.29). The crack width increases toward the mid span preliminarily due to the increase of the principal tensile strain ε_1. Hence, it is found that the diagonal crack spacing s_θ remains rather constant (Equation 5.27) . The principal tensile strain ε_1 increases because the transverse tensile strain ε_z increases towards the mid-depth (Equation 5.19). Therefore, $\tau_{ci,max}$ and consequentially τ_{ci}, are minimum around mid-depth. Based on these finding, one could argue that the aggregate interlock at mid-depth is less representative for the entire crack surface. Assuming the aggregate interlock at mid-span as representative for the entire crack could lead to an underestimation of contribution of the aggregate interlock. However, considering τ_{ci} in Figure 7.6 it is appears that this effect is less significant. Hence, for a part of the cross-section $\tau_{ci,max}$ is not limiting τ_{ci} (area where $\tau_{ci} < \tau_{ci,max}$). Moreover, because the crack penetrates into the bottom flange, the contribution of the aggregate interlock increases toward the bottom surface due to an increasing width of the cross-section. Considering the distribution of the distributed aggregate interlock force over the crack (see $b_z\,\tau$ for aggregate interlock in Figure 7.6), the assumption to consider the aggregate interlock stress at mid-depth as representative for the entire crack surface is also plausible for this girder.

The stresses of the stirrups at the crack (σ_{szcr}) were found to be equal to the yielding strength over almost the entire cracked height. Locally the stresses were about two percent higher because of tension hardening. This is caused by high transverse strains ε_z that are associated with failure due to concrete crushing. It is noted that Equations 6.4

to 6.6 are derived assuming no tension hardening. Using these equations could potentially lead to underestimation of the capacity. However, for the considered girders, the effect is negligible as appears from the distribution of σ_{szcr} in Figure 7.6. Just like for HX1-A, also for HCP1TE the crack angle was found as rather constant over the cracked height with only some increase in the part of the bottom flange that is cracked. To consider the contribution of the stirrups at mid-depth as representative for the entire crack surface is a plausible assumption also for this girder (see $b_z \tau$ for stirrup contribution in Figure 7.6).

Based on the results of the *Response* analyses, the assumption that the resistance of the aggregate interlock and the stirrups at mid-depth represents the entire crack surface, was found appropriate for the considered girders and associated failure mechanism. The contributions of the aggregate interlock and the stirrups together was found rather constant along the diagonal tension crack (see vertical dotted lines in Figure 7.3 and 7.6). But even for the parts of the web that are not cracked, the distributed shear force is about the same magnitude as for the cracked part. This corresponds to the linear elastic stress distribution for a girder with an I-shape and a thin web, in which the distributed shear stress is rather constant in the web. Hence, due to the thin web the first moment of area will hardly increase between the intersection of the flange and the web and the centre of gravity. Based on these two observations the resistance of only the web could be predicted by multiplying the resisted shear stress at mid-depth, the web height and the web width.

Both considered girders failed because the ultimate resistance of the web was reached, due to slipping of the crack or crushing of the compression field in the web. At failure, also the flanges resisted a significant part of the shear force, mainly by shear transfer of the uncracked concrete. Although failure of the flange was not governing, the contribution by the flanges was found to be significant (Figure 7.3 and 7.6). In Section 7.3 it is investigated how the additional contribution of the flanges can be accounted for.

7.3 Shear transfer in uncracked concrete

At a maximum shear force (the shear resistance) the shear is not only resisted by aggregate interlock and stirrups but also by a contribution of uncracked concrete. The contribution by the uncracked concrete was found to be significant, as shown in Figures 7.3 and 7.6. This section analyses the contribution of the uncracked concrete to the shear resistance.

The model that is proposed in this dissertation (Chapter 8) to determine the contribution of the uncracked concrete to the shear resistance is simple, to make the model more appealing for engineering practice. The contribution of uncracked concrete will not be

accounted for explicitly. Instead, the contribution of the uncracked concrete is accounted for by increasing the contribution of the aggregate interlock and the stirrups.

In the Section 7.2 it was found that the resistance of the web could be approached by multiplying the shear stress that can be resisted by aggregate interlock and stirrups at mid-depth ($\tau_{R,md}$) with the web height (h_w) and the web width (b_w). To determine the total resistance for a girder, this resistance should be increased with the shear transferred by the uncracked flange. In the proposed model (Chapter 8), this is accounted for by replacing the web height (h_w) by the effective shear depth (z'). The total shear resistance of a girder, based on z', is shown in Equation 7.5. The increase from h_w to z' concerns the contribution of the shear transferred by the flanges. In the proposed model τ_{Rmd} is determined using Equations 6.4 – 6.6. The apostrophe used in the parameters, indicates that the equations are derived for regions without flexural cracks.

$$V'_R = b_w \, z' \tau_{Rmd} \tag{7.5}$$

The effective shear depth is derived from the assumption that the shear resistance found using Equation 7.5 equals the shear resistance found from *Response* according to Equation 7.6. In Equation 7.6 the distribution of $\tau_{R,R2k}$ along the diagonal crack is considered. The associated shear resistance ($V_{R,R2k}$) is determined by integrating the distributed shear force ($\tau_{R,R2k,z} \, b_z$) over the height. Equation 7.5 also assumes $\tau_{R,md}$ equals $\tau_{R,R2k}$ so the effective shear depth is the only unknown.

$$V_{R,R2k} = \int \tau_{R,R2k,z} \, b_z \delta z \tag{7.6}$$

Figures 7.3 and 7.6 show the distribution of the total distributed shear force (continuous lines) and the contributions of aggregate interlock (fine dashed lines) and the stirrups (course dashed lines) over the height of the cross-section as found from the *Response* analyses, for the two girders analysed in Section 7.2.

Figure 7.7 show the total distributed shear force ($\tau_{R2k,z} \, b_z$, continuous lines) for both girders and the proposed approximation Equation 7.5 ($\tau_{R,md} \, b_z$, dashed line). Equation 7.5 assumes a constant distributed shear force over a limited height of the cross-section, whereas the distribution varies over the total height according to Equation 7.6. This figure also shows the linear elastic distributed shear force ($\tau_{LE,z} b_z$), which is the dotted line (which is hardly to see because it almost coincides with the continuous line). These linear elastic distributions are derived, assuming a linear elastic stress distribution that results in the same shear resistance as found from *Response* ($V_{R,LE} = V_{R,R2k}$). As can be seen the shape of the linear elastic distributed shear force and the distributed shear force as found from *Response* are very similar. In literature examples are found of *Response* analyses for cross-sections with flexural cracks (Esfandiari et al. 2009). It is found that

the shear stress distribution according to *Response* of girders with flexural cracks can deviate strongly from the linear elastic distribution. For the current dissertation, investigating the shear resistance in regions without flexural cracks, the observation that both shear force distributions (*Response* and linear elastic) are similar, is used for the derivation of *z'* for regions without flexural cracks.

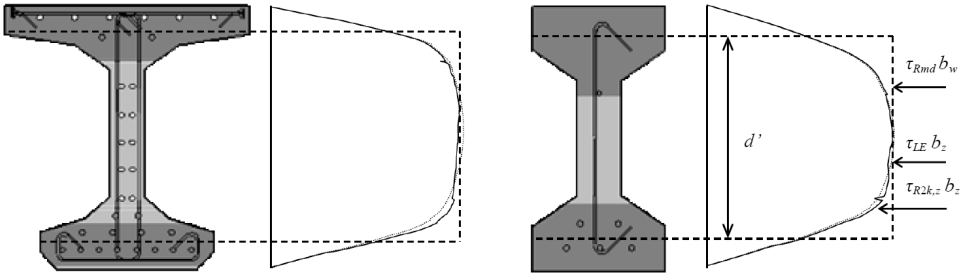

Figure 7.7. Distributed shear force R2k (continuous), linear elastic (dotted) and approached with *z'*(dashed)

The method to derive *z'* is explained in Figure 7.8. As the shapes of both the *Response* distribution and the linear elastic distribution are similar, *z'* is derived assuming a linear elastic distribution. With this assumption, the shape of the distribution only depends on the geometric proportions of the cross-section. Therefore, it is possible to investigate the effect of the geometric properties on the shear resisted by the uncracked concrete. A parametric study is carried out, considering geometric properties, and the results are used for the derivation *z'*. For the parametric study, the relative properties of various cross-sections are considered, that are representative for Dutch Highway bridges. Eventually, the predicted resistance based on the effective shear depth is compared with the predicted resistance according to *Response*. The resistances are compared for 26 girders of the database, which is described in Section 5.2. In this way it can be determined to what extend the proposed simple equation for the effective shear depth can accurately approximate the resistance found with R2K.

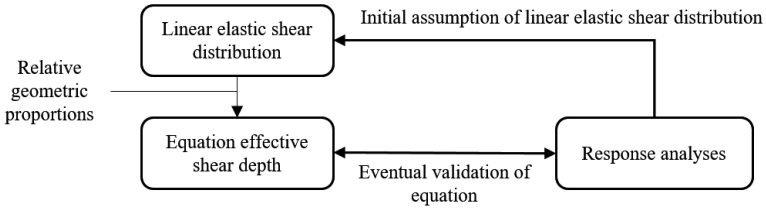

Figure 7.8. Method to derive the effective shear depth for regions without flexural cracks

It is assumed that the effective shear depth equals the height of the web increased with a contribution of the flanges. The linear elastic stress distribution is used to determine

the distribution of the contributions of the web and the flanges. These contributions depend on geometric properties. The effective shear depth is derived by multiplying the web height (h_w) with the ratio of total shear ($V_{tot,LE}$) and the shear transferred by the web ($V_{w,LE}$, Equation 7.7).

$$z' = {V_{tot,LE}}/{V_{w,LE}}\ h_w \tag{7.7}$$

An example how *z'* is derived is shown in the left part of Figure 7.9.

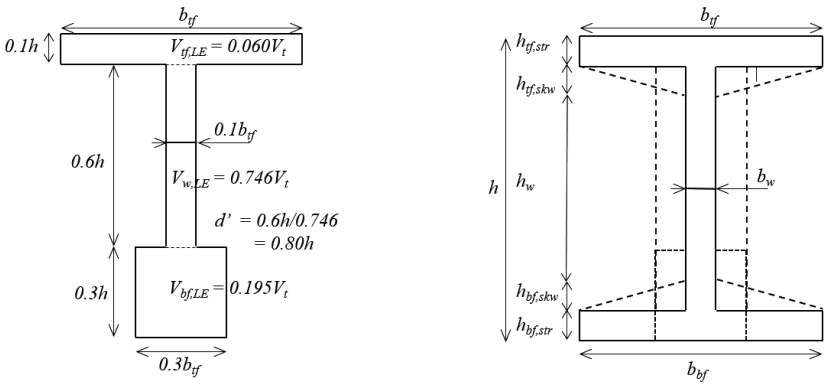

Figure 7.9. Example of distribution of shear force over the web and the flanges and definition of the geometric properties

The effective shear depth, based on the linear elastic stress distribution, is determined for several relative combinations of the geometric properties (Table 7.1).

Table 7.1. Considered geometric ratios

Figure 7.10	line a	line b	line c	line d	line e
$h_{tf,str}$ / h	0.05-0.30	0.05-0.30	0.05-0.30	0.05-0.30	0.05-0.30
$h_{tf,str}$ / $h_{bf,str}$	1	1	1	3	1
$h_{tf,skw}$ / $h_{tf,str}$	0	0	0	0	1
b_w / b_{tf}	0.1	0.3	0.2	0.2	0.2
b_{bf} / b_{tf}	1	1	0.3	0.3	1

The results of each combination is shown in Figure 7.10 with a line indicated with a letter. The height of the top flange is varied between 0.05 and 0.30 of the girder height for al considered combinations. This range covers all possible practical girder types. For the web width the extremes of 0.1 (line a) and 0.3 (line b) times the width of the top flange are used (and 0.2 for the other combinations). The width of the bottom flange can be smaller than the width of the top flange. This can be combined with equal heights of the flanges (line c, typically for an edge girder of a box-girder bridge) or with dissimilar

heights of both flanges (line d, typically for a bulb T-girder). Also the presence of skew sides of the flanges is investigated (line e).

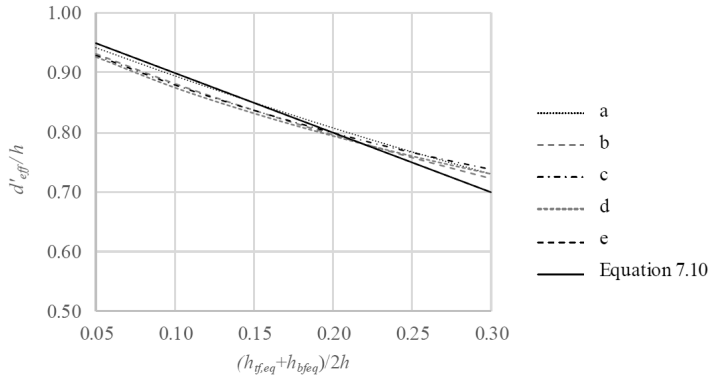

Figure 7.10. Effective shear depth versus half of average equivalent flange heights both as ratio of girder height

The results of the parameter study are shown in Figure 7.10. On the vertical axis, the calculated effective shear depth is shown as ratio of the height of the girder. On the horizontal axis the ratio of the average equivalent flange height and the girder height is plotted. The equivalent flange height is defined as the height of the straight flanges increased with a half of the heights of the skew flanges, which is present over the width of the flange (Equations 7.8 and 7.9). If the skew flange is only present for a (small) part of the flange, the presence can be ignored. For a symmetric I shaped girder without skew heights, the equivalent flange height corresponds to the flange height.

All considered combinations of geometric parameters show a comparable trend. The trend can be approached with Equation 7.10. The predictions of the effective shear depth according to this equation is also shown in Figure 7.10 (continuous line). Although the predicted line is somewhat steeper than the average trend of the other lines, the equation is attractive because of its simplicity.

If the intend use is out of the range of the investigated parameters, the effective shear depth can be calculated from the distribution of the contributions of the web and the flanges assuming a linear elastic shear stress distribution (Equation 7.7).

$$h_{tf,eq} = h_{tf,str} + {}^{h_{tf,skw}}/_{2} \tag{7.8}$$

$$h_{bf,eq} = h_{bf,str} + {}^{h_{bf,skw}}/_{2} \tag{7.9}$$

$$z' = h - {}^{(h_{tf,eq} + h_{bf,eq})}/_{2} \tag{7.10}$$

Finally the proposed equations for the effective shear depth are validated by comparing the resistances calculated using *Response* and the resistances determined using the proposed equations for the effective shear depth (Equations 7.8 to 7.10). The resistances are compared for 26 girders (Appendix I). This concerns girders of experiments of Elzanaty et al. (1986), Choulli (2005), Hanson (1964) and Leonhardt (1973), with the exception of CW17 and ŢP4. The properties of the girders, necessary for the comparison, are listed in Appendix I. The *Response* analyses are carried out for cross-sections at a distance of ½ (h - $h_{bf,str}$ - $h_{bf,skw}$) / tan30 from the point load ($x = a$ - ½ (h - $h_{bf,str}$ - $h_{bf,skw}$) / tan30). However, if flexural cracks were predicted in the bottom flange, the load increments were adjusted in a way that no flexural cracks were predicted in the bottom flange. Hence, the effective shear depth for regions without flexural cracks is investigated. The shear resistance $V_{R,R2k}$ follows directly from *Response*. To determine the resistance V'_R according to Equation 7.5, both the effective shear depth z' and $\tau_{R,md}$ are needed. The effective shear depth is found using Equations 7.8 to 7.10. To determine the equivalent flange height, only the heights of the skew flanges ($h_{tf,skw}$, $h_{bf,skw}$) are considered which are present over the full width of the flanges (Equations 7.8 and 7.9). The shear stress at mid-depth $\tau_{R,md}$ is found from the *Response* analyses ($\tau_{R,md} = \tau_{R,R2k}$ at mid-depth). Based on τ_{ci}, f_{ywm}, and θ at mid-depth, $\tau_{R,R2k}$ is determined. Eventually, the ratio $V_{R,R2k}/V'_R$ is determined (Appendix I).

The results are shown in Figure 7.11. Based on the analyses for 26 girders, a mean ratio of $V_{R,R2k}/V'_R$ was found of 0.99 and a coefficient of variation of 2%. Apparently, the simplifications of determining the resistance on the effective shear depth and assuming a constant shear resistance, hardly effects the accuracy, in comparison with a *Response* analysis. Therefore, it is justifiable to determine the resistance based on z', b_w and the shear stress that can be resisted at mid–depth.

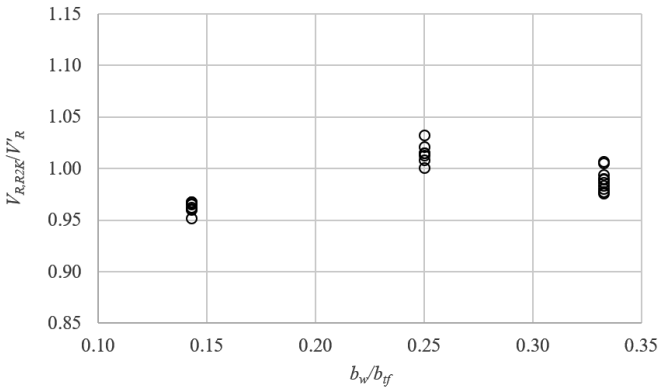

Figure 7.11. Ratio of resistances found from R2K and approached using Equations 7.5 and 7.8 to 7.10.

8

Proposed model for shear resistance of girders with stirrups

In this dissertation a model is derived for the shear resistance of prestressed girders with stirrups in regions without flexural cracks. The model describes the transfer of shear force by aggregate interlock, stirrups and uncracked concrete. Chapter 6 derives equations for the maximum shear stress that can be resisted at the mid-depth of the web by aggregate interlock and stirrups. Chapter 7 demonstrates that the shear stress that can be resisted at mid-depth of the web is representative for shear stress that can be resisted along the diagonal tension crack. Also the additional shear that can be transferred by uncracked concrete is described in Chapter 7. The current chapter describes the proposed model, referred to as model B1, and its application conditions and is based on the results of Chapter 6 and 7 (Figure 6.1).

Section 8.1 describes the method to determine the regions of the girder without flexural cracks in the ultimate limit state for which he model is intended. Section 8.2 describes the models that can be used to determine the maximum and minimum shear resistances. The minimum shear resistance concerns the resistance to diagonal tension cracking and can be governing for girders with a low amount of shear reinforcement. The maximum resistance concerns the shear resistance to crushing of the concrete before the stirrups yield and can be governing for girders with a high amount of shear reinforcement. Section 8.3 summarizes the proposed model using the equations derived in the previous chapters. Section 8.4 evaluates the accuracy of the proposed model, using test data from the database on shear failure for girders with stirrups (Section 5.3). The effect of various parameters on the accuracy is also described in this section. Additionally, the accuracy is compared to the accuracy of models from literature. Section 8.5 determines the design value of the proposed model. Section 8.6 describes an alternative for the proposed model. This concerns the variable angle truss model which is modified for regions without flexural cracks. Just like the proposed model in Section 8.3, this alternative model is based on the resistances of membranes at zero longitudinal strain that are determined using the MCFT (Section 6.3).

8.1 Method to determine the regions without flexural cracks

The model that is proposed to determine the shear resistance of girders with stirrups is applicable for regions without flexural cracks. In this section a method is proposed to determine this region.

A distinction should be made between whether diagonal tension cracking is governing or additional shear can be resisted after diagonal tension cracking. If diagonal tension cracking is governing, the presence of flexural cracks can be determined by assuming a linear stress distribution. Subsequently, it can be verified whether the tensile stress in the ultimate fibre exceeds the flexural tensile strength. However, if additional shear force can be resisted after diagonal tension cracking, diagonal tension cracks will be present, and the stresses are no longer linear distributed. Therefore, another method is necessary to determine whether flexural cracks are present.

A more appropriate method to determine the presence of flexural cracks, assuming that the lower limit of the resistance is not governing, is described in Section 5.1.5 (Bentz et al. 2006a). This method assumes a compression chord and tension chord at a vertical distance of the internal lever arm. Both chords are connected by a compression field. This method assumes the presence of diagonal cracks. This approach is adopted in the method proposed in the current section. However, in two aspects the proposed method deviates from the method described in Section 5.1.5:

1. According to the method described in Section 5.1.5, the compression chord is located at a vertical distance of $0.1h$ from the most compressed side. The tension chord is located at the centre of the tensile forces, which is determined based on the forces in both the prestressing steel and the reinforcing steel (Figure 5.15). However, in regions without flexural cracks, the centre of the tensile forces is unsuitable as chord as only a compression chord is present. It could be considered to locate both the most compressed chord and the least compressed chord at a distance of $0.1h$ from the most and least compressed sides. However, a more accurate predicting can be expected if both chords are assumed to be located at the centre of the concrete compressive stresses in the flanges. If this approach is followed, than the lever arm almost corresponds to the suggested equations for the effective shear depth (Equations 7.8 to 7.10). Therefore, it is proposed to use a lever arm equal to the effective shear depth (as derived in Section 7.3) and use the symbol z' for both parameters. At the end of this section, the proposed method to determine whether flexural cracks are present will be evaluated. This way also the suitability to use the effective shear depth as lever arm is evaluated. The apostrophe in z' indicates that the parameter is only applicable for regions without flexural cracks. It is noted that, as a consequence of this adapted approach, the internal lever arm can significantly deviate between the proposed method and the method described in Section 5.1.5.methods.
2. In this dissertation prestress is considered as part of the external load. This is called the ‘equivalent load prestressing method’ (Walraven et al. 2018). Therefore, the proposed method is based on the equivalent load prestressing method. This is in contrast

to the method described in Section 5.1.5, which does consider prestressing as part of the resistances, instead of part of the external load.

The application of the equivalent load prestressing method is demonstrated in Figure 8.1. The applied prestress results in a horizontal force P (prestressing force), a moment $P\,e_{p0}$ (e_{p0} is the eccentricity of the prestressing steel at the end of the girder relative to the centroidal axis) and a distributed load q_p, which is the result of the curvature of the prestressing steel. Because the prestressing steel is at an angle at the girder end, the prestress can be decomposed into a horizontal force somewhat smaller than P and a small vertical force. For small angles, the effect of decomposing the prestress force is usually not significant. As simplification only a horizontal force is shown in Figure 8.1 with the magnitude P.

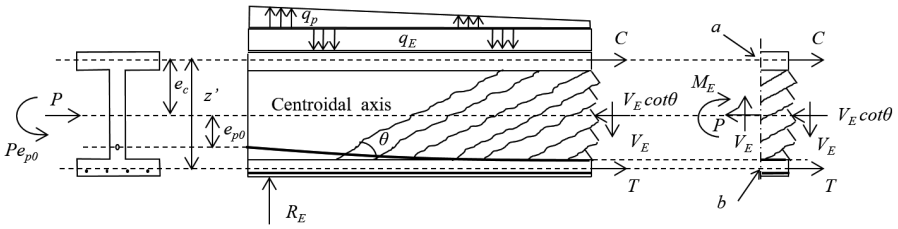

Figure 8.1. Derivation of the force in least compressed chord based on equivalent load prestressing method

A cross-section can be represented by a slice (right part of Figure 8.1). The cross sectional forces on the slice (M_E, V_E, P) can be determined from the external loads and the prestress loads on the considered free body diagram (left part of Figure 8.1). Hence, M_E includes the moment as result of R_E, q_E, q_p and Pe_{p0}. Subsequently, the force T in de least compressed chord can be found from moment equilibrium around point a. Note that the component V_E cotθ is located at a vertical distance of ½ z' from point a, which corresponds to the centre of the web, whereas P is located a vertical distance of e_c from point a, which is the distance from the most compressed chord to the centre of gravity of the cross-section (these distances coincide for the I shaped cross-section of Figure 8.1 because it is a symmetrical cross-section). The result is shown in Equation 8.1.

$$T = {}^{M_E}/_{z'} + \frac{1}{2} V_E \cot\theta + {}^{e_c}/_{z'}\ P \tag{8.1}$$

If it is assumed that ½ cotθ = 1 (this corresponds to θ = 26.6°), the equation can be simplified to Equation 8.2.

$$T = {}^{M_E}/_{z'} + V_E + {}^{e_c}/_{z'}\ P \tag{8.2}$$

For the ease of use in engineering practice, it is proposed to simply assume that flexural cracks are present in a cross-section if the force in the least compressed chord T is larger than zero (this corresponds to the method described in Section 5.1.5).

The method to determine whether flexural cracks are present as described in this section, is evaluated. For this purpose the longitudinal strains at the least compressed chord ε_t are calculated accurately using the programme *Response* (R2k). The longitudinal strains according to R2k are compared to the strains derived using the proposed method. For the comparison, strains are used instead of forces, because only these are determined by *Response*. The strains are calculated for the same 26 experiments that were used to validate the effective shear depth in Section 7.3. Also the same load increments are used that result in a bottom flange without flexural cracks. Appendix J illustrates how T is determined using the proposed method. The strain ε_t is subsequently determined using the stiffness of the chords according to CSA code (CSA 2006), as explained in Section 5.1.5.

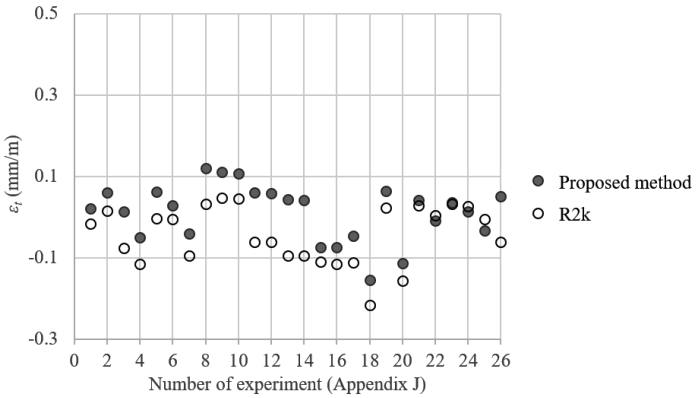

Figure 8.2. Longitudinal strain at tensile chord according to method proposed in this section and R2K

The results are also shown in Figure 8.2. The least compressed (or most tensioned) flange remains uncracked if ε_t is smaller than the cracking strain ε_{cr}, which is equal to $f_{ctm,fl} / E_c$. For commonly used concrete strengths ($40 \leq f_{cm} \leq 100$ N/mm^2), the cracking strain ε_{cr} is about 0.1 mm/m. As can be seen (Figure 8.2), the proposed method results in the prediction of flexural cracks for three of the experiments. This is more conservative than *Response*, for which the load increments were adapted to ensure that no flexural cracks would be present (Section 7.3). For almost all experiments a higher longitudinal strain is predicted compared to *Response*. For the few experiments for which the average strain according to *Response* is higher, the underestimation is insignificant. For the considered experiments it can be concluded the proposed method is conservative. This

also confirms the suitability of the use z' and the assumption ½ cotθ = 1 in the proposed method.

In section 8.4 the accuracy of the proposed model will be evaluated. Experiments of the database (Section 5.3) will be selected that meet the condition $\varepsilon_x \leq 0$. To determine if this condition is met, also the strains in the most and the least compressed chord are considered (Appendix L). Therefore, for the selection of experiments, also the force in the most compressed chord C is needed. The force C in de most compressed chord, found from moment equilibrium around point b, equals $-M_E/z' + V_E + (z' - e_c)/z' P$ (Figure 8.1).

8.2 Minimum and maximum shear resistance

The model derived in Chapter 6 is intended to determine the shear resistance of the web in which shear is transferred by stirrups and aggregate interlock. The model covers failure due to crushing of the concrete or slipping of the crack, after the stirrups start to yield. However, also uncracked concrete can resist shear. This corresponds to the resistance to diagonal tension cracking as described in Chapters 2 to 4. For higher amounts of shear reinforcement the resistance after diagonal tension cracking, by aggregate interlock, stirrups and the uncracked flanges, will be higher than the resistance to diagonal tension cracking. However, if the amount of shear reinforcement is low, it is possible that the resistance of after diagonal tension cracking is lower than the resistance to diagonal tension cracking. The highest of both resistances will be governing. It is not necessary to determine a minimum shear reinforcement ratio (or minimum ψ) to determine which failure mode is governing. It is sufficient to determine the resistance using the proposed model for cracked concrete and subsequently verify if the found resistance is higher than the resistance to diagonal tension cracking. Therefore, the resistance to diagonal tension cracking is defined as the minimum shear resistance for girders with stirrups in regions without flexural cracks ($V'_{R,c}$). The apostrophe indicates that the model is only applicable for regions without flexural cracks.

For the regions in which no flexural cracks are present in the ultimate limit state, the maximum principal tensile stress $\sigma_{1E}(z)$ should be limited by the tensile strength of the web $f_{ctm,web}$ (Equation 8.3). The shear force at which this condition is just met, corresponds to the minimum shear resistance $V'_{R,c.}$ For girders that remain free of flexural cracks in the ultimate limit state, $f_{ctm,web}$ corresponds to $0.89f_{ctm}$ (model A1, Section 3.4). For girders with flexural cracks in the ultimate limit state, $f_{ctm,web}$ corresponds to $1.01f_{ctm}$ (Section 3.5, model A2). In Equation 8.3, $\sigma_{1E,\max}$ is the maximum principal tensile stress in the regions without flexural cracks. The principal tensile stress can be determined using Equation 8.4. In Equation 8.4, $\sigma_{x,E}(z)$ is the normal stress in the longitudinal direction and $\tau_E(z)$ is the shear stress, assuming a linear elastic stress distribution. The

parameter z indicates that the associated parameter varies, or could vary, over the height z of the cross-section. If the cross-section opposite the support remains free of flexural cracks, $\sigma_{1E}(z)$ is considered as not critical between a vertical line through the support and a vertical line through a point that is the intersection of the elastic centroidal axis and a line inclined from the inner edge of the support at an angle of 45°(Figure 3.7 and Figure 4.1). These regions do not have to be considered for the determination of $\sigma_{1E,\max}$.

$$\sigma_{1\max,E} \leq f_{ctm,web} \tag{8.3}$$

$$\sigma_{1E}(z) = \frac{\sigma_{x,E}(z)}{2} + \sqrt{\left(\frac{\sigma_{x,E}(z)}{2}\right)^2 + \tau_E(z)^2} \tag{8.4}$$

As described earlier in this section, the proposed model is intended to determine the shear resistance to crushing of the concrete or to slipping of the crack, both while the stirrups yield simultaneously. For girders with a high amount of shear reinforcement, it is possible that the resistance is limited because the concrete crushes before the stirrups yield. Using a model that assumes that the stirrups yield would lead to an overestimation of the shear resistance. The proposed model does not cover this failure mode. Therefore, it should be verified if resistance found with the proposed model is lower than the resistance to crushing of the concrete before the stirrups yield. The resistance to crushing of the concrete before the stirrups yield is defined as the maximum shear resistance ($V'_{R\max}$). The apostrophe indicates that the derived model is only applicable for regions without flexural cracks.

Section 5.1.4.2 already derived the upper limit of the shear force $V_{R\max}$ using the MCFT (Equation 5.31, Bentz et al. 2006b). This derivation conservatively assumed that ε_x = 0.002. For regions without flexural cracks, it can be assumed that ε_x is zero. Zero longitudinal strain can still be considered as a rather conservative assumption as explained in Section 6.1. If the other assumptions of the derivation remain the same, Equation 8.5 can be derived using the same approach. As the condition concerns crushing of the concrete, ε_2 is assumed to be -2 mm/m. Because the transverse reinforcement is not yielding, the strain ε_z is lower than 2 mm/m. As a lower strain increases the maximum capacity, conservatively 2 mm/m is assumed for ε_z. These values are used sequentially in Equations 5.18, 5.19, 5.23, 5.24 and 5.17. Based on these values for the strains, an associated value for the maximum shear stress $\tau_{R\max}$ is found of $0.32 f_{cm}$ as average for all concrete strengths. For lower strengths of concrete a maximum shear stress is found of $0.33 f_{cm}$, which is conservatively neglected. Equation 8.5 is found if $\tau_{R\max}$ is multiplied with the width of the web b_w and the effective shear depths z'.

$$V'_{R\max} = 0.32\, f_{cm}\, b_w\, z' \tag{8.5}$$

It is found that the strength of the compression field in a region without flexural cracks is higher than in a region with flexural cracks (Hence, in Section 5.1.2 a factor of 0.28 was found instead of 0.32). This is caused by smaller longitudinal strains, that are associated with regions without flexural cracks, that consequentially result in smaller principal tensile strains and therefore higher values of $\sigma_{2,max}$ (Equation 5.23).

8.3 Model B1: shear resistance of prestressed girders with stirrups

This section summarizes the model proposed to determine the shear resistance of prestressed girders with stirrups in regions without flexural cracks, referred to as model B1. Equations from previous chapters are repeated (and renumbered) to get a clear overview. Model B1 is derived for normal weight concrete.

For regions of prestressed girders without flexural cracks the shear resistance can be determined using Equations 8.6 to 8.12. The apostrophe used in the parameters, indicates that the equations are only applicable for regions without flexural cracks (Section 8.1). The first term in Equation 8.6 represents the contribution of the aggregate interlock. The contribution depends on ψ, which equals $\rho_w f_{ywm} / f_{cm}$. In this equation, ρ_w is the shear reinforcement ratio, f_{ywm} is the yielding strength of the stirrups and f_{cm} the concrete cylinder compressive strength. In the equation for ρ_w, A_{sw} is the area of the stirrups, b_w is the width of the web and s is the centre to centre distance of the stirrups. The contribution of aggregate interlock reduces if ψ increases (Equations 8.7 and 8.8). The aggregate interlock contribution is also lower for $f_{cm} \geq 60$ N/mm^2. This is because in higher strength concrete the cracks run through the aggregates due to the strong paste (Bentz et al. 2006a). Therefore, the aggregate interlock contribution reduces for higher strength concrete.

$$V'_R = \beta \sqrt{f_{cm}}\, b_w z' + A_{sw}/s \;\; f_{ywm}\, z' \cot\theta \tag{8.6}$$

$$\beta = 0.38 - 2.5\psi \qquad \text{for } f_{cm} \leq 60 \text{ N/mm}^2 \tag{8.7}$$

$$\beta = 0.30 - 2.5\psi \qquad \text{for } f_{cm} \geq 80 \text{ N/mm}^2 \tag{8.8}$$

With $\psi = \rho_w f_{ywm} / f_c$, $\rho_w = A_{sw} / (b_w\, s)$ and $\theta = 26°$.

For $60 < f_{cm} < 80$ N/mm^2, β can be interpolated linearly.

The second part of Equation 8.6 represents the contribution of stirrups to the shear resistance. The cracking angle (θ) that would have been found using the MCFT could deviate from 26° as described in Section 6.4. Nevertheless, it is demonstrated in Section 6.4 that the total shear resistance corresponds to the total shear resistance as found from the MCFT, using an angle of 26°.

The contribution of aggregate interlock and stirrups is attributed to the web as the diagonal tension crack will be primarily located in the web. Even if a part of the web remains uncracked, it was found that the shear resisted by the web could be determined assuming aggregate interlock and stirrups along a crack over the height of the web (Section 7.2). The additional contribution due to shear transfer in uncracked concrete (mainly the flanges) is accounted for by replacing the web height by the effective shear depth z' (Section 7.3). The effective shear depth in regions without flexural cracks can be determined from Equations 8.9 – 8.11, for which the parameters are shown in Figure 8.3. The equivalent flange height in Equations 8.10 and 8.11 is defined as the height of the straight flanges increased with a half of the heights of the skew flanges. Only, the heights of skew flanges need to be considered, that are present over the full width of the flanges. Alternatively, the effective shear depth can be calculated from the distribution of the contributions between the web and the flanges assuming a linear elastic shear stress distribution (Section 7.4).

$$z' = h - \frac{1}{2}\left(h_{tf,eq} + h_{bf,eq}\right) \tag{8.9}$$

$$h_{tf,eq} = h_{tf,str} + \frac{1}{2}h_{tf,skw} \tag{8.10}$$

$$h_{bf,eq} = h_{bf,str} + \frac{1}{2}h_{bf,skw} \tag{8.11}$$

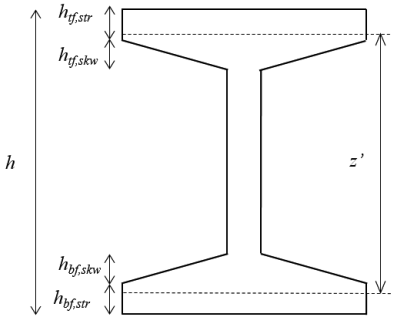

Figure 8.3. Effective shear depth z'

Model B1 is derived for a diagonal crack spacing s_θ of 300 mm. If the diagonal crack spacing is significant larger, the contribution for the aggregate interlock reduces and model B1 could overestimate the resistance. The orthogonal crack spacing for each of the directions (s_x and s_y) can be determined using Equation 7.4. The diagonal crack spacing can be determined from the cracks spacing in orthogonal directions using Equation 5.28. Only if the centre to centre distances of both the longitudinal reinforcing steel and

the stirrups (s) is large (for instance both larger than 400 mm) the diagonal crack spacing s_θ will be larger than 300 mm. For elements that contain both stirrups and longitudinal reinforcing steel, the crack spacing will be typically less than 300 mm (Bentz et al. 2006a, b). Therefore, for simplicity, the application of model B1 is limited for centre to centre distance (s) between the stirrups of maximum 300 mm (so the associated $s_x \leq 300$ mm). For larger values of s the limit of the diagonal crack spacing of 300 mm should be verified when the newly proposed model is used to determine the shear resistance.

The method to determine the regions without flexural cracks is described in Section 8.1.

The shear resistance is limited by $V'_{R,c}$ and $V'_{R\max}$ (Equation 8.12) as described in section 8.2.

$$V'_{R,c} \leq V'_R \leq V'_{R\max} \tag{8.12}$$

8.4 Accuracy of the proposed model

In this section, the accuracy of model B1 (Section 8.3) is evaluated, based on test data from the database described in Section 5.3. In this evaluation, the shear resistance determined with model B1 is compared to resistance obtained from experiments. The accuracy is expressed in terms of a test-to-predicted shear resistance ratio. A model is accurate if the mean value of the test-to-predicted shear resistance ratio is close to one and the associated coefficient of variation is low.

Section 8.4.1. describes the experiments from the database that are used to evaluate the accuracy. Section 8.4.2 describes the accuracy found for model B1. Also the effect of the parameters shear span to depth ratio, the maximum aggregate size, the diagonal crack spacing and the longitudinal strain on the accuracy is investigated in this section. Finally in Section 8.4.3, the accuracy of the proposed model is compared to the accuracy found using other models from literature. The results are reflected with earlier findings from literature regarding the accuracy of the models from literature.

8.4.1 Selection of experiments for the evaluation of the accuracy

The accuracy of model B1 evaluated by the test data from the experiments from the database on shear failure of girders with stirrups (Section 5.3). Model B1 is derived assuming a longitudinal strain at mid-depth equal to or smaller than zero ($\varepsilon_x \leq 0$, Section 6.1). The database, on the other hand, is compiled of experiments on prestressed girders with stirrups for which failure could be related to diagonal tension cracks (Section 5.3). Whether the experiments also meet the condition of a longitudinal strain at mid-depth smaller zero is uncertain. Therefore, only experiments that meet this condition are selected for the evaluation of the accuracy. Whether the condition $\varepsilon_x \leq 0$ is met,

is based on calculations with the proposed method as described in Section 8.1. A second selection criterion is that only experiments with predicted resistances between $V'_{R,c}$ and $V'_{R\max}$ (Equation 8.5) are selected to evaluate the accuracy. The selection will be carried out by the following steps considering both selection criteria:

1. For all experiments in the database described in Section 5.3 the resistance V'_R is determined using Equations 8.6 to 8.11 (Appendix K).
2. For all experiments in the database described in Section 5.3 the strain at mid-depth ε_x associated with V'_R is calculated and it is determined whether $\varepsilon_x \leq 0$ (Appendix L).
3. For the experiments that meet the condition $\varepsilon_x \leq 0$, the resistances $V'_{R,c}$ and $V'_{R\max}$ are determined (Appendix M). Experiments that meet both conditions $\varepsilon_x \leq 0$ and $V'_{R,c} \leq V'_R \leq V'_{R\max}$ are used for the evaluation of the accuracy of the model (Appendix N).

In the first step, resistances V'_R are determined for all the experiments of the database on shear failure related to diagonal tension cracks of girders with stirrups (Section 5.3, Appendix F). The used parameters, intermediate results and the resulting resistances V'_R are listed in Appendix K 'Shear resistance according to proposed model for prestressed girders with stirrups'. The effective shear depth z' is determined using Equations 8.9 to 8.11. As the cross-section of the experiments of Choulli were found to be irregular (Section 7.3), z' was calculated from the linear elastic shear stress distribution, using Equation 7.7, instead of using Equations 8.9 to 8.11. Subsequently, the shear reinforcement ratio ρ_w and, ψ and β (using Equations 8.7 or 8.8) were determined. Finally, V'_R was determined using Equation 8.6. Although the resistance for all experiments of the initial database are shown, the experiments that were eventually not selected are struck through in Appendix K (as these don't meet the criteria of Appendices L and N). It is further noted that all experiments of the initial database meet the condition $s \leq 300$ mm (Section 8.3).

In step 2, the strain at mid-depth ε_x at V'_R is determined for all experiments. As model B1 is derived for experiments with $\varepsilon_x \leq 0$, only experiments that meet this condition are used in the evaluation. To determine ε_x, it is necessary to assume a critical cross-section. For the selection, the cross-section at location $x = a - (h - h_{bf,str} - h_{bf,skw}) \cot\theta$ is assumed to be critical. In this equation a is the shear span, h the height of the girder, $h_{bf,str}$ is the height of the straight parts of the bottom flange and $h_{bf,skw}$ is the height of the skew part of the bottom flange. For continuously supported girders, where the most tensioned chord will be at the top flange, $h_{tf,str}$ and $h_{tf,skw}$ will be used instead of $h_{bf,str}$ and $h_{bf,skw}$. The location of the critical cross-section is determined from subtracting the longitudinal projection of the diagonal crack $(h - h_{bf,str} - h_{bf,skw}) \cot\theta$, from the shear span. The terms

$h_{bf,str}$ and $h_{bf,skw}$ are subtracted as the crack through the bottom flange is about perpendicular to the longitudinal axis.

The location x is used to determine the strain in the chord at the location of the least compressed flange (ε_t). Cracks at a distance further away from the support than x are assumed to be flexural cracks and do not concern the shear resistance ('Shear critical region' in Figure 8.4). The angle is found based on the analyses of photos and figures of crack patterns of the 25 experiments, both simply and continuously supported, for which clear cracking patterns were present. These experiments are CW10, CW11, CW13, CW14, CW16 (Elzanaty et al. 1986), HCP2TE, HCP2TW, HAP2TW, HCP1TE, HCP1TW, HAP1TE, HAP1TW (Choulli 2005), F1B, F3A, F3B, F5A, F5B,F19A (Hanson 1964), ŢP2 (Leonhardt 1973), LB2, LB3, LB6, LB7, LB8, LB10 (Xie 2009). It is conservatively assumed that shear failure could be related to the diagonal crack at x. The analyses of data from the observations result in an average angle of the first diagonal crack of 30°.

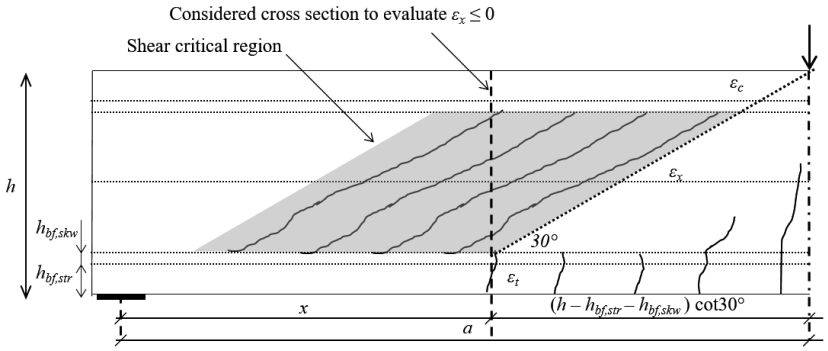

Figure 8.4. Considered cross-section for determination the strains

Assuming the critical cross-section at $x = a - (h - h_{bf,str} - h_{bf,skw})$ results in an overestimation of ε_c. Hence, the top of the diagonal crack will be more compressed than the top of the assumed cross-section. This is conservative, as an overestimation ε_c results in an overestimation of ε_x. One could argue to assume the critical cross-section at $x = a - ½ (h - h_{bf,str} - h_{bf,skw})$ so the overestimation of ε_c would be compensated by an underestimation of ε_t. However, the effect of ε_t on ε_x can be much more significant than the effect of ε_c on ε_x. This is because the stiffness of the chord reduces significantly if ε_t is positive. Hence, if the most tensile chord is under tension, only the stiffness of steel is ascribed to the chord. Therefore, the critical cross-section is chosen at $x = a - (h - h_{bf,str} - h_{bf,skw})$ and the effect of underestimating ε_c is considered acceptable. Hence, the overestimation of ε_x only results in a stricter selection.

Based on V'_R, z' (Appendix K) and x, the strain ε_x can be determined for all experiments of the database described in Section 5.3. Appendix L lists the determined strains and the conclusion whether experiments meet the condition $\varepsilon_x \leq 0$, including intermediate results. The longitudinal strain of ε_x is determined in accordance to Section 8.1. Based on the distance x and V'_R, the moment due to the external load M_F is determined. Based on e_p, which is the vertical distance between location of the centroidal axis and the prestress force P, the moment due to the prestressing M_P is determined. The continuously supported girders required more extensive calculations to determine M_p and M_F than the simply supported girders. The internal lever arm z' is already determined in Appendix K. Based on these values, the forces in the compression chord (C) and tension chord (T) are determined using respectively equations $T = M_E/z' + V_E + e_c / z' P$ and $C = -M_E/z' + V_E + (z' - e_c)/z' P$ (Section 8.1). Subsequently, ε_t and ε_c are determined from the forces in the compression chord (C) and tension chord (T) and the stiffness of the chords. The stiffness of the least compressed chord and the most compressed chord are determined based on the defined steel areas and the measured stiffness of the reinforcement and the prestressing steel. The stiffness of the concrete is calculated from area of the associated chord (Figure 5.15) and the measured compressive strength f_{cm}, using the equation $E_c = 3000 \sqrt{f_{cm}} + 6900$ as described in the CSA (2006). For positive values of C and T the stiffness of the concrete and steel are added together. For negative values of C and T, the stiffness equals the stiffness of the steel. The strain at mid-depth, ε_x, equals the mean of ε_t and ε_c. Eventually, experiments are selected that meet the condition $\varepsilon_x \leq 0$.

It was found that of the 57 experiments of the initial database for shear failure of girders with stirrups, 28 experiments meet the condition $\varepsilon_x \leq 0$ (of which 19 also meet the condition $\varepsilon_t \leq 0$) and 29 do not meet the condition $\varepsilon_x \leq 0$. It is noted that the selection is strict as consequence of the assumption that the most tensioned chord is immediately cracked when $T > 0$ (tensile strength of zero).

The third step concerns the selection of the experiments that meet the condition $V'_{R,c} \leq V'_R \leq V'_{R\max}$ for the 28 experiments that meet the condition $\varepsilon_x \leq 0$ (Appendix M). $V'_{R,c}$ is determined using Equations 8.3 and 8.4. For some of the experiments diagonal tension cracking is predicted before flexural cracking. For these experiments $V'_{R,c}$ is found by adapting V'_E until the condition $\sigma_{1E,\max}$ equals $0.89 f_{ctm}$ is met (Section 3.4) in the considered region (Figure 3.5). Other experiments are predicted to have flexural cracks before diagonal tension cracking. For these experiments, both V'_E and the dimension of the region without flexural cracks (Figure 3.11) are adapted until the condition $\sigma_{1E,\max}$ equals $1.01 f_{ctm}$ is met (Section 3.5). Appendix M lists both whether flexural cracks are predicted at diagonal tension cracking and the determined $V'_{R,c}$.

Using these models results in a mean value of the ratio experimentally found to predicted resistance for diagonal tension cracking of about unity (Section 4.3). The mean value of

the ratio experimentally found to predicted resistance for girders with stirrups is about 30% higher than unity (Section 8.4.2). Therefore, some of the experiments are selected despite $V'_{R,c} / V'_R$ exceeds unity but for which $V'_{R,c} / V'_R \leq 1.3$. Eventually it could be confirmed for these experiments that $V'_{R,c}$ was indeed not governing, by increasing V'_R with a factor depending on a/d (Section 8.4.2). One experiment is not used to evaluate the accuracy of model B1 because it is likely that it failed as result of diagonal tension cracking (CW17). Although in the experiment additional shear could be resisted after diagonal tension cracking (the shear force could be raised from 123kN to 142 kN), the predictions made it likely that the additional resistance could not be ascribed to the presence of stirrups. Hence, considering the contribution of stirrups after diagonal tension cracking a resistance was predicted of 81kN, whereas a resistance to diagonal tension cracking was predicted of 123kN (Appendix M). In Section 2.1 it is explained that also girders without stirrups can sometimes resist some additional shear force after diagonal tension cracking.

$V'_{R\max}$ is determined using Equation 8.5. For none of the experiments $V'_{R\max}$ is predicted to be governing (Appendix M).

Experiment ŢP4 is further considered, although the predicted ε_x is larger than zero, and the experiment was not used for the evaluation of the accuracy of model B1. This experiment contains a high amount of shear reinforcement (ρ_w= 2.32%). The experimentally found resistance (V_{Rexp} = 883 kN) reasonably agrees with the maximum predicted resistance ($V'_{R\max}$ = 770 kN, predicted using Equation 5.31 as ε_x is larger than zero). From the experimentally measured stirrup strains it was found that the maximum resistance was reached before the stirrups yielded (Leonhardt et al. 1973). This shows that the maximum shear resistance can be governing and that the maximum resistance is reasonably predicted using the applicable equation.

Eventually, 26 of the 57 experiments of the database described in Section 5.3 meet all selection criteria and will be used for the evaluation of model B1.

8.4.2 Accuracy of model B1

To evaluate the accuracy, the shear resistance determined with the proposed model (Appendix K) is compared to the experimentally found resistance (Appendix N). The accuracy is expressed in terms of the test-to-predicted shear resistance ratio. The results in terms of mean value of the test-to-predicted shear resistance ratio and the associated coefficient of variation are listed in Table 8.1 and shown in Figure 8.5.

Table 8.1. Statistical properties of test-to-predicted shear resistance ratio for model B1

		$a/d > 2.5$	$a/d > 5.0$
Number of experiments	26	21	6
Mean	1.39	1.33	1.12
Coefficient of variation	17.5%	14.6%	8.5%

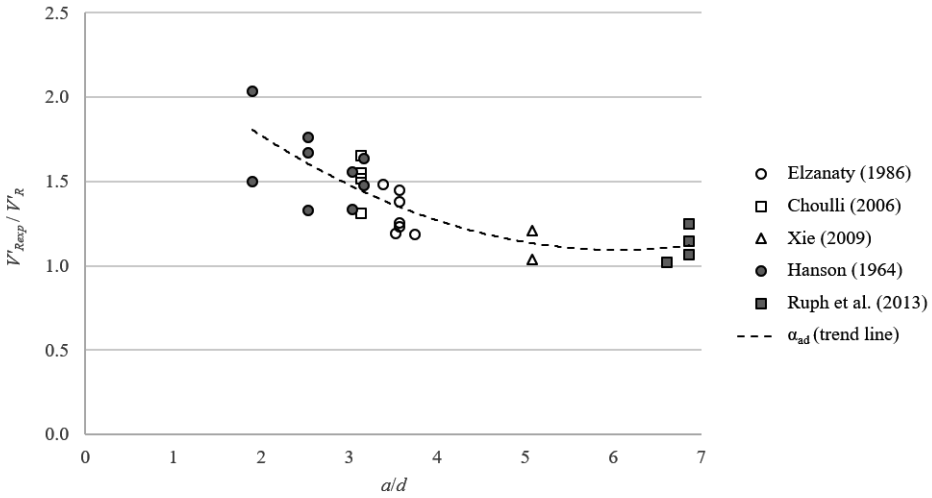

Figure 8.5. Test-to-predicted shear resistance ratio versus the ratio *a*/*d* for proposed model

Model B1 assumes sectional behaviour and conservatively neglects the contribution of direct load transfer mechanism. The proposed model further assumes that the shear force is only resisted by aggregate interlock, stirrups and the uncracked flanges. In literature it is frequently assumed that direct load transfer contributes to the shear resistance up to a value of *a*/*d* of 2.4. The value *a*/*d* of 2.4 is assumed for instance as selection criterion for the Reineck database for slender girders (Reineck et al. 2012). The value is also used as selection criterion to evaluate the accuracy of the sectional analyses programme *Response* (Bentz 2000). In this dissertation, also experiments with *a*/*d* smaller than 2.4 are selected in the current research to be able to investigate the effect of *a*/*d* on the accuracy (Section 5.3.2). Figure 8.5 and Table 8.1 show that the test-to-predicted shear resistance ratio strongly depends on the *a*/*d* ratio. For decreasing values of *a*/*d*, the test-to-predicted shear resistance ratio increases, which indicates that the actual resistance is underestimated when *a*/*d* is low. This observed trend corresponds well to the theory of arch action models (Section 5.1.8), that predict that a larger part of the shear will be resisted by direct load transfer if *a*/*d* decreases. When *a*/*d* is smaller than 5, direct load transfer will already increase the shear resistance. An adaption of model B1 to account for this additional resistance is a promising topic to further reduce the conservatism for low *a* over *d* ratios. However, this topic will not further be addressed in the current research.

Also the effect of crack spacing s_θ and the maximum aggregate size d_{max} on the accuracy of the proposed model is considered. Table 8.2 lists the maximum aggregate size as used in the experiments. The maximum aggregate size as used in the experiments is often smaller than 31.5 mm which is used to derive the proposed model (Section 6.3). As a result the contribution of aggregate interlock is overestimated (Equation 5.29). This is only the case for experiments with f_{cm} smaller than 80 N/mm^2, because above this value the aggregate size is assumed to have no effect (Equation 6.3a). Table 8.2 also lists the diagonal crack spacing at mid-depth as measured from photos or crack diagram figures. Crack patterns were not available for all experiments. Therefore, the average of the diagonal crack spacing based on the experiments for which photos or crack diagram figures were available was assumed to be representative for the whole test series. As shown in Table 8.2, the diagonal crack spacing found from observations was much lower than the assumed value of 300 mm. Because a too large diagonal cracking spacing is assumed, the contribution of aggregate interlock is underestimated (Equations 5.27 and 5.29) when the proposed model is used. This in contrast to the effect of assuming a to large assumed maximum aggregate size, which causes an overestimation of the aggregate interlock contribution.

Table 8.2. d_{max} and s_θ as assumed in models and as used in experiments and found from measurements

		Model (Section 8.3)	Elzanaty et al. (1986)	Choulli (2005)	Hanson (1964)	Rupf et al. (2013)	Xie (2009)
d_{max}	(mm)	31.5	12.7	12.0	19.1	16.0	10.0
s_θ	(mm)	300	90	100	70	75	90

The shear stress that can be resisted is determined using Equations 6.4 to 6.6. The equations are derived assuming a diagonal cracking spacing of 300 mm and a maximum aggregate size d_{max} of 31.5 mm. The maximum shear stress that can be resisted can also be determined using the MCFT by using the programme *Membrane* (Section 6.3). This way, d_{max} and s_θ can be explicitly considered. The resistances are determined using both approaches and they are listed in Appendix O. The resistances using *Membrane* are determined for f_{cm}, f_{yz} and ρ_w associated with each experiment. To consider the fact that in high strength concrete, cracks go through the coarse aggregates, the maximum aggregate size is linearly reduced from d_{max} (Table 8.2) at f_{cm} = 60 N/mm^2 to 0 mm at f_{cm} = 80 N/mm^2 (Bentz et al. 2001). The aggregate size which is adjusted at high f_{cm} is also listed in Appendix O and defined as $d_{max}(f_{cm})$. *Membrane* determines the diagonal crack spacing from the longitudinal crack spacing s_x and the vertical crack spacing s_z. As a simplification, s_x is equalized to the vertical distance between the bars in longitudinal direction (at mid-depth) and s_z is equalized to the centre to centre distance of the stirrups (Bentz et al. 2006b).

Figure 8.6 shows the ratio of $\tau'_{R,Eq6.4\text{-}6.6}$, which is the shear resistance according to the proposed model, assuming s_θ =300 mm and d_{max} = 31.5 mm, and $\tau'_{R,M2k}$ which is the shear resistance according to *Membrane* at $\varepsilon_x = 0$, using the actual d_{max} and resulting s_θ, as function of s_θ (Appendix O). Figure 8.6 shows that assuming a constant diagonal crack spacing of 300 mm leads to a more conservative prediction of the shear resistance compared to the smaller values of the diagonal crack spacing calculated using the MCFT. When the smaller d_{max} as used in the experiments (Table 8.2) would not have been considered, the predictions would have become even more conservative.

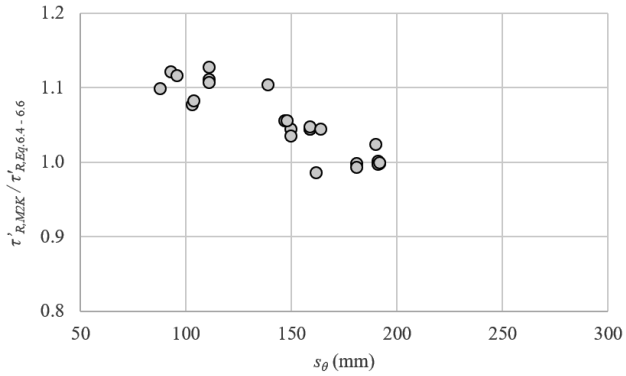

Figure 8.6. Ratio $\tau'_{R,Eq.6.4\text{-}6.6}$ (s_θ =300 mm and d_{max} = 31.5 mm) and $\tau'_{R,M2K}$ (calculated s_θ and d_{max})

The predicted V'_R for the model that explicitly considers d_{max} and s_θ can be found by multiplying the resistance found for the proposed model with $\tau'_{R,M2k} / \tau'_{R,Eq6.4\text{-}6.6}$. Based on the predicted V'_R , and considering the 21 experiments with $a/d > 2.5$ (Table 8.3), a mean value of 1.28 is found for the test-to-predicted shear resistance ratio and an associated coefficient of variation of 14.1%.

The assumption of a diagonal crack spacing of 300 mm turns out to be rather significant according to Figure 8.6. The assumed s_θ clearly contributes to the conservatism found in the predictions of the proposed model. On the other hand, the coefficient of variation is not significantly reduced when s_θ and d_{max} are explicitly considered. This could possibly be ascribed to the poor prediction of the diagonal crack spacing. This is evident if the average diagonal crack spacing of 82 mm found in the experiments (Table 8.2) is compared to the average diagonal crack spacing of 149 mm found from the *Membrane* calculations (Appendix O). Nevertheless, an adaption of the model to account for this additional resistance is a promising topic to further reduce the conservatism of the proposed model, but will not be further addressed in the current research.

Finally the effect of the longitudinal strain ε_x is investigated. The models of Bentz et al. (2006b) and Esfandiari (2009) explicitly consider ε_x. This is logical, as these models are

also applicable for the regions with flexural cracks where $\varepsilon_x > 0$. It is however questionable whether considering values of ε_x smaller than zero contributes to more accurate predictions of the resistance. As described in Section 6.1, the model is developed for $\varepsilon_x = 0$. This significantly simplifies the application of the model, as extensive calculation in which the areas, the locations and the stiffness of the concrete, the prestressing- and reinforcing steel, have to be considered are not necessary. As shown in Figure 8.5, a/d significantly affects the accuracy. Therefore, to be able to analyse the effect of the longitudinal strain, the test-to-predicted shear resistance ratio is divided by α_{ad} and plotted versus the longitudinal strain (Figure 8.7). The factor α_{ad} equals the second degree polynomial for the trend line as shown in Figure 8.5 as a function of a/d (dashed black line). Figure 8.7 shows that no significant effect of ε_x on the test-to-predicted shear resistance ratio is observed. Based on this observation it is plausible that considering the strain will not significantly improve the accuracy of the proposed model for regions without flexural cracks.

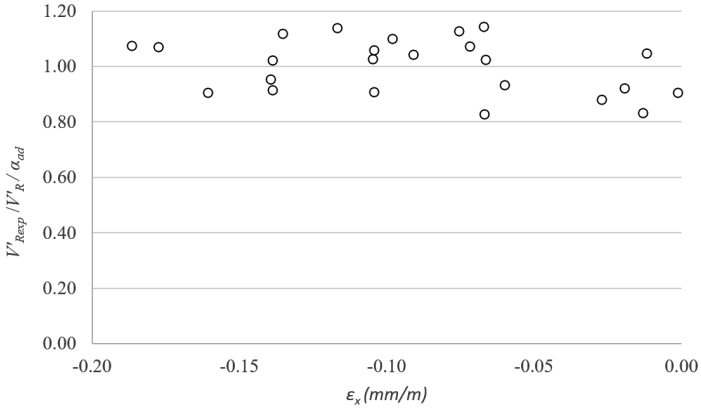

Figure 8.7. Test-to-predicted shear resistance versus the longitudinal strain

8.4.3 Comparison with models from literature

The accuracy of model B1 is compared to other models from literature using the test data. To compare the accuracy of the models, the accuracy of model B1 for the 21 experiments with an $a/d > 2.5$, is listed in Table 8.3 as reference. Additionally, the accuracy of the model of Bentz et al. (Section 5.1.5), the model of Esfandiari (Section 5.1.6) and the Variable Angle Truss model (Section 5.1.1) are listed in Table 8.3. The steps necessary to predict the resistance for each of these models are listed in Appendix P. Section 8.6 derives the variable angle truss model modified for regions without flexural cracks (also referred to as model B2). Also the accuracy of this model is listed in Table 8.3. The test-to-predicted shear resistance ratio for all models, including some intermediate results, are listed in Appendix N.

Table 8.3. Accuracy prop. model compared to models from literature for 21 experiments with $a/d > 2.5$

	Model B1: Proposed model (Section 8.3)	Model of Bentz et al. (Section 5.1.5)	Model of Esfandiari (Section 5.1.6)	Variable angle truss model (Section 5.1.1)	Model B2: Modified variable angle truss model (Section 8.6)
Mean	1.33	1.25	1.41	2.04	1.36
CoV	14.6%	16.9%	12.8%	32.6%	13.0%

For the model of Bentz et al., a mean value for the test-to-predicted shear resistance ratio of 1.25 was found for the 21 experiments that failed in regions without flexural cracks, with an associated coefficient of variation of 16.9% (Appendix N). This matches the results described in Section 5.1.5 reasonably, where a mean value for the test-to-predicted shear resistance ratio of 1.31 was found for 88 simply supported prestressed girders that failed in shear, with an associated coefficient of variation of 15.8%. Apparently the accuracy for regions with and without flexural cracks is about equal using the model of Bentz et al.. The mean value of the test-to-predicted shear resistance ratio is somewhat lower compared to model B1. This corresponds to the finding of Section 6.5. Hence, in Table 6.4, a lower mean value was found for test-to-predicted resistance for membrane elements at a longitudinal strain of zero using the model of Bentz et al. than using the proposed approximation equations. The found coefficient of variation using the model of Bentz et al., is higher than for model B1, despite that the longitudinal strain is explicitly calculated. This finding confirms that it is plausible that considering the strain will not significant improve the accuracy of model B1 for regions without flexural cracks (as also found from Figure 8.7).

For the model of Esfandiari, a mean value for the test-to-predicted shear resistance ratio of 1.41 was found for the 21 experiments that failed in regions without flexural cracks with an associated coefficient of variation of 12.8%. Section 5.1.6 describes the accuracy for 88 simply supported prestressed girders that failed in shear. For these experiments, a mean value for the test-to-predicted shear resistance ratio of 1.27 was found with an associated coefficient of variation of 16.7%. Esfandiari (2009) already concluded that the prediction became more conservative for values of the longitudinal strain smaller than 0.1 mm/m. Also for the current selection with a longitudinal strain smaller than 0 mm/m conservative predictions were found. The coefficient of variation of the model of Esfandiari is somewhat lower than the coefficient of variation of model B1.

For the variable angle truss model, a mean value for the test-to-predicted shear resistance ratio was found of 2.04 for the 21 experiments that failed in regions without flexural cracks with an associated coefficient of variation of 32.6%. The predictions are found to be extremely conservative and inconsistent, which can be attributed to the limitation

of angle of the compressive struts to 21.8° for low values of ψ (Section 5.1.1). In Section 8.6 a modified variable angle truss model is suggested for regions without flexural cracks, in which the strength of the compressive struts depends on ψ (model B2). With the modified variable angle truss model, the limitation of 21.8° is not necessary anymore. The predictions with this modified model become much more accurate, as shown in Table 8.3.

8.5 Design value of model B1

The design value of model B1 is determined by using the simple approach described in Annex D7.3 of the NEN (2011), with the statistical properties of V'_{Rexp}/V'_R as described in Appendix N as the basic input. These statistical properties concern the uncertainty of the proposed model with respect to the experimentally result, which therefore implicitly include the uncertainties regarding the model, the geometry and the material. This section determines the design value for the proposed model, for a failure probability of 10^{-4} for a 50 year reference period (the target reliability index $\beta_t = 3.8$). If another failure probability is envisaged, the same approach can be used to determine the associated partial factors.

The design value X_d for the basic variable X (in which X equals V'_{Rexp}/V'_R) can be determined using Equation 8.13 as described in NEN (2011). X is assumed to follow a lognormal distribution, which is a common distribution function for the resistance and is also used in the design value format of the Eurocode.

$$X_d = \eta_d e^{(m_y - k_{d,\eta} s_y)} \tag{8.13}$$

Equation 8.14 concerns the equation for m_y, which is the mean of the basic variable in a lognormal distribution. As the number of experiments is 21, and $\sum \ln(V'_{Rexp}/V'_R) = 5.77$, $m_y = 0.275$ (Table 8.4).

$$m_y = {}^1\!/_n \sum \ln\left(\frac{V'_{Rexp}}{V'_R}\right) \tag{8.14}$$

Equation 8.15 concerns the equation for s_y which is the coefficient of variation of the basic variable in a lognormal distribution. In this equation V_x is the coefficient of variation. The coefficient of variation is listed in Table 8.1, which results in $s_y = 14.5\%$ (Table 8.4).

$$s_y = \sqrt{\ln({V_x}^2 + 1)} \tag{8.15}$$

Table 8.4. Derivation of design value X_d

	n	m_y	s_y	$k_{d,\eta}$	X_d
All experiments	21	0.275	14.5%	3.16	0.833

The design value for the fractile factor, $k_{d,\eta}$, is found from Table D2 in NEN (2011). The value corresponds to $1.04\alpha_R\beta_t$, in which $\alpha_R = 0.8$ and $\beta_t = 3.8$. The factor α_R is the first-order reliability method sensitivity factor for the resistance and β_t concerns the target reliability index. Given the limited number of experiments ($n = 21$), an additional factor of 1.04 is required according to the referred Table D2.

In Equation 8.13, η_d is de design value of the conversion factor and should cover all uncertainties in a real structure that are not covered by the considered experiments. To be consistent with the design value format of the Eurocode η_d is equated to 1/1.15 for concrete and to 1.00 for reinforcing steel. Besides, an additional factor of 1/1.05 is introduced to ensure that the conservative that was intended by assuming s_θ of 300 mm is maintained and not included in the bias. Section 8.4.2 demonstrates that the resistances would have been average 5% higher if diagonal crack spacing and the maximum aggregate size would have been explicitly considered (Appendix O). The additional factor of 1/1.05 also covers a smaller $d_{\max}$ in the experiments than assumed for model B1. This avoids, on contrast to s_θ, that the design values becomes too conservative.

The mean value for the shear resistance for regions of prestressed girders with stirrups in regions without flexural cracks can be determined using Equation 8.6. The design value is found by multiplying Equation 8.6 with $X_d = 0.833$ and the additional factor 1/1.05 and f_{cm} and f_{ywm} with η_d, which results in Equation 8.16. X_d is the partial factor of the whole equation which already covers the uncertainty of the material properties and other uncertainties, it is sufficient to use the mean value of the material properties. However, this equation has to be converted into a design equation using f_{cd} and f_{ywd} instead of respectively f_{cm} and f_{ywm} (Equation 8.17). Accordingly, the correction factors α_1 and α_2 are introduced in the equation. Both α_1 and α_2 are derived by equalizing Equation 8.16 and 8.17.

$$V'_{Rd} = 0.833\frac{1}{1.05}\beta\sqrt{\eta_d f_{cm}}\, b_w z' + 0833\frac{1}{1.05}A_{sw}/s\ \eta_d f_{ywm}\, z'\cot\theta \tag{8.16}$$

$$V'_{Rd} = \alpha_1\,\beta\sqrt{f_{cd}}\, b_w z' + \alpha_2\, A_{sw}/s\ \ f_{ywd}\, z'\cot\theta \tag{8.17}$$

with $f_{cd} = \frac{f_{ck}}{\gamma_c}$ and $f_{ywd} = \frac{f_{ywk}}{\gamma_s}$

The correction factor α_1 for concrete is derived by equating the first part of Equation 8.16 and the first part of Equation 8.17. The ratio between f_{ck}/f_{cm}, which is necessary to derive α_1, depends on the mean value of the concrete compressive strength. Therefore,

α_1 is derived for a range of concrete strengths (Table 8.4). Table 8.4 show that the determined values of α_1 vary between 1.00 and 0.95. For simplicity it is proposed to conservatively use a α_1 of 0.95 for all concrete compressive strengths. The correction factor is taken into account by reducing β according to Equation 8.7 and 8.8 which will be explained hereafter. It is noted that, when a design code is compiled, f_{cm} in Equation 8.16 is frequently replaced by f_{ck} for practical considerations, but given the approach used in this section this is not considered as necessary for this dissertation.

Table 8.4. Correction factor for design value of concrete based on $f_{cm} = f_{ck} + 8$ (NEN 2005)

f_{ck}	f_{cm}	f_{ck}/f_{cm}	α_1
N/mm^2	N/mm2	-	-
35	43	0.81	1.00
45	53	0.85	0.98
55	63	0.87	0.97
65	73	0.89	0.96
75	83	0.90	0.95
85	93	0.91	0.95

The correction factor α_2 for the reinforcing steel is derived by equating the second part of Equation 8.16 and the second part of Equation 8.17. The ratio between f_{ywk} / f_{ywm}, which is necessary to derive α_2, depends on the characteristic value of the yield strength of the reinforcing steel. Therefore, α_2 is derived for a range of yields strengths (Table 8.5). A partial factor for the reinforcing steel γ_s is assumed of 1.15. This partial factor covers the uncertainties regarding the model, the geometry and the material. Table 8.5 show that the determined values of α_2 vary between 1.16 and 1.02. For simplicity it is proposed to conservatively use α_2 of 1.00 for all yield strengths.

Table 8.5. Correction factor for design value of reinforcing steel based on $f_{ywm} = f_{ywk} + 60$ (JCSS 2002)

f_{ywk}	f_{ywm}	f_{ywk}/f_{ywm}	α_2
N/mm^2	N/mm^2	-	-
220	280	0.79	1.16
300	360	0.83	1.09
400	460	0.87	1.05
500	560	0.89	1.02

Equations 8.18 to 8.20 concern the design value for model B1. Only α_1 has to be considered because a value for α_2 of unity is used. Equations 8.19 and 8.20 are found by multiplying Equations 8.7 and 8.8 with α_1= 0.95. This reduces the first parts of β from respectively 0.38 (Equation 8.7) and 0.30 (Equation 8.8) to 0.36 (Equation 8.19) and 0.28 (Equation 8.20). The second parts of equations 8.7 and 8.8 are conservatively not multiplied with α_1, because -2.5 is a nicely rounded value. Equation 8.18 should be used

in combination with $\gamma_c = 1.5$ and $\gamma_s = 1.15$, for a target reliability index $\beta_t = 3.8$ for a 50 year reference period.

$$V'_{Rd} = \beta \sqrt{f_{cd}}\, b_w z' + A_{sw}/s \;\; f_{ywd}\, z' \cot\theta \tag{8.18}$$

$$\beta = 0.36 - 2.5\psi \qquad \text{for } f_{cm} \leq 60 \text{ N/mm}^2 \tag{8.19}$$

$$\beta = 0.28 - 2.5\psi \qquad \text{for } f_{cm} \geq 80 \text{ N/mm}^2 \tag{8.20}$$

With $\psi = \rho_w f_{ywm} / f_{cm}$, $\rho_w = A_{sw} / (b_w\, s)$ and $\theta = 26°$

8.6 Model B2: modified variable angle truss model

Section 8.3 proposes a model for the shear resistance for prestressed girders with stirrups in regions without flexural cracks, referred to as model B1. Model B1 explicitly takes into account the contribution of aggregate interlock and stirrups. In the current section an alternative presentation of model B1 is described. This concerns a modification of the variable angle truss model specifically intended for regions without flexural cracks, referred to as model B2. Model B2 ascribes the shear resistance completely to the stirrups. The contribution of aggregate interlock is taken into account implicitly by using a smaller angle of the compressive struts than the cracking angle.

Like model B1 (Section 8.3), model B2 is based on the resistances determined for membrane elements at a longitudinal strain of zero (Section 6.3). This approach solves the following two issues regarding the application of the currently used variable angle truss model (Section 5.1.1) in regions without flexural cracks:

1. The currently used variable angle truss model does not distinguish between regions with and without flexural cracks. The additional resistance due to the smaller longitudinal strains and smaller crack width, is not considered. This additional resistance is however considered in the modified model described in this section, because the model is based on membrane resistances at a longitudinal strain of zero (Sections 6.1 to 6.4). It is noted that the version of the Eurocode that is currently under development (CEN 2020), relates the limitation of the angle of the compressive struts to the average axial compressive stresses.
2. The effective concrete strength of the struts according to the current variable angle truss model is derived for high values of ψ, for which crushing of the struts is governing. For lower values of ψ, for which sliding of the crack can be governing, the derived effective concrete strength of the struts is not suitable and could lead to an overestimation of the shear resistance. Therefore, the angle of the compression strut is limited to a minimum of 21.8° in the current model. However, this limitation results

in extremely conservative predictions for values of ψ for which the limit is governing, as shown in Table 5.1. In contrast to the current variable angle truss model, the modified version is based on membrane resistances based on the resistance associated with the governing failure mode. Thus both crushing of the compression fields and sliding of the cracks can be governing and the model is capable of determining associated resistances.

In the modified variable angle truss model, model B2, the effective strength of the compression struts is back calculated from the resistance for membrane elements as determined in Section 6.3. For the modified model, the effectiveness factor of the concrete strength in regions without flexural cracks is defined as one parameter v' (instead of $v\alpha_{cw}$, which is used in the current variable truss model). In Section 6.3, the values for $v\alpha_{cw}$ (replaced in the proposed model by v') are calculated and related to f_{cm} and ψ. The concrete effectiveness factor v', found from back calculations of the resistances of the MCFT, is shown in Figure 8.8 with black bullets (notice that of $v\alpha_{cw}$ is replaced by v'). It is noted that the angle of the compressive struts follows from the back calculations and therefore there is no need to limit this angle.

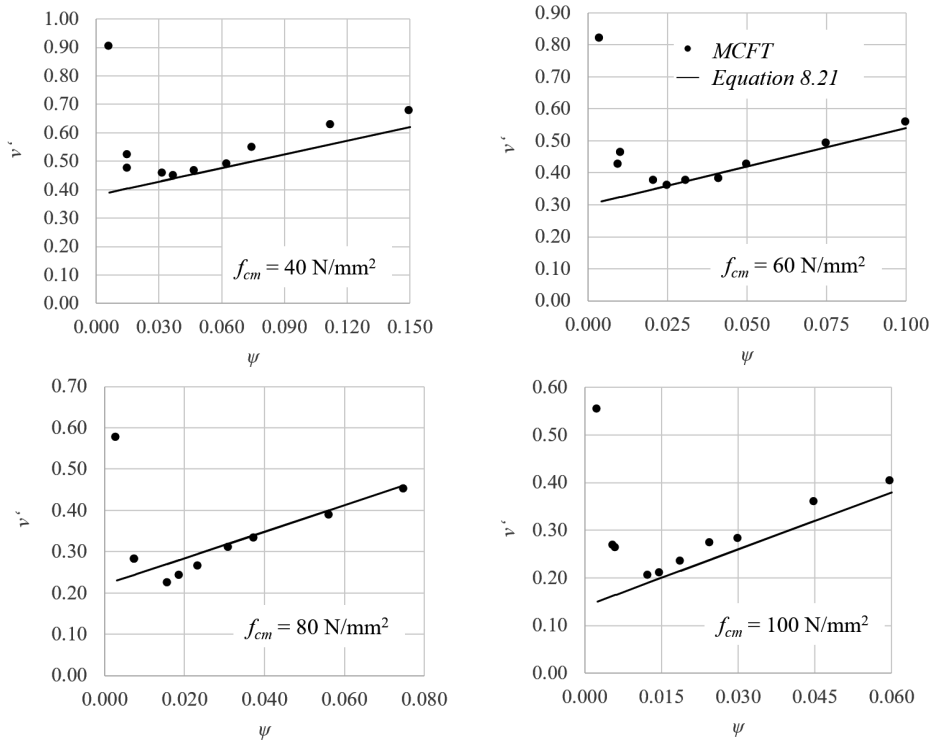

Figure 8.8. Comparison of v' according to MCFT and predicted with the variable angle truss model .

As shown in Figure 8.8, the highest values for v' are found, for the lowest values of ψ. This is explained considering Figure 6.11. For values of ψ approaching zero, the contribution of aggregate interlock can still be significant, whereas the contribution for the stirrups approaches zero. As the shear resistance is fully ascribed to the stirrups, the effective strength of the compressive struts must be significantly increased to find the associated resistance. The observation that the highest values for v' are found for the lowest values of ψ, is not considered in model B2. Hence, for values of ψ that approach zero, the resistance to diagonal tension cracking ($V'_{R,c}$) will be governing.

To derive an approximation equation for the effectiveness factor of the concrete strength, an equation $v' = (a - b\,f_{cm}) + c\,\psi\,f_{cm}$ is assumed. The part $a - b\,f_{cm}$ accounts for the different values of v' for the considered values of f_{cm}, at $\psi = 0$. The part $c\,\psi\,f_{cm}$ accounts for the different slopes of the graphs for the considered values of f_{cm}. For a combination of a, b and c it is possible to determine the ratio of the approached resistance and the resistance according to the MCFT. For the 32 membranes that meet the condition $\psi \geq 0.010$, the mean values of the ratio of both resistances are determined with the associated coefficient of variation. The values of a, b and c are adapted until the mean value of the ratio of the resistances approaches 1.00 (eventually 1.03) and a minimum coefficient of variation is found (eventually 6%). This results in values for a, b and c of respectively 0.54, -0.004, 0.04 (Equation 8.21, with f_{cm} and f_{ywm} in N/mm^2). Eventually, $\psi\,f_{cm}$ Is rewritten as $\rho_w f_{ywm.}$

The concrete effectiveness factor according to Equation 8.21 is shown in Figure 8.8 with a continuous black line for each concrete strength. Note that this equation is only valid for regions without flexural cracks, because the equation is based on the resistance of membrane elements with $\varepsilon_x = 0$. For regions with flexural cracks in the ultimate limit state, for which $\varepsilon_x > 0$, lower resistances will be found for the membranes elements. Therefore, if flexural cracks are present, the effective strength of the concrete v' will also be lower than follows from Equation 8.21.

$$v' = 0.54 - 0.004 f_{cm} + 0.04 \rho_w f_{ywm} \tag{8.21}$$

The modified variable angle truss model, model B2, is summarized in the following text. For regions of prestressed girders without flexural cracks the shear resistance can be determined using model B2 according to Equation 8.21 – 8.24. The apostrophe used in the parameters, indicates that the equations are derived for regions without flexural cracks. In these equations, θ is the angle of the compressive strut (this in in contrast to model B1, in which θ represents the angle of the cracks). The angle of the compressive strut is steeper than the cracking angle. This is possible because aggregate interlock enables shear transfer across the crack. The resistance by the aggregate interlock and

stirrups is expressed as a resistance by the stirrups only, as appears from Equation 8.22. In this equation A_{sw} is the area of shear reinforcement, s is the distance between the stirrups and f_{ywm} the yielding strength of the stirrups. The effective shear depth z' in regions without flexural cracks can be determined from Equations 8.9 – 8.11.

$$V'_R = A_{sw}/s \; f_{ywm} \; z' \cot\theta \tag{8.22}$$

$$\tan\theta = \sqrt{\psi_{VAT}/(1-\psi_{VAT})} \tag{8.23}$$

$$\psi_{VAT} = \rho_z f_{yw} / \nu' f_{cm} \tag{8.24}$$

With $\rho_z = A_{sw} / (b_w \, s)$

Equation 8.21 is found from the assumption that the struts fail due to or concrete crushing or crack sliding, after the stirrups start to yield. Note that in Equation 8.24 for ψ_{VAT}, the strength of the compressive struts $\nu' f_{cm}$ comprises the denominator whereas in the equation for ψ (Equation 8.8), the concrete cylinder compressive f_{cm} comprises the denominator. Equation 8.21 is found from back calculations of the resistance determined with the MCFT (Section 6.5.2).

The conditions regarding the diagonal crack spacing, as described at the end of Section 8.3, are also applicable for model B2. Also $V'_{R,c}$ and $V'_{R\max}$ should be considered if the resistance is determined with model B2 (Section 8.2).

Finally, the accuracy is evaluated for model B2. The shear resistance determined with model B2 is compared to the experimentally found resistance (Appendix N). To determine the shear resistance, firstly, the internal lever arm (which equals the effective shear depth) is determined from Equations 8.9 – 8.11. Secondly, ν' is determined using Equation 8.21. Thereafter, ψ_{VAT}, θ and V'_R are determined using successively Equations 8.24, 8.23 and 8.22. Note that the angles of the compressive struts, determined with model B2, vary between 9.0° and 20.8° (Appendix N). Using the variable angle truss model, a mean value for the test-to-predicted shear resistance ratio was found, for 21 experiments that failed in regions without flexural cracks, of 1.36 and an associated coefficient of variation of 13.0%. The accuracy is comparable with model B1 (Table 8.3). The predictions are a little more conservative compared to model B1, which can be ascribed to the conservative approximation of ν' for low values of ψ. (Figure 8.8). The coefficient of variation is found to be somewhat lower than for model B1.

The design value for model B2 can be determined in the same way as for model B1 (Section 8.5). Again the statistical properties of V'_{Rexp}/V'_R as described in Appendix N can be used as the basic input. Equation 8.14 results in a mean of the basic variable in a lognormal distribution (m_y) of 0.298, as the number of experiments = 21 and

$\sum \ln(V'_{Rexp}/V'_R) = 6.25$. Equation 8.15 results in a coefficient of variation of the basic variable in a lognormal distribution (s_y) of 12.9%, as $V_x = 13.0\%$. The design value for the fractile factor $k_{d,\eta} = 3.16$, considering the number of experiments. Equation 8.13 results in $X_d = 0.896$. As for reinforcing steel $\eta_d = 1$, only the additional factor of 1/1.05 is used that ensures that the conservative that was intended by assuming s_θ of 300 mm is maintained and not included in the bias. By equating the second part of Equation 8.16 and the second part of Equation 8.17, a correction factor for the reinforcing steel (α_2) of 1.10 is found for a yield strength f_{ywk} = 500 N/mm^2 (which is the yield strength that results in a minimum α_2, Table 8.5). For simplicity it is proposed to conservatively use $\alpha_2 = 1.00$ for all yield strengths. The design value, which can be used with a partial factor for the reinforcing steel γ_s of 1.15, is shown in Equation 8.25.

$$V'_{Rd} = A_{sw}/s \ f_{ywd} \ z' \cot\theta \tag{8.25}$$

8.7 Minimum shear reinforcement ratio

A minimum amount of shear reinforcement should ensure that failure does not occur immediately upon shear cracking and that truss action can develop (*fib* 2012, article 7.13.5.2). Based on this definition, the minimum shear reinforcement ratio for regions without flexural cracks ($\rho'_{w,\min}$) can be derived by equating the shear resistance of girders with stirrups (V'_R) and the resistance to diagonal tension cracking ($V'_{R,c}$). The apostrophes indicate that the parameters are applicable for regions without flexural cracks.

The most consistent way to determine both resistances is by using models A1, A2 and B1 (respectively in sections 4.1, 4.2 and 8.3). In engineering practice, both resistances will be determined and the highest of both resistances will be governing. Therefore, there is no need to have an equation for $\rho'_{w,\min}$ for engineering practice. Nevertheless, an equation for $\rho'_{w,\min}$ will be derived because it provides insight in the conditions under which diagonal tension cracking is governing and when additional shear can be resisted after diagonal tension cracking.

Because the equation for $\rho'_{w,\min}$ is only derived to provide insight, models from literature will be used that are further simplified and lead to a simple equation for $\rho'_{w,\min}$. To determine $V'_{R,c}$, Equation 8.26 is used which combines Equations 2.19 and 2.20 (ACI 2008). Furthermore, the effective height of the prestressing steel (d_p) is assumed to be $0.9h$, as investigated in Section 2.1.5. To determine V'_R, Equation 8.27 is used, which combines Equations 5.30, 5.36 and 5.37 (Bentz et al. 2006a). Furthermore, ε_x is assumed to be zero and z is assumed to be $0.8h$, as investigated in respectively Sections 6.1 and 7.3.

$$V'_{R,c} = 0.9h\, b_w \left(0.291\sqrt{f_{cm}} + 0.3\,\sigma_{cp}\right) \tag{8.26}$$

$$V'_{R} = 0.8h\, b_w \left(0.4\sqrt{f_{cm}} + \frac{\rho_w f_{ywm}}{\tan 29°}\right) \tag{8.27}$$

The experimentally found resistances will not exactly match the predicted shear resistances. To get a realistic value for $\rho'_{w,\min}$, the predicted resistances will be multiplied by the mean value of the test-to-predicted shear resistance ratio. The mean values are determined for the 26 experiments which were found suitable to evaluate models for regions without flexural cracks of girders with stirrups (Section 8.4.1). Considering experiments without stirrups is not useful to determine $\rho'_{w,\min}$. A mean value for $V'_{R,c,exp} / V'_{R,c(Eq8.26)}$ was found of 1.01, which is in line with the earlier found values for the proposed models A1 and A2 for diagonal tension cracking (Table 3.8). A mean value for $V'_{Rexp} / V'_{R(Eq8.27)}$ was found of 1.27, which is also in line with the earlier found values for model B1 for girders wit stirrups (Table 8.1). The equation for the minimum shear reinforcement ratio (Equation 8.28) is found by equating $1.27V'_R$ and $1.01V'_{R,c}$. It is noted the associated coefficients of variation for the simple models are both 18%, which is indeed more than for models A1, A2 and B1.

$$\rho'_{w,\min} = \frac{\left(0.15\sigma_{cp} - 0.08\sqrt{f_{cm}}\right)}{f_{ywm}} \tag{8.28}$$

For the selected 26 experiments $\rho'_{w,\min}$ is determined using equation 8.28. This is also done for experiment CW17, that was not selected because the experiment was considered to have failed due to diagonal tension cracking (Section 8.4.1). In Figure 8.9 the of ratio ρ'_w and $\rho'_{w,\min}$ is plotted versus the ratio of the experimentally found ultimate resistance and the experimentally found resistance to diagonal tension cracking. For all experiments, except CW17, it is found that $V'_{R,exp} / V'_{R,c,exp}$ is indeed larger than unity if ρ'_w is larger than $\rho'_{w,\min}$ (shown with a grey area). For values of $\rho'_w / \rho'_{w,\min}$ that decrease towards unity, also $V'_{Rexp} / V'_{R,c,exp}$ approaches unity. This trend confirms that Equation 8.28 is suitable to determine $\rho'_{w,\min}$.

For experiment CW17, it was found that $V'_{Rexp} / V'_{R,c,exp} > 1$ despite that $\rho'_w < \rho'_{w,\min}$. In Section 2.1 is it shown that also girders without stirrups can sometimes resist some additional shear force after diagonal tension cracking (Figure 2.2). It is plausible that this is the case for CW17. It is noted that regarding the selection criterion $V'_R > V'_{R,c}$ (Section 8.4.1), the same experiments would have been selected if Equation 8.28 was used instead of considering the highest resistance determined with the more accurate models (A1, A2 and B1, Appendix M).

For one experiment (SR23) a negative value for $\rho'_{w,\min}$ was found (this result is not shown in Figure 8.9). This negative value was caused by the ratio V'_{Rexp} and $V'_{R(Eq8.27)}$ of 0.96 which was substantial lower than the mean value of 1.27. If a test to predict resistance ratio of 0.96 was used instead of 1.27, a positive value for $\rho'_{w,\min}$ would have been found and a $\rho'_w / \rho'_{w,\min}$ of 1.3, which fits well into the range of $\rho'_w / \rho'_{w,\min}$ shown in Figure 8.9.

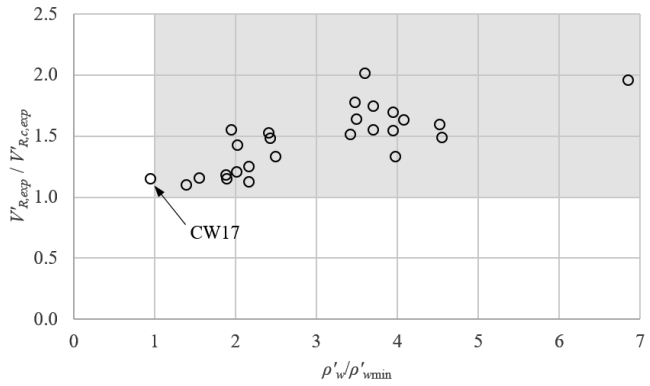

Figure 8.9. ratio of ρ'_w and $\rho'_{w,\min}$ versus $V'_{R,exp} / V'_{R,c,exp}$ for selected 26 experiments & CW17

Figure 8.10 shows $\rho'_{w,\min}$ according to Equation 8.28 versus σ_{cp} for some combinations of f_{cm} and f_{ywm} that are representative for practice (Table 1.1).

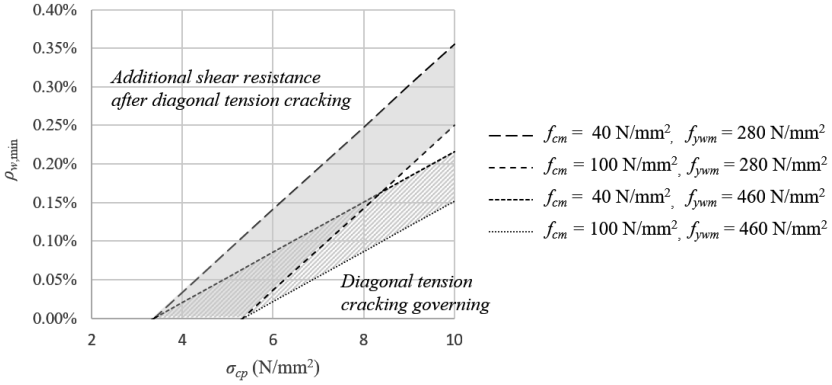

Figure 8.10. $\rho'_{w,\min}$ versus σ_{cp} for combinations of f_{cm} and f_{ywm} representative for practice.

It is noted that for low values of σ_{cp} the minimum shear reinforcement approaches zero. A value of zero means that the resistance by the aggregate interlock in the diagonal tension crack (after diagonal tension cracking) equals the resistance to diagonal tension cracking. That these values could be equal follows from Equations 8.26 and 8.27. For low values of σ_{cp}, diagonal tension cracking occurs at a lower load, and $V'_{R,c}$ will be

small (Equation 8.26). On the other hand, low values of σ_{cp} will not affect V'_R (Equation 8.27). There is however another phenomenon that reduces the chance that both values could be equal. This is because the aggregate interlock part of V'_R remains high according to Equation 8.27, because it is located in a region without flexural cracks ($\varepsilon_x = 0$). For low values of σ_{cp}, the chance that a regions remains uncracked reduces. Therefore, the chance that the equations are applicable reduces if σ_{cp} reduces.

Figure 8.10 shows that diagonal tension cracking is governing for high values of σ_{cp} and low values of ρ'_w. For low values of σ_{cp} and high values of ρ'_w additional shear can be resisted after diagonal tension cracking.

9

Conclusions and recommendations

This chapter summarizes the results of this dissertation and gives recommendations regarding the use of the proposed models in practice and for future research. Section 9.1 summarizes the main scientific results and Section 9.2 addresses the answers to the research questions. Section 9.3 summarizes the proposed models and their application conditions. Section 9.4 describes the implications of the use of the proposed models for the structural assessments of bridges. Finally, Section 9.5 suggests topics for further research.

9.1 Scientific results

This dissertation investigated two aspects of the shear resistance of prestressed girders in regions without flexural cracks: (i) the resistance to diagonal tension cracking and (ii) the shear resistance after diagonal tension cracking. The latter is only relevant if stirrups are present. The main scientific results for these two topics are described in respectively Sections 9.1.1 and 9.1.2.

9.1.1 Resistance to diagonal tension cracking

1. This dissertation provides an overview of models from literature for the resistance of prestressed girders to diagonal tension cracking (Section 2.1). The models, as applied in the Eurocode (NEN 2005), the Model Code 2010 (*fib* 2012) and the ACI (ACI 2008), all assume diagonal tension cracking at the instant the maximum principal tensile stress equals the tensile strength of the web. However, different simplifications are used to determine the maximum principal tensile stress. Also, different models use different values for the tensile strength of the web. These two issues are further investigated.
2. In this dissertation a database is composed, containing 70 experiments from seven test series of prestressed girders (Appendix A), in which diagonal tension cracking was reported. The main parameters of the experiments vary between the ranges: $-11.3 \leq \sigma_{cp} \leq -2.3$ N/mm^2, $-0.23 \leq \sigma_{cp} / f_{cm} \leq -0.05$, $24 \leq f_{cm} \leq 99$ N/mm^2. These ranges of parameters are reasonably representative for the parameters of existing bridges (Table 1.1).

3. Diagonal tension cracking occurs at a principal tensile stress lower than the uniaxial tensile strength of concrete. This can be ascribed to the presence of principal compressive stresses that reduce the tensile strength of concrete (bi-axial behaviour, Section 3.2).
4. The tensile strength of the web relates to the size of the region exposed to high principal tensile stresses (statistical size effect). This dissertation derives an equation for the tensile strength of the web that combines the statistical size effect and the effect of bi-axial behaviour (Equation 3.10). Using Equation 3.10 to determine the tensile strength of the web for the 14 experiments without flexural cracks, instead of the uniaxial tensile strength, results in a reduction of the bias of the mean ratio of $\sigma_{1\max} / f_{ctm,web}$ from 0.84 to 1.01 and reduction of the associated coefficient of variation from 6.7% to 2.3% (Section 3.2).
5. The maximum principal tensile stresses are not present in the disturbed area around the support, as long as no flexural cracks are present in this disturbed area. This is due to the vertical stresses and the more favourable distribution of the longitudinal and shear stresses in the disturbed areas (Section 3.3).
6. The distribution of principal tensile stresses in the region without flexural cracks cannot be considered as independent of flexural cracks on the edge of this region. This is because the formation of a flexural crack on the edge of the region without flexural cracks can increase the principal tensile stresses in the uncracked region and trigger diagonal tension cracking (Section 3.5).
7. When the maximum principal tensile stresses $\sigma_{1\max}$ are based on σ_1 along the centroidal axis instead of over the web area (light grey area of Figure 3.7), the consistency of the predicted resistance to diagonal tension cracking decreases significantly.
8. This dissertation proposes a model to predict the resistance to diagonal tension cracking for girders in which no flexural cracks are present, referred to as model A1 (Section 3.4). The accuracy of model A1 is investigated considering 16 experiments in which no flexural cracks are present. A mean value of the test-to-predicted shear resistance ratio was found of 1.00 and an associated coefficient of variation of 5.2% (Section 3.4).
9. This dissertation proposes a model to predict the resistance to diagonal tension cracking for girders in which flexural cracks are present, referred to as model A2 (Section 3.5). The accuracy of model A2 is investigated considering 37 experiments in which flexural cracks are present. A mean value of the test-to-predicted shear resistance ratio was found of 1.01 and an associated coefficient of variation of 12.3% (Section 3.5).

9.1.2 Shear resistance of prestressed girders with stirrups

1. This dissertation provides an overview of models from literature that are intended to determine the shear resistance of prestressed girders with stirrups for regions without flexural cracks (Section 5.1). These concern empirical models as derived by MacGregor et al. (1960) and Leonhardt (1973), the variable angle truss model, which is a lower bound approach based on the theory of plasticity (Walraven 2002), models based on the MCFT (Bentz et al. 2006a, Esfandiari 2009) and the arch action model as proposed by Huber (2016). Based on a comparative study of the models (Section 5.2) and an evaluation of the models (Section 5.4), it was decided to base the proposed model on the MCFT theory (Section 5.1.3). This is because the MCFT is capable to predict the shear resistance for the low longitudinal strains that are present in regions without flexural cracks and for low shear reinforcement ratios that are present in existing bridges (Tables 1.1 and 6.3).

2. In this dissertation a database is composed, containing 57 experiments of prestressed girders with stirrups that failed in shear and for which the shear failure could be related to diagonal tension cracks. Of these 57 experiments, 21 are considered suitable to use for the validation of the proposed model because it could be demonstrated that (i) the failure occurred in the region without flexural cracks, (ii) sufficient stirrups were present to prevent instant failure at diagonal tension cracking and (iii) the shear span to depth ratio was larger than 2.5 (Section 8.4.1). These 21 experiments consist of five test series, containing both simply as well as continuously supported girders, containing experiments with post-tensioned and pre-tensioned prestressing steel with straight, draped and curved geometries of the prestressing steel. The main parameters vary as follows: $0.06\% \leq \rho_w \leq 0.79\%$, $28 \leq f_{cm} \leq 91$ N/mm^2, $298 \leq f_{ywm} \leq 585$ N/mm^2. These ranges of parameters are representative for the parameters of existing bridges (Table 1.1).

3. This dissertation derives an equation to determine the shear resistance by aggregate interlock and stirrups at mid-depth of the web (Section 6.4) which will be used in the model proposed in this dissertation (model B1). This equation (Equation 6.4) is based on the resistances found for a series of membranes for a range of parameters, which are determined using the MCFT (Section 6.3). It was found possible to cover the possible failure modes with just this one equation. Equation 6.4 determines the resistances found from the MCFT more accurately (Table 6.4) than equations used in existing models (Bentz et al. 2006a, Esfandiari 2009) and is also more simple to use. For the considered 40 membranes, the mean value of the ratio of the resistance according to the proposed equation and the MCFT was found to be 1.00 and an associated coefficient of variation of 4%. The proposed equation differs in a number of aspects from equations used in these cited existing models:

a. The range of parameters considered for the determination of the resistances of the membranes is extended to become representative for the intended application of the proposed model (Table 1.1). This implies that the lowest value for ρ_w has been reduced from 0.2% to 0.1% and the highest value for f_{cm} has been increased from 60 N/mm^2 to 100 N/mm^2. Moreover a value for $d_{\max}$ is used of 31.5 mm, which is a common value for $d_{\max}$ applied in Dutch bridges up to 2000.

b. The proposed model assumes a longitudinal strain of zero as it is specifically intended to predict the shear resistance in regions without flexural cracks. It was found that explicitly considering the longitudinal strain for this condition did not increase the accuracy (Figure 8.7).

c. The way in which the decreasing contribution of aggregate interlock for higher strength concrete ($f_{cm} \geq 80$ N/mm^2) is taken into account, is adapted (Section 6.4).

4. The model of Bentz et al. (2006b) assumes that the resistance of the aggregate interlock and stirrups at mid-depth is representative for the resistances along the entire crack surface. The validity of this assumption is demonstrated for regions without flexural cracks (Section 7.2).

5. For the parts of the web that are not cracked, the distributed shear force is approximately the same magnitude as for the cracked part of the web. Therefore, the resistance of the web in the regions without flexural cracks can be accurately predicted by multiplying the shear resistance at the web at mid-depth, the web height and the average web width.

6. The contribution of the uncracked concrete to the shear transfer was found to depend mainly on the height of the straight and skew flanges (Section 7.3). It was found that the effect of the width of the flanges on the contribution by uncracked concrete was insignificant. Based on these findings, an equation for the effective shear depth was derived (Equation 7.10). The effective shear depth accounts for an increase of the shear that can be resisted by aggregate interlock and stirrups along the crack, by shear transferred in the uncracked concrete. This is in contrast to the existing models (Bentz et al. 2006a, Esfandiari 2009) which relate the effective shear depth to the effective depth of the reinforcing steel and prestressing steel, which are irrelevant if no flexural cracks are present.

7. The shear resistance calculated with a non-linear sectional analyses programme based on the MCFT, that predicts the shear flow over the height (*Response*), can be predicted accurately by using the simple equation proposed for the effective shear depth (Equation 7.10), which will be used in the model proposed in this dissertation. This

is evaluated by comparing the resistances determined using the proposed equations for the effective shear depth for 26 experiments of the database, for cross-sections in which no flexural cracks were predicted. A mean value of the ratio of both resistances was found of 0.99 and a coefficient of variation of 2% (Section 7.3, Figure 7.11).

8. This dissertation proposes a model, referred to as model B1, to predict the shear resistance of prestressed girders with stirrups in regions without flexural cracks, based on the derived equations for the shear resistance at mid-depth and the effective shear depth (Chapter 8). The accuracy of the model is evaluated by comparing the shear resistance determined with the proposed model (Appendix K) and the experimentally found resistance (Appendix N). For the 21 experiments that are considered suitable for the evaluation (Section 8.4.1), a mean value of the test-to-predicted shear resistance ratio was found of 1.33 with an associated coefficient of variation 14.6% (Table 8.1).
9. Neglecting the effect of direct load transfer in the proposed model was found to affect the accuracy of the predictions significantly. The influence appears from Figure 8.5, which shows that, despite the observation that the level of conservatism reduces for increasing shear span to depth ratios, the effect remains significant even for higher shear span to depth ratios.
10. This dissertation also offers an alternative for the proposed model B1. This alternative is the variable angle truss model modified for regions without flexural cracks (Section 8.6), which is referred to as model B2. This model ascribes the shear resistance completely to the stirrups. The contribution of aggregate interlock is taken into account implicitly by using a smaller angle for the strut angle than the cracking angle. In the modified variable angle truss model, the effective strength of the compression struts is determined from back calculations of the resistances found from the MCFT for the considered series of membrane elements (Section 6.3). The effective concrete strength (v') was found to depend not only on the mean compressive strength of the concrete (Equation 5.4), but also on the mean yielding strength of the stirrups and the shear reinforcement ratio (Equation 8.21). As this equation is also applicable for low shear reinforcement ratios, it is no longer needed to limit the angle of the compressive strut as prescribed in the current variable angle truss model (Section 5.1.1).
11. Model B2, the variable angle truss model modified for regions without flexural cracks, is found to be slightly more accurate than model B1 and significantly more accurate than the currently used variable angle truss model (Table 8.3). The accuracy of model B2 is evaluated using the 21 experiments that are considered suitable for the evaluation (Section 8.4.1). As a result, the mean value of the test-to-predicted

shear resistance ratio was found to be 1.36 and the associated coefficient of variation of 13.0% (Table 8.3).

9.2 Answers to research questions

This section explicitly addresses the answers to the research questions as posted in Section 1.4.

Research question A: 'Does the accuracy of the predictions increase if bi-axial behaviour and statistical size effect are taken into account?'

Related part of dissertation: Sections 3.2, 3.4 and 3.5

The accuracy of the predictions was found to increase if the bi-axial behaviour and statistical size effect are taken into account (Table 3.5). Moreover, the bi-axial behaviour was found as the main explanation for the finding that diagonal tensile cracking occurred at stresses below the uniaxial tensile strength (Equation 3.8). Nevertheless, for girders without flexural cracks, diagonal tension cracking can be predicted accurately based on a fraction of the uniaxial tensile strength, without considering bi-axial behaviour and statistical size effect (Table 3.7). Also for girders with flexural cracks, diagonal tension cracking could be predicted consistently without considering bi-axial behaviour and statistical size effect (Table 3.8, Appendix E).

Research question B 'How are the principal stresses distributed around the supports and the concentrated loads and is it possible to determine the maximum principal tensile stress using the Euler-Bernoulli girder theory and neglecting the vertical stresses?'

Related part of dissertation: Sections 3.3 and 3.5

To answer research question B, a distinction should be made between girders with and without flexural cracks in the flange opposite to the concentrated load (Figures 3.7, 4.1 and 4.2).

For girders without flexural cracks in the flange opposite to the concentrated load, the maximum principal tensile stresses are found in the undisturbed regions (Section 3.3). Therefore, the maximum principal tensile stress can be fairly accurate approached using the Euler-Bernoulli girder theory in the undisturbed regions. Moreover, it is appropriate to neglect the influence of the vertical stresses to the principal tensile stresses, as at the governing location, the vertical stresses are relatively small. Because the maximum principal tensile stresses are not present around the support, a region is defined around the support (Figure 3.5) which can be neglected when determining the maximum principal tensile stress. In Appendix C, column σ_{1max} (Eq. 3.1, 3.2 and 3.4)/ σ_{1max}(LEFEA)), it is

demonstrated that the maximum principal tensile stresses can be accurately determined using this approach.

For girders with flexural cracks in the flange opposite to the concentrated load , it was found that also the formation of a flexural crack at the edge of the region without flexural cracks can initiate diagonal tension cracking in the regions without flexural cracks (Section 3.5). Whether this is the case, can be rather accurately determined by assessing the principal tensile stresses in the web in the cross-section at the edge of the uncracked region. The principal tensile stresses in this cross-section can be approximated using the Euler-Bernoulli girder theory and neglecting the vertical stresses. Although assuming a linear elastic stress distribution in the vicinity of a flexural crack might seem questionable, it was found that diagonal tension cracking can be predicted accurately by using this assumption (Table 3.8, Appendix E).

Research question C 'How does the presence of flexural cracks affect the distribution of principal tensile stresses?'

Related part of dissertation: Section 3.5

It was found that for experiments with flexural cracks, diagonal cracking occurred at higher ratios of $\sigma_{1\max}$ and f_{ctm} than for the experiments without flexural cracks (Table 3.8, Appendix E). The principal tensile stresses are overestimated in the regions without flexural cracks, if these are determined with the Euler-Bernoulli girder theory, when flexural cracks are present. Nevertheless, it was found that diagonal tension cracking can be predicted accurately for girders with flexural cracks by using the approach described above (see answer to research question B).

Research question D 'What are the possible shear failure modes for prestressed girders with stirrups in the regions without flexural cracks and is it possible to relate the shear resistance to the potential failure modes?'

Related part of dissertation: Chapters 6 and 7

When sufficient stirrups are present to prevent instant failure after diagonal tension cracking, two failure modes are possible in regions without flexural cracks. The two failure modes are sliding of the crack and crushing of the compression field, after the stirrups start to yield (Section 6.2.1). Sliding of the crack is predicted as governing failure mode for low concrete strengths (Figure 6.7). Also for high concrete strengths in combination with low values of ψ ($= f_{ywm}\rho_w / f_{cm}$) sliding of the crack is found governing (Figure 6.7). Crushing of compression field is predicted as the governing failure mode for high concrete strength in combination with high values of ψ (Figure 6.7). The shear resistance can be found for both failure modes and the higher resistance is considered to be governing (Section 6.2). However, the difference between the resistances associated

with the two failure modes is found to be limited (Figure 6.7). Therefore, it is proposed to determine the shear resistance using just one set of equations, that covers both failure modes. Theoretically, failure due to crushing of the compression field could also occur without yielding of the stirrups. However, this is only relevant for girders with a very high shear reinforcement ratio. It is unlikely that this will be the case for existing bridges. Nevertheless, an equation for this maximum shear resistance is derived for regions without flexural cracks (Section 8.2).

Research question E 'How does the low longitudinal strain, that is associated with regions without flexural cracks, affect the shear force transfer mechanism along the diagonal tension crack?'

Related part of dissertation: Chapter 5

It was found that the low longitudinal strain results in high contributions of aggregate interlock and stirrups to the shear resistance (Table 5.6). It is noted that the high contributions are considered in the proposed model B1, because the contributions of aggregate interlock and stirrups are derived at a longitudinal strain of zero (Section 6.1 and 6.3).

Research question F 'How can the contribution of the shear force transferred by the uncracked flanges be determined and how is this contribution affected by the cross sectional properties?'

Related part of dissertation: Chapter 7

For regions without flexural cracks, the ratio of the shear transferred by the web and the flange at failure reasonably corresponds to the ratio of the shear transferred by the web and the flange assuming uncracked concrete. The proposed model B1 includes the effects of uncracked concrete in the flanges by the 'effective shear depth', which replaces the height of the web (Section 7.3). This effective shear depth is mainly determined by the relative height of the straight and skew flanges. It was further found that the width of the flanges does not significantly affect the contribution of the uncracked concrete to the shear resistance (Figure 7.10). The scientific conclusions about the shear transfer by the uncracked flanges are already discussed in Section 9.1.2.

9.3 Summary of proposed models and their application conditions

Section 9.3.1 provides an overview of the models for the determination of the shear resistance of prestressed girders and describes a step wise procedure to apply the different models. Section 9.3.2 describes the model to determine the resistance of prestressed girders to diagonal tension cracking. Section 9.3.3 describes the model to determine the shear resistance of prestressed girders with stirrups for regions without flexural cracks after diagonal tension cracking.

9.3.1 Overview shear resistance models for a prestressed girder

This dissertation proposes a model for the shear resistance of girders with stirrups in regions without flexural cracks, referred to as model B1 (Section 8.5, V'_{Rd}). As an example for how to determine the shear resistance for the regions of girders with flexural cracks(V_{Rd}), the equations given by the Eurocode (NEN 2005) are used (for which the partial factors should be applied for a reliability class 2 to achieve $\beta_t = 3.8$ for a 50 year reference period). The equations that are applicable for this combination of models are shown in Figure 9.1 for girders with stirrups. Figure 9.1 also shows the equation proposed to determine the regions with and without flexural cracks (Section 8.1), so it is clear in which region each model is applicable.

This dissertation also proposes a model that can be applied to determine the resistance to diagonal tension cracking of girders without stirrups ($V'_{Rd,c}$, Section 4.3), referred to as model A. This model is applicable for the regions in which $\sigma_{x,Ed} < f_{ctd,fl}$. For the regions (of a girder without stirrups) with flexural cracks, the shear resistance ($V_{Rd,c}$) can be determined with, for example, the equations given by the Eurocode (NEN 2005). The equations that are applicable for this combination of models are shown in Figure 9.2.

For girders that contain nonconforming shear reinforcement (Figure 1.3), it is unknown to what extend the stirrups contribute to the shear resistance. In practice, the shear resistance is usually determined neglecting the contribution of nonconforming shear reinforcement. For that assumption, the models for a girder without stirrups are applicable (Figure 9.2).

For girders that contain (conforming) shear reinforcement (Figure 1.3), the resistance can be determined by using the following step wise procedure:

1. verify whether sufficient shear resistance is present if the resistance models for girders with stirrups are used (Figure 9.1). If this does not result in sufficient shear resistance:
2. neglect the presence of stirrups and verify whether sufficient shear resistance is present if the resistance models for girders without stirrups are used (Figure 9.2). If this also does not result in sufficient shear resistance:
3. verify whether sufficient shear resistance is present in the region with flexural cracks using the resistance model for girders with stirrups (Figure 9.1) and verify whether sufficient shear resistance is present in the region without flexural cracks using the resistance model for girders without stirrups (Figure 9.2).

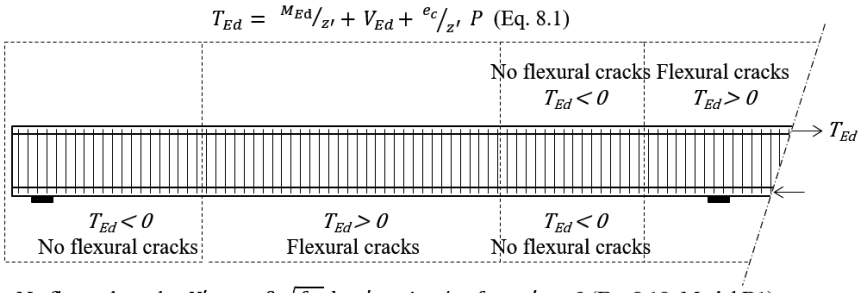

No flexural cracks: $V'_{Rd} = \beta \sqrt{f_{cd}}\, b_w z' + A_{sw}/s\ \ f_{ywd}\, z' \cot\theta$ (Eq. 8.18, Model B1)

β acc. to Eq. 8.19 & 8.20, z' acc. to Eq. 8.9 to 8.11, $\theta = 26°$, $V'_{Rd} \leq V'_{Rd,\max}$ (Eq. 8.5)

Flexural cracks: $V_{Rd,s} = A_{sw}/s\ \ f_{ywd}\, z \cot\theta$ (Eq. 6.8 of Eurocode NEN 2005)

$21.8° \leq \theta \leq 45°$, $V_{Rd,s} \leq V_{Rd,\max}$ (Eq. 6.9 of Eurocode NEN 2005)

Figure 9.1. Model B1 combined with Eurocode model for girders with stirrups[3]

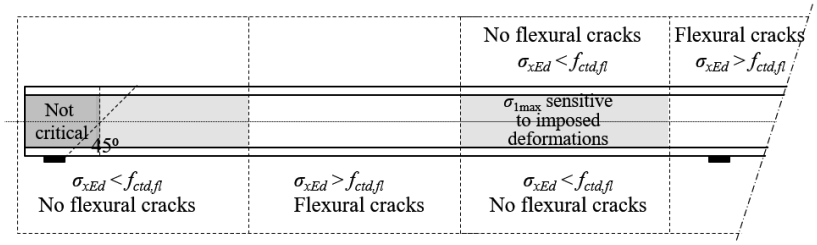

No flexural cracks: $V'_{Rd,c} = \frac{I_c b_w(z)}{S_c(z)} \sqrt{(1.28 f_{ctd})^2 + \sigma_x(z)(1.28 f_{ctd})}$ (Eq. 4.10, Model A)

Flexural cracks: $V_{Rd,c} = \left(C_{Rd,c}\, k\, (100\rho_1 f_{ck})^{\frac{1}{3}} + k_1 \sigma_{cp}\right) b_w d$ (Eq. 6.2a of Eurocode, NEN 2005)

Figure 9.2. Model A combined with Eurocode model for girders without stirrups

Sufficient shear resistance is present if this is demonstrated for all cross sections by one of these steps. Sufficient resistance to diagonal tension cracking should be considered for the whole region without flexural cracks. This is because diagonal tension cracks itself can cause an increase of the principal tensile stresses, leading to new diagonal tension cracks (Section 3.5).

The proposed models are validated for both simply supported and continuously supported girders (Section 3.5 and 8.4.2). Girders without stirrups do not have the possibility to redistribute stresses before failure. Therefore, the failure mode is brittle

[3] Model B2 (Equation 8.25) can be used as an alternative for Model B1. Equation 8.25 is $V_{Rd,s} = A_{sw}/s\ \ f_{ywd}\, z' \cot\theta$, in which θ can be determined from Equations 8.21, 8.23 and 8.24 (Section 8.6).

and these girders could instantly fail at diagonal tension cracking (Section 2.1). Consequently, also the effect of imposed deformations and transverse bending should be considered when determining the maximum principal tensile stress. Especially in the regions around the point of contraflexure on both sides of the mid support, imposed deformations could affect the maximum principal tensile stress (Figure 9.2 '$\sigma_{1\max}$ sensitive to imposed deformations'). For the continuously supported girders it is therefore preferable to only use the model proposed for girders with stirrups (Figure 9.1) to demonstrate sufficient shear resistance. Otherwise, it is less certain that all load effects can be adequately considered when determining the maximum principal tensile stress.

9.3.2 Model A: resistance to diagonal tension cracking

The proposed model, referred to as model A, assumes that diagonal tension cracks form when the maximum principal tensile stress in the web equals the tensile strength of the web. Although potentially some redistribution of stresses can occur before a diagonal tension crack forms, it is not necessary to consider this phenomenon in the proposed model, given the accuracy found.

According to model A, the maximum principal tensile stress $\sigma_{1Ed,\max}$ is determined as follows:

- The Euler-Bernoulli girder theory can be used and the longitudinal stresses and shear stresses can be determined using Equations 4.3 and 4.4. The principal tensile stress can be determined from the longitudinal stresses and shear stresses by Equation 4.2. The effect of vertical stresses on the principal tensile strength can be neglected. The cross-sectional properties of the concrete can be used in Equations 4.3 and 4.4. It is, given the accuracy found, not necessary to consider the effect of the stiffness of the reinforcing steel and prestressing steel to determine the stresses.
- The principal tensile stresses in the entire web area should be considered to determine the maximum principal tensile stress. The accuracy significantly decreases if only the principal tensile stresses along the centroidal axis are considered (Section 3.4).
- Under the condition that the flange opposite to the support remains free of flexural cracks, the maximum principal stress can be accurately determined by considering the principal tensile stresses (determined with Equations 4.2 to 4.4) in the undisturbed areas such as defined in Figures 4.1 and 4.2 (light grey). The principal tensile stresses in the disturbed areas around the supports do not have to be considered.
- The principal tensile stresses in the web area should be considered up to and including the cross-section at the edge of the uncracked region such as defined in Figure 4.2 (light grey). The maximum principal tensile stress in this cross-section is decisive for

whether a diagonal tension crack occurs that is caused by the formation of a flexural crack (Section 3.5).

To achieve a target reliability index β_t of 3.8 for a 50 year reference period, a design value for the tensile strength of the web should be used of $0.599f_{ctm}$ (thus $\sigma_{1Ed,\max} \leq 0.599f_{ctm}$). If the relations $f_{ctk} = 0.7f_{ctm}$, $f_{ctd} = f_{ctk} / \gamma_c$ and $\gamma_c = 1.5$ are used, this could also be written as $\sigma_{1Ed,\max} \leq 1.28f_{ctd}$ (Equation 4.9, see also Figure 9.2). The design value is derived for the model for girders in which flexural cracks are present (Section 3.5). As the design value for the model without flexural cracks (Section 3.4) is just a bit higher ($0.652f_{ctm}$, see Table 4.1), it is proposed to use $1.28f_{ctd}$ regardless of whether flexural cracks are present. Some conservatism is desirable for girder without flexural cracks, to compensate for the less favourable distribution of the shear stresses in bridges, which are loaded with distributed loads, compared to the experiments used to derive the design value, which are loaded with a concentrated load.

If diagonal tension cracking is predicted by a (linear elastic) finite element analysis, bi-axial behaviour should be considered by using the Mohr-Coulomb approximation (Equation 2.7), to prevent an overestimation of the resistance to diagonal tensile cracking (Section 3.1).

9.3.3 Model B1: shear resistance of prestressed girders with stirrups

The proposed model, referred to as model B1, should be applied in combination with the 'equivalent load prestressing method'. This means that the prestress should be considered as part of the load instead of part of the resistance (Section 8.1).

The proposed model is applicable for regions without flexural cracks. A simple method is proposed to determine this region (Section 8.1). The method assumes two longitudinal chords, which can be under compression or tension, at a vertical distance of the internal lever arm. The internal level arm is equated to the effective shear depth and both chords are connected by a compression field (Figure 8.1). The force in the least compressed chord can be determined using Equation 8.1. It is assumed that the region is free of flexural cracks when the force in the least compressed chord is negative. This simple method leads to a conservative prediction of the region without flexural cracks (Figure 8.2).

Model B1 is given by Equations 8.18 to 8.20 (see also Figure 9.1). These equations concern the design value of the model to achieve a target reliability index β_t of 3.8 for a 50 year reference period. The proposed model assumes a diagonal tension crack in the web and describes the shear force that can be transferred by aggregate interlock (first part of Equation 8.18) and stirrups (second part of Equation 8.18). This resistance is further increased with the contribution of the uncracked flanges to the shear transfer.

The contribution of the uncracked concrete is incorporated in Equation 8.20 by using the effective shear depth instead of the height of the cracked web. Model B1 is based on the Modified Compression Field Theory (Section 5.1.3). The shear resistance is based on failure of the web, either by crushing of the concrete compression fields or slipping along the diagonal tension crack (Section 6.2). For both failures modes, the stirrups yield simultaneously.

As shown from Equation 8.19 and 8.20, the aggregate interlock contribution decreases for increasing shear reinforcement ratios, for increasing yielding strengths of the stirrups and for decreasing concrete compressive strengths (Figure 6.8). According to Equations 8.19 and 8.20, the contribution of the aggregate interlock is lower for $f_{cm} \geq 80$ N/mm^2 than for $f_{cm} \geq 60$ N/mm^2. This is because for $f_{cm} \geq 80$ N/mm^2 the cracks are assumed to run through the aggregates, due to the strong paste. Model B1 is intended for girders with $d_{max} = 31.5$ mm. The model should only be used for girders with a centre to centre distance of the stirrups $s \leq 300$ mm. Larger centre to centre distances can cause larger cracking distances which causes wider cracks and reduces the contribution of aggregate interlock. In such a case, the proposed model is still applicable when it can be verified with more refined calculations (Equation 7.4) that the diagonal crack spacing s_θ at mid-depth is less than 300 mm (Section 8.3).

For the cracking angle, a fixed value of 26° is used. This angle belongs to the failure mode crack sliding (Figure 6.9), which is the most likely failure mode for regions without flexural cracks (Figure 6.7). For conditions in which crushing of the compression field is found to be the governing failure mode, lower values for the cracking angle are found. However, for this failure mode, the overestimation of the cracking angle is compensated by an overestimation of the aggregate interlock contribution (Figure 6.7). Therefore, if a cracking angle of 26° is assumed, the prediction of the total resistance along the diagonal tension crack still remains accurate.

For girders with a high shear reinforcement ratio a model is proposed to determine the maximum shear resistance in the region without flexural cracks (Section 8.2). The proposed model for girders with stirrups (Equation 8.18) is intended to determine the shear resistance to crushing of the concrete or to slipping of the crack, after the stirrups start to yield (Section 6.4). However, it is possible that the resistance for these assumed failure mechanisms should be limited because the concrete crushes before the stirrups yield. This maximum resistance (Equation 8.5) limits the shear resistance for model B1 for girders with stirrups (Equation 8.18).

9.4 Implications for the structural assessments of bridges

This section describes the implications of the use of the proposed models for the structural assessments of bridges. Section 9.4.1 describes the implications that apply for both models. Section 9.4.2 describes the implications regarding the proposed model for diagonal tension cracking, model A. Section 9.4.3 describes the implications regarding the proposed model for shear resistance of prestressed girders with stirrups for regions without flexural cracks, model B1.

9.4.1 Implications for both proposed models

The main implication of this research for the assessment of bridges in practice is that models have become available that are capable to accurately determine the shear resistance in regions without flexural cracks.

This dissertation also provides insight into which parameters and conditions significantly affect the accuracy of the shear resistance and should be considered to ensure an accurate determination of the resistance. Accordingly, the study indicates the parameters that affect the accuracy of the shear resistance less significantly. Because these less influential parameters are omitted from the proposed models, the application in engineering practice becomes more simple than models in which these parameters are considered.

Another important result is that design values of the models are derived. This makes it possible to relate the results of assessments to a target level of safety. This is not possible with the currently used models as data about the accuracy of the models is lacking.

As the proposed models are shown to be accurate, these models allow substantiated decisions about whether to maintain, strengthen or replace prestressed bridges and viaducts with a thin web.

Commissioned by RWS, an engineering company assessed 15 bridges using the models for shear resistance as proposed in this dissertation (De Boer 2020). This concerns the 15 bridges for which the shear resistance was insufficient in the regions without flexural cracks according to the current guideline for the assessment of existing structures (Section 1.1, RWS 2013). In these assessments, the resistance to diagonal tension cracking was conservatively determined assuming a reduction of the tensile strength of concrete with 15% because of the sustained loading. By using the newly proposed models it was found possible to demonstrate sufficient shear resistance for 13 of these 15 bridges. For 7 bridges sufficient shear resistance could be demonstrated using the proposed model for diagonal tension cracking, model A (Section 9.3.2). For 6 bridges sufficient shear resistance could be demonstrated using the proposed model for prestressed girders with

stirrups for regions without flexural cracks, model B1 (Section 9.3.3). Chapter 1 indicated that for approximately 75 of the entire group of 540 older bulb-T-girders and precast girders, it will not be possible to demonstrate sufficient shear resistance in the regions without flexural cracks if the current assessment guideline (RWS 2013) is used. Based on the additional assessments, it can be expected, by extrapolation, that by using the proposed models it will be possible to demonstrate sufficient shear resistance for another 65 of these 75 bridges.

9.4.2 Implications for resistance to diagonal tension cracking

The proposed model for diagonal tension cracking, model A, approximately corresponds to the model used in current assessments (Section 1.2, Chapter 2). An important result is that, given the gained insights, the doubts about the applicability of the model can be dispelled.

As model A was found to predict the resistance to diagonal tension cracking fairly accurate, the currently used design value for the tensile strength of the web was found to be too strict. Therefore, the target level of safety can be obtained with an increase of 28% compared to the currently used design value of the concrete tensile strength of the web. As a consequence, it is possible to demonstrate the structural safety of more prestressed bridges by using the proposed model, as found from the additional assessments (De Boer 2020). Especially for the bridges that consist of girders with a low shear reinforcement ratio and a high prestress level. For these conditions, diagonal tension cracking is the governing failure mode as no additional shear force can be resisted after diagonal tension cracking (Figure 8.10).

9.4.3 Implications for girders with stirrups

The proposed model for prestressed girders with stirrups, model B1, concerns a newly developed model for regions without flexural cracks based on the principles as described by Bentz et al. (2006a) and Esfandiari (2009). In contrast to the currently used variable angle truss model (Sections 1.3 and 5.1.1), the proposed model is suitable to predict the shear resistance for regions without flexural cracks and is suitable for all shear reinforcement ratios present in existing bridges. Model B1 is based on the Modified Compression Field Theory and it was not necessary to calibrate the model with experimental data.

As an alternative to model B1, a modified version of the variable angle truss model is derived for regions without flexural cracks, model B2 (Section 8.6). The accuracy of model B2 is about the same as for model B1 (Table 8.3). Nevertheless, model B1 is preferred above model B2 because the physical phenomena ‘aggregate interlock’ and ‘shear transfer by the stirrups in the crack’ are explicitly part of the proposed model, which contributes to a better insight of how the shear force is transferred.

The proposed model B1 is shown to be considerably less conservative than the currently used variable angle truss model (Sections 1.3, 5.1.1 and Table 8.3). In current assessments, also another model is used to determine the shear resistance for regions without flexural cracks, which is actually intended for the regions with flexural cracks (Section 1.3, RWS 2013). This is considered an conservative approach because the shear resistance in regions without flexural cracks is assumed to be higher than in the regions with flexural cracks (Section 1.3). Therefore, it is likely that the currently used model (intended for the regions with flexural cracks) is more conservative for regions without flexural cracks than model B1. This is indeed confirmed with the results of the additional assessments (De Boer 2020). In summary, it can be concluded that it will be possible to demonstrate the structural safety of more prestressed bridges by using model B1. Especially for the bridges that consist of girders with a high shear reinforcement ratio and a low prestress level. For these bridges, additional shear force can be resisted after diagonal tension cracking (Figure 8.10).

9.5 Future research

The following topics are suggested either to further improve the accuracy of the proposed models or to investigate adjacent topics which could contribute to make better substantiated decisions about the structural safety of existing prestressed bridges:

1. For girders with a low shear reinforcement ratio, which is the case for most of the existing bridges in the Dutch Highways (Table 1.1, Table 6.3), the contribution of aggregate interlock to the total shear resistance is significant (Figure 6.11). The aggregate interlock resistance depends on the diagonal crack spacing s_θ (Equation 5.29), which is assumed to be 300 mm for model B1 (Section 6.3). It is suggested to investigate whether the experimentally found diagonal crack spacing can be predicted more accurately and whether explicitly considering the diagonal cracking improves the accuracy of the proposed model.
2. Due to direct load transfer, model B1 is still found to be conservative for lower shear span to effective depth ratios (Figure 8.5). It is suggested to investigate whether this additional resistance can be quantified.
3. Instead of neglecting the contribution of non-conforming stirrups, it is suggested to investigate to what extent the nonconforming stirrups contribute to the shear resistance.
4. Model B1 is derived for regions without flexural cracks. It is suggested to extend this model to regions with flexural cracks using the same approach as used in this dissertation for regions without flexural cracks. Ideally, future study should lead to one

model which is capable of predicting the shear resistance for prestressed girders with stirrups, irrespectively of whether flexural cracks are present.

5. It is suggested to further investigate the uncertainties that are present in real bridges which are not covered by experiments. An overview of these uncertainties and their magnitude will help to substantiate and improve the currently used conversion factors which are used to determine the design value of resistance models.

References

AASHTO 2004	AASTHO, American Association of State Highway and Transportation Officials: LRFD Bridge Design Specifications and commentary, 1st edition, 2004
ACI 2008	ACI Committee 318: Building Code Requirements for Structural Concrete (ACI 318-08) and Commentary, American Concrete Institute, 2008
Arthur 1965	Arthur, P. D.: The shear strength of pre-tensioned I beams with unreinforced webs, Magazine of Concrete Research, Vol. 17, pp.199-210, 1965
Avendano et al. 2008	Avendano, A.R.; Bayrak, O.; Shear Strength and Behavior of Prestressed Concrete Beams, Technical Report: IAC-88-5DD1A003-3, Center for Transportation Research, the University of Texas at Austin, 2008
Bentz 2000	Bentz, E. C.: Sectional Analyses of Reinforced Concrete Members, PhD dissertation, University of Toronto, 2000
Bentz et al. 2001	Bentz, E. C.; Collins, M. P.: Response-2000, Shell-2000, Triax 2000, Membrane-2000, User Manual, 2001
Bentz et al. 2006a	Bentz, E. C.; Collins, M. P.: Development of the 2004 Canadian Standards Association (CSA) A23.3 shear provisions for reinforced concrete, Canadian Journal of Civil Engineering, Vol. 33, pp. 521-534, 2006
Bentz et al. 2006b	Bentz, E. C.; Vecchio, F. J.; Collins, M. P.: Simplified modified compression field theory for calculating shear strength of reinforced concrete elements, ACI Structural Journal, Vol. 103, pp. 614 -624., 2006
Bentz 2019	Bentz, E. C.: Empirical Modelling of Cracking in Reinforced Concrete, ACI Structural Journal, Vol. 116, pp. 233-242., 2019
Bentz 2020	Bentz, E. C.: The size effect in reinforced concrete cracking stress: testing an empirical model, Concrete Structures for Resilient Society: *fib* Symposium Proceedings, 2020, pp. 1037-1044, 2020
Birrcher et al. 2009	Birrcher, D; Tuchscherer , R.; Huizinga, M; Bayrak, O.; Wood, S.; Jirsa, J.O.: Strength and Serviceability Design Reinforced Deep Beams, Report No.0-5253-1; Center for Transportation Research, the University of Texas, 2009

CEN 2020	CEN Comité Européen de Normalisation; Design of concrete structures – Part 1-1: General rules – Rules for buildings, bridges and civil engineering structures, prEN 1992-1-1 D6, Working file, Eurocode, unpubl., 2020
Choulli 2005	Choulli, Y.: Shear behaviour of full-scale prestressed I-beams made with self-compacting concrete, PhD dissertation, Universitat politécnica de Catalunya, 2005
Choulli et al. 2008	Choulli, Y.; Mari, A. R.; Cladera, A.: Shear behaviour of full-scale prestressed i-beams made with self-compacting concrete, Materials and Structures, Vol. 41, pp. 131-141, 2008
Collins et al. 1996	Collins, M. P.; Mitchel, D.; Adebar, P; Vecchio, F.J.: A General Shear Design Method, ACI Structural Journal, Vol. 93, pp. 36-45, 1996.
Collins et al. 1997	Collins, M. P.; Mitchel, D.: Prestressed Concrete, Book, 1997
Collins et al. 2009	Collins, M.P.; Xie, L.; Mihaylow B.I.; Bentz, E.C.: Shear Response of Prestressed Thin-Webbed Continuous Girders, ACI Structural Journal, pp. 447-457, 2009
CSA 2006	CSA: Canadian Highway Bridge Design Code CAN/CSA-S6-06 and commentary, Canadian Standard Association, 2006
De Boer et al. 2016	De Boer, M, Vergoossen, R.P.H.: Quick Scan statisch bepaalde liggerviaducten DR8, Report, Royal HaskoningDHV, 2016
De Boer 2020	De Boer, M.: Impactanalyse dwarskrachtregels, Prefab liggers s.b. en T-liggers, Royal HaskoningDHV, 2020
Dubbeldeman 2009	Dubbeldam, M.: Onderzoek borgen constructieve veiligheid bruggen & viaducten, VROM Inspectie, Ministerie van Volkshuisvesting Ruimtelijke Ordening en Milieubeheer, Research Report, 2009
Elzanaty 1985	Elzanaty A.H.: Shear-critical High-strength concrete beams, Research report, Cornell University, 1985
Elzanaty et al. 1986	Elzanaty, A. H.; Nilson, A. H.; Slate, F. O.: Shear capacity of prestressed concrete beams using high-strength concrete, Journal of the American Concrete Institute, Vol. 83, pp. 359-368, 1986
Esfandiari 2009	Esfandiari, A: Shear strength of structural concrete members using a uniform shear element approach, PhD dissertation, The University of British Columbia, Vancouver, 2009
Esfandiari et al. 2009	Esfandiari, A.; Adebar, P: Shear strength Evaluation of Concrete Bridge Girders, ACI Structural Journal, pp. 416-426, 2009

fib 1993	*fib* Model Code for Concrete Structures 1990, Thomas Telford, 1993
fib 2012	*fib:* Model Code for Concrete Structures 2010, Ernst & Sohn, a Wiley brand, 2012
Gleich et al. 2015	Gleich, P.; Maurer, R.: Investigations into the shear load bearing capacity of a prestressed two-span concrete beam - Findings from a large scale experiment, Concrete - Innovation and Design: *fib* Symposium Proceedings, 2015, pp. 57-58, 2015
Gleich et al. 2016	Gleich, P.; Maurer, R.: An analytical model to determine the shear capacity of prestressed continuous concrete beams, IABSE Congress Stockholm, 2016, pp. 1544-1555, 2016
Gleich et al. 2018	Gleich, P.; Maurer, R.: Bridge Reassessments – Realistic Shear Capacity Evaluation Using Arch Action Model, Proceedings of the 2017 *fib* Symposium, pp. 1822-1831, 2018
Hampel 2006	Hampel, T; Experimentelle Analyse des Tragverhaltens von Hochleistungsbeton unter mehraxialer Beanspruchung, PhD dissertation, Technische Universität Dresden, 2006
Hanson 1964	Hanson, J. M.: Ultimate shear strength of prestressed concrete beams with web reinforcement, PhD dissertation, Lehigh University, 1964
Hanson et al. 1964	Hanson, J. M.; Hulsbosch, C.L.: Ultimate Shear tests of prestressed concrete I-beams under concentrated and uniform loadings, PCI Journal, pp. 15-28, 1964
Hawkins et al. 2007	Hawkins, N.M.; Kuchma, D.A.: Application of LRFD Bridge Design Specifications to High-Strength Structural Concrete Shear Provisions, NCHRP Report 579, Transport Research Board, National Research Council, 2007
Hegger et al. 2015	Hegger, J.; Marzahn, G.; Teworte, F.; Herbrand, M.: Zur Anwendung des Hauptzugspannungskriteriums bei Nachrechnung bestehender Spannbetonbrücken, Beton- und Stahlbau, Vol. 110, pp. 82-95, 2015
Herbrand et al. 2013	Herbrand, M.; Hegger, J.: Experimentelle Untersuchungen zum Einfluss einer extern Vorspannung auf die Querkrafttragfähigkeit vorgespanter Durchlaufträger, Bauingenieur, Vol. 88, pp. 509-517, 2013
Herbrand et al. 2015	Herbrand, M.; Claßen, M.; Hegger, J.: Finite Element Analysis of Post-Tensioned Continuous Prestressed Concrete Beams under Shear Loading, 16th European Bridge Conference in Edinburgh, 2015

Herbrand et al. 2017	Herbrand, M.; Kueres, D.; Claßen, M.; Hegger, J.: Experimental Investigations on the Shear Capacity of Prestressed Concrete Continuous Beams with Rectangular and I-Shaped Cross-Sections, Proceedings of the 2017 *fib* Symposium, pp. 658-666, 2017
Hicks 1958	Hicks, A. B.: The influence of shear span and concrete strength upon the shear resistance of a pre-tensioned prestressed concrete beam, Magazine of Concrete Research, Vol. 10, pp. 115-122, 1958
Hordijk 1991	Hordijk, D.A.: Local Approach to Fatigue of Concrete, PhD dissertation, Delft University of Technology, 1991
Huber 2016	Huber, P.: Assessment of shear strength of existing reinforced and prestressed concrete bridges, PhD dissertation, Technical University of Wien, 2016
Huber et al. 2016a	Huber, P.; Kromoser, B.; Huber; T., Kleiser, M.; Kollegger, J.: Investigation of the shear behavior of RC beams on the basis of measured crack kinematics, Engineering Structures, Vol. 113, pp. 41-58, 2016
Huber et al. 2016b	Huber, P.; Kromoser, B.; Huber; T., Kleiser, M.; Kollegger, J.: Experimentelle Untersuchung zum Querkrafttragverhalten von Spanbetonträgern mit geringen Schubbewehrung, Bauingenieur, Vol. 91, 2016
Huber et al. 2016c	Huber, P.; Kratzer, K.; Huber; T., Kleiser, M.; Kollegger, J.: Rechnerische Beurteilung der Schubtragfähigkeit einer Spannbetonbrücke mit geringem Querkraft bewehrungsgrad, Beton- und Stahlbetonbau, Vol 111, pp. 706-715, 2016
Hussein 1998	Hussein, A. A.: Behaviour of high-strength concrete under bi-axial loading conditions, PhD dissertation, Memorial University of Newfoundland, 1998
JCSS 2002	JCSS, Joint Committee on Structural Safety, Probabilistic Model Code, Part 3: Resistance models, 2002.
Jena et al. 1972	Jena, B.; Pannell, F. N.: The diagonal cracking strength of continuous prestressed concrete beams, Magazine of Concrete Research, Vol. 24, pp. 3-14, 1972
Kamp 2017a	Kamp C.L.: Quick scan T- liggers 2017 / Samenvatting en advies, Report, Movares, 2017
Kamp 2017b	Kamp C.L.: Quick scan T- liggers 2017 / Beoordeling kunstwerken groep A, Report, Movares, 2017
Kamp 2017c	Kamp C.L.: Quick scan T- liggers 2017 / Beoordeling kunstwerken groep B, Report, Movares, 2017

Klatter 2019	Klatter, L.: Prognose rapport V&R, Vervanging en Renovatie, prognose voor de periode 2020 tot en met 2050 , Rijkswaterstaat, 2019
Kraczla 2016	M.J. Kraczla: Analytical and Numerical Analysis of the Shear Tension Critical Prestressed Beams, Master thesis, Delft University of Technology, 2016
Kroeze 2018	Kroeze, S.J.: Resistance to Diagonal Tension Cracking in Prestressed Beams, Master thesis, Delft University of Technology, 2018
Kupfer et al. 1969	Kupfer, H.; Hilsdorf, H. K.; Rusch, H.: Behaviour of concrete under biaxial stresses, ACI Structural Journal, Vol 66, pp. 656-666, 1969
Kupfer 1973	Kupfer, H.: Das Verhalten des Betons unter mehrachsiger Kurzzeitbelastung unter besonderer Berücksichtigung der zweiachsigen Beanspruchung, 1973
Leonhardt et al. 1973	Leonhardt, F.; Koch, R.; Rostásy, S.: Schubversuche an Spannbetonträgern, Deutscher Ausschuss für Stahlbeton, Vol. 227, 1973
Levi et. al. 1993	Levi, F.; Marro, P.; Shear test on HSC prestressed beams – proposals of new interpretative models, conference paper, Conference High Strength Concrete, Lillehammer, pp. 295-305, 1993
Lyngberg 1976	Lyngberg, B.S.: Ultimate shear resistance of partially prestressed concrete I-beams, ACI Structural Journal, pp. 214-221, 1976
MacGregor et al. 1960	MacGregor J.C.; Sozen, M.A.; Siess C.P.: Strength and behavior of prestressed concrete beams with web reinforcement, Research report, University of Illinois, 1960
Mattock et al. 1961	Mattock, A.H.; Kaar, P.H.: Pre-cast-prestressed concrete bridges, 4. Shear test of continuous girdles, Journal of the PCA Research and Development Laboratories, 1961
Muttoni et al. 2013	Muttoni, A.; Ruiz, M.F.: The levels-of-approximation approach in MC2010: application to punching shear provisions, Structural Concrete, pp. 32-41, 2013
Nakamura 2011	Nakamura, E.: Shear database for Prestressed Concrete Members, Master thesis, University of Texas, 2011
NEN 1974	NEN, Nederlands Normalisatie Instituut: Voorschriften Beton 1974, NEN3861, 1974
NEN 2005	NEN, Nederlands Normalisatie Instituut: NEN-EN 1992-1-1 Eurocode 2: Design of concrete structures – Part 1-1: General rules and rules for buildings, Nederlands Normalisatie Instituut, 2005

NEN 2011	NEN, Nederlands Normalisatie Instituut: NEN-EN 1990 Eurocode: Basis of structural design, Nederlands Normalisatie Instituut, 2011
Nielsen et al. 2011	Nielsen, M.P.; Hoang, L.C.: Limit Analyses and Concrete Plasticity, 3rd Edition, CRC Press, Taylor & Francis Group, 2011
Olesen et al. 1967	Olesen, S.O.; Sozen, M.A.; Siess C.P.: Investigation of Prestressed Reinforced Concrete for Highway Bridges, Part IV: Strength in Shear of Beams with Web Reinforcement, Engineering Experiment Station Bulletin 493, Vol. 64, University of Illinois, 1967.
Reineck et al. 2012	Reineck, K.-H.; Fitik D.; Kuchma D.A: Erweiterte Datenbanken zur Überprüfung der Querkraftbemessung für Konstruktionsbauteilen mit und Ohne Bügel, Deutscher Ausschuss für Stahlbeton, Vol. 597, 2012
Rupf 2014	Rupf, M: Querkraftwiderstand von Stahlbeton- und Spannbetonträgern mittels Spannungsfeldern, PhD dissertation, École polytechnique Fédérale de Lausanne, 2014
Rupf et al. 2012	Rupf, M; Muttoni, A.: Schubversuche an vorgespannten Stahlbetonträgern mit ungenügender Schubbewehrung, Research Report, École polytechnique Fédérale de Lausanne, 2012
Rupf et al. 2013	Rupf, M; Ruiz, M.F.; Muttoni, A: Post-tensioned girders with low amounts of hear reinforcement: Shear strength and influence of flanges, Engineering Structures, pp. 357-371, 2013
RWS 2013	Rijkswaterstaat: Richtlijnen beoordelen kunstwerken, RTD1006, RBK1.1, 2013
RWS 2018	Rijkswaterstaat, Roosen, M.A.; Sliedrecht, H.: Areaalbeoordeling bruggen uit T-liggers, Report, Rijkswaterstaat, concept, unpubl., 2018
RWS 2020	Rijkswaterstaat, Hendriks M.A.N.; Roosen M.A.: Guideline for Nonlinear Finite Element Analyses of Concrete Structures, RTD1016, 2020
Sethunarayanan 1960	Sethunarayanan, R.: Ultimate strength of pre-tensioned I beams in combined bending and shear, Magazine of Concrete Research, Vol. 12, pp. 83-90, 1960
Slobbe et al. 2017	A.T. Slobbe, A.J. Bigaj - van Vliet: Validating the guidelines for nonlinear finite element analysis of three prestressed concrete beams - blind predictions, TNO 2017 R11413, TNO report, 2017
Sozen et al. 1959	Sozen, M. A.;. Zwoyer, E.M; Siess, C. P.: Strength in shear of beams without web reinforcement, Research report, University of Illinois, 1959

Sugianto 2019	Sugianto, A.: Numerical Investigation into Size Effect, Master thesis, Delft University of Technology, 2019
Tuitjer 2019	M.P. Tuitjer: Effect of Flexural Cracks on web-shear cracking of prestressed concrete continuous members, Master thesis, Delft University of Technology, 2019
Vecchio et al. 1986	Vecchio F.J.;. Collins, M.P.: The Modified Compression-Field Theory for Reinforced Concrete Elements Subjected to Shear, ACI Journal, Vol. 83, pp. 219-231, 1986
Vecchio et al. 1994	Vecchio, F.J.; Collings, M.P.; Aspiotis J.: High-Strength Concrete Elements Subjected to Shear, ACI Structural Journal, Vol. 91, 1994
Vergeer 2019	M.C. Vergeer: Shear tension resistance of prestressed concrete beams with shear reinforcement, Master thesis, Delft University of Technology, 2019
Verruijt 1987	Verruijt, A.: Toegepaste Mechanica II, Delftse Uitgevers Maatschappij, book, 1987
Walraven 1980	Walraven, J. C.: Aggregate Interlock: A theoretical and experimental analyses, PhD dissertation, Delft University of Technology, 1980.
Walraven 1981	Walraven, J. C.: Fundamental Analyses of Aggregate Interlock, Journal of the Structural Engineering, ASCE, V.107, pp. 2245-2270, 1981.
Walraven 1987	Walraven, J. C.: Shear in prestressed concrete members : a state-of-the-art report, Bulletin d'information, Comité Euro-International du Béton, Vol. 180, 1987
Walraven 2002	Walraven, J. C.: Background document for prENV 1992-1-1: 2002, Report, Delft University of Technology, 2002
Walraven et al. 1995	Walraven, J. C.; Al-zubi, N.: Shear capacity of lightweight concrete beams with shear reinforcement, International Symposium on Structural Lightweight Aggregate Concrete, pp. 91-104, 1995
Walraven et al. 1999	Walraven, J. C.; Stroband, J.: Shear capacity of high strength concrete beams with shear reinforcement, Symposium on Utilization of High Strength/High Performance Concrete, pp. 693-700, 1999
Walraven et al. 2018	Walraven J.C.; C.R. Braam, C.R.: Prestressed Concrete, lecture notes, 2018
Xie 2009	Xie, L: The Influence of Axial Load and Prestress on the Shear Strength of Web-critical Reinforced Concrete Elements, PhD dissertation, University of Toronto, 2009

Yang 2014 Yang, Y: Shear behaviour of Reinforced Concrete Members without Shear Reinforcement, PhD dissertation, Delft University of Technology, 2014

Appendix A

Database on diagonal tension cracking

	Researcher	Experiment	Resistance	Prestress		Prestress level	Geometry			Material
			$V'_{R,c,exp}$	P	σ_{cp}	σ_{cp}/f_{cm}	h	b_w	A	f_{cm}
			kN	kN	N/mm^2	-	mm	mm	mm^2	N/mm^2
1	Elzanaty et al. (1986)	CW1	138	-607	-11.20	-0.15	457	51	54193	76.6
2		CW2	125	-603	-11.13	-0.15	457	51	54193	76.6
3		CW3	117	-596	-11.01	-0.14	457	51	54193	76.6
4		CW4	127	-614	-11.33	-0.14	457	51	54193	78.6
5		CW5	124	-606	-11.18	-0.14	457	51	54193	77.9
6		CW6	112	-455	-8.40	-0.11	457	51	54193	77.9
7		CW7	106	-444	-8.19	-0.11	457	51	54193	77.6
8		CW8	90	-451	-8.33	-0.20	457	51	54193	41.4
9		CW9	101	-447	-8.25	-0.14	457	51	54193	61.0
10		CW10	109	-439	-8.11	-0.11	457	51	54193	73.1
11		CW11	96	-429	-7.91	-0.14	457	51	54193	55.9
12		CW12	85	-431	-7.94	-0.20	457	51	54193	40.0
13		CW13	123	-604	-11.15	-0.15	457	51	54193	72.4
14		CW14	124	-610	-11.26	-0.15	457	51	54193	73.8
15		CW15	101	-433	-7.99	-0.11	457	51	54193	70.3
16		CW16	122	-607	-11.20	-0.15	457	51	54193	73.1
17		CW17	123	-608	-11.22	-0.16	457	51	54193	69.7
18	Choulli (2005)	HAP1E	416	-1859	-9.56	-0.10	750	100	194500	99.2
19		HAP1TE	409	-1859	-9.56	-0.10	750	100	194501	91.2
20		HAP1TW	438	-1859	-9.56	-0.10	750	100	194502	91.2

	Researcher	Experiment	Resistance	Prestress		Prestress level	Geometry			Material
			$V'_{R,c,exp}$	P	σ_{cp}	σ_{cp}/f_{cm}	h	b_w	A	f_{cm}
			kN	kN	N/mm^2	-	mm	mm	mm^2	N/mm^2
21	Choulli (2005)	HAP1TW	359	-1225	-6.30	-0.07	750	100	194503	96.0
22		HCP1TW	421	-1859	-9.56	-0.12	750	100	194504	81.2
23		HCP1TE	502	-1859	-9.56	-0.12	750	100	194505	81.2
24		HCP2TE	463	-1225	-6.30	-0.07	750	100	194506	90.2
25		HAP1W	419	-1859	-9.56	-0.10	750	100	194507	99.2
26		HAP2TW	367	-1225	-6.30	-0.07	750	100	194508	96.0
27		HAP2E	340	-1225	-6.30	-0.07	750	100	194509	96.3
28		HAP2W	361	-1225	-6.30	-0.07	750	100	194510	96.3
29		HCP2TW	404	-1225	-6.30	-0.07	750	100	194511	96.3
30	Hanson (1964)	F-X1A	133	-408	-6.20	-0.14	457	76	65806	45.9
31		F-X1B	126	-408	-6.20	-0.14	457	76	65806	45.9
32		F-1A	146	-411	-6.24	-0.13	457	76	65806	47.0
33		F-1B	150	-411	-6.24	-0.13	457	76	65806	47.0
34		F-2A	151	-384	-5.83	-0.13	457	76	65806	45.2
35		F-2B	133	-384	-5.83	-0.13	457	76	65806	45.2
36		F-3A	138	-390	-5.93	-0.13	457	76	65806	47.2
37		F-3B	125	-390	-5.93	-0.13	457	76	65806	47.2
38		F-4A	149	-421	-6.39	-0.15	457	76	65806	43.7
39		F-4B	142	-421	-6.39	-0.15	457	76	65806	43.7
40		F-5A	124	-387	-5.88	-0.13	457	76	65806	44.2
41		F-5B	124	-387	-5.88	-0.13	457	76	65806	44.2
42		F-7A	129	-417	-6.33	-0.14	457	76	65806	45.7
43		F-7B	125	-417	-6.33	-0.14	457	76	65806	45.7
44		F-8A	120	-407	-6.18	-0.13	457	76	65806	47.4
45		F-8B	120	-407	-6.18	-0.13	457	76	65806	47.4
46		F-10A	120	-399	-6.06	-0.12	457	76	65806	48.6

	Researcher	Experiment	Resistance	Prestress		Prestress level	Geometry			Material
			$V'_{R,c,exp}$	P	σ_{cp}	σ_{cp}/f_{cm}	h	b_w	A	f_{cm}
			kN	kN	N/mm^2	-	mm	mm	mm^2	N/mm^2
47	Hanson (1964)	F-10B	110	-399	-6.06	-0.12	457	76	65806	48.6
48		F-11A	120	-406	-6.17	-0.15	457	76	65806	41.6
49		F-11B	116	-406	-6.17	-0.15	457	76	65806	41.6
50		F-12A	111	-394	-5.99	-0.13	457	76	65806	44.8
51		F-12B	102	-394	-5.99	-0.13	457	76	65806	44.8
52		F-13A	113	-392	-5.96	-0.13	457	76	65806	44.5
53		F-19A	133	-399	-6.07	-0.12	457	76	65806	51.1
55	Xie (2009)	LB2	156	-786	-8.99	-0.14	506	74	87400	63.2
56		LB3	103	-408	-4.69	-0.07	506	72	86980	63.2
57		LB7	80	-255	-3.47	-0.05	506	72	73430	63.5
58		LB8	111	-512	-7.03	-0.11	504	73	72780	63.5
59		LB10	138	-822	-11.16	-0.18	506	74	73670	62.3
60		LB11	144	-809	-10.97	-0.18	506	74	73740	62.3
61	Leonhardt et al. (1973)	TP2	294	-1912	-5.62	-0.23	970	150	340500	24.0
62		TP4	255	-1871	-6.46	-0.14	900	80	289750	46.6
63	Rupf et al. (2013)	SR21	321	-749	-2.40	-0.08	780	150	312000	30.8
64		SR22	311	-743	-2.38	-0.07	780	150	312000	33.7
65		SR23	307	-764	-2.45	-0.07	780	150	312000	35.3
66		SR24	292	-743	-2.38	-0.08	780	150	312000	31.3
67		SR25	432	-1476	-4.73	-0.14	780	150	312000	33.1
68		SR26	420	-1504	-4.82	-0.13	780	150	312000	36.9
69		SR29	277	-736	-2.36	-0.08	780	150	312000	29.8
70		SR30	289	-711	-2.28	-0.07	780	150	312000	31.4

Appendix B

Categorization of experiments on whether flexural cracks are present

	Researcher	ID	f_{cm}	f_{ctm}	$f_{ctm,fl}$	$V'_{R,c,exp}$	σ_x at loaded cross-section	$\sigma_x/f_{ctm,fl}$	Flexural cracks observed?	Categorization
			N/mm^2	N/mm^2	N/mm^2	N	N/mm^2	-		
1	Elzanaty et al. (1986)	CW1	76.6	4.58	5.23	138	0.00	0.00	Unknown	No flexural cracks
2		CW2	76.6	4.58	5.23	125	3.61	0.69	Unknown	No flexural cracks
3		CW3	76.6	4.58	5.23	117	10.96	2.10	Unknown	Flexural cracks present
4		CW4	78.6	4.63	5.29	127	3.77	0.71	Unknown	No flexural cracks
5		CW5	77.9	4.61	5.27	124	3.40	0.65	Unknown	No flexural cracks
6		CW6	77.9	4.61	5.27	112	6.80	1.29	Yes	Flexural cracks present
7		CW7	77.6	4.60	5.26	106	5.88	1.12	Unknown	Flexural cracks present
8		CW8	41.4	3.35	3.83	90	2.04	0.53	Unknown	No flexural cracks
9		CW9	61.0	4.16	4.75	101	4.67	0.98	Unknown	Unknown
10		CW10	73.1	4.49	5.13	109	6.96	1.36	Yes	Flexural cracks present
11		CW11	55.9	4.00	4.57	96	4.51	0.99	Yes	Unknown
12		CW12	40.0	3.27	3.74	85	2.15	0.58	Yes	Unknown
13		CW13	72.4	4.47	5.11	123	3.54	0.69	No	No flexural cracks
14		CW14	73.8	4.51	5.15	124	3.49	0.68	No	No flexural cracks
15		CW15	70.3	4.42	5.05	101	5.44	1.08	Yes	Flexural cracks present
16		CW16	73.1	4.49	5.13	122	3.33	0.65	No	No flexural cracks
17		CW17	69.7	4.40	5.03	123	3.48	0.69	No	No flexural cracks
18	Choulli (2005)	HAP1E	99.2	5.07	5.07	416	2.26	0.45	No	No flexural cracks
19		HAP1TE	91.2	4.91	4.91	409	1.87	0.38	No	No flexural cracks
20		HAP1TW	91.2	4.91	4.91	438	2.89	0.59	Yes	Unknown
21		HAP2TE	96.0	5.00	5.00	359	7.25	1.45	Yes	Flexural cracks present

	Researcher	ID	f_{cm}	f_{ctm}	$f_{ctm,fl}$	$V'_{R,c,exp}$	σ_x at loaded cross-section	$\sigma_x/f_{ctm,fl}$	Flexural cracks observed?	Categorization
			N/mm^2	N/mm^2	N/mm^2	N	N/mm^2	-		
22	Choulli (2005)	HCP1TW	81.2	4.69	4.69	421	2.24	0.48	Yes	Unknown
23		HCP1TE	81.2	4.69	4.69	502	7.11	1.52	Yes	Flexural cracks present
24		HCP2TE	90.2	4.89	4.89	463	13.10	2.68	Yes	Flexural cracks present
25		HAP1W	99.2	5.07	5.07	419	1.82	0.36	No	No flexural cracks
26		HAP2TW	96.0	5.00	5.00	367	7.09	1.42	Yes	Flexural cracks present
27		HAP2E	96.3	5.01	5.01	340	6.18	1.23	No	Unknown
28		HAP2W	96.3	5.01	5.01	361	6.75	1.35	No	Unknown
29		HCP2TW	96.3	5.01	5.01	404	9.18	1.83	No	Unknown
30	Hanson (1964)	F-X1A	45.9	3.62	4.13	133	9.70	2.35	Yes	Flexural cracks present
31		F-X1B	45.9	3.62	4.13	126	8.47	2.05	Yes	Flexural cracks present
32		F-1A	47.0	3.68	4.21	146	2.10	0.50	No	No flexural cracks
33		F-1B	47.0	3.68	4.21	150	2.53	0.60	No	No flexural cracks
34		F-2A	45.2	3.58	4.09	151	9.15	2.24	Yes	Flexural cracks present
35		F-2B	45.2	3.58	4.09	133	6.57	1.61	Yes	Flexural cracks present
36		F-3A	47.2	3.69	4.22	138	7.03	1.67	Yes	Flexural cracks present
37		F-3B	47.2	3.69	4.22	125	5.10	1.21	Yes	Flexural cracks present
38		F-4B	43.7	3.49	3.99	142	11.86	2.97	Yes	Flexural cracks present
39		F-5A	44.2	3.52	4.02	124	9.75	2.42	Yes	Flexural cracks present
40		F-5B	44.2	3.52	4.02	124	9.75	2.42	Yes	Flexural cracks present
41		F-19A	51.1	3.91	4.47	133	6.19	1.38	No	Unknown
42	Xie (2009)	LB2	63.2	4.22	4.62	156	6.72	1.46	Yes	Flexural cracks present
43		LB3	63.2	4.22	4.62	103	5.92	1.28	Yes	Flexural cracks present
44		LB7	63.5	4.23	4.63	80	6.38	1.38	Yes	Flexural cracks present
45		LB8	63.5	4.23	4.63	111	6.46	1.40	Yes	Flexural cracks present
46		LB10	62.3	4.19	4.59	138	5.16	1.12	No	Unknown
47		LB11	62.3	4.19	4.59	144	5.88	1.28	No	Unknown

	Researcher	ID	f_{cm}	f_{ctm}	$f_{ctm,fl}$	$V'_{R,c,exp}$	σ_x at loaded cross-section	$\sigma_x/f_{ctm,fl}$	Flexural cracks observed?	Categorization
			N/mm^2	N/mm^2	N/mm^2	N	N/mm^2	-		
48	Hanson (1964)	F-4A	43.7	3.49	3.99	149	8.94	2.24	Yes	Flexural cracks present
49		F-7A	45.7	3.60	4.12	129	14.47	3.51	Yes	Flexural cracks present
50		F-7B	45.7	3.60	4.12	125	13.41	3.25	Yes	Flexural cracks present
51		F-8A	47.4	3.71	4.24	120	12.82	3.03	Yes	Flexural cracks present
52		F-8B	47.4	3.71	4.24	120	12.82	3.03	Yes	Flexural cracks present
53		F-10A	48.6	3.77	4.31	120	17.26	4.00	Yes	Flexural cracks present
54		F-10B	48.6	3.77	4.31	110	14.81	3.43	Yes	Flexural cracks present
55		F-11A	41.6	3.37	3.85	120	13.56	3.52	Yes	Flexural cracks present
56		F-11B	41.6	3.37	3.85	116	16.84	4.38	Yes	Flexural cracks present
57		F-12A	44.8	3.56	4.07	111	19.62	4.83	Yes	Flexural cracks present
58		F-12B	44.8	3.56	4.07	102	17.04	4.19	Yes	Flexural cracks present
59		F-13A	44.5	3.54	4.04	113	16.70	4.13	Yes	Flexural cracks present
60		F-19B	51.1	3.91	4.47	143	12.94	2.89	Yes	Flexural cracks present
61	Leonhardt et al. (1973)	TP2	24.0	2.21	2.21	294	0.00	0.00	No	No flexural cracks
62		TP4	46.6	3.66	3.66	255	0.00	0.00	No	No flexural cracks
63	Rupf et al. (2013)	SR21	30.8	2.69	2.69	321	5.37	2.00	Yes	Flexural cracks present
64		SR22	33.7	2.88	2.88	311	5.06	1.76	Yes	Flexural cracks present
65		SR23	35.3	2.98	2.98	307	4.72	1.58	Yes	Flexural cracks present
66		SR24	31.3	2.72	2.72	292	4.37	1.61	Yes	Flexural cracks present
67		SR25	33.1	2.84	2.84	432	4.20	1.48	Yes	Flexural cracks present
68		SR26	36.9	3.08	3.08	420	3.53	1.15	Yes	Flexural cracks present
69		SR29	29.8	2.62	2.62	277	3.88	1.48	Yes	Flexural cracks present
70		SR30	31.4	2.73	2.73	289	5.61	2.06	Yes	Flexural cracks present

Appendix C

Ratio of σ_{1max} and f_{ctm} for experiments without flexural cracks

	Researcher	ID	f_{ctm}	$V'_{R,c,exp}$	Linear elastic FEM Maximum σ_1		Equations 3.1, 3.2, 3.4 Maximum σ_1 in web		Equations 3.1, 3.2, 3.4 Maximum σ_1 along the centroidal axis		
					σ_{1max}	σ_{1max}/f_{ctm}	σ_{1max}	σ_{1max}/f_{ctm}	σ_{1max}	σ_{1max}/f_{ctm}	σ_{1max} (Eq.3.1, 3.2 & 3.4) / σ_{1max} (LEFEM)
			N/mm²	N	N/mm²	-	N/mm²	-	N/mm²	-	-
1	Elzanaty et al. (1986)	CW1	4.58	138	4.36	0.95	4.40	0.96	4.17	0.91	1.01
2		CW2	4.58	125	3.76	0.82	4.04	0.88	3.55	0.78	1.07
3		CW4	4.63	127	3.80	0.82	4.14	0.90	3.63	0.78	1.09
4		CW5	4.61	124	3.68	0.80	3.98	0.86	3.52	0.76	1.08
5		CW8	3.35	90	2.65	0.79	2.81	0.84	2.53	0.75	1.06
6		CW13	4.47	123	3.64	0.81	3.95	0.88	3.47	0.78	1.09
7		CW14	4.51	124	3.66	0.81	3.97	0.88	3.49	0.77	1.08
8		CW16	4.49	122	3.62	0.81	3.90	0.87	3.44	0.77	1.08
9		CW17	4.40	123	3.65	0.83	3.95	0.90	3.48	0.79	1.08
10	Choulli (2005)	HAP1E	5.07	418	4.19	0.83	4.33	0.85	3.99	0.79	1.04
11		HAP1TE	4.91	411	4.09	0.83	4.24	0.86	3.89	0.79	1.04
12		HAP1W	5.07	415	4.02	0.79	4.23	0.83	3.88	0.77	1.04
13	Hanson (1964)	F-1A	3.68	146	3.38	0.92	3.42	0.93	3.39	0.92	1.01
14		F-1B	3.68	150	3.51	0.95	3.53	0.96	3.53	0.96	1.00
15	Leonhardt et al. (1973)	TP2	2.21	294	n/a	n/a	1.79	0.81	1.21	0.55	n/a
16		TP4	3.66	255	n/a	n/a	3.53	0.96	2.61	0.71	n/a
	Mean (experiments 1-14)					0.84					1.06
	Mean (experiments 1-14)					6.7%					2.9%
	Mean (experiments 1-16)							0.89		0.79	
	Mean (experiments 1-16)							5.2%		11.8%	

Appendix D

Ratio of σ_{1max} and f_{ctm} for experiments considering bi-axial behaviour and statistical size effect

	Researcher	ID	f_{cm}	f_{ctm}	Linear elastic FEM $\sigma_{1max}/f_{ctm,eff}$			Explored model for bi-axial behaviour and statistical size effect						
					Uniaxial	Mohr-Coulomb Approximation	Huber	σ_{2m}	$1+\sigma_2/f_{cm}$	$l_{\sigma 1}$	$(750/l_{\sigma 1})^{1/4}$	$f_{ctm(Eq3.10)}$	σ_{1m}	σ_{1m} / $f_{ctm(Eq3.10)}$
					Equations 3.6 and 3.7	Equation 2.7	Equation 2.8	Equation 3.10						
			N/mm²	N/mm²	-			N/mm²	-	mm	-	N/mm²	N/mm²	-
1	Elzanaty et al. (1986)	CW1	76.6	4.58	0.95	1.18	1.50	-15.73	0.79	410	1.16	4.23	4.35	1.03
2		CW2	76.6	4.58	0.82	1.02	1.29	-15.30	0.80	750	1.00	3.66	3.72	1.02
3		CW4	78.6	4.63	0.82	1.03	1.32	-15.91	0.80	740	1.00	3.70	3.73	1.01
4		CW5	77.9	4.61	0.80	0.99	1.26	-15.67	0.80	710	1.01	3.73	3.62	0.97
5		CW8	41.4	3.35	0.79	1.07	1.05	-11.54	0.72	680	1.02	2.59	2.57	0.99
6		CW13	72.4	4.47	0.81	1.01	1.25	-15.51	0.79	740	1.00	3.53	3.57	1.01
7		CW14	73.8	4.51	0.81	1.02	1.27	-15.63	0.79	740	1.00	3.56	3.60	1.01
8		CW16	73.1	4.49	0.81	1.00	1.24	-15.53	0.79	730	1.01	3.56	3.54	0.99
9		CW17	69.7	4.40	0.83	1.03	1.24	-15.57	0.78	740	1.00	3.43	3.59	1.05
10	Choulli (2005)	HAP1E	99.2	5.07	0.83	0.95	1.39	-13.71	0.86	1100	0.91	3.97	3.99	1.01
11		HAP1TE	91.2	4.91	0.83	0.97	1.35	-13.79	0.85	1075	0.91	3.81	3.87	1.02
12		HAP1W	99.2	5.07	0.79	0.91	1.33	-13.75	0.86	1075	0.91	3.99	3.81	0.96
13	Hanson (1964)	F-1A	47.0	3.68	0.92	n/a	n/a	-9.69	0.79	270	1.29	3.37	3.36	1.00
14		F-1B	47.0	3.68	0.95	n/a	n/a	-9.81	0.79	400	1.17	3.41	3.50	1.03
	Mean (experiments 1-12)				0.83	1.01	1.29							1.00
	CoV (experiments 1-12)				5.2%	6.7%	8.2%							2.5%
	Mean (experiments 1-14)				0.84	n/a	n/a							1.01
	CoV (experiments 1-14)				6.7%	n/a	n/a							2.3%

Appendix E

Type of diagonal tension cracking and statistical properties for σ_{1max}/f_{ctm}

	Researcher	ID	Categorization					f_{cm}	f_{ctm}	σ_{1max}	σ_{1max}/f_{ctm}	$\ln(\sigma_{1max}/f_{ctm})$
			Flexural cracks Present?	Diagonal tension Cracks caused by flexural crack?	Based on observation	Based on calculation	Categorization Type of crack-ing					
								N/mm^2	N/mm^2	N/mm^2	-	-
1	Elzanaty	CW1	no	n/a	n/a	n/a	Type a	76.6	4.58	4.40	0.96	-0.04
2	Elzanaty	CW2	no	n/a	n/a	n/a	Type a	76.6	4.58	4.04	0.88	-0.12
3	Elzanaty	CW4	no	n/a	n/a	n/a	Type a	78.6	4.63	4.14	0.90	-0.11
4	Elzanaty	CW5	no	n/a	n/a	n/a	Type a	77.9	4.61	3.98	0.86	-0.15
5	Elzanaty	CW8	no	n/a	n/a	n/a	Type a	41.4	3.35	2.81	0.84	-0.18
6	Elzanaty	CW13	no	n/a	n/a	n/a	Type a	72.4	4.47	3.95	0.88	-0.12
7	Elzanaty	CW14	no	n/a	n/a	n/a	Type a	73.8	4.51	3.97	0.88	-0.13
8	Elzanaty	CW16	no	n/a	n/a	n/a	Type a	73.1	4.49	3.90	0.87	-0.14
9	Elzanaty	CW17	no	n/a	n/a	n/a	Type a	69.7	4.40	3.95	0.90	-0.11
10	Choulli	HAP1E	no	n/a	n/a	n/a	Type a	99.2	5.07	4.33	0.85	-0.16
11	Choulli	HAP1TE	no	n/a	n/a	n/a	Type a	91.2	4.91	4.24	0.86	-0.15
12	Choulli	HAP1W	no	n/a	n/a	n/a	Type a	99.2	5.07	4.23	0.83	-0.18
13	Hanson	F-1A	no	n/a	n/a	n/a	Type a	47.0	3.68	3.42	0.93	-0.08
14	Hanson	F-1B	no	n/a	n/a	n/a	Type a	47.0	3.68	3.53	0.96	-0.04
15	Leonhardt	TP2	no	n/a	n/a	n/a	Type a	24.0	2.21	1.79	0.81	-0.21
16	Leonhardt	TP4	no	n/a	n/a	n/a	Type a	46.6	3.66	3.53	0.97	-0.03
17	Elzanaty	CW3	yes	no	yes	yes	Type b	76.6	4.58	4.90	1.07	0.07
18	Elzanaty	CW6	yes	no	yes	yes	Type b	77.9	4.61	5.19	1.13	0.12
19	Elzanaty	CW7	yes	no	yes	yes	Type b	77.6	4.60	4.90	1.07	0.06
20	Hanson	F-X1A	yes	no	yes	yes	Type b	45.9	3.62	4.05	1.12	0.11

	Researcher	ID	Categorization					f_{cm}	f_{ctm}	σ_{1max}	σ_{1max}/f_{ctm}	$\ln(\sigma_{1max}/f_{ctm})$
			Flexural cracks Present?	Diagonal tension Cracks caused by flexural crack?	Based on observation	Based on calculation	Categorization Type of crack-ing					
								N/mm^2	N/mm^2	N/mm^2	-	-
21	Hanson	F-X1B	yes	no	yes	yes	Type b	45.9	3.62	3.80	1.05	0.05
22	Hanson	F-2A	yes	no	yes	yes	Type b	45.2	3.58	4.75	1.33	0.28
23	Hanson	F-2B	yes	no	yes	yes	Type b	45.2	3.58	4.12	1.15	0.14
24	Hanson	F-3A	yes	no	yes	yes	Type b	47.2	3.69	4.28	1.16	0.15
25	Hanson	F-3B	yes	no	yes	yes	Type b	47.2	3.69	3.81	1.03	0.03
26	Hanson	F-4B	yes	no	yes	yes	Type b	43.7	3.49	4.29	1.23	0.21
27	Hanson	F-5A	yes	no	yes	yes	Type b	44.2	3.52	3.79	1.08	0.07
28	Hanson	F-5B	yes	no	yes	yes	Type b	44.2	3.52	3.79	1.08	0.07
29	Xie	LB2	yes	yes	yes	yes	Type c	63.2	4.22	4.40	1.04	0.04
30	Xie	LB3	yes	yes	yes	yes	Type c	63.2	4.22	3.69	0.88	-0.13
31	Xie	LB7	yes	yes	yes	yes	Type c	63.5	4.23	3.67	0.87	-0.14
32	Xie	LB8	yes	yes	yes	yes	Type c	63.5	4.23	3.76	0.89	-0.12
33	Hanson	F-4A	yes	yes	yes	yes	Type c	43.7	3.49	4.44	1.27	0.24
34	Hanson	F-7A	yes	yes	yes	yes	Type c	45.7	3.60	3.89	1.08	0.08
35	Hanson	F-7B	yes	yes	yes	yes	Type c	45.7	3.60	3.72	1.03	0.03
36	Hanson	F-8A	yes	yes	yes	yes	Type c	47.4	3.71	3.63	0.98	-0.02
37	Hanson	F-8B	yes	yes	yes	yes	Type c	47.4	3.71	3.63	0.98	-0.02
38	Hanson	F-10A	yes	yes	yes	yes	Type c	48.6	3.77	3.65	0.97	-0.03
39	Hanson	F-10B	yes	yes	yes	yes	Type c	48.6	3.77	3.30	0.88	-0.13
40	Hanson	F-11A	yes	yes	yes	yes	Type c	41.6	3.37	3.64	1.08	0.08
41	Hanson	F-11B	yes	yes	yes	yes	Type c	41.6	3.37	3.48	1.04	0.03
42	Hanson	F-12A	yes	yes	yes	yes	Type c	44.8	3.56	3.35	0.94	-0.06
43	Hanson	F-12B	yes	yes	yes	yes	Type c	44.8	3.56	3.03	0.85	-0.16
44	Hanson	F-13A	yes	yes	yes	yes	Type c	44.5	3.54	3.48	0.98	-0.02

	Researcher	ID	Categorization					f_{cm}	f_{ctm}	$\sigma_{1\max}$	$\sigma_{1\max}/f_{ctm}$	$\ln(\sigma_{1max}/f_{ctm})$
			Flexural cracks Present?	Diagonal tension Cracks caused by flexural crack?	Based on observation	Based on calculation	Categorization Type of crack-ing					
								N/mm^2	N/mm^2	N/mm^2	-	-
45	Hanson	F-19B	yes	yes	yes	yes	Type c	51.1	3.91	4.44	1.13	0.13
46	Rupf	SR21	yes	yes	yes	yes	Type c	30.8	2.69	2.65	0.99	-0.01
47	Rupf	SR22	yes	yes	yes	yes	Type c	33.7	2.88	2.65	0.92	-0.08
48	Rupf	SR23	yes	yes	yes	yes	Type c	35.3	2.98	2.59	0.87	-0.14
49	Rupf	SR24	yes	yes	yes	yes	Type c	31.3	2.72	2.41	0.89	-0.12
50	Rupf	SR25	yes	yes	yes	yes	Type c	33.1	2.84	2.61	0.92	-0.08
51	Rupf	SR26	yes	yes	yes	yes	Type c	36.9	3.08	2.53	0.82	-0.20
52	Rupf	SR29	yes	yes	yes	yes	Type c	29.8	2.62	2.25	0.86	-0.15
53	Rupf	SR30	yes	yes	yes	yes	Type c	31.4	2.73	2.45	0.90	-0.11
54	Elzanaty	CW9	unknown	n/a	n/a	n/a	unknown	61.0	4.16	3.65	0.88	-0.13
55	Elzanaty	CW10	yes	unknown	n/a	n/a	unknown	73.1	4.49	5.03	1.12	0.11
56	Elzanaty	CW11	unknown	n/a	n/a	n/a	unknown	55.9	4.00	3.46	0.87	-0.14
57	Elzanaty	CW12	unknown	n/a	n/a	n/a	unknown	40.0	3.27	2.70	0.82	-0.19
58	Elzanaty	CW15	yes	unknown	n/a	n/a	unknown	70.3	4.42	4.62	1.05	0.04
59	Choulli	HAP1TW	unknown	n/a	n/a	n/a	unknown	91.2	4.91	4.49	0.91	-0.09
60	Choulli	HAP2TE	yes	unknown	n/a	n/a	unknown	96.0	5.00	5.47	1.09	0.09
61	Choulli	HCP1TW	unknown	n/a	n/a	n/a	unknown	81.2	4.69	4.33	0.92	-0.08
62	Choulli	HCP1TE	yes	unknown	n/a	n/a	unknown	81.2	4.69	6.88	1.47	0.38
63	Choulli	HCP2TE	yes	unknown	n/a	n/a	unknown	90.2	4.89	7.08	1.45	0.37
64	Choulli	HAP2TW	yes	unknown	n/a	n/a	unknown	96.0	5.00	5.42	1.08	0.08
65	Choulli	HAP2E	unknown	n/a	n/a	n/a	unknown	96.3	5.01	5.18	1.03	0.03
66	Choulli	HAP2W	unknown	n/a	n/a	n/a	unknown	96.3	5.01	5.33	1.06	0.06
67	Choulli	HCP2TW	unknown	n/a	n/a	n/a	unknown	96.3	5.01	5.98	1.19	0.18
68	Hanson	F-19A	unknown	n/a	n/a	n/a	unknown	51.1	3.91	3.54	0.91	-0.10

	Researcher	ID	Categorization					f_{cm}	f_{ctm}	$\sigma_{1\max}$	$\sigma_{1\max}/f_{ctm}$	$\ln(\sigma_{1max}/f_{ctm})$
			Flexural cracks Present?	Diagonal tension Cracks caused by flexural crack?	Based on observation	Based on calculation	Categorization Type of crack-ing					
								N/mm²	N/mm²	N/mm²	-	-
69	Xie	LB10	unknown	n/a	n/a	n/a	unknown	62.3	4.19	3.72	0.89	-0.12
70	Xie	LB11	unknown	n/a	n/a	n/a	unknown	62.3	4.19	3.92	0.93	-0.07
Mean (Experiments 1 – 16)											0.89	$\sum \ln(\sigma_{1max}/f_{ctm}) = -1.94$
CoV (Experiments 1 – 16)											5.2%	
Mean (Experiments 17 – 28)											1.12	$\sum \ln(\sigma_{1max}/f_{ctm}) = 1.37$
CoV (Experiments 17 - 28)											7.6%	
Mean (Experiments 29 – 53)											0.96	$\sum \ln(\sigma_{1max}/f_{ctm}) = -1.10$
CoV (Experiments 29 - 53)											10.9%	
Mean (Experiments 17 – 53)											1.01	$\sum \ln(\sigma_{1max}/f_{ctm}) = 0.26$
CoV (Experiments 17 - 53)											12.3%	
Mean (Experiments 1 – 70)											0.99	$\sum \ln(\sigma_{1max}/f_{ctm}) = 0.26$
CoV (Experiments 1 - 70)											14.4%	

Appendix F

Database on shear failure of prestressed girders with stirrups

Researcher	Experiment	Resistance		Prestress	Geometry										Materials		
		$V'_{R,c,exp}$	V'_{Rexp}	P	h	A_p	d_p	A_s	d_s	b_w	A_c	A_{sw}	s	a	f_{ywm}	f_{cm}	d_{max}
		kN	kN	kN	mm	mm^2	mm	mm^2	mm	mm	mm^2	mm^2	mm	*mm*	N/mm^2	N/mm^2	mm
Elzanaty et al. (1986)	CW10	109	173	-439	457	568	362	214	426	50.8	54193	71.3	254	1356	434	73.1	13
	CW11	96	157	-429	457	568	362	214	426	50.8	54193	71.3	254	1356	434	55.9	13
	CW12	85	141	-431	457	568	362	214	426	50.8	54193	71.3	254	1356	434	40.0	13
	CW13	123	182	-604	457	568	362	214	426	50.8	54193	71.3	254	1356	434	72.4	13
	CW14	124	188	-610	457	568	362	0	426	50.8	54193	71.3	178	1356	434	73.8	13
	CW15	101	150	-433	457	395	362	214	426	50.8	54193	71.3	254	1356	434	70.3	13
	CW16	122	187	-607	457	568	362	1164	419	50.8	54193	71.3	254	1356	434	73.1	13
	CW17	123	142	-608	457	568	362	214	426	50.8	54193	31.7	254	1356	379	69.7	13
Choulli (2005)	HCP2TE	463	723	-1225	750	792	700	0	-	100	194500	100.5	200	2100	525	90.2	12
	HCP2TW	404	679	-1225	750	792	700	0	-	100	194500	100.5	200	2100	525	90.2	12
	HAP2TW	367	601	-1225	750	792	700	0	-	100	194500	100.5	200	2100	525	96.0	12
	HCP1TE	502	781	-1859	750	1386	671	0	-	100	194500	100.5	200	2100	525	81.2	12
	HCP1TW	421	737	-1859	750	1386	671	0	-	100	194500	100.5	200	2100	525	81.2	12
	HAP1TE	409	634	-1859	750	1386	671	0	-	100	194500	100.5	200	2100	525	91.2	12
	HAP1TW	438	745	-1859	750	1386	671	0	-	100	194500	100.5	200	2100	525	91.2	12
Hanson (1964)	FX1A	133	167	-408	457	359	401	0	-	76.2	65806	31.7	203	1219	410	45.9	19
	FX1B	126	142	-408	457	359	401	0	-	76.2	65806	31.7	203	1219	410	45.9	19
	F1A	146	286	-411	457	359	401	0	-	76.2	65806	71.3	127	762	360	47.0	19
	F1B	150	267	-411	457	359	401	0	-	76.2	65806	31.7	127	762	410	47.0	19
	F2A	151	214	-384	457	359	401	0	-	76.2	65806	71.3	127	1016	360	45.2	19
	F2B	133	178	-384	457	359	401	0	-	76.2	65806	31.7	203	1016	410	45.2	19
	F3A	138	224	-390	457	359	401	0	-	76.2	65806	71.3	169	1016	360	47.2	19

Researcher	Experiment	Resistance		Prestress	Geometry										Materials		
		$V'_{R,c,exp}$	V'_{Rexp}	P	h	A_p	d_p	A_s	d_s	b_w	A_c	A_{sw}	s	a	f_{ywm}	f_{cm}	d_{max}
		kN	kN	kN	mm	mm²	mm	mm²	mm	mm	mm²	mm²	mm	*mm*	N/mm²	N/mm²	mm
Hanson (1964)	F3B	125	178	-390	457	359	401	0	-	76.2	65806	17.8	102	1016	298	47.2	19
	F4B	142	169	-421	457	359	401	0	-	76.2	65806	31.7	212	1270	410	43.7	19
	F5A	124	179	-387	457	359	401	0	-	76.2	65806	31.7	127	1270	410	44.2	19
	F5B	124	143	-387	457	359	401	0	-	76.2	65806	17.8	106	1270	298	44.2	19
Leonhardt et al. (1973)	ŢP2	294	746	-1912	970	2801	825	302	895	150	347800	157	150	3250	423	24.0	15
	ŢP4	255	883	-1870	900	2801	825	302	825	80	295800	157	85	3250	423	47	15
Rupf et al. (2013)	SR21	N/A	285	-749	780	600	645	4279	738	150	312000	28.3	220	4800	585	30.8	16
	SR22	N/A	346	-743	780	600	645	4279	738	150	312000	56.5	300	4800	585	33.7	16
	SR23	N/A	248	-764	780	600	645	4279	738	150	312000	28.3	300	4800	585	35.3	16
	SR24	N/A	466	-743	780	600	645	4279	738	150	312000	56.5	150	4800	575	31.3	16
	SR25	N/A	297	-1476	780	1200	606	3223	734	150	312000	28.3	220	4800	585	33.1	16
	SR26	N/A	266	-1504	780	1200	606	3223	734	150	312000	28.3	300	4800	585	36.9	16
	SR27	N/A	414	-1513	780	1200	606	3223	734	150	312000	56.5	200	4800	575	28.3	16
	SR29	N/A	473	-736	780	600	645	4279	738	150	312000	56.5	150	4800	575	29.8	16
	SR30	N/A	473	-711	780	600	647	1847	730	150	312000	56.5	150	4800	585	31.4	16
Mattock et al. (1961)	S1	252	668	-778	648	46	527	1330	606	88.9	90242	63.3	64	609.6	341	45.7	19
	S2	186	483	-778	648	46	527	1330	606	88.9	90242	63.3	64	1219	341	45.4	19
	S3	169	603	-778	648	46	527	1330	606	88.9	90242	63.3	64	914.4	341	44.8	19
	S5	217	568	-778	648	46	527	1330	606	88.9	90242	63.3	127	609.6	341	41.9	19
	S6	188	472	-778	648	46	527	1330	606	88.9	90242	63.3	127	914.4	341	43.8	19
	S7	208	429	-778	648	46	527	1330	606	88.9	90242	63.3	127	1219	341	43.7	19
	S8	220	362	-778	648	46	527	1330	606	88.9	90242	63.3	127	1981	341	47.3	19
	S9	332	481	-778	648	46	527	1330	606	88.9	90242	63.3	191	609.6	341	44.9	19
	S10	187	374	-778	648	46	527	1330	606	88.9	90242	63.3	191	1219	341	43.2	19
	S11	197	314	-778	648	46	527	1330	606	88.9	90242	63.3	191	1981	341	43.2	19

Researcher	Experiment	Resistance		Prestress	Geometry										Materials		
		$V'_{R,c,exp}$	V'_{Rexp}	P	h	A_p	d_p	A_s	d_s	b_w	A_c	A_{sw}	s	a	f_{ywm}	f_{cm}	d_{max}
		kN	kN	kN	mm	mm^2	mm	mm^2	mm	mm	mm^2	mm^2	mm	*mm*	N/mm^2	N/mm^2	mm
Mattock et al. (1961)	S12	227	275	-778	648	46	527	1330	606	88.9	90242	63.3	191	2743	341	45.4	19
	S13	181	300	-778	648	46	527	1330	606	88.9	90242	63.3	127	2743	341	44.5	19
	S21	224	364	-778	648	46	527	1330	606	88.9	90242	63.3	191	1219	341	46.3	19
Xie (2009)	lb2	156	172	-786	506	507	473	534	473	74.0	87400	24.2	175	2400	529	63.2	10
	lb3	103	149	-475	506	507	473	400	473	73.0	86980	24.2	175	2400	529	63.2	10
	lb6	148	156	-797	506	507	473	934	473	73.0	73230	24.2	175	2400	529	63.5	10
	lb7	80	138	-319	506	507	473	934	473	73.0	73430	24.2	175	2400	529	63.5	10
	lb8	111	134	-512	504	507	471	934	471	73.0	72780	24.2	175	2400	529	63.5	10
	lb10	138	215	-822	506	507	473	934	473	74.0	73670	24.2	87.5	2400	529	62.3	10

Appendix G

Resistances of membrane elements determined with the MCFT for $\varepsilon_x = 0$, $s_\theta = 300$ mm, $d_{max} = 32$ mm

	Combination of parameters				Crack sliding ($\tau_{ci} = \tau_{ci,max}$)				Yielding of stirrups ($\sigma_{sz,cr} = f_{yz}$)				Crushing of concrete ($\sigma_2 = \sigma_{2,max}$)			
					input	results			input	results			input	results		
	f_{cm}	f_{yz}	ρ_z	ψ	s_x	τ_R	τ_{ci}	θ	s_x	τ_R	τ_{ci}	θ	s_x	τ_R	τ_{ci}	θ
	N/mm²	N/mm²	-	-	mm	N/mm²	N/mm²	°	mm	N/mm²	N/mm²	°	mm	N/mm²	N/mm²	°
1	40	250	0.0010	0.006	397	3.00	2.42	24.7	397	2.74	2.10	22.4	397	1.31	0.19	12.5
2	40	600	0.0010	0.015	391	3.34	1.85	22.2	391	3.12	1.36	19.1	391	2.45	0.31	15.8
3	40	250	0.0025	0.016	400	3.56	2.23	25.4	400	3.55	2.12	24.1	400	2.56	0.32	15.8
4	40	600	0.0025	0.038	395	5.00	1.48	23.2	395	5.01	1.31	22.2	395	4.47	0.48	20.9
5	40	250	0.0050	0.031	405	4.61	2.07	26.4	405	4.61	2.07	26.4	405	3.90	0.41	19.8
6	40	600	0.0050	0.075	400	7.55	1.30	25.8	400	7.56	1.20	25.4	400	7.22	0.73	25.3
7	40	250	0.0075	0.047	405	5.62	1.97	27.5	405	5.62	1.97	27.5	405	5.00	0.50	22.5
8	40	600	0.0075	0.113	407	9.68	1.26	28.3	407	9.66	1.17	28.1	407	9.32	0.91	28.5
9	40	250	0.0100	0.063	412	6.57	1.98	28.8	412	6.57	1.98	28.8	412	6.37	0.63	23.9
10	40	600	0.0100	0.150	412	11.30	1.15	30.8	412	11.21	1.10	31.1	412	10.40	0.96	32.2
11	60	250	0.0010	0.004	397	3.50	2.91	24.4	397	3.17	2.49	21.6	397	1.48	0.16	11.3
12	60	600	0.0010	0.010	391	3.87	2.40	22.6	391	3.44	1.61	18.4	391	2.54	0.24	14.5
13	60	250	0.0025	0.010	400	4.13	2.77	24.9	400	4.03	2.55	23.6	400	2.69	0.25	14.5
14	60	600	0.0025	0.025	391	5.52	1.91	22.8	391	5.46	1.55	21.2	391	4.97	0.41	18.4
15	60	250	0.0050	0.021	400	5.16	2.57	26.0	400	5.16	2.46	25.1	400	4.21	0.34	17.8
16	60	600	0.0050	0.050	400	8.19	1.64	24.8	400	8.24	1.49	24.2	400	7.91	0.59	22.5
17	60	250	0.0075	0.031	405	6.22	2.51	27.1	405	6.22	2.51	27.1	405	5.59	0.43	19.9
18	60	600	0.0075	0.075	402	10.58	1.55	26.6	402	10.58	1.55	26.6	402	10.41	0.75	25.4
19	60	250	0.0100	0.042	406	7.18	2.36	27.7	406	7.18	2.36	27.7	406	6.97	0.52	21.4
20	60	600	0.0100	0.100	406	12.84	1.45	28.0	406	12.84	1.45	28.0	406	12.34	0.87	27.7

	Combination of parameters				Crack sliding ($\tau_{ci} = \tau_{ci,max}$)				Yielding of stirrups ($\sigma_{sz,cr} = f_{yz}$)				Crushing of concrete ($\sigma_2 = \sigma_{2,max}$)			
					input	results			input	results			input	results		
	f_{cm}	f_{yz}	ρ_z	ψ	s_x	τ_R	τ_{ci}	θ	s_x	τ_R	τ_{ci}	θ	s_x	τ_R	τ_{ci}	θ
	N/mm^2	N/mm^2	-	-	mm	N/mm^2	N/mm^2	°	mm	N/mm^2	N/mm^2	°	mm	N/mm^2	N/mm^2	°
21	100	250	0.0010	0.003	407	3.70	3.19	28.3	407	2.42	1.65	18.8	407	1.70	0.04	10.0
22	100	600	0.0010	0.006	403	3.95	2.70	26.6	403	2.94	0.91	16.5	403	2.86	0.06	12.4
23	100	250	0.0025	0.006	404	4.00	2.74	27.1	404	3.40	1.76	21.1	404	2.82	0.06	12.7
24	100	600	0.0025	0.015	397	5.19	1.73	23.6	397	5.13	0.89	19.6	370	5.39	0.11	15.9
25	100	250	0.0050	0.013	405	4.88	2.44	27.3	405	4.62	1.67	23.3	405	4.70	0.09	15.1
26	100	600	0.0050	0.030	380	7.97	1.17	24.0	380	8.13	0.89	22.6	385	8.64	0.16	19.4
27	100	250	0.0075	0.019	404	5.89	2.21	27.1	404	5.79	1.75	25.1	375	6.30	0.13	16.9
28	100	600	0.0075	0.045	400	10.48	1.03	25.6	400	10.66	0.89	24.9	390	11.87	0.22	21.4
29	100	250	0.0100	0.025	379	6.77	2.00	27.9	379	6.90	1.67	25.8	379	7.85	0.15	18.1
30	100	600	0.0100	0.060	402	12.95	0.91	26.6	402	13.19	0.81	26.0	395	14.30	0.25	23.4
31	80	250	0.0010	0.003	407	3.38	2.89	28.7	407	2.25	1.49	18.9	402	1.45	0.04	10.3
32	80	600	0.0010	0.008	402	3.63	2.37	26.1	375	2.85	0.87	17.0	375	2.62	0.07	13.2
33	80	250	0.0025	0.008	405	3.69	2.43	27.1	405	3.20	1.59	21.5	405	2.81	0.07	13.3
34	80	600	0.0025	0.019	395	4.92	1.48	23.7	395	4.92	0.83	20.2	375	5.15	0.13	16.7
35	80	250	0.0050	0.016	403	4.59	2.14	27.2	403	4.42	1.53	23.6	372	4.50	0.11	15.9
36	80	600	0.0050	0.038	397	7.76	1.02	24.4	397	7.81	0.79	23.3	385	8.43	0.20	20.1
37	80	250	0.0075	0.023	405	5.52	1.85	27.3	405	5.56	1.55	25.3	377	6.01	0.14	17.8
38	80	600	0.0075	0.056	401	10.16	0.88	25.9	401	10.45	0.72	25.0	395	10.97	0.24	23.0
39	80	250	0.0100	0.031	404	6.46	1.71	28.0	404	6.49	1.49	26.8	382	7.48	0.18	19.1
40	80	600	0.0100	0.075	404	12.48	0.48	27.4	404	12.65	0.75	26.9	399	13.42	0.29	24.8

Notes:

1. For s_y the same value is used as for s_x
2. For steel no strain hardening is assumed

Appendix H

Ratio of the resistances determined with the MCFT and with the proposed approximation equations & other models

Membranes					**MCFT**		**Approximation equations**		**Model of Bentz et al.**		**Variable angle truss model**					
	f_{cm}	f_{yz}	ρ_z	ψ	*Failure mode*	τ_R	τ_R	$\tau_{R,MCFT}/\tau_{R,model}$	τ_R	$\tau_{R,MCFT}/\tau_{R,model}$	ν	ψ_{VAT}	θ_{calc}	θ_{gov}	τ_R	$\tau_{R,MCFT}/\tau_{R,model}$
	N/mm²	N/mm²	-	-	-	N/mm²	N/mm²	-	N/mm²		-	-	°	°	N/mm²	
1	40	250	0.0010	0.006	slipping	3.00	2.82	1.06	2.98	1.01	0.50	0.011	6.1	21.8	0.63	4.80
2	40	600	0.0010	0.015	slipping	3.34	3.40	0.98	3.61	0.92	0.50	0.027	9.5	21.8	1.50	2.23
3	40	250	0.0025	0.016	slipping	3.56	3.44	1.04	3.66	0.97	0.50	0.028	9.7	21.8	1.56	2.28
4	40	600	0.0025	0.038	slipping	5.00	4.89	1.02	5.24	0.95	0.50	0.068	15.1	21.8	3.75	1.33
5	40	250	0.0050	0.031	slipping	4.61	4.47	1.03	4.78	0.96	0.50	0.056	13.7	21.8	3.13	1.48
6	40	600	0.0050	0.075	slipping	7.55	7.37	1.02	7.94	0.95	0.50	0.135	21.6	21.8	7.50	1.01
7	40	250	0.0075	0.047	slipping	5.62	5.51	1.02	5.91	0.95	0.50	0.085	16.9	21.8	4.69	1.20
8	40	600	0.0075	0.113	slipping	9.68	9.85	0.98	10.65	0.91	0.50	0.203	26.8	26.8	8.92	1.09
9	40	250	0.0100	0.063	slipping	6.57	6.54	1.00	7.04	0.93	0.50	0.113	19.6	21.8	6.25	1.05
10	40	600	0.0100	0.150	slipping	11.30	12.33	0.92	13.35	0.85	0.50	0.271	31.3	31.3	9.85	1.15
11	60	250	0.0010	0.004	slipping	3.50	3.38	1.04	3.55	0.99	0.46	0.008	5.2	21.8	0.63	5.60
12	60	600	0.0010	0.010	slipping	3.87	3.98	0.97	4.18	0.93	0.46	0.020	8.1	21.8	1.50	2.58
13	60	250	0.0025	0.010	slipping	4.13	4.02	1.03	4.23	0.98	0.46	0.021	8.3	21.8	1.56	2.64
14	60	600	0.0025	0.025	slipping	5.52	5.53	1.00	5.80	0.95	0.46	0.050	12.9	21.8	3.75	1.47
15	60	250	0.0050	0.021	slipping	5.16	5.10	1.01	5.35	0.96	0.46	0.042	11.8	21.8	3.13	1.65
16	60	600	0.0050	0.050	slipping	8.19	8.13	1.01	8.51	0.96	0.46	0.100	18.4	21.8	7.50	1.09
17	60	250	0.0075	0.031	slipping	6.22	6.18	1.01	6.48	0.96	0.46	0.062	14.5	21.8	4.69	1.33
18	60	600	0.0075	0.075	slipping	10.58	10.72	0.99	11.22	0.94	0.46	0.150	22.7	22.7	10.73	0.99
19	60	250	0.0100	0.042	slipping	7.18	7.26	0.99	7.61	0.94	0.46	0.083	16.8	21.8	6.25	1.15
20	60	600	0.0100	0.100	slipping	12.84	13.31	0.96	13.92	0.92	0.46	0.199	26.5	26.5	12.02	1.07

Membranes					MCFT		Approximation equations		Model of Bentz et al.		Variable angle truss model					
	f_{cm}	f_{yz}	ρ_z	ψ	*Failure mode*	τ_R	τ_R	$\tau_{R,MCFT}/\tau_{R,model}$	τ_R	$\tau_{R,MCFT}/\tau_{R,model}$	ν	ψ_{VAT}	θ_{calc}	θ_{gov}	τ_R	$\tau_{R,MCFT}/\tau_{R,model}$
	N/mm²	N/mm²	-	-	-	N/mm²	N/mm²	-	N/mm²		-	-	°	°	N/mm²	
21	100	250	0.0010	0.003	slipping	3.70	3.49	1.06	3.68	1.01	0.36	0.006	4.6	21.8	0.63	5.92
22	100	600	0.0010	0.006	slipping	3.95	4.12	0.96	4.31	0.92	0.36	0.015	7.1	21.8	1.50	2.63
23	100	250	0.0025	0.006	slipping	4.00	4.17	0.96	4.35	0.92	0.36	0.016	7.2	21.8	1.56	2.56
24	100	600	0.0025	0.015	crushing	5.39	5.74	0.94	5.93	0.91	0.36	0.038	11.2	21.8	3.75	1.44
25	100	250	0.0050	0.013	slipping	4.88	5.29	0.92	5.48	0.89	0.36	0.032	10.2	21.8	3.13	1.56
26	100	600	0.0050	0.030	crushing	8.64	8.44	1.02	8.64	1.00	0.36	0.076	16.0	21.8	7.50	1.15
27	100	250	0.0075	0.019	crushing	6.30	6.42	0.98	6.61	0.95	0.36	0.047	12.6	21.8	4.69	1.34
28	100	600	0.0075	0.045	crushing	11.87	11.14	1.07	11.34	1.05	0.36	0.114	19.7	21.8	11.25	1.06
29	100	250	0.0100	0.025	crushing	7.85	7.54	1.04	7.74	1.01	0.36	0.063	14.6	21.8	6.25	1.26
30	100	600	0.0100	0.060	crushing	14.30	13.84	1.03	14.05	1.02	0.36	0.152	22.9	22.9	14.20	1.01
31	80	250	0.0010	0.003	slipping	3.38	3.16	1.07	3.68	0.92	0.41	0.007	4.8	21.8	0.63	5.41
32	80	600	0.0010	0.008	slipping	3.63	3.78	0.96	4.31	0.84	0.41	0.017	7.4	21.8	1.50	2.42
33	80	250	0.0025	0.008	slipping	3.69	3.83	0.96	4.35	0.85	0.41	0.017	7.6	21.8	1.56	2.36
34	80	600	0.0025	0.019	crushing	5.15	5.38	0.96	5.93	0.87	0.41	0.042	11.8	21.8	3.75	1.37
35	80	250	0.0050	0.016	slipping	4.59	4.93	0.93	5.48	0.84	0.41	0.035	10.8	21.8	3.13	1.47
36	80	600	0.0050	0.038	crushing	8.43	8.03	1.05	8.64	0.98	0.41	0.084	16.8	21.8	7.50	1.12
37	80	250	0.0075	0.023	crushing	6.01	6.04	1.00	6.61	0.91	0.41	0.052	13.2	21.8	4.69	1.28
38	80	600	0.0075	0.056	crushing	10.97	10.69	1.03	11.34	0.97	0.41	0.125	20.7	21.8	11.25	0.98
39	80	250	0.0100	0.031	crushing	7.48	7.15	1.05	7.74	0.97	0.41	0.070	15.3	21.8	6.25	1.20
40	80	600	0.0100	0.075	crushing	13.42	13.34	1.01	14.05	0.96	0.41	0.167	24.1	24.1	13.39	1.00
	Mean							1.00		0.94						1.89
	CoV							4.1%		5,2%						63.9%

Appendix I

Ratio of the resistance of girders according to Response and predicted using Equations 7.5 and 7.8 to 7.10

Girder	Properties girder										Response analyses						Eq.7.5,7.8-7.10		
	h	$h_{tf,str}$	$h_{tf,skw}$	$h_{bf,str}$	$h_{bf,skw}$	b_w	A_{sw}	s	a	x	f_{ywm}	θ	τ_s	τ_{ci}	$\tau_{R,R2k}$	$V_{R,R2K}$	z'	V'_R	$V'_{R,R2K}/V'_R$
	mm	mm	mm	mm	mm	mm	mm^2	mm	mm	mm	N/mm^2	°	N/mm^2	N/mm^2	N/mm^2	N	mm	N	-
cw10	457	89	25	89	25	50.8	71.3	254	1356	600	508	19.5	7.92	0.31	8.23	1.51E+05	356	1.49E+05	1.02
cw11	457	89	25	89	25	50.8	71.3	254	1356	990	481	20.6	7.07	0.50	7.57	1.38E+05	356	1.37E+05	1.01
cw12	457	89	25	89	25	50.8	71.3	254	1356	760	434	22.3	5.86	0.99	6.85	1.24E+05	356	1.24E+05	1.00
cw13	457	89	25	89	25	50.8	71.3	254	1356	760	507	19.4	7.95	0.32	8.27	1.52E+05	356	1.50E+05	1.02
cw14	457	89	25	89	25	50.8	71.3	178	1356	760	481	21.0	9.86	0.50	10.36	1.90E+05	356	1.87E+05	1.01
cw15	457	89	25	89	25	50.8	71.3	254	1356	600	505	19.8	7.77	0.34	8.11	1.51E+05	356	1.47E+05	1.03
cw16	457	89	25	89	25	50.8	71.3	254	1356	760	508	19.4	7.98	0.31	8.29	1.53E+05	356	1.50E+05	1.02
HCP2TE	750	80	30	100	40	100	100.5	200	2100	950	529	23.2	6.21	1.87	8.08	4.94E+05	643	5.19E+05	0.95
HCP2TW	750	80	30	100	40	100	100.5	200	2100	860	536	20.7	7.13	1.05	8.18	5.08E+05	643	5.25E+05	0.97
HAP2TW	750	80	30	100	40	100	100.5	200	2100	840	537	20.4	7.25	1.02	8.27	5.14E+05	643	5.31E+05	0.97
HCP1TE	750	80	30	100	40	100	100.5	200	2100	1148	545	18.8	8.04	0.70	8.74	5.40E+05	643	5.62E+05	0.96
HCP1TW	750	80	30	100	40	100	100.5	200	2100	1148	544	18.8	8.03	0.69	8.71	5.39E+05	643	5.60E+05	0.96
HAP1TE	750	80	30	100	40	100	100.5	200	2100	1148	542	19.7	7.59	0.86	8.45	5.21E+05	643	5.43E+05	0.96
HAP1TW	750	80	30	100	40	100	100.5	200	2100	1148	543	19.7	7.63	0.75	8.38	5.20E+05	643	5.39E+05	0.97
FX1A	457	76	51	76	51	76.2	31.7	203	1219	647	410	18.0	2.58	1.16	3.74	1.00E+05	356	1.01E+05	0.99
FX1B	457	76	51	76	51	76.2	31.7	203	1219	647	410	18.0	2.58	1.17	3.75	1.00E+05	356	1.02E+05	0.99
F1A	457	76	51	76	51	76.2	71.3	127	762	190	360	23.5	6.08	1.34	7.42	2.03E+05	356	2.01E+05	1.01
F1B	457	76	51	76	51	76.2	31.7	127	762	190	410	19.8	3.74	1.33	5.06	1.35E+05	356	1.37E+05	0.98
F2A	457	76	51	76	51	76.2	71.3	127	1016	444	360	24.8	5.73	0.90	6.63	1.75E+05	356	1.80E+05	0.98
F2B	457	76	51	76	51	76.2	31.7	203	1016	444	410	18.4	2.53	1.20	3.73	1.00E+05	356	1.01E+05	0.99

Girder	Properties girder											Response analyses					Eq.7.5,7.8-7.10		
	h	$h_{tf,str}$	$h_{tf,skw}$	$h_{bf,str}$	$h_{bf,skw}$	b_w	A_{sw}	s	a	x	f_{ywm}	θ	τ_s	τ_{ci}	$\tau_{R,R2k}$	$V_{R,R2K}$	z'	V'_R	$V'_{R,R2K}/V'_R$
	mm	mm	mm	mm	mm	mm	mm^2	mm	mm	mm	N/mm^2	°	N/mm^2	N/mm^2	N/mm^2	N	mm	N	-
F3A	457	76	51	76	51	76.2	71.3	169	1016	444	360	21.3	5.09	1.08	6.17	1.68E+05	356	1.67E+05	1.01
F3B	457	76	51	76	51	76.2	17.8	102	1016	900	376	15.4	3.13	0.40	3.53	9.36E+04	356	9.57E+04	0.98
F5A	457	76	51	76	51	76.2	31.7	127	1270	640	410	20.2	3.64	1.34	4.98	1.32E+05	356	1.35E+05	0.98
F5B	457	76	51	76	51	76.2	17.8	106	1270	1050	298	16.7	2.19	1.13	3.32	8.83E+04	356	9.01E+04	0.98
F19A	457	76	51	76	51	76.2	31.7	127	1016	444	410	19.7	3.74	1.31	5.06	1.36E+05	356	1.37E+05	0.99
ŢP2	970	175	0	150	0	150	157	150	3250	1000	427	28.5	5.50	0.98	6.48	7.59E+05	808	7.85E+05	0.97
Mean																			0.99
CoV																			2%

Appendix J

Comparison of ε_x at the least compressed chord between Response and the proposed method

Number	Researcher	Experiment	*Location*	*Response*		*Parameters*			*Suggested model using z'*				
			x	$V_{R,R2K}$	ε_t	P	e_{p0}	e_c	z'	M_F	M_P	T	ε_t
			m	kN	mm/m	kN	mm	mm^2	mm	kNm	kNm	kN	mm/m
1	Elzanaty et al. (1986)	CW10	0.600	151	-0.017	-439	133	178	356	91	-59	21.6	0.021
2		CW11	0.760	138	0.014	-429	133	178	356	105	-57	57.2	0.060
3		CW12	0.760	124	-0.077	-431	133	178	356	94	-57	11.2	0.013
4		CW13	0.760	152	-0.117	-604	133	178	356	115	-81	-52.3	-0.051
5		CW14	0.760	190	-0.004	-610	133	178	356	144	-81	61.3	0.061
6		CW15	0.600	151	-0.005	-433	133	178	356	91	-58	27.7	0.028
7		CW16	0.760	153	-0.096	-607	133	178	356	116	-81	-51.5	-0.042
8	Choulli (2005)	HCP2TE	0.950	494	0.032	-1225	231	202	652	469	-283	400.6	0.120
9		HCP2TW	0.860	508	0.046	-1225	231	202	652	437	-283	365.8	0.110
10		HAP2TW	0.840	514	0.045	-1225	231	202	652	432	-283	363.0	0.106
11		HCP1TE	1.148	540	-0.061	-1859	251	202	652	620	-467	198.4	0.060
12		HCP1TW	1.148	539	-0.061	-1859	251	202	652	619	-467	195.6	0.059
13		HAP1TE	1.148	521	-0.095	-1859	251	202	652	598	-467	147.1	0.042
14		HAP1TW	1.148	520	-0.096	-1859	251	202	652	597	-467	143.2	0.041
15	Hanson (1964)	FX1A	0.647	100	-0.110	-408	131	178	356	65	-54	-71.3	-0.074
16		FX1B	0.647	100	-0.116	-408	131	178	356	65	-54	-71.9	-0.075
17		F1A	0.190	203	-0.111	-411	131	178	356	38	-54	-46.0	-0.047
18		F1B	0.190	135	-0.217	-411	131	178	356	26	-54	-149.6	-0.154
19		F2A	0.444	175	0.023	-384	131	178	356	78	-50	60.6	0.063
20		F2B	0.444	100	-0.157	-384	131	178	356	44	-50	-108.4	-0.114
21		F3A	0.444	168	0.028	-390	131	178	356	75	-51	39.0	0.040

Number	Researcher	Experiment	*Location*	*Response*		*Parameters*			*Suggested model using z'*				
			x	$V_{R,R2K}$	ε_t	P	e_{p0}	e_c	z'	M_F	M_P	T	ε_t
			m	kN	mm/m	kN	mm	mm^2	mm	kNm	kNm	kN	mm/m
22		F3B	0.900	94	0.004	-390	131	178	356	84	-51	-8.5	-0.009
23		F5A	0.640	132	0.032	-387	131	178	356	84	-51	33.0	0.035
24		F5B	1.050	88	0.026	-387	131	178	356	93	-51	12.7	0.013
25		F19A	0.444	140	-0.007	-399	131	178	356	62	-52	-33.2	-0.033
26	Leonhardt (1973)	ŢP2	1.200	763	-0.062	-1912	479	259	808	915	-915	149.4	0.050

x = the distance from the centre of the support (considered cross-section)
$M_E = M_F + M_P$ in which M_E is the total moment at the considered the cross-section
M_F is the moment as result of the external force. For the considered girders with only a point load M_F is equal to $V_{R,R2k}$ multiplied with x.
M_P is the moment as result of the prestressing. For the considered girders with straight tendons M_P is equal to P multiplied with e_{po}.

Appendix K

Shear resistance according to the proposed model for prestressed girders with stirrups

Number	Researcher	Experiment	h	$h_{tf,str}$	$h_{tf,skw}$	$h_{bf,str}$	$h_{bf,skw}$	z'	A_{sw}	s	b_w	f_{ywm}	f_{cm}	ρ_z	ψ	β	V'_R
			mm	mm	mm	mm	mm	mm	mm^2	mm	mm	N/mm^2	N/mm^2	-	-	-	kN
1	Elzanaty et al. (1986)	cw10	457	89	25	89	25	356	71.3	254	50.8	434	73.1	0.553%	0.0328	0.246	127
2		cw11	457	89	25	89	25	356	71.3	254	50.8	434	55.9	0.553%	0.0429	0.273	126
3		cw12	457	89	25	89	25	356	71.3	254	50.8	434	40.0	0.553%	0.0600	0.230	115
4		cw13	457	89	25	89	25	356	71.3	254	50.8	434	72.4	0.553%	0.0331	0.248	127
5		cw14	457	89	25	89	25	356	71.3	178	50.8	434	73.8	0.789%	0.0464	0.209	159
6		cw15	457	89	25	89	25	356	71.3	254	50.8	434	70.3	0.553%	0.0341	0.254	127
7		cw16	457	89	25	89	25	356	71.3	254	50.8	434	73.1	0.553%	0.0328	0.246	127
~~8~~		~~cw17~~	~~457~~	~~89~~	~~25~~	~~89~~	~~25~~	~~356~~	~~31.7~~	~~254~~	~~50.8~~	~~379~~	~~69.7~~	~~0.246%~~	~~0.0134~~	~~0.308~~	~~81~~
~~9~~	Choulli (2005)	~~HCP2TE~~	~~750~~	~~80~~	~~100~~	~~100~~	~~100~~	~~652~~[1)]	~~100.5~~	~~200~~	~~100~~	~~525~~	~~90.2~~	~~0.503%~~	~~0.0293~~	~~0.227~~	~~494~~
~~10~~		~~HCP2TW~~	~~750~~	~~80~~	~~100~~	~~100~~	~~100~~	~~652~~[1)]	~~100.5~~	~~200~~	~~100~~	~~525~~	~~90.2~~	~~0.503%~~	~~0.0293~~	~~0.227~~	~~494~~
~~11~~		~~HAP2TW~~	~~750~~	~~80~~	~~100~~	~~100~~	~~100~~	~~652~~[1)]	~~100.5~~	~~200~~	~~100~~	~~525~~	~~96.0~~	~~0.503%~~	~~0.0275~~	~~0.231~~	~~501~~
12		HCP1TE	750	80	100	100	100	652[1)]	100.5	200	100	525	81.2	0.503%	0.0325	0.219	482
13		HCP1TW	750	80	100	100	100	652[1)]	100.5	200	100	525	81.2	0.503%	0.0325	0.219	482
14		HAP1TE	750	80	100	100	100	652[1)]	100.5	200	100	525	91.2	0.503%	0.0289	0.228	495
15		HAP1TW	750	80	100	100	100	652[1)]	100.5	200	100	525	91.2	0.503%	0.0289	0.228	495
16	Hanson (1964)	FX1A	457	76	51	76	51	356	31.7	203	76.2	410	45.9	0.205%	0.0183	0.334	108
17		FX1B	457	76	51	76	51	356	31.7	203	76.2	410	45.9	0.205%	0.0183	0.334	108
18		F1A	457	76	51	76	51	356	71.3	127	76.2	360	47.0	0.736%	0.0564	0.239	192
19		F1B	457	76	51	76	51	356	31.7	127	76.2	410	47.0	0.327%	0.0286	0.309	132
~~20~~		~~F2A~~	~~457~~	~~76~~	~~51~~	~~76~~	~~51~~	~~356~~	~~71.3~~	~~127~~	~~76.2~~	~~360~~	~~45.2~~	~~0.736%~~	~~0.0587~~	~~0.233~~	~~190~~
21		F2B	457	76	51	76	51	356	31.7	203	76.2	410	45.2	0.205%	0.0186	0.334	107
~~22~~		~~F3A~~	~~457~~	~~76~~	~~51~~	~~76~~	~~51~~	~~356~~	~~71.3~~	~~169~~	~~76.2~~	~~360~~	~~47.2~~	~~0.552%~~	~~0.0421~~	~~0.275~~	~~162~~

Number	Researcher	Experiment	h	$h_{tf,str}$	$h_{tf,skw}$	$h_{bf,str}$	$h_{bf,skw}$	z'	A_{sw}	s	b_w	f_{ywm}	f_{cm}	ρ_z	ψ	β	V'_R
			mm	mm	mm	mm	mm	mm	mm^2	mm	mm	N/mm^2	N/mm^2	-	-	-	kN
23	Hanson (1964)	F3B	457	76	51	76	51	356	17.8	102	76.2	298	47.2	0.230%	0.0145	0.344	102
24		F4B	457	76	51	76	51	356	31.7	212	76.2	410	43.7	0.196%	0.0184	0.334	105
~~25~~		~~F5A~~	~~457~~	~~76~~	~~51~~	~~76~~	~~51~~	~~356~~	~~31.7~~	~~127~~	~~76.2~~	~~410~~	~~44.2~~	~~0.327%~~	~~0.0304~~	~~0.304~~	~~129~~
26		F5B	457	76	51	76	51	356	17.8	106	76.2	298	44.2	0.221%	0.0149	0.343	98
27		F19A	457	76	51	76	51	356	31.7	127	76.2	410	51.1	0.327%	0.0263	0.314	135
~~28~~	~~Leonhardt et al. (1973)~~	~~TP2~~	~~970~~	~~175~~	~~0~~	~~150~~	~~0~~	~~808~~	~~157~~	~~150~~	~~150~~	~~423~~	~~24.0~~	~~0.698%~~	~~0.1230~~	~~0.073~~	~~776~~
~~29~~		~~TP4~~	~~900~~	~~175~~	~~0~~	~~150~~	~~0~~	~~738~~	~~157~~	~~85~~	~~80~~	~~423~~	~~47.0~~	~~2.309%~~	~~0.2096~~	~~-0.144~~	~~1123~~
~~30~~	~~Rupf et al. (2013)~~	~~SR21~~	~~780~~	~~140~~	~~20~~	~~140~~	~~20~~	~~630~~	~~28.3~~	~~220~~	~~150~~	~~585~~	~~30.8~~	~~0.086%~~	~~0.0163~~	~~0.339~~	~~275~~
~~31~~		~~SR22~~	~~780~~	~~140~~	~~20~~	~~140~~	~~20~~	~~630~~	~~56.5~~	~~300~~	~~150~~	~~585~~	~~33.7~~	~~0.126%~~	~~0.0218~~	~~0.325~~	~~321~~
32		SR23	780	140	20	140	20	630	28.3	300	150	585	35.3	0.063%	0.0104	0.354	270
~~33~~		~~SR24~~	~~780~~	~~140~~	~~20~~	~~140~~	~~20~~	~~630~~	~~56.5~~	~~150~~	~~150~~	~~575~~	~~31.3~~	~~0.251%~~	~~0.0462~~	~~0.265~~	~~420~~
34		SR25	780	140	20	140	20	630	28.3	220	150	585	33.1	0.086%	0.0151	0.342	283
35		SR26	780	140	20	140	20	630	28.3	300	150	585	36.9	0.063%	0.0100	0.355	275
36		SR27	780	140	20	140	20	630	56.5	200	150	575	28.3	0.188%	0.0383	0.284	353
~~37~~		~~SR29~~	~~780~~	~~140~~	~~20~~	~~140~~	~~20~~	~~630~~	~~56.5~~	~~150~~	~~150~~	~~575~~	~~29.8~~	~~0.251%~~	~~0.0485~~	~~0.259~~	~~413~~
~~38~~		~~SR30~~	~~780~~	~~140~~	~~20~~	~~140~~	~~20~~	~~630~~	~~56.5~~	~~150~~	~~150~~	~~585~~	~~31.4~~	~~0.251%~~	~~0.0468~~	~~0.263~~	~~424~~
~~39~~	~~Mattock et al. (1961)~~	~~S1~~	~~648~~	~~165~~	~~57~~	~~89~~	~~95~~	~~483~~	~~63.3~~	~~64~~	~~88.9~~	~~341~~	~~45.7~~	~~1.122%~~	~~0.0836~~	~~0.171~~	~~386~~
~~40~~		~~S2~~	~~648~~	~~165~~	~~57~~	~~89~~	~~95~~	~~483~~	~~63.3~~	~~64~~	~~88.9~~	~~341~~	~~45.4~~	~~1.122%~~	~~0.0841~~	~~0.170~~	~~385~~
~~41~~		~~S3~~	~~648~~	~~165~~	~~57~~	~~89~~	~~95~~	~~483~~	~~63.3~~	~~64~~	~~88.9~~	~~341~~	~~44.8~~	~~1.122%~~	~~0.0853~~	~~0.167~~	~~384~~
~~42~~		~~S5~~	~~648~~	~~165~~	~~57~~	~~89~~	~~95~~	~~483~~	~~63.3~~	~~127~~	~~88.9~~	~~341~~	~~41.9~~	~~0.561%~~	~~0.0457~~	~~0.266~~	~~242~~
~~43~~		~~S6~~	~~648~~	~~165~~	~~57~~	~~89~~	~~95~~	~~483~~	~~63.3~~	~~127~~	~~88.9~~	~~341~~	~~43.8~~	~~0.561%~~	~~0.0436~~	~~0.271~~	~~245~~
~~44~~		~~S7~~	~~648~~	~~165~~	~~57~~	~~89~~	~~95~~	~~483~~	~~63.3~~	~~127~~	~~88.9~~	~~341~~	~~43.7~~	~~0.561%~~	~~0.0438~~	~~0.271~~	~~245~~
~~45~~		~~S8~~	~~648~~	~~165~~	~~57~~	~~89~~	~~95~~	~~483~~	~~63.3~~	~~127~~	~~88.9~~	~~341~~	~~47.3~~	~~0.561%~~	~~0.0404~~	~~0.279~~	~~250~~
~~46~~		~~S9~~	~~648~~	~~165~~	~~57~~	~~89~~	~~95~~	~~483~~	~~63.3~~	~~191~~	~~88.9~~	~~341~~	~~44.9~~	~~0.374%~~	~~0.0284~~	~~0.309~~	~~201~~
~~47~~		~~S10~~	~~648~~	~~165~~	~~57~~	~~89~~	~~95~~	~~483~~	~~63.3~~	~~191~~	~~88.9~~	~~341~~	~~43.2~~	~~0.374%~~	~~0.0295~~	~~0.306~~	~~199~~
~~48~~		~~S11~~	~~648~~	~~165~~	~~57~~	~~89~~	~~95~~	~~483~~	~~63.3~~	~~191~~	~~88.9~~	~~341~~	~~43.2~~	~~0.374%~~	~~0.0295~~	~~0.306~~	~~199~~
~~49~~		~~S12~~	~~648~~	~~165~~	~~57~~	~~89~~	~~95~~	~~483~~	~~63.3~~	~~191~~	~~88.9~~	~~341~~	~~45.4~~	~~0.374%~~	~~0.0281~~	~~0.310~~	~~202~~
~~50~~		~~S13~~	~~648~~	~~165~~	~~57~~	~~89~~	~~95~~	~~483~~	~~63.3~~	~~127~~	~~88.9~~	~~341~~	~~44.5~~	~~0.561%~~	~~0.0430~~	~~0.273~~	~~246~~

Number	Researcher	Experiment	h	$h_{tf,str}$	$h_{tf,skw}$	$h_{bf,str}$	$h_{bf,skw}$	z'	A_{sw}	s	b_w	f_{ywm}	f_{cm}	ρ_z	ψ	β	V'_R
			mm	mm	mm	mm	mm	mm	mm^2	mm	mm	N/mm^2	N/mm^2	-	-	-	kN
~~50~~		~~S13~~	~~648~~	~~165~~	~~57~~	~~89~~	~~95~~	~~483~~	~~63.3~~	~~127~~	~~88.9~~	~~341~~	~~44.5~~	~~0.561%~~	~~0.0430~~	~~0.273~~	~~246~~
~~51~~		~~S21~~	~~648~~	~~165~~	~~57~~	~~89~~	~~95~~	~~483~~	~~63.3~~	~~191~~	~~88.9~~	~~341~~	~~46.3~~	~~0.374%~~	~~0.0275~~	~~0.311~~	~~203~~
52		LB2	506	84	25	72	25	416	24.2	175	74.0	529	63.2	0.187%	0.0156	0.328	143
~~53~~	Xie (2009)	~~LB3~~	~~506~~	~~80~~	~~25~~	~~76~~	~~25~~	~~416~~	~~24.2~~	~~175~~	~~73.0~~	~~529~~	~~63.2~~	~~0.189%~~	~~0.0159~~	~~0.328~~	~~141~~
~~54~~		~~LB6~~	~~506~~	~~51~~	~~25~~	~~55~~	~~25~~	~~441~~	~~24.2~~	~~175~~	~~73.0~~	~~529~~	~~63.5~~	~~0.189%~~	~~0.0158~~	~~0.327~~	~~150~~
~~55~~		~~LB7~~	~~506~~	~~51~~	~~25~~	~~55~~	~~25~~	~~441~~	~~24.2~~	~~175~~	~~73.0~~	~~529~~	~~63.5~~	~~0.189%~~	~~0.0158~~	~~0.327~~	~~150~~
~~56~~		~~LB8~~	~~504~~	~~53~~	~~25~~	~~51~~	~~25~~	~~440~~	~~24.2~~	~~175~~	~~73.0~~	~~529~~	~~63.5~~	~~0.189%~~	~~0.0158~~	~~0.327~~	~~149~~
57		LB10	506	56	25	50	25	441	24.2	87.5	74.0	529	62.3	0.374%	0.0317	0.291	207

All experiments of the database of shear failure related to diagonal tension cracks of girder with stirrups (Appendix F) are listed. The experiments that are eventually not selected (Appendix L and M), are struck through.

[1] The cross-section of the experiments of Choulli were found to be irregular. Therefore, z' was calculated from the linear elastic shear stress distribution, using Equation 7.6, instead of using Equations 7.7 - 7.9.

Appendix L

Selection of experiments for the evaluation of the accuracy of the proposed model based on ε_x

	Researcher	Experiment	V'_R	x	M_F	e_p	P	M_p	z'	e_c	C	T	EA_c	EA_t	ε_c	ε_t	ε_x	$\varepsilon_x \leq 0$
			kN	m	kNm	mm	kN	kNm	mm	mm	kN	kN	10^8 N	10^8 N	mm/m	mm/m	mm/m	
1	Elzanaty et al. (1986)	cw10	127	0.762	97	134	-439	-59	355	178	-200	14	8.95	1.56	-0.223	0.090	-0.066	yes
2		cw11	126	0.762	96	134	-429	-57	355	178	-197	19	8.07	1.56	-0.244	0.124	-0.060	yes
3		cw12	115	0.762	88	134	-431	-58	355	178	-185	-16	7.14	8.57	-0.260	-0.018	-0.139	yes
4		cw13	127	0.762	97	134	-604	-81	355	178	-220	-130	8.91	10.35	-0.247	-0.126	-0.186	yes
5		cw14	159	0.762	121	134	-610	-81	355	178	-258	-34	8.98	9.99	-0.287	-0.034	-0.161	yes
6		cw15	127	0.762	97	134	-433	-58	355	178	-199	21	8.81	1.21	-0.226	0.172	-0.027	yes
7		cw16	127	0.762	97	134	-607	-81	355	178	-220	-133	8.95	12.28	-0.246	-0.108	-0.177	yes
8		cw17	81	0.762	62	134	-608	-81	355	178	-168	-278	8.78	10.22	-0.191	-0.272	-0.232	yes
9	Choulli (2005)	HCP2TE	494	1.147	566	231	-1225	-283	652	202	-787	549	37.69	1.84	-0.209	2.981	1.386	no
10		HCP2TW	494	1.147	566	231	-1225	-283	652	202	-787	549	38.00	2.16	-0.207	2.547	1.170	no
11		HAP2TW	501	1.147	575	231	-1225	-283	652	202	-793	569	38.93	2.16	-0.204	2.639	1.218	no
12		HCP1TE	482	1.147	553	251	-1859	-467	652	202	-933	37	36.15	2.99	-0.258	0.124	-0.067	yes
13		HCP1TW	482	1.147	553	251	-1859	-467	652	202	-933	37	36.47	3.30	-0.256	0.113	-0.072	yes
14		HAP1TE	495	1.147	568	251	-1859	-467	652	202	-944	74	37.85	2.99	-0.249	0.247	-0.001	yes
15		HAP1TW	495	1.147	568	251	-1859	-467	652	202	-944	74	38.16	3.30	-0.247	0.224	-0.012	yes
16	Hanson (1964)	FX1A	108	0.647	70	131	-408	-54	356	178	-142	-50	9.08	9.60	-0.156	-0.052	-0.104	yes
17		FX1B	108	0.647	70	131	-408	-54	356	178	-142	-50	9.08	9.60	-0.156	-0.052	-0.104	yes
18		F1A	192	0.190	36	131	-411	-54	356	178	35	-63	9.17	9.68	0.039	-0.065	-0.013	yes
19		F1B	132	0.190	25	131	-411	-54	356	178	8	-154	9.17	9.68	0.008	-0.159	-0.075	yes
20		F2A	190	0.444	84	131	-384	-50	356	178	-97	93	9.03	0.64	-0.108	1.444	0.668	no
21		F2B	107	0.444	48	131	-384	-50	356	178	-77	-92	9.03	9.55	-0.085	-0.096	-0.091	yes

	Researcher	Experiment	V'_R	x	M_F	e_p	P	M_p	z'	e_c	C	T	EA_c	EA_t	ε_c	ε_t	ε_x	$\varepsilon_x \leq 0$
			kN	m	kNm	mm	kN	kNm	mm	mm	kN	kN	10^8 N	10^8 N	mm/m	mm/m	mm/m	
22		F3A	162	0.444	72	131	-390	-51	356	178	-91	24	9.18	0.64	-0.099	0.375	0.138	no
23		F3B	102	0.444	45	131	-390	-51	356	178	-76	-110	9.18	9.69	-0.083	-0.113	-0.098	yes
24		F4B	105	0.698	73	131	-421	-55	356	178	-156	-56	8.93	9.44	-0.175	-0.059	-0.117	yes
25		F5A	129	0.698	90	131	-387	-51	356	178	-175	47	8.96	0.64	-0.196	0.730	0.267	no
26		F5B	98	0.698	69	131	-387	-51	356	178	-145	-45	8.96	9.48	-0.162	-0.047	-0.105	yes
27		F19A	135	0.444	60	131	-399	-52	356	178	-86	-42	9.46	9.97	-0.091	-0.043	-0.067	yes
28	Leonhardt et al. (1973)	TP2	776	1.830	1420	479	-1912	-915	808	259	-1148	788	53.34	6.28	-0.215	1.255	0.520	no
29		TP4	1123	1.951	2192	525	-1870	-982	738	212	-1848	2225	59.95	6.28	-0.308	3.545	1.618	no
30	Rupf et al. (2013)	SR21	275	6.326	365	0	-749	-151 [2)]	630	315	-439	240	45.29	9.73	-0.097	0.247	0.075	no
31		SR22	321	6.326	426	0	-743	-150 [2)]	630	315	-488	229	46.49	9.73	-0.105	0.236	0.065	no
32		SR23	270	6.326	358	0	-764	-154 [2)]	630	315	-436	53	47.13	9.73	-0.093	0.054	-0.019	yes
33		SR24	420	6.326	557	0	-743	-150 [2)]	630	315	-598	529	45.50	9.73	-0.131	0.543	0.206	no
34		SR25	283	6.326	375	0	-1476	-248 [2)]	630	315	-657	-596	44.14	46.48	-0.149	-0.128	-0.139	yes
35		SR26	275	6.326	365	0	-1504	-253 [2)]	630	315	-655	-650	45.64	47.98	-0.143	-0.135	-0.139	yes
36		SR27	353	6.326	468	0	-1513	-254 [2)]	630	315	-743	-417	42.11	44.45	-0.176	-0.094	-0.135	yes
37		SR29	413	6.326	548	0	-736	-148 [2)]	630	315	-589	515	44.87	9.73	-0.131	0.530	0.199	no
38		SR30	424	6.326	562	0	-711	-143 [2)]	630	315	-597	594	40.68	4.86	-0.147	1.220	0.537	no
39	Mattock et al. (1961)	S1	386	0.000	N/A [2)]	N/A [2)]	-788	N/A [2)]	483	N/A [2)]	-877	870	16.09	2.63	-0.545	3.306	1.380	no
40		S2	385	0.482	N/A [2)]	N/A [2)]	-788	N/A [2)]	483	N/A [2)]	-1118	1110	16.06	2.63	-0.696	4.215	1.760	no
41		S3	384	0.177	N/A [2)]	N/A [2)]	-788	N/A [2)]	483	N/A [2)]	-1001	991	15.98	2.63	-0.626	3.764	1.569	no
42		S5	242	0.000	N/A [2)]	N/A [2)]	-788	N/A [2)]	483	N/A [2)]	-828	533	15.61	2.63	-0.530	2.026	0.748	no
43		S6	245	0.177	N/A [2)]	N/A [2)]	-788	N/A [2)]	483	N/A [2)]	-908	620	15.86	2.63	-0.573	2.355	0.891	no
44		S7	245	0.482	N/A [2)]	N/A [2)]	-788	N/A [2)]	483	N/A [2)]	-982	693	15.84	2.63	-0.620	2.632	1.006	no
45		S8	250	1.244	N/A [2)]	N/A [2)]	-788	N/A [2)]	483	N/A [2)]	-1152	874	16.28	2.63	-0.707	3.320	1.306	no
46		S9	201	0.000	N/A [2)]	N/A [2)]	-788	N/A [2)]	483	N/A [2)]	-814	437	15.99	2.63	-0.509	1.661	0.576	no
47		S10	199	0.482	N/A [2)]	N/A [2)]	-788	N/A [2)]	483	N/A [2)]	-937	556	15.79	2.63	-0.594	2.110	0.758	no
48		S11	199	1.244	N/A [2)]	N/A [2)]	-788	N/A [2)]	483	N/A [2)]	-1067	686	15.79	2.63	-0.676	2.605	0.964	no
49		S12	202	2.006	N/A [2)]	N/A [2)]	-788	N/A [2)]	483	N/A [2)]	-1181	806	16.05	2.63	-0.736	3.061	1.163	no

	Researcher	Experiment	V'_R	x	M_F	e_p	P	M_p	z'	e_c	C	T	EA_c	EA_t	ε_c	ε_t	ε_x	$\varepsilon_x \leq 0$
			kN	m	kNm	mm	kN	kNm	mm	mm	kN	kN	10^8 N	10^8 N	mm/m	mm/m	mm/m	
50	Mattock et al. (1961)	S13	246	2.006	N/A[2)]	N/A[2)]	-788	N/A[2)]	483	N/A[2)]	-1277	991	15.94	2.63	-0.801	3.765	1.482	no
51		S21	203	0.482	N/A[2)]	N/A[2)]	-788	N/A[2)]	483	N/A[2)]	-941	569	16.17	2.63	-0.582	2.161	0.789	no
52	Xie (2009)	LB2	143	0.688	73.0	0	-786	0	416	205	-432	-69	14.51	14.51	-0.298	-0.048	-0.173	yes
53		LB3	141	0.695	71.4	0	-475	0	416	207	-269	77	14.51	1.34	-0.186	0.572	0.193	no
54		LB6	150	0.745	68.2	0	-797	0	441	221	-402	-96	13.23	13.23	-0.304	-0.072	-0.188	yes
55		LB7	150	0.745	68.2	0	-319	0	441	221	-164	144	13.23	2.16	-0.124	0.669	0.273	no
56		LB8	149	0.738	69.0	0	-512	0	440	219	-264	51	13.23	2.16	-0.200	0.237	0.019	no
57		LB10	207	0.736	96.1	0	-822	0	441	219	-425	17	13.15	2.16	-0.323	0.079	-0.122	yes

1) Distance from girder end according to Rupf (2013) instead of distance from support (other listed experiments)
2) The forces are determined based on the CSA method (Section 5.1.5). As none of the experiments meet the condition $\varepsilon_x \leq 0$ (which is logical as hardly any prestress is present in the most tensioned chord), it is not worthwhile to adjust the calculations based on the equivalent load prestressing method.

Depending on the sign of T, EA_c and EA_t consist if the stiffness of the concrete, prestressing steel and reinforcing steel (Section 5.1.5).

Appendix M

Selection of experiments for the evaluation of the accuracy of the proposed model based on $V'_{R,c}$ and V'_{Rmax}

	Researcher	Experiment	V'_R	f_{cm}	b_w	z'	V'_{Rmax}	V'_R/V'_{Rmax}	*Flexural cracks predicted*	$V'_{R,c}$	$V'_{R,c}/V'_R$	Selected
			kN	N/mm^2	mm	mm	kN	-	10^9 mm^4	kN	-	
1	Elzanaty et al. (1986)	cw10	127	73.1	50.8	355	422	0.30	No	97	0.76	Yes
2		cw11	126	55.9	50.8	355	323	0.39	Yes	96	0.76	Yes
3		cw12	115	40.0	50.8	355	231	0.50	No	88	0.77	Yes
4		cw13	127	72.4	50.8	355	418	0.30	No	123	0.97	Yes
5		cw14	159	73.8	50.8	355	426	0.37	No	124	0.78	Yes
6		cw15	127	70.3	50.8	355	406	0.31	Yes	99	0.78	Yes
7		cw16	127	73.1	50.8	355	422	0.30	No	124	0.98	Yes
8		cw17	81	69.7	50.8	355	403	0.20	No	123	**1.52**	No
9	Choulli (2005)	HCP1TE	482	81.2	100	652	1694	0.28	No	403	0.84	Yes
10		HCP1TW	482	81.2	100	652	1694	0.28	No	409	0.85	Yes
11		HAP1TE	495	91.2	100	652	1904	0.26	No	419	0.85	Yes
12		HAP1TW	495	91.2	100	652	1904	0.26	No	429	0.87	Yes
13	Hanson (1964)	FX1A	108	45.9	76.2	356	398	0.27	Yes	122	1.13	Yes[1]
14		FX1B	108	45.9	76.2	356	398	0.27	Yes	122	1.13	Yes[1]
15		F1A	192	47.0	76.2	356	408	0.47	No	143	0.74	Yes
16		F1B	132	47.0	76.2	356	408	0.32	No	143	1.08	Yes[1]
17		F2B	107	45.2	76.2	356	392	0.27	Yes	119	1.11	Yes[1]
18		F3B	102	47.2	76.2	356	409	0.25	Yes	122	1.20	Yes[1]
19		F4B	105	43.7	76.2	356	379	0.28	Yes	120	1.14	Yes[1]
20		F5B	98	44.2	76.2	356	383	0.26	Yes	118	1.20	Yes[1]
21		F19A	135	51.1	76.2	356	443	0.31	Yes	129	0.96	Yes

	Researcher	Experiment	V'_R	f_{cm}	b_w	z'	V'_{Rmax}	V'_R/V'_{Rmax}	*Flexural cracks predicted*	$V'_{R,c}$	$V'_{R,c}/V'_R$	Selected
			kN	N/mm^2	mm	mm	kN	-	10^9 mm^4	kN	-	
22	Rupf et al. (2013)	SR23	270	35.3	150	630	1067	0.25	Yes	235	0.87	Yes
23		SR25	283	33.1	150	630	1001	0.28	Yes	272	0.96	Yes
24		SR26	275	36.9	150	630	1116	0.25	Yes	292	1.06	Yes[1]
25		SR27	353	28.3	150	630	856	0.41	Yes	250	0.71	Yes
26	Xie (2009)	LB2	143	63.2	74	416	622	0.23	Yes	151	1.07	Yes[1]
27		LB6	150	63.5	73	441	653	0.23	Yes	150	1.00	No[2]
28		LB10	207	62.3	74	441	650	0.32	Yes	157	0.76	Yes
	Leonhardt et al. (1973)	TP4	1123	46.6	80	738	880	**1.28**	No	250	0.22	No

[1] Selected despite $V'_{R,c} / V'_R$ somewhat exceeds 1. This is because the experimentally found shear resistance V'_{Rexp} is higher (average 30%) than the predicted shear resistance V'_R. Eventually the selection could be verified per experiment by evaluating V'_R that considers the effect of a/d (Section 8.4.2).
[2] LB6 is accidentally not selected despite this experiment meets the selection criteria.

Appendix N

Accuracy of models for the determination of the shear resistance of prestressed girders with stirrups

	Re-search	Exp.	V'_{Rexp}	*Proposed model (Section 8.3)*				*Model of Bentz et al. (Section 5.1.5)*				*Model of Esfandiari (Section 5.1.6)*				*Variable angle truss model (Section 5.1.1)*			*Modified variable angle truss model (Section 8.5)*		
				θ	β	V'_R	V'_{Rexp}/V'_R	θ	β	V'_R	V'_{Rexp}/V'_R	θ	β	V'_R	V'_{Rexp}/V'_R	θ	V'_R	V'_{Rexp}/V'_R	θ	V'_R	V'_{Rexp}/V'_R
			kN	°	-	kN	-	°	-	kN	-	°	-	kN	-	°	kN	-	°	kN	-
1	Elza-naty et al. (1986)	cw10	175	26.0	0.25	127	1.38	29.2	0.38	127	1.36	22.2	0.17	126	1.37	21.8	108	1.62	18.0	133	1.31
2		cw11	158	26.0	0.27	126	1.26	29.2	0.39	125	1.26	22.6	0.17	122	1.29	21.8	108	1.46	18.8	127	1.24
3		cw12	142	26.0	0.23	115	1.23	28.8	0.42	122	1.16	23.1	0.17	116	1.21	21.8	108	1.31	20.8	114	1.24
4		cw13	184	26.0	0.25	127	1.45	27.8	0.53	153	1.19	19.4	0.17	142	1.28	21.8	108	1.70	18.0	133	1.38
5		cw14	189	26.0	0.21	159	1.19	28.8	0.42	160	1.17	22.6	0.17	160	1.17	21.8	149	1.26	20.4	166	1.14
6		cw15	152	26.0	0.25	127	1.19	29.4	0.36	126	1.19	22.7	0.17	125	1.20	21.8	109	1.39	18.1	133	1.14
7		cw16	188	26.0	0.25	127	1.48	27.9	0.52	160	1.17	19.6	0.17	149	1.26	21.8	112	1.69	18.0	133	1.41
8	Choulli (2005)	HCP1TE	796	26.0	0.22	482	1.65	28.7	0.43	497	1.60	20.7	0.15	494	1.61	21.8	421	1.89	18.6	513	1.55
9		HCP1TW	746	26.0	0.22	482	1.55	28.7	0.43	497	1.50	20.7	0.15	494	1.51	21.8	421	1.77	18.6	513	1.46
10		HAP1TE	648	26.0	0.23	495	1.31	28.7	0.43	496	1.31	20.6	0.15	496	1.31	21.8	421	1.54	18.7	508	1.28
11		HAP1TW	749	26.0	0.23	495	1.51	28.7	0.43	496	1.51	20.6	0.15	496	1.51	21.8	421	1.78	18.7	508	1.48
12	Hanson (1964)	FX1A	168	26.0	0.33	108	1.56	29.3	0.37	111	1.51	18.9	0.18	100	1.67	21.8	61	2.76	12.5	103	1.64
13		FX1B	144	26.0	0.33	108	1.33	29.3	0.37	111	1.29	18.9	0.18	100	1.42	21.8	61	2.36	12.5	103	1.40
14		F1A	288	26.0	0.24	192	1.50	30.2	0.32	185	1.55	22.3	0.07	186	1.54	21.8	193	1.49	20.5	192	1.50
15		F1B	269	26.0	0.31	132	2.04	28.6	0.44	151	1.77	20.5	0.18	132	2.02	21.8	98	2.75	15.4	132	2.03
16		F2B	180	26.0	0.33	107	1.67	28.7	0.42	121	1.48	19.2	0.18	99	1.79	21.8	61	2.94	12.6	102	1.76
17		F3B	180	26.0	0.34	102	1.76	28.5	0.45	120	1.48	18.9	0.21	94	1.88	21.8	50	3.61	11.3	93	1.93

	Re-search	Exp.	V'_{Rexp}	*Proposed model (Section 8.3)*				*Model of Bentz et al. (Section 5.1.5)*				*Model of Esfandiari (Section 5.1.6)*				*Variable angle truss model (Section 5.1.1)*			*Modified variable angle truss model (Section 8.5)*		
				θ	β	V'_R	V'_{Rexp} /V'_R	θ	β	V'_R	V'_{Rexp} /V'_R	θ	β	V'_R	V'_{Rexp}/ V'_R	θ	V'_R	V'_{Rexp} /V'_R	θ	V'_R	V'_{Rexp} /V'_R
			kN	°	-	kN	-	°	-	kN	-	°	-	kN	-	°	kN	-	°	kN	-
18	Han-son (1964)	F4B	171	26.0	0.33	105	1.64	29.2	0.38	109	1.55	18.8	0.18	98	1.73	21.8	59	2.92	12.4	99	1.73
19		F5B	145	26.0	0.34	98	1.48	29.3	0.37	101	1.42	18.8	0.21	91	1.57	21.8	48	3.03	11.3	90	1.62
20		F19A	180	26.0	0.31	135	1.33	29.8	0.34	132	1.34	21.7	0.18	128	1.39	21.8	98	1.84	15.1	135	1.33
21	Rupf et al. (2013)	SR23	275	26.0	0.35	270	1.02	29.4	0.37	277	0.99	18.8	0.13	182	1.51	21.8	91	*3.03*	9.1	216	1.27
22		SR25	324	26.0	0.34	283	1.14	28.4	0.46	339	0.96	18.4	0.13	213	1.52	21.8	120	*2.70*	10.8	247	1.31
23		SR26	293	26.0	0.36	275	1.07	28.4	0.46	330	0.89	17.8	0.13	182	1.61	21.8	88	*3.34*	9.0	219	1.34
24		SR27	441	26.0	0.28	353	1.25	28.5	0.45	413	1.07	20.7	0.13	338	1.30	21.8	259	*1.70*	16.6	344	1.28
25	Xie (2009)	LB2	172	26.0	0.33	143	1.21	28.7	0.43	164	1.05	17.8	0.15	133	1.29	21.8	80	2.14	12.6	136	1.27
26		LB10	215	26.0	0.29	207	1.04	29.4	0.37	202	1.06	21.5	0.15	194	1.11	21.8	159	1.35	17.0	210	1.02
	Mean						1.39				1.31				1.47			2.13			1.43
	Coefficient of variation						17.5%				17.6%				15.8%			33.5%			17.0%
	Mean ($a/d > 2.5$)						1.33				1.25				1.41			2.04			1.36
	Coefficient of variation ($a/d > 2.5$)						14.6%				16.9%				12.8%			32.6%			13.0%
	Mean ($a/d > 5.0$)						1.12				1.00				1.39			2.38			1.25
	Coefficient of variation ($a/d > 5.0$)						8.5%				7.1%				13.5%			32.6%			9.1%

Appendix O

Effect on resistance of assuming s_θ = 300 mm and d_{max} = 31.5 mm

			Prop model Eq. 6.4-6.6	Data experiment							Membrane 2000					$\tau'_{RM2k}/\tau'_{R6.4-6}$	V'_{Rexp}/V'_R	V'_{Rexp}/V'_R
											Sliding	Crushing	Governing				Prop. model	Cons. s_θ and d_{max}
			τ'_R	s_x	s_z	d_{max}	d_{max} (f_{cm})	f_{cm}	f_{ywm}	ρ_z	τ'_{RM2k}	τ'_{RM2k}	τ'_{RM2k}		s_θ			
			N/mm^2	mm	mm	mm	mm	N/mm^2	N/mm^2		N/mm^2	N/mm^2	N/mm^2		mm			
1	Elza-naty et al. (1986)	cw10	7.02	255	254	13	4	73.1	434	0.553%	7.00	6.84	7.00	sliding	192	1.00	1.38	1.38
2		cw11	6.96	255	254	13	13	55.9	434	0.553%	6.95	6.71	6.95	sliding	191	1.00	1.26	1.26
3		cw12	6.37	255	254	13	13	40.0	434	0.553%	6.52	6.14	6.52	sliding	190	1.02	1.23	1.20
4		cw13	7.02	255	254	13	5	72.4	434	0.553%	7.03	6.82	7.03	sliding	191	1.00	1.45	1.45
5		cw14	8.81	255	178	13	4	73.8	434	0.789%	8.92	9.20	9.20	crushing	150	1.04	1.19	1.14
6		cw15	7.04	255	254	13	6	70.3	434	0.553%	7.02	6.92	7.02	sliding	191	1.00	1.19	1.20
7		cw16	7.02	255	254	13	4	73.1	434	0.553%	7.01	6.84	7.01	sliding	192	1.00	1.48	1.49
8	Choulli (2005)	HCP1TE	7.38	80	200	12	0	81.2	525	0.503%	7.95	7.86	7.95	sliding	103	1.08	1.65	1.53
9		HCP1TW	7.38	160	200	12	0	81.2	525	0.503%	7.67	7.79	7.79	crushing	147	1.06	1.55	1.47
10		HAP1TE	7.59	80	200	12	0	91.2	525	0.503%	8.21	8.07	8.21	sliding	104	1.08	1.31	1.21
11		HAP1TW	7.59	160	200	12	0	91.2	525	0.503%	7.84	8.01	8.01	crushing	148	1.06	1.51	1.43
12	Hanson (1964)	FX1A	3.98	222	203	19	19	45.9	410	0.205%	4.16	3.15	4.16	sliding	159	1.04	1.56	1.49
13		FX1B	3.98	222	203	19	19	45.9	410	0.205%	4.16	3.15	4.16	sliding	159	1.04	1.33	1.28
14		F1A	7.07	222	127	19	19	47.0	360	0.736%	7.86	7.43	7.86	sliding	111	1.11	1.50	1.35
15		F1B	4.87	222	127	19	19	47.0	410	0.327%	5.49	4.67	5.49	sliding	111	1.13	2.04	1.81
16		F2B	3.96	222	203	19	19	45.2	410	0.205%	4.15	3.14	4.15	sliding	159	1.05	1.67	1.60
17		F3B	3.77	222	102	19	19	47.2	298	0.230%	4.22	3.03	4.22	sliding	93	1.12	1.76	1.57
18		F4B	3.86	222	212	19	19	43.7	410	0.196%	4.03	2.94	4.03	sliding	164	1.04	1.64	1.57
19		F5B	3.63	222	106	19	19	44.2	298	0.221%	4.05	2.89	4.05	sliding	96	1.12	1.48	1.32
20		F19A	5.00	222	127	19	19	51.1	410	0.327%	5.53	4.53	5.53	sliding	111	1.11	1.33	1.20

			Prop model Eq. 6.4-6.6	Data experiment							Membrane 2000					$\tau'_{R6.4\text{-}6}/\tau'_{RM2k}$	V'_{Rexp}/V'_R	V'_{Rexp}/V'_R
											Sliding	Crushing	Governing				Prop. model	Cons. s_θ and d_{max}
			τ'_R	s_x	s_z	d_{max}	d_{max} (f_{cm})	f_{cm}	f_{ywm}	ρ_z	τ'_{RM2k}	τ'_{RM2k}	τ'_{RM2k}		s_θ			
			N/mm^2	mm	mm	mm	mm	N/mm^2	N/mm^2		N/mm^2	N/mm^2	N/mm^2		mm			
21	Rupf et al.(2013)	SR23	2.86	150	300	16	16	35.3	585	0.063%	2.85	1.66	2.85	sliding	181	1.00	1.02	1.02
22		SR25	3.00	150	220	16	16	33.1	585	0.086%	3.10	2.09	3.10	sliding	150	1.03	1.14	1.11
23		SR26	2.91	150	300	16	16	36.9	585	0.063%	2.89	1.68	2.89	sliding	181	0.99	1.07	1.07
24		SR27	3.73	150	200	16	16	28.3	575	0.188%	4.12	3.45	4.12	sliding	139	1.10	1.25	1.13
25	Xie (2009)	lb2	4.64	426	175	10	8	63.2	529	0.187%	4.57	3.71	4.57	sliding	162	0.99	1.21	1.22
26		lb10	6.35	426	88	10	9	62.3	529	0.374%	6.98	6.24	6.98	sliding	88	1.10	1.04	0.94
	Mean														149	1.05	1.39	1.32
	Coefficient of variation																17.5%	15.6%
	Mean ($a/d > 2.5$)																1.33	1.28
	Coefficient of variation ($a/d > 2.5$)																14.6%	14.1%

Appendix P

Steps to determine shear resistance for models from literature

The predicted resistance using the model of Bentz et al. (Section 5.1.5) is determined iteratively. This is because the resisted load depends on the strain at mid-depth and the strain at mid-depth depends on the applied load. The predicted resistance is determined by the following steps:

1. The effective depth d is determined using a weighted mean of the effective depth of the reinforcing steel and the prestressing steel. For the internal lever arm z, the maximum of $0.9d$ and $0.72h$ is used (CSA 2006).
2. The stiffness of the most tensioned chord and the most compressed chord are determined based on the defined steel areas and the measured stiffness of the reinforcement and the prestress tendons. The stiffness of the concrete is calculated from the defined area and the measured compressive strength f_{cm}, using the equation $E_c = 3000\sqrt{f_{cm}} + 6900$ as described in the CSA (2006). Because it is unclear in advance if a cracked or uncracked most tensioned flange should be assumed, both a cracked stiffness and uncracked stiffness are determined.
3. The resistance is determined for both a cracked most tensioned chord as an uncracked most tensioned chord.
4. As initial resistance, the experimentally found resistance is used.
5. The strain at mid-depth ε_x is calculated for the initially resistance using the equations from Section 5.1.5. The strain at mid-depth ε_x is the minimum of the calculated strain and -2 mm/m (Section 5.1.5).
6. β and θ are determined using the determined value of ε_x, using Equations 5.36 and 5.37
7. The resisted shear force is calculated using Equation 5.30. A maximum value of 65 N/mm^2 is used for f_{cm} (CSA 2006).
8. The assumed resistance is adapted until the assumed and calculated resistances match. Both resistances are assumed to match if the difference between both is less than 0.1%.
9. The sign of the force in the most tensioned flange associated with the calculated resistance determines which of the both calculated resistances is applicable for the considered experiment (a cracked or an uncracked most tensioned chord).

The predicted resistance using the model of Esfandiari (Section 5.1.6) is determined iteratively. The predicted resistance is determined by the following steps:

1. The effective depth d is determined identical as for the model of Bentz et al..

2. The stiffness's of the most tensioned chord and the most compressed chord are determined identical as for the model of Bentz et al..
3. The resistances are determined for both the failure mode yielding of the stirrups and crushing of the concrete.
4. For each failure mode, the resistance is determined for both a cracked most tensioned chord as an uncracked most tensioned chord.
5. As an initial resistance, the experimentally found resistance is used.
6. The strain at mid-depth ε_x is calculated identical as for the model of Bentz et al..
7. For each failure mode, β and θ are determined using the determined value of ε_x, using Equations 5.38–5.44.
8. The resisted shear force is calculated from Equation 5.30. A maximum value for f_{cm} is used of 65 N/mm^2.
9. The assumed resistance is adapted for each failure mode until the assumed and calculated resistances matches. Both resistances are assumed to match if the difference between both is less than 0.1%.
10. The sign of the force in the most tensioned flange associated with the calculated resistance determines which of the both calculated resistances is applicable for the considered experiment (a cracked or an uncracked most tensioned chord).
11. Finally, the highest of the resistances to yielding of the stirrups and crushing of the concrete is considered governing.

The predicted resistance for the variable angle truss model is determined by the following steps:

1. The internal lever arm is determined assuming $z_s = 0.9d_s$ and $z_p = 0.95d_p$ and using Equation 5.2 (as described in Section 5.1.1).
2. The factor ν, which accounts for the reduced strength, is determined using equation $\nu = 0.6\ (1 - f_{cm}/250)$. The factor α_{cw}, which addresses the effect of prestressing, is determined as described in Section 5.1.1.
3. The parameter ψ_{VAT} and successively angle of the compressive struts θ was determined using Equations 5.5 and 5.6. If cable ducts were present it is assumed that these are fully filled. Hence, the resistance is predicted using a non-reduced web width b_w.
4. If the angle of the compressive struts θ determined with Equation 5.5 is lower than 21.8°, a value of 21.8° is used (which appear to be the case for all experiments, see Appendix N)
5. The shear resistance $V_{R,s}$ is predicted using Equation 5.1.

Notations

Roman lower case letters

a	Shear span
b	Width of cross section
b_{bf}	Width of bottom flange
b_{tf}	Width of top flange
b_w	Width of web on T or I girders
c	Diagonal distance from the considered depth to the nearest reinforcement in the section
d	Effective height, distance from extreme compression fiber to centroid of longitudinal tension reinforcing steel
d_b	Diameter of the nearest bar
$d_{\max}$	Maximum aggregate size
d_{p}	Effective depth for prestressing steel
d_{s}	Effective depth of longitudinal reinforcing steel
e_c	Distance from the most compressed chord to the centre of gravity of the cross-section
e_{p0}	Eccentricity of the prestressing steel at the end of the girder relative to the centroidal axis
f'_c	Specified compressive strength of concrete (ACI)
$f_{c,cu,200}$	Concrete compressive strength determined for a cube with a rib length of 200 mm
$f_{cm,red}$	Reduced value of the cylinder compressive strength of concrete depending on principal tensile strain
f_{cd}	Design value of concrete cylinder compressive strength
f_{ck}	Characteristic value of concrete cylinder compressive strength
f_{ck}	Characteristic value of concrete cylinder compressive strength
$f_{ck.cube}$	Characteristic value of cube compressive strength of concrete
f_{cm}	Mean value of concrete cylinder compressive strength
f_{cr}	Cracking strength of concrete
$f_{ct,eff}$	Effective tensile strength of concrete depending on principle compression stresses
f_{ctd}	Design value of axial tensile strength of concrete
$f_{ctd,fl}$	Design value of flexural tensile strength of a concrete member
f_{ctk}	Characteristic value of axial tensile strength of concrete
f_{ctm}	Mean value of axial tensile strength of concrete

$f_{ctm,eff}$	Mean value of tensile strength considering bi-axial behaviour
$f_{ctm,fl}$	Mean value of flexural tensile strength of a concrete member
$f_{ctm,2s}$	Mean value of tensile strength considering bi-axial behaviour and the statistical size effect
$f_{ctm,sp}$	Mean value of splitting tensile strength of concrete
$f_{ctm,web}$	Mean value of tensile strength of concrete in a web used to predict diagonal tensile cracking
f_{ywd}	Design value of yield strength of shear reinforcing
f_{ywk}	Characteristic value of yield strength of shear reinforcing
f_{ywm}	Mean yield strength of shear reinforcing
f_{yx}	Yield strength of reinforcing in longitudinal direction (MCFT)
f_{yz}	Yield strength of reinforcing in vertical direction (MCFT)
h	Overall depth of member
$h_{bf,eq}$	Equivalent height of the bottom flange
$h_{bf,skw}$	Height of the skew part of the bottom flange
$h_{bf,str}$	Height of the straight part of the bottom flange
h_{cr}	Depth of the crack
h_f	Depth of flange
h_{fc}	Height of the compression flange
$h_{tf,eq}$	Equivalent height of the top flange
$h_{tf,skw}$	Height of the skew part of the top flange
$h_{tf,str}$	Height of the straight part of the top flange
h_w	Web height
l_0	Value of $l_{\sigma 1}$ for which no size effect is present.
$l_{\sigma 1}$	The length along the longitudinal axis over which the principal tensile stresses are between 90% and 100% of the maximum principal tensile stresses
n	Number of experiments
q_p	Distributed load which is the result of the curvature of the prestressing steel
s	Spacing of stirrups, spacing of bars
s_x	Spacing of cracks in longitudinal direction (MCFT)
s_z	Spacing of cracks in vertical direction (MCFT)
s_θ	Diagonal crack spacing (MCFT)
w	Crack width
x_{crit}	Distance from critical cross section to support
z	Internal lever arm, the vertical distance to the centroidal axis

z'	Effective shear depth in regions without flexural cracks, the level arm in regions without flexural cracks
$z_{c,0}$	Distance between ultimate top fibre and the centre of gravity
z_{Fc}	Distance between ultimate top fibre and centre of concrete compressive force
z_p	Internal lever arm of prestressing
z_s	Internal lever arm of longitudinal reinforcing steel

Greek lower case letters

$k_{d,\eta}$	Design value for the fractile factor
α_{cc}	Angle of the compressive strut in arch action model
α_{cw}	Factor intended to address the effect of prestressing on maximum compressive stress in compressive struts
α_R	First-order reliability method sensitivity factor for the resistance
β	Concrete contribution factor
β_t	Target reliability index
γ_c	Partial factor for concrete
γ_s	Partial factor for the reinforcing steel
γ_{xz}	Shear strain relative to x- z axis (MCFT)
ε_1	Principle tensile strain in concrete (MCFT)
ε_2	Principle compressive strain in concrete (MCFT)
ε_c	Concrete strain in a concrete cylinder at peak stress
ε_c	Strain at the flexural compressive side of a member
ε_{cr}	Cracking strain of concrete
ε_s	Steel strain
ε_t	Strain at the flexural tension side of a member
ε_x	Strain in x-direction (MCFT), strain at mid-depth of a section (MCFT)
ε_y	Yielding strain of the transverse reinforcing steel
ε_z	Strain in z-direction (MCFT)
η_d	Design value of the conversion factor which should cover all uncertainties in a real structure that are not covered by the considered experiments
θ	Inclination of the compressive struts (Variable Angle Truss model) or angle of inclination of compressive stresses in concrete to x-axis (MCFT, original notation θ_c).
θ_{cr}	Angle of diagonal crack to the longitudinal axis
θ_ε	Angle of inclination op principle strains to x-axis (MCFT, original notation θ)
ν	Effectiveness factor for concrete
ν'	Effectiveness factor of the concrete strength in regions without flexural cracks
ν_c	Strength reduction factor by micro cracks

ν_s	Strength reduction factor by sliding
ρ	Ratio of (longitudinal) tension reinforcing steel
$\rho'_{w,\min}$	Minimum shear reinforcement ratio for regions without flexural cracks
ρ_w	Reinforcement ratio of shear reinforcement
ρ_x	Ratio of reinforcing steel in x direction
ρ_z	Ratio of reinforcing steel in z direction
σ_1	Highest principle stress, principal tensile stress in concrete (MCFT, original notation f_1)
$\sigma_{1\mathrm{Ed,max}}$	Design value of the maximum value of the highest principle stress for a considered area
σ_{1m}	Principal tensile stress at the point at the mid-length of $l_{\sigma 1}$ and at mid-height of the points defining $l_{\sigma 1}$
$\sigma_{1\max}$	Maximum value of the principle tensile stress for a considered area
σ_{1R}	Principle tensile stress resistance according to Leonhardt
σ_2	Lowest principle stress, principal compressive stress in concrete (MCFT, original notation f_2)
$\sigma_{2,\max}$	Maximum stress in compression field
σ_{2m}	Principal compressive stress at the point at the mid-length of $l_{\sigma 1}$ and at mid-height of the points defining $l_{\sigma 1}$
σ_c	Concrete compression stress
σ_{cp}	Stress in the concrete in longitudinal direction in the centre of gravity
σ_{cR}	Reduction parameter indicating the difference between the stresses in the stirrups and the principle tensile stresses in the centre of gravity (Leonhardt, original notation σ_{1D})
$\sigma_{p'0}$	Initial stress in prestressed reinforcing steel at the compression side of a member
σ_{p0}	Initial stress in prestressed reinforcing steel at the tensile side of a member
σ_{pe}	Compressive stress in the concrete from effective prestressing force only at the extreme fibre
σ_{sw}	Stress in the stirrups
σ_{sx}	Average stress in x-reinforcing steel (MCFT, original notation f_{sx})
$\sigma_{sx,cr}$	Stress in x-reinforcing steel at crack location (MCFT, original notation f_{sxcr})
σ_{sz}	Average stress in z-reinforcing steel (MCFT, original notation f_{sz})
$\sigma_{sz,cr}$	Stress in z-reinforcing steel at crack location (MCFT, original notation f_{szcr})
σ_x	Stress in the longitudinal direction, stress in x-direction (MCFT, original notation f_x)
σ_{xEd}	Design value of the stress in the longitudinal direction
σ_z	Stress in the vertical direction
σ_z	Stress in the depth direction (MCFT, original notation f_z)
τ	Shear stress (MCFT, original notation v)

$\tau'_{R,c}$	Maximum shear stress that can be resisted for diagonal tension cracking
τ_{ci}	Shear stress on crack surface (MCFT)
$\tau_{ci,\max}$	Maximum shear stress on crack surface (MCFT)
τ_R	Maximum shear stress that can be resisted
$\tau_{R,c}$	Concrete contribution to shear strength
$\tau_{R,\max}$	Maximum shear strength associated with crushing of the concrete without yielding of the stirrups
$\tau'_{REq6.4\text{-}6.6}$	Maximum shear stress that can be resisted according to Equations 6.4 to 6.6
$\tau'_{R,M2k}$	Maximum shear stress that can be resisted according to membrane at $\varepsilon_x = 0$
$\tau_{R,R2k}$	Maximum shear stress that can be resisted according to Response
$\tau_{R,s}$	Steel contribution to shear strength
τ_{Rmd}	Maximum shear stress that can be resisted at mid-depth
τ_s	Shear stress resisted by transverse reinforcement
τ_{uncr}	Shear transferred by uncracked concrete
φ_{cr}	Angle of the principal stresses at a diagonal tension cracking
ψ	$\rho_{sw} f_{ywm} / f_{cm}$
ψ_{vat}	$\rho_{sw} f_{ywm} / v f_{cm}$

Roman capital letters

A'_s	Area of reinforcing steel on the flexural compression side of a member
A_c	Area of concrete cross section
A_{cc}	Area of concrete cross section on the flexural compression side of a member
A_{ct}	Area of concrete cross section area of concrete on the flexural tension side of a member
A_p	Area of prestressing steel on the flexural tensile side of a member
A_p'	Area of prestressing steel on the flexural compression side of a member
A_s	Area of reinforcing steel on the flexural tensile side of a member
A_{sw}	Area of shear reinforcing steel
A_{sz}	Area of transverse reinforcement
C	Force in the compressive chord of a girder
E_c	Modulus of elasticity of concrete
E_p	Modulus of elasticity of prestressing steel
E_s	Modulus of elasticity of reinforcing steel
F	Applied load
F_c	Strut force (compression force), resulting concrete compressive force (F_c) in cross section
F_t	Tie force (tension force)

I	Second moment of area of the uncracked concrete cross section (including reinforcement)
I_c	Second moment of area of the uncracked concrete cross section (excluding reinforcement)
M_{ct}	Moment required to cause cracking in the ultimate fiber
M_E	Applied internal; bending moment
M_r	Cracking moment
N_E	Applied axial force
P	Prestressing force
P_x	Component of the prestressing force parallel to the girder axis
S	First moment of area of the uncracked concrete cross section (including reinforcement)
S_c	First moment of area of the uncracked concrete cross section (excluding reinforcement)
$S_{c,cg}$	First moment of area of the uncracked concrete cross section in the centre of gravity (excluding reinforcement)
T	Force in the tensile chord of a girder
V'_R	Shear resistance in a region without flexural cracks
$V'_{R,c}$	Resistance to diagonal tension cracking, the minimum shear resistance for girders with stirrups in regions without flexural cracks
$V'_{R,c,exp}$	Experimentally obtained resistance to diagonal tension cracking
$V'_{R,exp}$	Experimentally obtained ultimate shear resistance in a regions without flexural cracks
$V'_{R\max}$	Resistance to crushing of the concrete before the stirrups yield in regions without flexural cracks
V_E	Applied shear force
V_R	Shear resistance
$V_{R,cc}$	Vertical component of compressive arch
$V_{R,ci}$	Shear that can be resisted by aggregate interlock
$V_{R,DC}$	Shear resistance to diagonal cracking
$V_{R,DTC}$	Shear resistance to diagonal tension cracking
$V_{R,exp}$	Experimentally obtained ultimate shear resistance
$V_{R,FC}$	Shear resistance to flexural cracking
$V_{R,FS}$	Shear resistance to flexural shear failure
$V_{R,FSC}$	Shear resistance to flexural shear cracking
$V_{R,\max}$	Resistance to crushing of the concrete before the stirrups yield
$V_{R,p}$	Vertical component of prestress force
$V_{R,R2k}$	Shear resistance according to Response
$V_{R,s}$	Shear that can be resisted by shear reinforcing steel

$V_{R,\mathrm{strut}}$	Maximum shear force which can be sustained by the member, limited by crushing of the compression struts with yielding of stirrups
$V_{R,uncr}$	Shear resistance by the uncracked concrete
$V_{tot,LE}$	Total shear force associated with a linear elastic stress distribution
$V_{w,LE}$	Shear force associated with a linear elastic stress distribution transferred by the web
V_x	Coefficient of variation.
X_d	Design value

Others

Φ	Diameter of a prestressing duct

Dankwoord

Mijn dank gaat op de eerste plaats uit naar mijn werkgever Rijkswaterstaat. Rijkswaterstaat heeft, gedurende de duur van het promotieonderzoek (April 2015 – September 2020), twee dagen per week beschikbaar gesteld voor het promotieonderzoek, waarvoor ik de organisatie zeer erkentelijk ben. Mijn bijzondere dank gaat hierbij uit naar Marès van den Hark en Albert Manenschijn. Ook mijn voormalig collega Ane de Boer wil ik bedanken voor de bemiddelende rol die hij heeft willen vervullen richting de TU Delft bij het opstarten van het promotieonderzoek.

Ik heb het geluk gehad promotoren en begeleiders te hebben die zeer betrokken waren bij het onderzoek, waarvoor ik hen zeer erkentelijk ben. Mijn dank gaat uit naar mijn promotor Max Hendriks. Max heeft de logische structuur van het proefschrift bewaakt en hij heeft me gedurende het onderzoek steeds het vertrouwen gegeven dat ik op de goede weg was. Halverwege het promotietraject was Max bereid de rol als promotor over te nemen, wat ik erg heb gewaardeerd. Ik heb Max' begeleiding als heel plezierig en effectief ervaren. Ik heb van Max verder ontzettend veel geleerd over niet-lineaire analyses, wat waardevol voor me is geweest tijdens het promoveren, maar nog meer voor mijn werk bij Rijkswaterstaat.

Verder gaat mijn dank uit naar mijn copromotor Yuguang Yang. Naast zijn rol als docent, onderzoeker en inhoudelijk coördinator van vrijwel alles binnen de groep betonconstructies, heeft Yuguang altijd tijd weten te vinden, meestal in de avond maar soms tot diep in de nacht, om de hoofdstukken van het proefstuk te lezen en van commentaar te voorzien. Als expert op het gebied van dwarskracht kon ik bij Yuguang altijd terecht voor de meest complexe vraagstukken over dwarskracht. Daarnaast heeft hij rapporten en artikelen aangedragen die erg relevant zijn gebleken voor het onderzoek. De vele vragen die hij heeft gesteld en de discussies die we samen hebben gevoerd, hebben veel bijgedragen aan het uiteindelijke resultaat en de onderbouwing van het proefschrift.

Zeker ook gaat mijn dank uit naar mijn begeleider Cor van der Veen. Zijn uitgebreide en brede kennis op het gebied van betonconstructies waren erg waardevol voor het onderzoek. Cor heeft er steeds voor gezorgd dat de focus van het onderzoek op de meest essentiële vraagstukken bleef liggen, de aandacht uitging naar het meest geschikte model en dat de onderzoeksresultaten praktisch toepasbaar zouden zijn. Ook ben ik Cor dankbaar voor zijn motiverende begeleiding en zijn bereidheid om mij te blijven begeleiden zelfs na zijn pensioen.

Verder gaat mijn dank uit naar Dick Hordijk die gedurende de eerste helft van het onderzoek mijn promotor was. Dick heeft de gave om de juiste vragen te stellen die het onderzoek verder helpen en ik heb zijn begeleiding als zeer inspirerend ervaren.

Ik ben mijn promotoren en begeleiders verder erkentelijk voor de vrijheid die ik heb gekregen om het onderzoek naar eigen inzicht in te vullen.

Mijn dank gaat uit naar Maaike Ritzen van Rijkswaterstaat. Dat het onderzoek binnen de beschikbare tijd is afgerond is mede te danken aan de aandacht die Maaike hiervoor bij ieder voortgangsoverleg heeft gevraagd. Verder wil ik haar danken voor het bewaken van de zichtbaarheid van de onderzoeksresultaten binnen Rijkswaterstaat. Ik ben Dick Schaafsma van Rijkswaterstaat dankbaar voor het reviewen van de algemene hoofdstukken van het proefschrift. Dat de modellen nu direct voor de praktijk toepasbaar zijn is vooral dankzij zijn reviewopmerkingen. Ook ben ik hem dankbaar voor het laten uitvoeren van de aanvullende beoordelingen door het ingenieursbureau waardoor inzicht kon worden gegeven in de aantallen bruggen en viaducten waarvoor het promotieonderzoek gevolgen heeft. Als laatste collega van Rijkswaterstaat wil ik Christien Mak bedanken voor de prettige afspraken die we hebben kunnen maken rondom de afronding van het promotietraject.

Daarnaast wil ik Gerrie Dieteren van TNO bedanken voor de feedback die hij heeft willen geven op de gebruikte methode voor het vaststellen van de rekenwaarden van de modellen. Ook wil ik Joost Walraven bedanken voor de ideeën die heeft aangedragen en de vakliteratuur die ik van hem heb gekregen. Ik heb het heel bijzonder gevonden om af en toe onverwachts bezoek te krijgen van de hoogleraar waarbij ik in 1996 ben afgestudeerd.

Mijn dank en waardering gaat verder uit naar de afstudeerders die met hun onderzoeken hebben bijgedragen aan de onderzoeksresultaten. Het promotieonderzoek is extra plezierig geweest door met hen gezamenlijk aan het onderzoek te werken. De volgende afstudeerders hebben bijgedragen aan het onderzoek:

- Maciej Kraczla, die onderzoek heeft verricht met de titel: *'Analytical and Numerical Analysis of the Shear Tension Critical Prestressed Beams'* (Kraczla 2016).
- Sijtse Jan Kroeze, die onderzoek heeft verricht met de titel: *'Resistance to Diagonal Tension Cracking in Prestressed Beams'* (Kroeze 2018).
- Andrew Sugianto, die onderzoek heeft verricht met de titel: *'Numerical Investigation into Size Effect on Prestressed Concrete Beam Resistance to Shear Tension Cracking'* (Sugianto 2019).
- Marieke Vergeer, die onderzoek heeft verricht met de titel: *'Shear tension resistance of prestressed concrete beams with shear reinforcement, Based on the MCFT'* (Vergeer 2019).
- Mathijs Tuitjer, die onderzoek heeft verricht met de titel: *'Effect of Flexural Cracks on web-shear cracking of prestressed concrete continuous members'* (Tuitjer 2019).

Ik wil verder de vele mensen bedanken die tijdens mijn promotie met me hebben meegeleefd en belangstelling hebben getoond voor het onderzoek. Mijn kinderen Ilse en Floris die als een van de weinigen de titel van het proefschrift feilloos uit hun hoofd kennen. Mijn ouders en broer, mijn andere familieleden, schoonfamilie en vrienden. Mijn goede vriend Erwin van Aalst wil ik bedanken voor het meedenken over het ontwerp van de omslag. Ook wil ik alle collega's van Rijkswaterstaat danken voor alle interesse die zij hebben getoond. Ik heb het ontzettend gewaardeerd dat de afdeling Bruggen en Viaducten tijdens het promoveren op bezoek is geweest bij de groep betonconstructies van de TU Delft.

Ook wil ik de collega's van de afdeling betonconstructies van de TU Delft danken voor de fijne tijd die ik daar heb gehad. Ik kijk met plezier terug op de vele etentjes, uitjes, de 'dangerous sports' activiteiten en de lunch- en koffiemomenten. De hoogtepunten in deze periode waren voor mij de week dat we Vechtbrug hebben laten bezwijken, de experimenten die ik samen met Rutger Koekkoek en Albert Bosman heb uitgevoerd met de prefab ZIP-liggers, het *fib* congres in Maastricht en het SEMC congres in Zuid Afrika. Met mijn leeftijds- en kamergenoot Sebastiaan Ensink heb ik het promoveren als gezamenlijk avontuur mogen beleven wat de promotie een extra plezierige ervaring heeft gemaakt.

Maar mijn meeste dankbaarheid gaat uit naar mijn partner Riemke Overal. Vanwege haar positieve reactie op het idee om naast het werk een promotieonderzoek te beginnen en mijn niet meer zo nodige 'pappadag' in te ruilen voor een 'promotie dag'. Vanwege alle klussen die ze heeft gedaan in ons nieuwe huis terwijl ik weer eens een weekend doorwerkte aan mijn promotie. Omdat ze alle belangrijke teksten nog heeft willen controleren op spellingsfouten voordat het proefschrift naar de drukker is gegaan. Maar vooral vanwege de vele uren waarin ze de verhalen over het onderzoek heeft willen aanhoren en heeft willen meedenken over alle vraagstukken die niet inhoudelijk waren. Ik heb het erg getroffen met haar.

Curriculum Vitae

2008 – heden	Senior Adviseur/ Specialist, Rijkswaterstaat, Grote Projecten en Onderhoud, afdeling Bruggen en Viaducten, Utrecht – Trekker beoordeling van de bestaande voorgespannen liggerbruggen en viaducten in het areaal RWS, m.n. de aansturing van het numerieke en experimentele onderzoek door kennisinstituten en de beoordelingen door ingenieursbureaus – Promovendus aan de TU Delft, faculteit Civiele Techniek en Geowetenschappen, Afdeling 'Engineering Structures', groep betonconstructies, voor 3 dagen per week (April 2015 – September 2020) – Opsteller PvA ter beoordeling van betonnen bruggen en viaducten – Adviseur techniek bij realisatieprojecten – Beheerder richtlijn niet-lineaire eindige-elementen analyses (RTD1016) – Beheerder Richtlijnen Ontwerp Kunstwerken (RTD1001, v1.1) – Beheerder kader borging constructieve veiligheid in de realisatiefase – Detachering als constructeur bij Volker Infra Design – Trekker kennisveld (programma) constructieve veiligheid – Lid van het Kernteam Bouwtechnologie – Deelname werkgroepen: Betonvereniging 'Compendium Aanpak Constructieve Veiligheid (editie 2011), CUR Platform Constructieve Veiligheid, CUR rapport 'Borging constructieve veiligheid bij geïntegreerde contracten', CROW College van Deskundigen TIS
2005 - 2008	Principal Engineer bij VECTRA Group Ltd., Utrecht – Safety Manager, Beveiligingssysteem EBS+, IPS Deventer (ProRail) – Safety Engineer, Beveiligings- en beheersysteem Amsterdam-Utrecht (ProRail, project BB21)
2002 –2005	Lead Auditor, Lloyd's Register Rail B.V., Rotterdam – Projectleider veiligheidsaudit bij de Belgische Spoorwegen (NMBS) – Auditor projecten, organisaties, kwaliteitsmanagementsystemen – Independent Safety Assessor Randstad Rail, Notified Body HSL Zuid
2000 – 2002	Constructeur van kantoorgebouwen en gevangenissen Rijksgebouwendienst, Den Haag
1996 – 2000	Constructeur van spoorviaducten, perrontunnels, stationskappen, voetgangersbruggen en technische gebouwen, Holland Railconsult, Utrecht
1990 - 1996	Technische Universiteit Delft, Faculteit der Civiele Techniek, vakgroep mechanica en constructies, sectie betonconstructies, Delft, afstudeeronderzoek: 'het genereren van benodigde wapeningshoeveelheden met behulp van de eindige elementen methode'
1984 - 1990	Carolus Borremeus College, VWO, Helmond
1972	Geboren op 23 februari in Helmond

In the design process of prestressed bridges and viaducts, the required amount of shear reinforcement is determined with a model that assumes the presence of flexural cracks. In order to keep the design process simple, this model is also prescribed to determine the amount of shear reinforcement for the regions of the structure in which, at the ultimate load, no flexural cracks are present. This is a conservative approach, as the conditions for shear transfer are more favourable in the regions without flexural cracks.

From structural assessments of existing prestressed bridges and viaducts, it is found that the amount of shear reinforcement is frequently too low in the regions that remain free of flexural cracks. Accordingly, these structures are considered as unqualified, although the actual shear resistance could possibly be sufficient. This is the prime motivation for this research, in which the shear behaviour of prestressed girders in regions without flexural cracks is investigated.

Two models are proposed in this dissertation for the determination of the shear resistance in the regions without flexural cracks:
- a model for diagonal tension cracking and
- a model that considers the contributions of stirrups, aggregate interlock and uncracked flanges after diagonal tension cracking.

Depending on the amount of shear reinforcement and the level of prestressing, the governing resistance will be present in either one of these stages.

With the proposed models it has become possible to determine the shear that can be resisted in regions without flexural cracks more accurately. The use of the proposed models will therefore prevent that numerous bridges and viaducts are strengthened or replaced while the actual shear resistance is sufficient.